EXPERIMENTAL AND NUMERICAL INVESTIGATION OF THE CONCRETE SHEAR STRENGTH OF REINFORCED CONCRETE BOX CULVERTS UNDER UNIFORMLY DISTRIBUTED LOAD

by

MASOUD GHAHREMANNEJAD

Presented to the Faculty of the Graduate School of

The University of Texas at Arlington in Partial Fulfillment

of the Requirements

for the Degree of

DOCTOR OF PHILOSOPHY

THE UNIVERSITY OF TEXAS AT ARLINGTON

August 2018

ACKNOWLEDGEMENTS

First of all, I would like to express my sincere gratitude to my supervising professor, Professor Abolmaali, for his endless support. This research would not have been successfully completed without his valuable knowledge and advice. I also appreciate my committee members, Professor Yazdani, Professor Chao, and Professor Wang, for providing me with their comments and contributions. Thanks go to all members of the Center for Structural Engineering Research/Simulation and Pipeline Inspection for their help.

I thank my family for their support and for encouraging me to go abroad for the PhD program. Their motivation and heartwarming support are always appreciated.

My warmest thanks go to my friends, Arash Emami Saleh, Maziar Mahdavi, Sina Abhaee, Amin Darabnoush Tehrani, Dr. Mahnaz Mostafazadeh, Bassam Al-lami, Dr. Himen Hojat Jalali, and Dr. Hamideh Habibi.

July 5, 2018

ABSTRACT

EXPERIMENTAL AND NUMERICAL INVESTIGATION OF THE CONCRETE SHEAR STRENGTH OF REINFORCED CONCRETE BOX CULVERTS UNDER UNIFORMLY DISTRIBUTED LOAD

Masoud Ghahremannejad, PhD

The University of Texas at Arlington, 2018

Supervising Professor: Seyedali Abolmaali

This research resulted in the development of a new method for performing displacement control analysis of distributed loads to obtain the ultimate shear strength of structural components. A framework, consisting of several sub-frames, was designed to convert the single displacement applied at the top of the framework to equivalent uniformly-distributed forces applied to the beam. To validate the loading mechanism, using the proposed framework, the load was applied on the top of a reinforced concrete beam in the laboratory, and numerical studies were conducted. The shear capacity of the beam under a concentrated load at mid-span was compared with the shear capacity of a uniform load for four different a/d ratios (3, 4, 5, and 7). The results indicated that the strain in the longitudinal rebar, which is dependent upon the loading condition, strongly impacts the shear strength of a critical section of structural components. The shear strength of the critical sections of the R.C. beams studied in this research had uniformly distributed loads that were, on average, 76% greater than the shear strength of the same beam with a concentrated load

at mid-span. The shear strength predictions of the AASHTO specification and the ACI318-14 code were evaluated for beams with shear behavioral mode. A parametric study of 24 RC beams was conducted, and the results indicated that AASHTO's prediction for strain in longitudinal rebar differed about 19%, on average, from the results of the finite element method (FEM). For prediction of the β factor, however, the difference was about 61%. The ACI318-14's formulation for the concrete shear strength (V_c) averaged 59% higher than the FEM results for the studied beams.

An increase in the fill height of buried box culverts leads to an increase in the thickness of the slab and wall, as well as in the number or size of longitudinal slab reinforcements required to resist flexure. This geometrical configuration imposes a shear behavioral mode. The second part of this study focuses on experimental and numerical approaches to determining the shear strength of reinforced concrete box culverts with uniformly distributed load on the top slab. Two sizes of reinforced concrete (R.C.) box culverts were experimentally and numerically investigated. The results from the verified numerical models differed from the ACI318-14 formulation for the shear strength of top slabs of R.C. box culverts. A parametric study of 108 cases using the verified analysis revealed that the shear strength of the top slabs of R.C. box culverts averaged 66% greater than the ACI318-14's shear formulation. The ratio of $\frac{V_{FEM}}{V_{ACI318-14}}$ decreased slightly when the span/rise increased; however, an increase in the span/top slab's thickness led to a significant decrease in the $\frac{V_{FEM}}{V_{ACI318-14}}$ ratio.

The finite element models of R.C. box culverts were calibrated by experimental data. Using the verified numerical models, several parameters were investigated that influence the shear strength of a R.C. box culvert's top slab, such as span, rise, top slab's thickness, etc. Consequently,

the results of 288 case studies assessed the AASHTO's methodology to determine the shear strength of the box culverts' top slab. A comparison of analysis results with the equations in the specification, using the AASHTO approach, indicated an underestimation in the prediction of the concrete shear strength (the β factor); however, the difference in prediction of the strain value in the longitudinal rebar was reasonably acceptable. The comparison revealed, on average, an 89% difference in prediction of the β factor and a 19% difference in prediction of the strain in the longitudinal rebar in the shear critical section, at distance "d" from haunch. The nonlinear regression analysis proposed multi-variable formulations to predict the concrete shear strength in the shear critical section of the top slab of R.C. box culverts.

Contents

ACKNOWLEDGEMENTS ii
ABSTRACT iii
LIST OF FIGURES ix
LIST OF TABLES xiv
CHAPTER 1. INTRODUCTION 1
1.1. Overview 1
1.2. Box Culverts 3
1.3. Literature Review 5
1.4. Research Objective 12
CHAPTER 2. LOADING MECHANISM 14
2.1. Overview 14
2.2. Concept and Theory 15
2.3. Framework Construction 18
2.3.1. Design and Drawings 18
2.3.2. Implementation 19
2.4. Experimental Tests 20
2.4.1. Specimens 20
2.4.2. Test Setup and Instrumentations 22
2.5. Finite Element Modeling 24
2.5.1. Material Properties 25
2.5.2. Boundary Conditions 27
2.5.3. Loading and Analysis 27
2.6. Results and Discussions 28
CHAPTER 3. SHEAR STRENGTH OF REINFORCED CONCRETE BEAMS 32
3.1. Overview 32
3.2. Experimental Tests by Other Researchers 32
3.2.1. Specimens 33
3.2.2. Material Properties 34
3.2.3. Test Setup and Instrumentations 34
3.2.4. Results 35
3.3. Numerical Modeling 35
3.3.1. Material Properties 35
3.3.2. Boundary Conditions 37
3.3.3. Loading and Analysis 37

3.3.4. Verification of Finite Element Models 37
3.4. Parametric Study 40
3.4.1. Results 42
3.5. Comparison with Design Codes 44
3.5.1. ACI318-14 45
3.5.2. AASHTO Specification 47
CHAPTER 4. EXPERIMENTAL AND NUMERICAL INVESTIGATION OF R.C. BOX CULVERTS 54
4.1. Overview 54
4.2. Specimens Size 54
4.3. Specimens Construction 56
4.4. Test Setup and Instrumentations 57
4.5. Results 59
4.6. Finite Element Modeling 61
4.7. Material Properties 62
4.7.1. Concrete 62
4.7.2. Rebar 63
4.7.3. Steel 63
4.8. Element Type 63
4.8.1. Solid Element 63
4.8.2. Truss Element 63
4.9. Boundary Conditions 63
4.10. Loading and Analysis 64
4.11. Finite Element Model Verifications 64
4.11. Effects of Box Culverts' Width 67
4.12. Size Effects in Shear Strength 69
4.12. Effects of Indeterminacy 70
4.13. Effects of Bedding 74
CHAPTER 5. PARAMETRIC STUDY AND DESIGN CODES ASSESSMENTS 77
5.1. Overview 77
5.2. Case Studies 78
5.3. Results and Discussions 80
5.4. ACI318-14 86
5.4.1. Methodology 86
5.4.2. Assessment 86

5.5. AASHTO Specification 92
5.5.1. Methodology 92
5.5.2. Assessment 95
CHAPTER 6. REGRESSION ANALYSIS 99
6.1. Overview 99
6.2. Assumptions 101
6.3. Shear Strength of Top Slab of Box Culverts using MLR 103
6.4. Proposed AASHTO Shear Design Equation for Top Slab 106
6.5. An Equation Independent of the Strain Value (Shear Capacity of Box Culvert) 108
CHAPTER 7. SUMMARY AND CONCLUSIONS 110
7.1. Summary and Conclusions 110
7.2. Recommendations for further investigations 113
APPENDIX 1. LOAD-DEFLECTION CURVES 114
APPENDIX 2. CRACKING PATTERN 163
APPENDIX 3. RESULTS OF PARAMETRIC STUDY 212
APPENDIX 4. GALLERY OF BEAM TEST PICTURES 224
APPENDIX 5. GALLERY OF BOX CULVERT TESTS 231
References 250
Biographical Information 256

LIST OF FIGURES

Figure 1. Application of box culvert as tunnel under roadway 1

Figure 2. Application of box culvert as small stream crossing 2

Figure 3. Application of box culvert for stormwater detention 2

Figure 4. Schematic section of box culverts 4

Figure 5. Typical box sections of ASTM C1577 [4] 5

Figure 6. Effect of using high-strength rebar on the shear capacity of R.C. beams [5] 6

Figure 7. Tested beams' configuration under uniformly distributed load [8] 7

Figure 8. Numerical model output for shear force and bending moment [12] 9

Figure 9. Box culvert test setup for studying the effects of wheel load [13] 9

Figure 10. Box culvert test setup for testing one-half of a specimen [14] 10

Figure 11. A simply supported beam under applied uniform displacement at the top 15

Figure 12. A simply supported beam under several applied single displacements at the top 16

Figure 13. Framework to apply displacement control of distributed uniform load 17

Figure 14. Experimental-tested beam and its cross section under uniform load [8] 17

Figure 15. Load-deflection curves to verify the frame 18

Figure 16. Dimensions of each part of the framework 19

Figure 17. The framework built for the experimental program 20

Figure 18. Beam-tested dimensions within the framework 21

Figure 19. Beam specimens prepared for tests in moisture chamber 22

Figure 20. Anchorage details 22

Figure 21. Beam specimen test setup 23

Figure 22. Strain gauge installation 23

Figure 23. Developed numerical model for the beam test 24

Figure 24. Strain-stress curves for 5100 psi concrete; a) for compression behavior; b) for tension behavior 25

Figure 25. Strain-stress curve for rebar (Grade 60 ksi, 420 MPa) 27

Figure 26. Load-deflection curve from experimental data and FEA 29

Figure 27. Comparison of the strain value in longitudinal rebar obtained from experimental data and FEA at failure 30

Figure 28. Obtained shear cracks from both experimental test and FEA 30

Figure 29. Load distribution through the framework in various loading steps 31

Figure 30. Cross sections of experimental case studies (Unit: mm) [34] 33

Figure 31. Test setup of the experiment (Unit: mm) [34] 34

Figure 32. d_c and d_t parameters for used concrete in compression and tension 36

Figure 33. Comparison of load-deflection curve of the beams for concentrated load and uniformly distributed load 39

Figure 34. Crack pattern of the designated beams: (a) OA1 Beam (a/d=4), (b) OA2 Beam (a/d=5), and (c) OA3 Beam (a/d=7) 40

Figure 35. Finite element model and proposed displacement loading 41

Figure 36. Variation of $V_{FEM}/V_{(ACI318\text{-}14)}$ versus a/d 47

Figure 37. Variation of strain in longitudinal steel along the span: (a) a/d=4, (b) a/d=5, and (c) a/d=7 49

Figure 38. Variation of the β factor along the span: (a) a/d=4, (b) a/d=5, and (c) a/d=7 51

Figure 39. Variation of $\beta_{FEM}/\beta_{AASHTO}$ and $\varepsilon FEM/\varepsilon AASHTO$ versus a/d 53

Figure 40. R.C. box culverts' examined characteristics 55

Figure 41. Wooden molds for the box culvert specimens 56
Figure 42. Reinforcement cages 56
Figure 43. Chemicals for strain gauge installation 57
Figure 44. Box culvert specimens..... 57
Figure 45. Test setup and instrumentations for the box culvert tests (box culvert size: 3×2×4).. 58
Figure 46. Crack patterns (box culvert size: 3 × 3 × 4) 60
Figure 47. Finite element model and assumptions..... 61
Figure 48. Stress-strain curve for concrete material in compression and tension 62
Figure 49. Comparison of numerical results with experimental data, a) for box culvert 3×2×4; b) for box culvert 3×3×4 65
Figure 50. Validation of numerical model's crack pattern via experimental data for box culvert examined 3×3×4- ρ=2.22%- f_c^'=4.8 ksi (33.1 MPa) 66
Figure 51. Comparison of numerical results with experimental data to predict the stain value in longitudinal rebar at failure..... 66
Figure 52. Comparison of box culvert's width in failure mode..... 68
Figure 53. Shear stress at distance "d" from haunch versus deflection of top slab's mid-span up to failure 68
Figure 54. Validity of finite element method to consider size effect..... 69
Figure 55. Comparison of the shear strength for box culverts and simply supported beams 71
Figure 56. Shear force and bending moment diagrams for box culvert 3 × 3 × 4 and beam 3 × 4 73
Figure 57. Comparison of crack propagation in box culverts and simply supported beams 74

Figure 58. Box culvert on a rigid bedding: a) on a rigid bedding; b) equivalent boundary condition; c) bending moment diagram; d) shear force diagram 75
Figure 59. Box culvert with upward loading: a) a uniform load applies to the bottom slab; b) bending moment diagram; c) shear force diagram 76
Figure 60.Finite element model and proposed framework for loading 77
Figure 61.Strain-stress curve for concrete material; a) in compression; b) in tension 79
Figure 62. Indication of failure mode based on cracking pattern 80
Figure 63. Total failure load and failure mode for each case study 81
Figure 64. Variations of the total failure load vs change in S/R 82
Figure 65. Variations of the total failure load vs change in S/T 82
Figure 66. Comparison of total shear force and the shear force at the critical section in top slab 83
Figure 67. Shear cracking location for case studies with shear failure mode 84
Figure 68. Different types of shear failure 84
Figure 69. The shear strength and bending moment of the critical shear section in top slab at failure from FEA for the examined box culverts 88
Figure 70. Comparison of analysis outcomes with ACI318-14's shear formulations: a) comparison with Equation 3-1a, b) comparison with Equation 3-1b, c) comparison with Equation 3-1c, d) comparison with ACI318-14's prediction (1 lbs. = 0.00445 kN) 90
Figure 71. Variations of $V_{FEM}/V_{(ACI318-14)}$ versus span/rise for R.C. box culverts' top slab under uniformly distributed loads 91
Figure 72. Variations of $V_{FEM}/V_{(ACI318-14)}$ versus span/top slab's thickness for R.C. box culverts' top slab under uniformly distributed loads 91

Figure 73. Comparison of the obtained β factor from FEA and AASHTO in the section at distance “d” from haunch..... 96

Figure 74. Comparison of the obtained strain value in longitudinal rebar from FEA and AASHTO in the section at distance “d” from haunch 96

Figure 75. Variations of $\beta_{AASHTO}/\beta_{FEA}$ ratio versus changing top slab’s thickness and R/S in the section at distance “d” from haunch: a) when f_c'=20.7 MPa & ρ=1.3%, b) when f_c'=20.7 MPa & ρ=2.3%, c) when f c'=34.5 MPa & ρ=1.3%, d) when f_c'=34.5 MPa & ρ=2 98

Figure 76. Change in the shear strength in the critical section versus a) fc', b) Top slab’s thickness (T), c) area of longitudinal rebar in tension times the strain value ($As\varepsilon$) where As is in mm^2 ; d) R/S..... 102

Figure 77. Evaluation of multiple linear regression model..... 105

Figure 78. Evaluation of nonlinear regression model..... 107

LIST OF TABLES

Table 1. The characteristics of tested specimens by Yee [14] 10

Table 2. Summary of code predictions and test capacities by Yee [14] 11

Table 3. Concrete damage parameters 26

Table 4. Cross section details of experimental case studies [34] 33

Table 5. Concrete characteristics of the beams [34] 34

Table 6. Experimental test results [34] 35

Table 7. Characteristics of case studies 41

Table 8. Parametric study results and comparison with AASHTO Specification 44

Table 9. Parametric study results and comparison with Equation (3-1) in ACI318-14 Code 46

Table 10. Concrete properties in the experimental program 55

Table 11. The experimental tests outputs 59

Table 12. Results of comparison of box culverts with simply supported beam 72

Table 13. The characteristics of case studies 78

Table 14. Characteristics of cases with S/T<6 85

Table 15. Case study characteristics for evaluation of ACI318-14 87

Table 16. Comparison of the examined R.C. box culverts with ACI318-14 88

Table 17. Correlation matrix 102

Table 18. Summary statistics 103

Table 19. Variance inflation factor 103

Table 20. ANOVA for training data sets 104

Table 21. Model parameters 104

Table 22. ANOVA table 108

Table 23. Model Parameters 108

CHAPTER 1. INTRODUCTION

1.1. Overview

Precast concrete box culverts are the ideal solution to a wide range of construction applications. Their traditional use is for diverting watercourses, but since they are available in a wide range of sizes and shapes, including round, elliptical, flat-bottomed, and pear-shaped and box [1], they are versatile and are used for many applications. These include attenuation tanks, pedestrian subways, access shafts, service tunnels (Figure 1), sea outfalls, road crossings, and a variety of other applications where strength, durability, and economy are of paramount importance. In the construction industry, culverts are structures that allow water to flow under a road, railroad, trail or other obstruction, as shown in Figure 2. They are typically embedded in and surrounded by soil.

Box culverts are used for intakes and outtakes, holding tanks, steam tunnels, corridor links, road crossings, service tunnels, storm-water detention (Figure 3), and utility trenches. They are one of the most useful structures in modern construction. Precast reinforced concrete box culverts are widely used throughout the world to provide safe and relatively economical structures.

Figure 1. Application of box culvert as tunnel under roadway

Figure 2. Application of box culvert as small stream crossing

Figure 3. Application of box culvert for stormwater detention

The installation of a box culvert involves preparation of the site, placement, and backfilling of the box culvert sections. Depending on the project size, preparation of the site may be completed in a matter of hours and may be performed just prior to delivery of the precast culverts. Placement of the culvert units is usually carried out with a crane and is a straightforward and rapid operation. Precast fabrication of box culvert units reduces the amount of work on-site and possible impact of weather on project schedules. The culvert sections can be installed, backfilled, and placed into service immediately after delivery to the site. Box culvert units can be preordered to allow projects to proceed on-site in early spring. When the work site involves a water course, a precast structure eliminates the need to maintain a dry site for the entire duration of the project to prevent damage or disruption to form work, rebar, etc., reducing water control requirements and costs. Precast

concrete culverts are a low maintenance solution, as precast concrete products have all of the durability advantages of high quality concrete, without the concern of breakdown of protective coatings, corrosion, or the various problems associated with other materials. Because of the nature of precast concrete products, designers have access to a large range of configurations of culvert layouts, geometry, alignment, and capacity, and special box sections can be fabricated to meet unusual conditions or design requirements. For example, radius box sections and angular bend sections can be fabricated to accommodate changes in alignment, transition units can be fabricated where a change in culvert size is required, and wyes and tees can be fabricated to allow connection of round pipe sections to the box culvert [2].

1.2. Box Culverts

Figure 4 illustrates a schematic section of box culverts. The internal distance between the top and bottom slabs is called “rise,” and the internal distance between two walls is called “span.” In most cases, the thickness of the slabs and walls is equal. The load that reaches the structure is governed by the buried depth of the box culverts. According to codes and specifications [3, 4], live loads, due to the wheels of vehicles, as well as dead loads, should be applied to box culverts with shallow cover since the effects of live loads are more critical than those of dead loads. Only soil pressure is considered as the design load for box culverts that are buried deep (up to 100 feet).

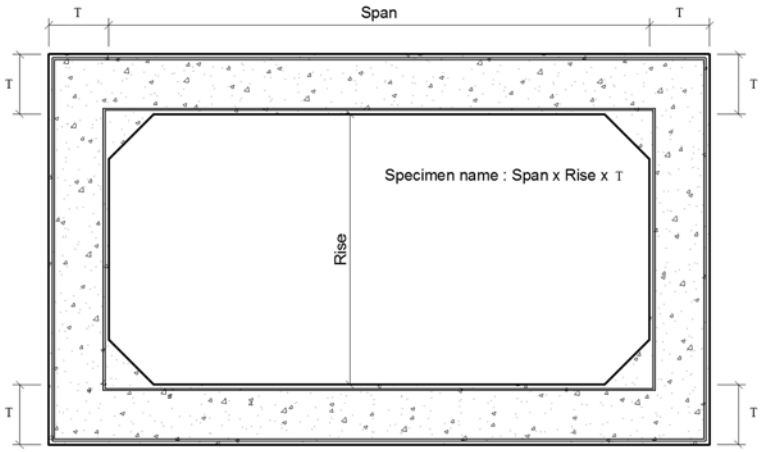

Figure 4. Schematic section of box culverts

ASTM C1577 [4] defines box sections based on their fill height. Figure 5 shows two typical box sections of ASTM C1577 [4]. This specification assigns specific names for each section's reinforcement. For example, the bottom longitudinal reinforcement of the top slab is called As2, and the outer vertical reinforcement of the walls is called As1. Because the depths of the structures incur different environmental hazards, the concrete cover of longitudinal reinforcement is assumed to be 2 inches (50 mm) for fill height of less than 2 feet (610 mm) and 1 inch (25 mm) for fill height greater than 2 feet (610 mm). The configuration of the reinforcement of the top slab is different, since live loads, such as those imposed by traffic, considerably affect shallow-depth box culverts and require more reinforcements in two perpendicular directions. Haunch is a triangular piece of concrete that is built into all four corners of rectangular sections of box culverts to strengthen the connection between the slab and the wall so that the angle remains perpendicular after deformation. The dimensions of the haunch (H) are usually equal to the thickness of the slabs and walls.

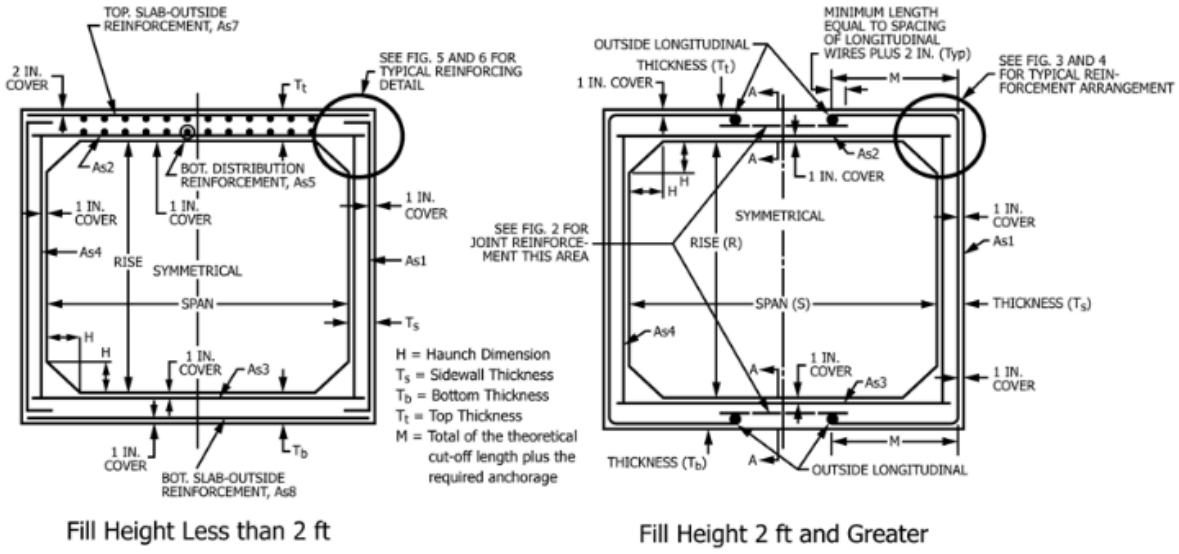

Figure 5. Typical box sections of ASTM C1577 [4]

The convention for the naming of box culverts used in ASTM C1577 [2] and this research is $span \times rise \times top\ slab's\ thickness$, where span and rise are in feet and the top slab's thickness is in inches.

1.3. Literature Review

Many researchers have investigated the shear strength of reinforced concrete (R.C.) members and the parameters that affect it, such as the material properties, size, loading conditions, etc. [5-9], resulting in guidelines and formulations for the shear design of R.C. elements [10, 11]. The literature review in this study is divided into two categories: previous investigations on the concrete shear strength of reinforced concrete beams, and the work of other researchers who specifically focused on the shear strength of reinforced concrete box culverts.

The shear behavior of R.C. beams and the different parameters affecting the shear strength of the beams have been studied for the past several decades. Unlike the flexural behavior of beams, there is no universal agreement or theory to justify the shear behavior of R.C. elements. Using higher strength materials in construction of the members leads to higher strength in both the flexural and

shear behavioral modes. Hassan et al. [5] studied the impact of high-strength rebar on the shear capacity of large concrete beams. They experimentally investigated a number of R.C. beams constructed with both conventional and high-strength steel. The comparison of the outputs revealed that using high-strength rebar considerably increases the shear capacity of the beams and confirmed that an increase in concrete compressive strength leads to an increase in the shear strength. Figure 6 illustrates a comparison of two beams which only differed in rebar material. This figure indicates that the beam constructed with high-strength steel showed significantly greater strength rather than the beam constructed with conventional steel.

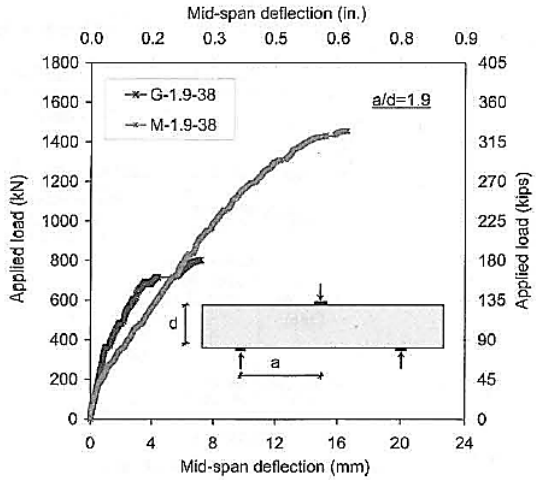

Figure 6. Effect of using high-strength rebar on the shear capacity of R.C. beams [5]

Adding various components, such as fibers, into the concrete mix can help strengthen R.C. elements against shear stresses. Zarrinpour and Chao [6] tested the shear capacity of reinforced concrete beams equipped with steel fibers. They examined a total of 12 large-scale simply supported steel-fiber-reinforced concrete (SFRC) and R.C. beams with an overall height from 12 to 48 in. (305 to 1220 mm) under monotonic point load up to failure. All of the beams were examined under a concentrated load at the mid-span. They concluded that the bridging action of fibers across the diagonal shear cracks enhances the shear capacity of beams and affects the

cracking patterns, and different distributions of internal stress and strain impact the shear strength of structural members. Shioya et al. [8] applied uniformly distributed loads to test six large R.C. beams without shear reinforcement. The geometry of the beams is shown in Figure 7; the spans of the beams were 12 times that of each cross section. The size effect of the beams was investigated, and it was concluded that an increase in the effective depth of the beam decreases the shear stress at the critical section at failure.

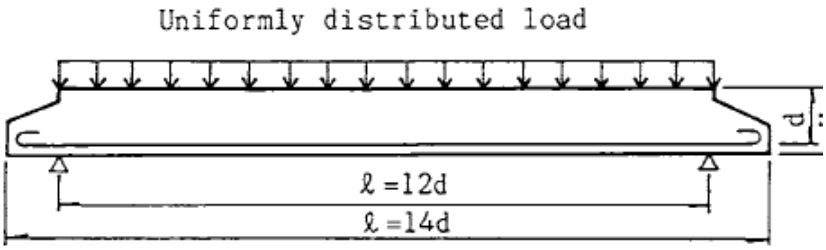

Figure 7. Tested beams' configuration under uniformly distributed load [8]

Some prominent studies emphasize the shear strength of reinforced concrete box culverts. Abolmaali and Garg [12] performed experimental and analytical studies to investigate the effects of wheel load, as it is the most critical live load that is applied to shallow box culverts. They applied a point load to a distance of "d" from the haunch to simulate the worst case scenario and developed a numerical model, coupled with nonlinear analysis, to predict the behavior of the specimens under the designated load. The finite element analysis (FEA) predicted the crack, with an increase in load, on the inside face of the top slab at the loading end. Figure 8 shows the ability of the developed finite element model to predict the bending moment and shear force in R.C. box culverts. Mostafazadeh [13] investigated the effects of wheel load on box culverts made from synthetic fibers, using the same test setup and loading protocol shown in Figure 9. The results revealed that adding synthetic fibers to the concrete mix design considerably increases the shear strength of the top slab of box culverts. Adding 0.52% synthetic fibers volume fraction to the

concrete mix designs not only increases the shear and flexural strength of concrete, but also changes the behavior of concrete from brittle to more ductile.

Yee [14] performed an experimental study on 12 different box culvert sizes, as presented in Table 1. He tested half of the culverts by applying distributed load, using several loading jacks, and investigated the failure strength of the culverts. The test setup for testing a half-box culvert is shown in Figure 10. He then compared them with code predictions and exhibited the results in Table 2. He found that CHBDC [15] and AASHTO [3] formulations underestimated the shear strength of the culvert sections by a considerable margin. Sherwood et al. [16] tested several thick slabs and wide beams to monitor the shear cracking changes that occur with variations of the member's width. The results revealed that the width of a member does not have a significant influence on the shear stress at failure. The slab of a box culvert acts like a one-way slab; therefore, its width does not influence it. The effects of truck loads on R.C. box culverts acting as a bridge were investigated by Orton et al. [17]. They studied 10 existing R.C. box culverts with different thickness of soil applied on the top of them. The outcomes indicated that for box culverts with less than two feet of fill height, the AASHTO [18] specification is conservative in its estimation of strains and displacements. Additionally, Kim and Yoo [19] used the finite element method (FEM) to study the loads applied to buried box culverts and the soil-structure interaction behavior caused by various installation methods, backfill height, etc.

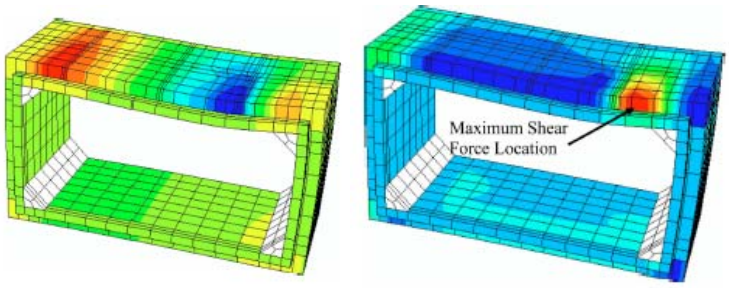

a) Contour for moment b) Contour for shear force

Figure 8. Numerical model output for shear force and bending moment [12]

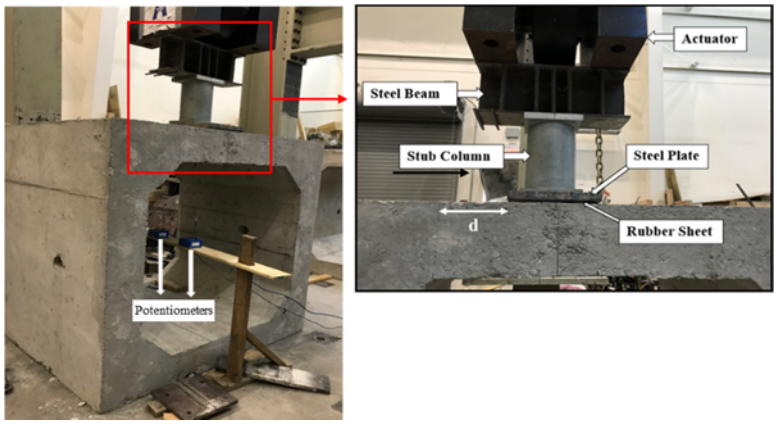

Figure 9. Box culvert test setup for studying the effects of wheel load [13]

Understanding the behavior of structural components under different loading scenarios and determining their failure strength is an important part of design strategy. The behavior and failure capacity of a structural component, such as a beam, differ considerably due to applications of a concentrated load or a uniformly distributed load [20]. In some cases, such as a buried box culvert, using a concentrated load on the top slab is not a reasonable representation of the real loading condition. Soil pressure is the only applied load on the top slab of a deeply buried box culvert; thus, it is essential to study this kind of infrastructure from the perspective of uniformly distributed loads.

Table 1. The characteristics of tested specimens by Yee [14]

Specified Full Box Geometry								Half-Box Specimen Measurements	
Specimen	OPSS1821 Section Name	Interior Span (mm)	Interior Rise (mm)	Slab depth (mm)	Exterior Span (mm)	Span to Haunch Edge (mm)	Width (mm)	Actual Width (mm)	Rise (mm)
RY1	1800 × 900 × 200	1829	914	203	2235	1423	2032	580	650
RY1P	1800 × 900 × 200	1829	914	203	2235	1423	2032	585	650
RY2	1800 × 900 × 200	1829	914	203	2235	1423	2032	560	650
RY2P	1800 × 900 × 200	1829	914	203	2235	1423	2032	555	650
RY3	2400 × 1500 × 200	2438	1524	203	2844	2032	2032	575	955
RY3P	2400 × 1500 × 200	2438	1524	203	2844	2032	2032	580	945
RY4	2400 × 1500 × 200	2438	1524	203	2844	2032	2032	575	950
RY4P	2400 × 1500 × 200	2438	1524	203	2844	2032	2032	570	945
RY5	3000 × 2400 × 250	3048	2438	254	3556	2540	2032	575	1470
RY5P	3000 × 2400 × 250	3048	2438	254	3556	2540	2032	560	1470
RY6	3000 × 2400 × 250	3048	2438	254	3556	2540	2032	590	1470
RY6P	3000 × 2400 × 250	3048	2438	254	3556	2540	2032	590	1470

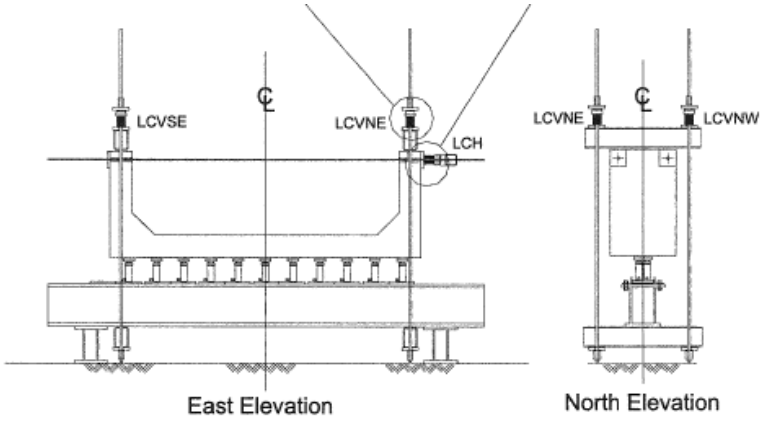

Figure 10. Box culvert test setup for testing one-half of a specimen [14]

Several studies have focused on applying uniformly distributed loads experimentally on structural components. Pang and Millar [21] studied the behavior of a fixed-ended aluminum beam under a simulated uniformly distributed load. They used several hydraulic pistons to apply equal point loads along the span of a beam. The pressure of the hydraulic system was incrementally increased up to failure. Brown and Bayrak [22] used the same method to simulate uniformly distributed loads

on deep beams, utilizing several hydraulic rams. Each of the rams was connected to the same hydraulic manifold with an identical hose and coupler to ensure that the same pressure was supplied to each ram. The shear strength of reinforced concrete beams under uniformly distributed loads was also studied by P. Zararis and I. Zararis [23]. They analytically and experimentally investigated the shear strength of beams under various loading conditions by applying ten identical point loads along the span to reach the ultimate load.

Table 2. Summary of code predictions and test capacities by Yee [14]

(Note: All values in kN/m^2)

		RY1	RY1P	RY2	RY2P	RY3	RY3P	RY4	RY4P	RY5	RY6	RY6P
Peak Test Load		606	552	735	610	351	319	655	580	427	427	441
Factored CHBDC Design Load		225	225	425	425	160	160	389	389	133	358	358
Load Causing Shear Failure		NA	NA	735	NA	NA	NA	655	580	NA	427	NA
Estimated shear Failure load (No axial Load)	CHBDC General	314	314	375	375	238	238	300	300	239	269	269
	CHBDC Simplified	418	418	428	428	285	285	568	268	298	287	287
	CHBDC 7.8.8.2.1	430	430	467	467	304	304	284	284	314	310	310
	AASHTO Box	564	564	578	578	384	384	348	346	418	399	399
Ratio of Estimated Failure Load to design load	CHBDC General	1.4	1.4	0.88	0.88	1.49	1.49	0.77	0.77	1.8	0.75	0.75
	CHBDC Simplified	1.88	1.88	1.01	1.01	1.78	1.78	0.69	0.69	2.24	0.8	0.8
	CHBDC 7.8.8.2.1	1.91	1.91	1.1	1.1	1.9	1.9	0.73	0.73	2.36	0.87	0.87
	AASHTO Box	2.51	2.51	1.36	1.36	2.4	2.4	0.89	0.89	3.14	1.11	1.11
Estimated shear Failure load (axial load)	CHBDC General	333	333	405	405	260	260	316	316	249	289	289
	CHBDC Simplified	418	418	428	428	285	285	268	268	298	287	287
	CHBDC 7.8.8.2.1	455	455	467	457	304	304	284	284	325	310	310
	AASHTO Box	564	564	578	578	384	384	355	355	418	399	399
Ratio of estimated failure load to peak load	CHBDC General	0.56	0.6	0.56	0.5	0.74	0.82	0.48	0.54	0.58	0.68	0.66
	CHBDC Simplified	0.69	0.76	0.58	0.53	0.81	0.89	0.41	0.46	0.7	0.67	0.65
	CHBDC 7.8.8.2.1	0.75	0.82	0.63	0.58	0.87	0.95	0.43	0.49	0.76	0.73	0.7
	AASHTO Box	0.93	1.02	0.79	0.71	1.09	1.2	0.54	0.61	0.98	0.93	0.9

Iguro et al. [24] applied uniformly distributed loads to reinforced concrete beams, using a synthetic rubber bag which exerted uniform hydraulic pressure, based on Pascal's Law. Loads were measured by pressure gauges and load cells; the pressure assured that the specified loads were active. The investigation of the shear strength of box culverts requires applying a uniformly distributed load on the top slab to mimic the real loading condition, which is soil pressure. Klaus [25] and Yee [14] used a hydraulic jack system to apply identical point loads on the top slabs of box culverts, increasing the pressure in the jacks to reach failure. All of the previous studies

required the use of several hydraulic jacks to perform a force control analysis to determine the ultimate strength of structural elements in the absence of post-failure behavior.

1.4. Research Objective

An increase in the fill height of buried box culverts leads to an increase in the thickness of the slab and wall, as well as in the number or size of longitudinal slab reinforcements required to resist flexure. This geometrical configuration imposes a shear behavioral mode. According to the literature, the existing design codes underestimate the shear capacity of concrete. This leads to an increase in the shear reinforcement and, consequently, an increase in the cost of the project. Therefore, this study focuses on experimental and numerical approaches to determining the shear strength of reinforced concrete box culverts with uniformly distributed load at the top slab.

The scope of this research is a modification of the shear design of reinforced concrete box culverts' top slabs that are buried deep enough to carry only soil pressure on the top slab as dead load. To this end, several steps were taken, as follows.

First, it is important to understand the shear design methodology used in AASHTO specification [3] and ACI318-14 [26]. The shear design equations in the AASHTO specification are based on a modified compression field theory (MCFT) [27]; hence a comprehensive knowledge of the theory was essential to this research.

Second, a loading mechanism was developed in this research to perform displacement control analysis for a uniformly distributed load in laboratory and numerical modeling. A framework, consisting of several sub-frames, was designed to convert the single displacement applied at the top of the framework to the equivalent uniformly distributed forces at the top slab of the culvert,

allowing a displacement control analysis algorithm to be performed. The proposed framework was investigated experimentally and numerically to validate the load-transferring mechanism.

Third, reinforced concrete box culverts were examined in the laboratory to determine the shear strength of the top slab. Then, finite element models were calibrated to mimic the experimental tests, using the similar material properties, boundary conditions, and loading protocol. Taking advantage of the verified finite element models, parametric studies of 288 cases were performed to evaluate the effects of different parameters, such as length of span, rise, top slab's thickness, etc.

Fourth, the prediction of the specification and code to estimate the concrete shear strength (V_c) of the top slabs of reinforced concrete box culverts was assessed, using the results of the parametric studies. And finally, nonlinear regression analysis proposed equations for the concrete shear strength (V_c) of top slabs of reinforced concrete box culverts in the critical shear section, at distance of "d" from haunch. The equation has the same format as ACI318-14 and AASHTO's equation to calculate V_c.

CHAPTER 2. LOADING MECHANISM

2.1. Overview

Understanding the behavior of structural components under different loading scenarios and determining their failure strength are important to design strategy [28]. The behavior and failure capacity of a structural component, such as a beam, differ considerably due to the application of a concentrated load or uniformly distributed load [20]. In some cases, such as a buried box culvert, using a concentrated load on the top slab is not a reasonable representation of the real loading condition. The soil pressure is the only applied load on the top slab of a deeply buried box culvert; thus it is essential to study this kind of infrastructure from the perspective of uniformly distributed loads. Several studies have discussed the displacement control method (DCM) for nonlinear analysis of reinforced concrete structures [20, 29, 30, 45], and post-failure behavior can be recorded by applying the DCM to experimental tests and numerical analyses. The post-failure behavior of a reinforced concrete (R.C.) one-way slab, the crack pattern, etc. are indicators that can be used to determine the failure mode of the slab. If a R.C. one-way slab fails due to flexural failure mode, with an almost constant load, the slab continues to deform; however, if the slab fails due to shear failure mode, a sudden drop in the load carried by the slab occurs after peak load. Although all of the box culverts in this study were designed to have shear behavioral mode (no shear reinforcements), the DCM recorded post-failure performance of the top slabs to monitor a decrease in the carried load. Due to some elaborations in applying uniformly distributed loads in experimental tests, many researchers prefer to study structural components under a concentrated load, which makes a more severe condition.

2.2. Concept and Theory

Problems are frequently encountered in performing the displacement-controlled analysis of a beam with a uniformly distributed load. Figure 11 illustrates a simply supported beam under an applied uniform displacement (δ) at the top. As the top surface of the beam is forced to move down incrementally, the sections of the beam near the supports endure intense compressive stresses. The beam does not deform like a simply supported beam under a uniformly distributed load, nor do the plane sections close to the supports remain plane. Applying several displacements along the span of the beam does not solve this problem. Figure 12 shows a simply supported beam under several applied displacements ($\delta_1, \delta_2, \delta_3, \dots, \delta_n$). If all of the target displacement values are identical ($\delta_1 = \delta_2 = \delta_3 = \cdots, = \delta_n$), the sections close to the supports carry high shear stress, and the span of the beam is forced to move down, while the sections near the supports are restrained. Assigning any specific pattern, such as a triangular or trapezoidal pattern, to the applied displacements ($\delta_1, \delta_2, \delta_3, \dots, \delta_n$) imposes a deformation shape to the beam, which may behave differently than one with a uniformly distributed load. Therefore, in order to perform a displacement control analysis of a uniformly distributed load, a framework is needed to convert the controlled displacement to the desired load pattern. To this end, it is necessary to identify several identical point loads along the beam's span that are not dependent upon deformation of the beam.

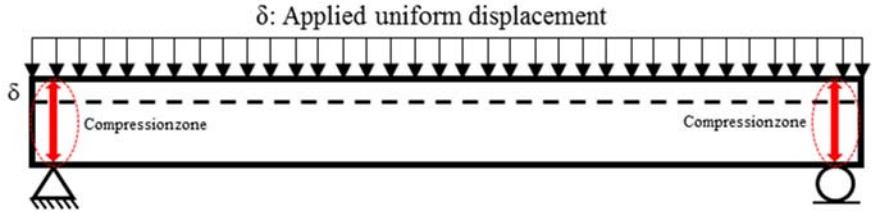

Figure 11. A simply supported beam under applied uniform displacement at the top

Figure 13 illustrates a framework that can be used to simulate a uniformly distributed load with a displacement control analysis algorithm. Each of the framework components acts like a simply

supported beam, transferring forces without bending moment. The beams in the framework are designed to be rigid, while the supports under the beams are an elastic material with a low module of elasticity. The low module of elasticity for the supports simulates placing a steel plate on a rubber shaft. The steel plate easily rotates on the shaft and compresses to transfer axial force to the lower beam. In the FEM modeling, a hard contact element is assigned between the reinforced concrete beams and 16 rigid plates of the last layer of the framework to transfer the normal forces from the framework to the top surface of the reinforced concrete beam. A frictionless contact is assumed for tangential behavior between the framework and the top of the reinforced concrete beam. All of the framework's supports are tied with connected beams to maintain integration of the framework during loading, and the movement of the framework is restricted in the z-direction and the rotation of it around the x and y axes.

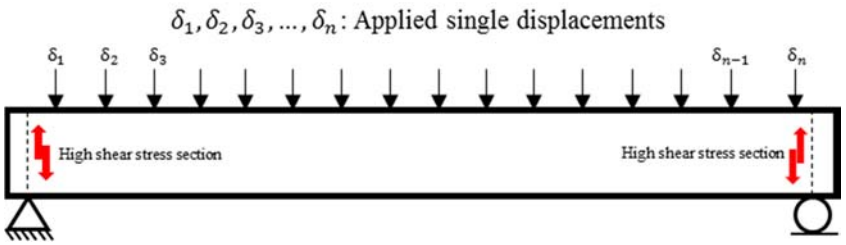

Figure 12. A simply supported beam under several applied single displacements at the top

Displacement is applied to the middle of the top rigid beam of the framework, and the corresponding force, due to the applied displacement, is distributed to two support reactions. According to Figure 13, the corresponding force of each increment is divided into 16 equal forces, which are distributed along the span. To increase the intensity of the distributed load for more accurate analysis, the framework can be constructed with additional layers of beams.

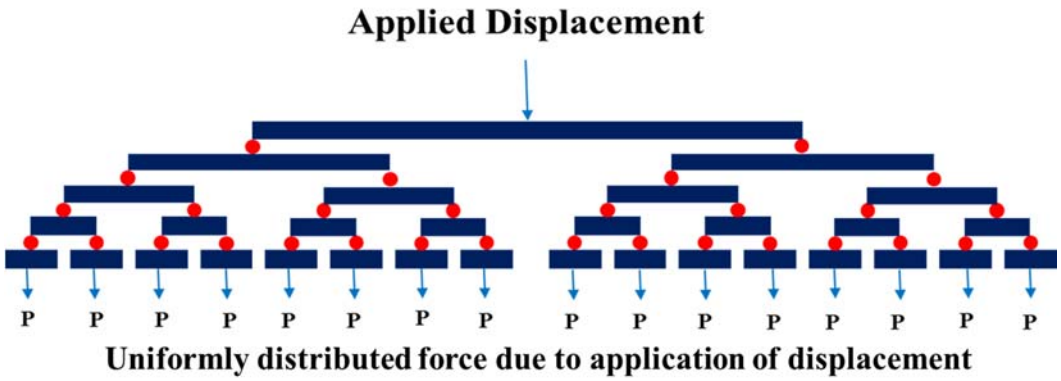

Figure 13. Framework to apply displacement control of distributed uniform load

To verify the frame, the results of an experimental-tested beam with uniformly distributed load were compared with a finite element analysis of force control and the displacement control analysis. Shioya et al. [8] tested a beam with uniformly distributed load. Figure 14 shows the designated beam and its cross section. The compressive strength of the concrete was 23.5 MPa (3400 Psi), and the rebar was Grade 44 ksi.

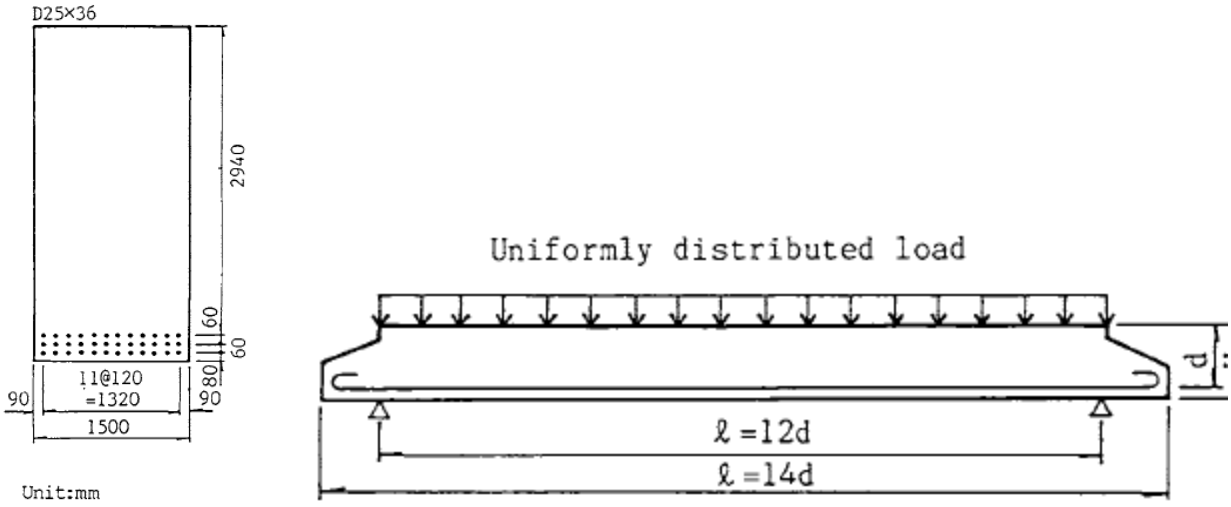

Figure 14. Experimental-tested beam and its cross section under uniform load [8]

A force control analysis was performed to verify the FEM model and duplicate the experimental research. Figure 15 shows load-deflection curves of the experimental test and FEM analyses, which reflect good agreement between the experimental result and force control analysis of

uniform pressure on the top of the beam. After verification of the model, the frame was added to perform displacement control analysis of uniformly distributed load. The load-deflection curve of the model with frame successfully duplicated the experimental and force control results, as shown in Figure 15. In this case, the governed failure mode was flexure; therefore, the FEM curve after failure went straight.

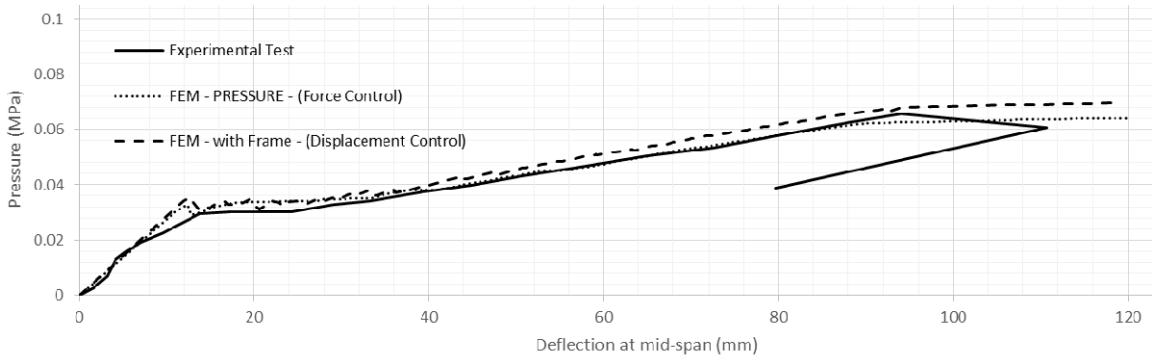

Figure 15. Load-deflection curves to verify the frame

2.3. Framework Construction

A small framework was built for this research to apply eight identical point loads. The framework had to fulfill the theoretical requirements, as well as keep proper performance under applied load. To this end, the first step was designing a framework for an estimated maximum load. The details of designed framework are in the following.

2.3.1. Design and Drawings

This framework was designed for 3-foot span components that are 6 inches wide. The total length of the framework, back-to-back of the first and last plates, is 37.5 inches, and there are eight 6 × 2.5 inch transfer loads from the framework to the beams or the top slab of box culverts. Figure 16 illustrates the dimensions of all of the parts of the framework.

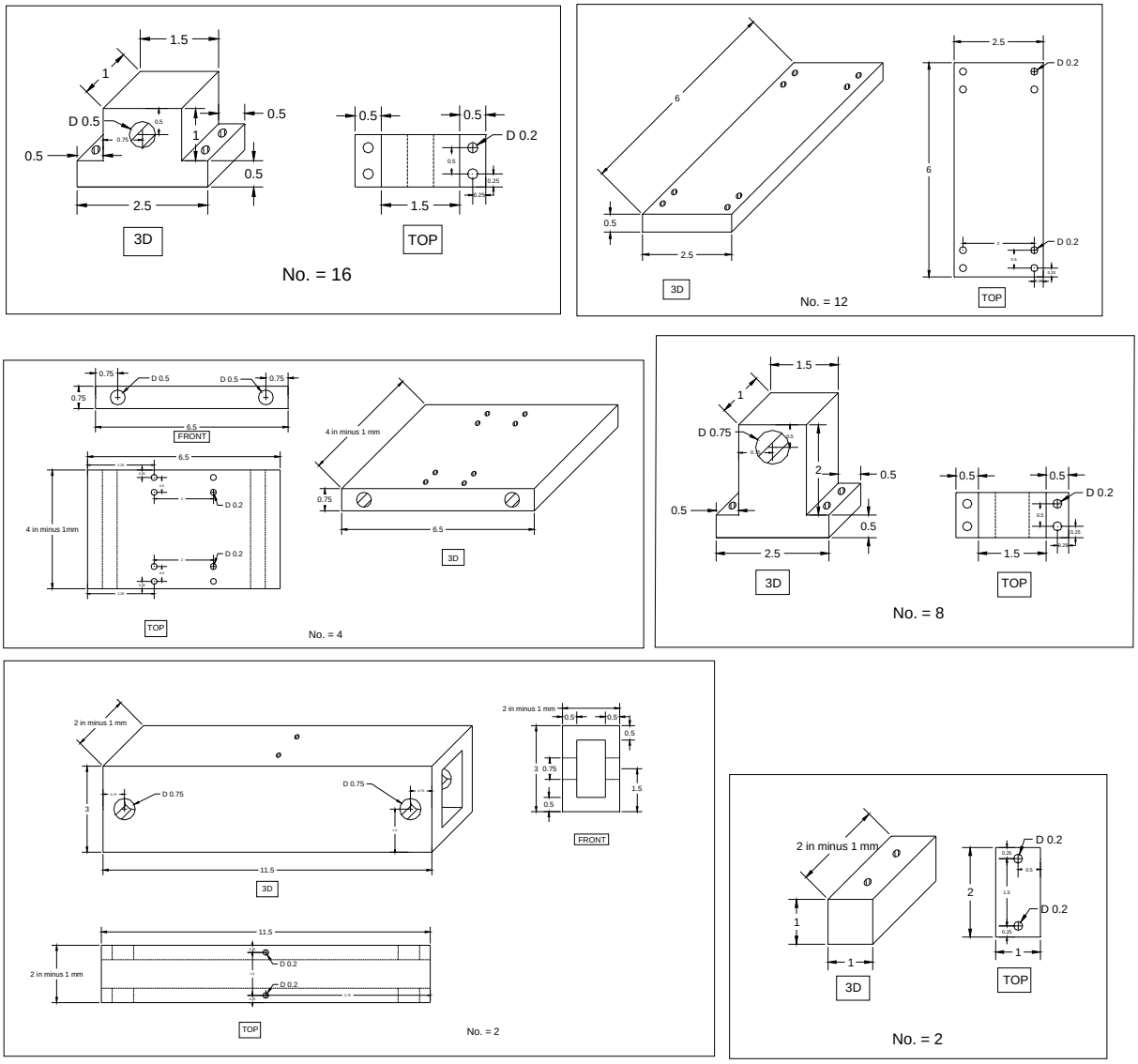

Figure 16. Dimensions of each part of the framework

2.3.2. Implementation

The framework was built by experts in the machine shop of the Mechanical Engineering Department at the University of Texas at Arlington. Each layer of the framework easily rotates around the shaft, only allowing the transfer of vertical forces without bending moment. Figure 17 shows the framework that was built for use in the laboratory testing. It was made of steel material to provide enough strength to transfer force through itself without either large deformations or

yielding. The material of the shafts is stronger than the plates, because flexural deformation of them will prevent rotations.

Figure 17. The framework built for the experimental program

2.4. Experimental Tests

To validate the load-transferring mechanism of the framework, the load was applied to the top of a reinforced concrete beam to measure the load applied by each of the plates in the last layer of the framework throughout the loading. The loading mechanism was validated as long as each plate applied identical point loads to the beam.

2.4.1. Specimens

A simply supported reinforced concrete beam with 40 in. (1016 mm) length (a/d = 2.9) and cross-sectional dimensions of 6×8 in. (152×203 mm) was constructed for this experiment. Two beams, with the dimensions specified in Figure 18, were cast from one batch and placed in a curing chamber for 28 days (Shown in Figure 19). The beams were designed to have shear behavior mode, and no stirrups were provided to strengthen versus shear force. A couple of #6 rebar (area = 0.4 in.2) were used for the bottom longitudinal reinforcement (ρ = %2.22) to assure that there was

enough reinforcement to resist flexure and impose shear behavioral mode. There was no longitudinal rebar at the top of the cross section. To prevent the possibility of bond failure from insufficient anchorage, the bottom longitudinal reinforcement was extended through the ends of the beam and was anchored to steel plates, rather than inside the concrete, via special anchor nuts. Figure 20 illustrates details of the mechanical anchorage for the longitudinal rebar. The supports were 35 in. (890 mm) center-to-center; one support was a roller, and the other was a pin. The longitudinal rebar were placed 2 in. (50 mm) apart, and the effective depth was assumed to be 6.5 in. (165 mm). A 1.5 in. (38 mm) concrete cover was provided on each side for the rebar.

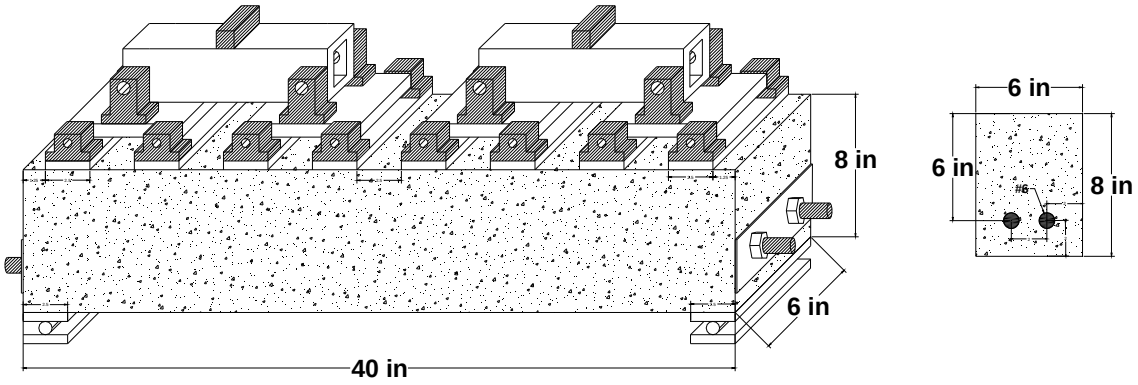

Figure 18. Beam-tested dimensions within the framework

A 5.1 ksi (35.2 MPa) 28-day compressive strength concrete and conventional Grade 60 (f_y = 60 ksi, 420 MPa) rebar were used to prepare the specimens. The maximum aggregate size of concrete was $3/8$ in. (10 mm), and the w/c ratio for the concrete mix design was assumed to be 0.4. A slump value of 6 in. (152 mm) was considered for the concrete mix design. It should be noted that the specimens were tested after being cured for 28 days in a moisture chamber. The reinforcing rebar in this research had an average modulus of elasticity of 29,000 ksi (200 GPa), and met the requirements of ASTM A615 [31].

Figure 19. Beam specimens prepared for tests in moisture chamber

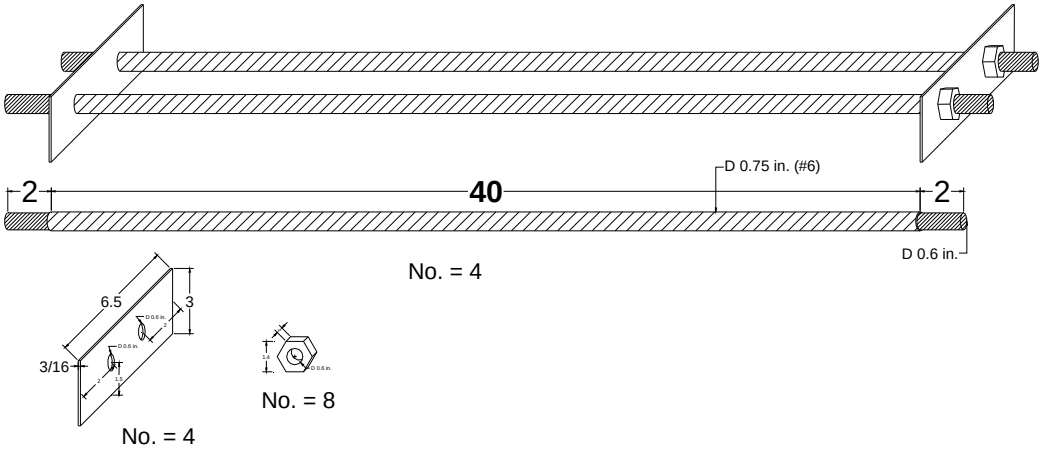

Figure 20. Anchorage details

2.4.2. Test Setup and Instrumentations

Figure 21 shows the test setup. A strong steel I-girder was placed beneath the beam to provide a rigid base. Before adding the framework to the top of the beam, the top surface was made flat and horizontal. It should be noted that the top surface of the beam was the bottom of the mold, which provided a smooth and flat surface. Three strain gauges were attached to the longitudinal rebar at mid-span and at distance “d” from supports to measure the strain value of the rebar during the test,

as shown in Figure 22. A linear variable displacement transducer (LVDT) measured the vertical deflection of the beam at mid-span. The test was employed via a displacement control method; the rate of applying displacement was 0.05 in/min (1.3 mm/min), using a 400 kips (1780 kN) hydraulic jack. A data acquisition (DAQ) system continuously recorded the outputs.

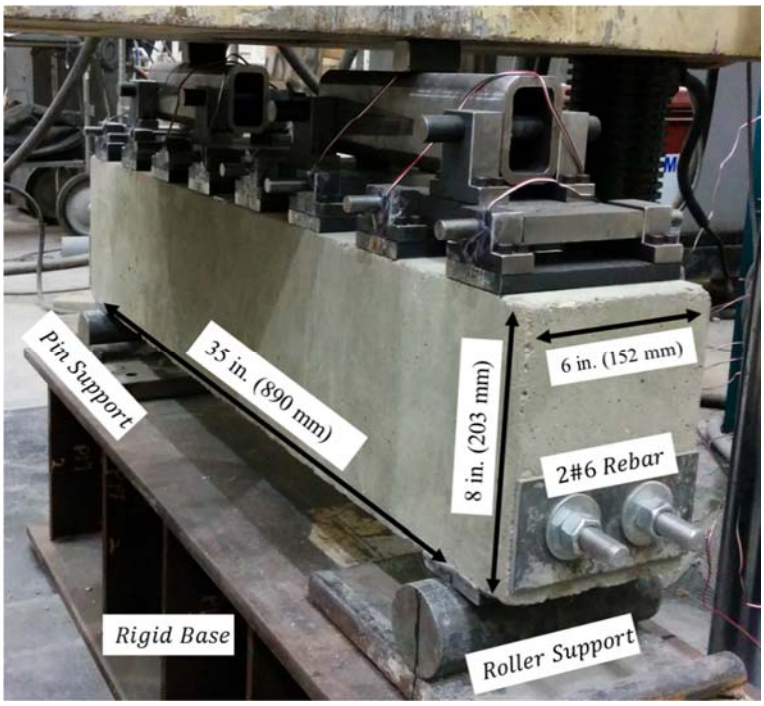

Figure 21. Beam specimen test setup

Figure 22. Strain gauge installation

2.5. Finite Element Modeling

A calibrated finite element model was developed for the experiment by ABAQUS software [32]. Figure 23 illustrates the numerical model for the beam and the framework. All material properties, dimensions, and boundary conditions used in the model were similar to those used in the experiment. The parts of the framework modeled by finite element could easily rotate around the shaft so as to not transfer bending moment.

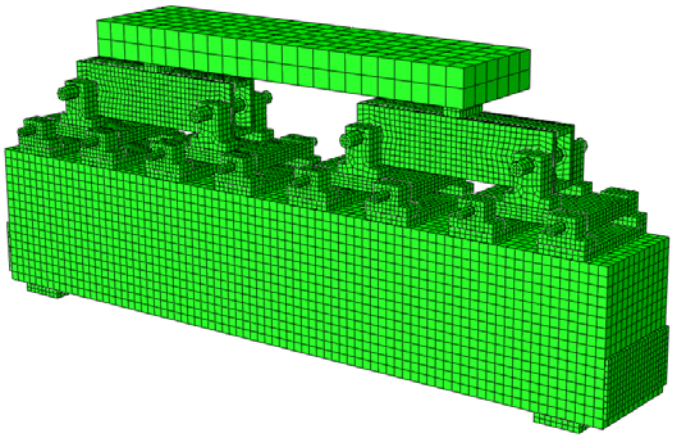

Figure 23. Developed numerical model for the beam test

The advantage of using a finite element model to mimic this experiment was that the load applied by each plate in different loading steps could be monitored. Generally, numerical models allow access to a wide range of data which are not accessible directly from experimental tests. The sectional force, bending moment, and the value of strain or stress in different locations in the specimens, etc. are examples of those type of outputs. Additionally, finite element models are very beneficial for studying different parameters that influence the behavior of specimens. Using a finite element model verified by experimental outcomes can be a reliable tool for investigating the behavior of structural components that is due to various loading conditions, boundary conditions,

and material properties. The assumptions used to duplicate the experiment are described in the following sections.

2.5.1. Material Properties

A regular concrete associated with 5100 psi specified compressive strength and 530 psi specified tensile strength was used to model the material properties of concrete in this numerical study. Figure 24 shows stress-strain curve for the concrete material, both in compression and tension behavior.

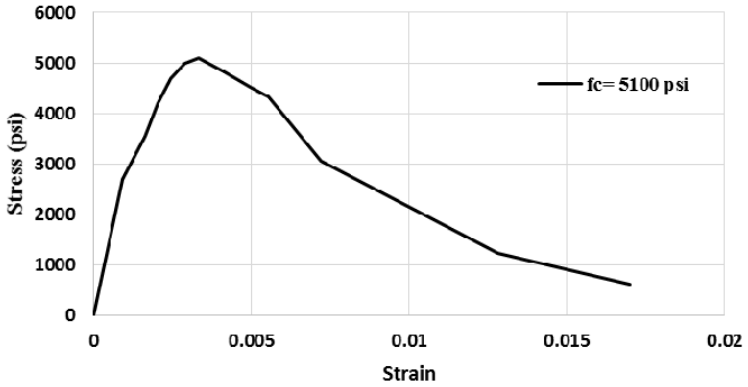

a) Strain-stress curve for compression

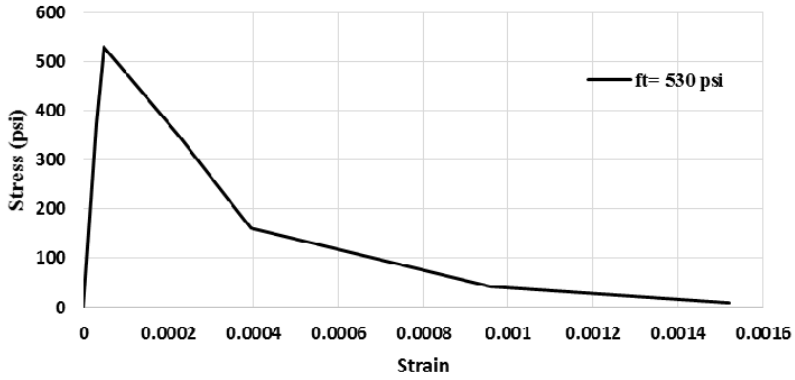

b) Strain-stress curve for tension

Figure 24. Strain-stress curves for 5100 psi concrete; a) for compression behavior; b) for tension behavior

A concrete damage plasticity (CDP) model, developed by Jankowiak and Lodygowski [33], was used to observe the after-damage compression and tension behavior of the concrete. It can model concrete and other quasi-brittle materials for all types of structures, and uses the concepts of

isotropic-damaged elasticity, in combination with isotropic tensile and compressive plasticity, to represent the inelastic behavior of concrete [32]. It is based on the assumption of scalar (isotropic) damage and is designed for applications in which the concrete is subjected to arbitrary loading conditions, including cyclic loading. The model takes into consideration the degradation of the elastic stiffness induced by plastic straining, both in tension and compression [32]. The parameters of the CDP model used in this study are presented in Table 3.

Table 3. Concrete damage parameters

Dilation Angle	**Eccentricity*[1]**	**fb0/fc0*[2]**	**K*[3]**	**Viscosity Parameter**
40	0.1	1.16	0.667	0

*[1] The eccentricity is a small positive number that defines the rate at which the hyperbolic flow potential approaches its asymptote

*[2] The ratio of initial equibiaxial compressive yield stress to initial uniaxial compressive yield stress

*[3] The ratio of the second stress invariant on the tensile meridian, q(TM) , to that on the compressive meridian, q(CM), at initial yield for any given value of the pressure invariant p such that the maximum principal stress is negative. It must satisfy the condition $0.5 < K \leq 1$

A conventional steel rebar with 60,000 psi tensile strength was assumed to model the material behavior of rebar. The reinforcing rebar in this research had an average modulus of elasticity of 29,000 ksi (200 GPa) and met the requirements of ASTM A615 [31]. The strain-stress curve of steel rebar in the linear and plastic parts is shown in Figure 25. The longitudinal rebar was embedded into the concrete to ensure that the concrete and steel had the same strain in every section.

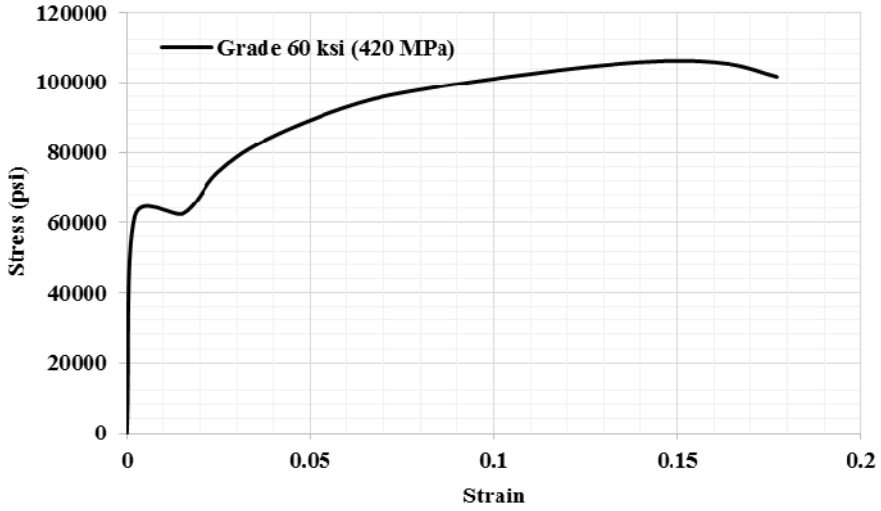

Figure 25. Strain-stress curve for rebar (Grade 60 ksi, 420 MPa)

2.5.2. Boundary Conditions

Since the beam was a simply supported beam, the movement of one of the supports, defined as a pin, was restricted in the x, y, and z axes; however, every rotation was free. The other support acted as a roller, and the movement along the y and z axes was restricted, while the movement along the x axis, as well as all rotations, were free. A hard contact element was assigned between the last layer of the framework and the top of the beam for normal behavior to prevent the framework from penetrating the beam specimen. A frictionless contact element was assigned for the tangential behavior. It should be noted that any friction would cause an imbalanced distribution of point loads along the span. The side plates used to anchorage the longitudinal rebar were tied to the concrete beam. Instead of modeling the nuts, the rebar was tied to the end plates in one node.

2.5.3. Loading and Analysis

General static analysis with displacement control of load was performed. The load was applied at a very low rate during a specific time, with the ramp placed linearly over the step to prevent any dynamic effects of load. The loading rate automatically changed between $10^{-6}$and 10^{-10} to attain convergence at each increment. The full Newton method was used to solve the equations.

Observation of the analyses continued after failure behavior of the beam. To avoid having local instabilities, such as surface wrinkling, material instability, or local buckling, an automatic stabilization method was selected to stabilize this class of problems by applying damping throughout the model. Thus, damping was utilized to eliminate fluctuation of the load during the analyses.

2.6. Results and Discussions

A comparison of the total shear force deflection curves obtained from the experimental test and FEM results, shown in Figure 26, indicates a good agreement between them. The strain values in longitudinal reinforcement, as well as the crack patterns at failure obtained from the FEM results, were verified and are shown in Figures 27 and 28, respectively. The strain obtained from the experimental test at mid-span was 2036 με at the failure, while the FEA predicted this value at 1941 με (a difference of 4.9%). For the sections at distance "d" from supports, the strain values of the longitudinal rebar were 1521 and 1529 με, which was an 11.9 percent difference from that predicted by the FEA outcome. The strain value demonstrated that the beam failed before the longitudinal rebar yielded. The diagonal tension cracks from both the experimental test and the FEA indicated shear failure mode.

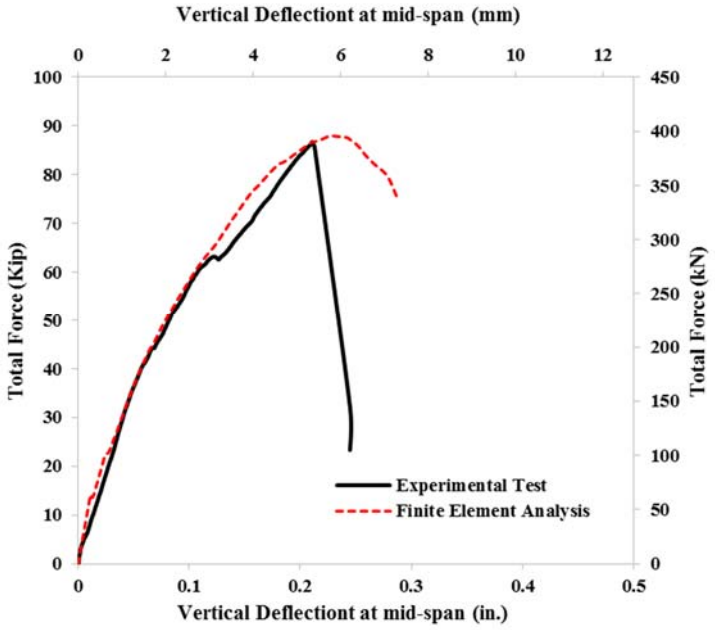

Figure 26. Load-deflection curve from experimental data and FEA

The loads applied by each of eight plates to the top surface of the beam during the experimental test were not accessible for monitoring; however, the validated finite element model reported this value for each load step. Figure 29 shows the value of the applied loads by each plate in four load steps (20, 40, and 60 kip, or 89, 178, and 267 kN, and the failure load).

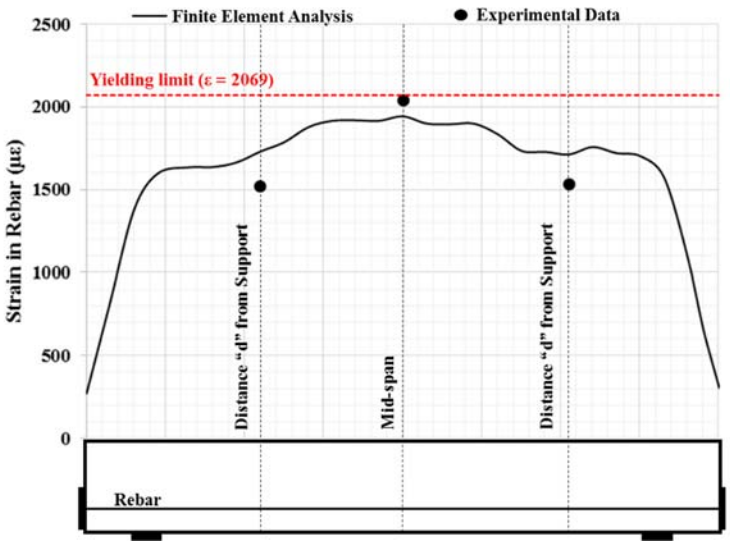

Figure 27. Comparison of the strain value in longitudinal rebar obtained from experimental data and FEA at failure

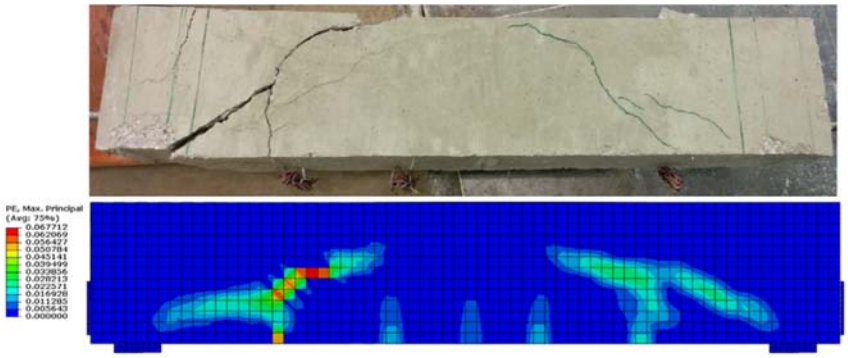

Figure 28. Obtained shear cracks from both experimental test and FEA

As Figure 29 illustrates, the plates applied almost identical loads to the top surface of the beam in each load step. The red line in the figure identifies the ideal load that each plate should apply. For instance, for the total load of 20 kip (89 kN), ideally each plate would apply 2.5 kip (20/8= 2.5). The maximum difference between loads applied by plates and the ideal load, when the total applied load was 20 kip (89 kN), was 3.4%. The difference in load steps of 40 and 60 kip (178 and 267 kN) and the failure load were 2.14%, 3.34% and 6.36%, respectively. Due to a sudden deformation of the beam at shear failure, this difference reached its highest value when the failure load was

applied. The framework applied almost identical eight point loads along the span of the beam, from the beginning of the loading to the failure load, with less than 10% error.

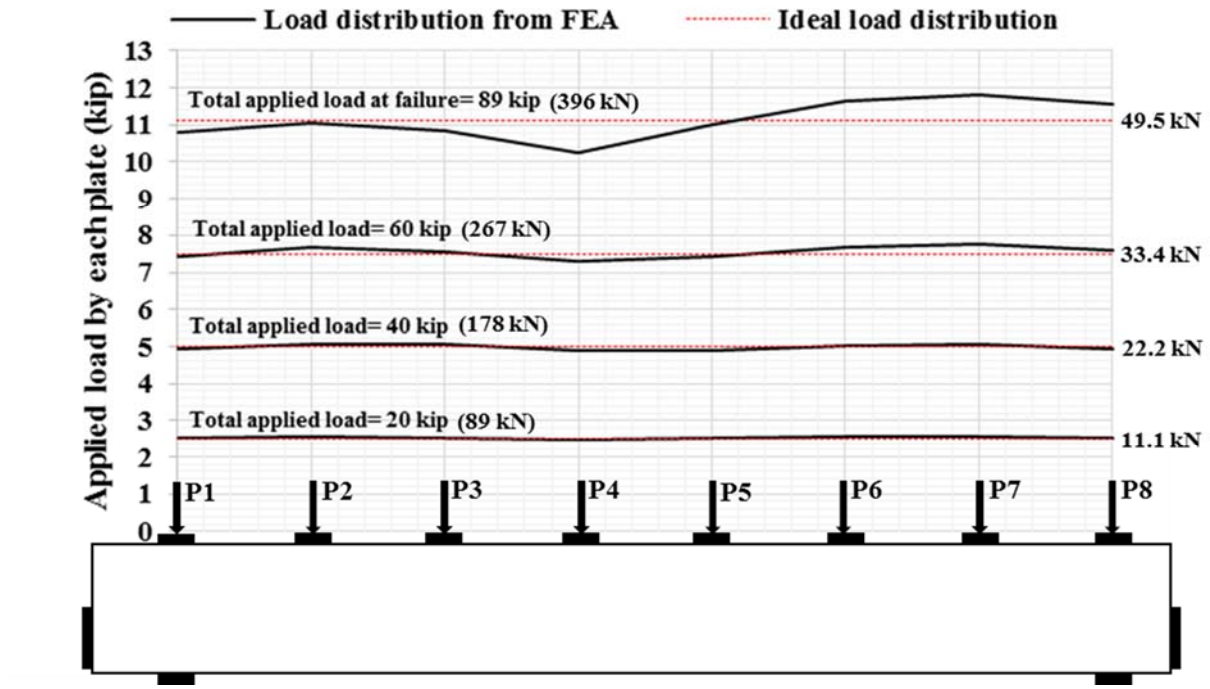

Figure 29. Load distribution through the framework in various loading steps

CHAPTER 3. SHEAR STRENGTH OF REINFORCED CONCRETE BEAMS

3.1. Overview

This research presents a numerical method with displacement control type loading to determine the shear capacity of reinforced concrete beams. In this method, a controlled displacement is applied to a specific node, and the total distributed force of the system is calculated for each increment of displacement. Thus, the structure's load-deformation graph can be obtained for any chosen ultimate displacement, and the shear capacity is determined when the structure can no longer support the load. It should be noted that application of uniform displacement is not an option since a displacement curve, due to uniformly distributed load, is not a straight line and varies along the beam, depending on support conditions.

This chapter focuses on the impact of various loading conditions, due to variations of strain in the longitudinal rebar of the critical section, on the shear strength of the RC beams. Comparisons were made between the shear capacity of RC beams under a concentrated load at mid-span and the shear capacity of RC beams under a uniformly distributed load. A parametric study was conducted to obtain the shear strength of reinforced concrete beams with various a/d ratios, amount of longitudinal reinforcements, and loading conditions. Finally, the shear strength of the beams, obtained by using the finite element method (FEM), was compared with the AASHTO's prediction and ACI318-14's shear design formulations.

3.2. Experimental Tests by Other Researchers

Vecchio and Shim [34] performed an experimental study at the University of Toronto to determine the shear strength of 12 reinforced concrete beams. They tested beams with and without transvers reinforcement and at three different a/d ratios: 4, 5, and 7.

3.2.1. Specimens

The three beams chosen for this study, referred to as OA1, OA2, and OA3, were without stirrups and were tested under a point load at mid-span. Figure 30 illustrates the cross sections of the beams without shear reinforcement. The cross section details and other dimensions are presented in Table 4. All three sections were 12 inches wide and 18 inches deep. Shear failure was imposed to the beams, according to the amount of longitudinal reinforcement needed to resist against flexural loading. The a/d ratio for the beam associated with OA1 cross section was 4, and for the OA2 and OA3 beams were 5 and 7, respectively.

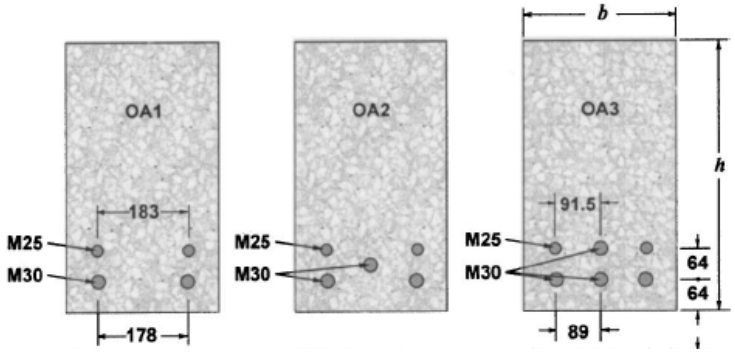

Figure 30. Cross sections of experimental case studies (Unit: mm) [34]

Table 4. Cross section details of experimental case studies [34]

Beam Name	b (mm)	h (mm)	d (mm)	L (mm)	Span (mm)	Bottom steel (ρ %)	Steel Yielding stress
OA1	305	552	457	4,100	3,660	2M30, 2M25 (1.72 %)	440 MPa
OA2	305	552	457	5,010	4,570	3M30, 2M25 (2.22 %)	440 MPa
OA3	305	552	457	6,840	6,400	4M30, 2M25 (2.72 %)	440 MPa

$1\ in. = 25.4\ mm$; $1\ ksi = 6.9\ MPa$

3.2.2. Material Properties

Table 5 presents the three material properties of the concrete used for the beams in this research. An increase in concrete compressive strength leads to an increase in shear and flexural capacity of reinforced concrete members.

Table 5. Concrete characteristics of the beams [34]

Material Name	Beam Name	f'_c (MPa)	ε_0 (mm/mm)	E_c (MPa)	f_{sp} (MPa)
I	OA1	22.6	0.0016	36,500	2.37
II	OA2	25.9	0.0021	32,900	3.37
III	OA3	43.5	0.0019	34,300	3.13

$1\ ksi = 6.9\ MPa$

3.2.3. Test Setup and Instrumentations

The schematic test setup is illustrated by Figure 31. Three linear transducers measured the deformation of the mid-span and supports. As was expected, the deflection at the supports was negligible - close to zero. A concentrated load following the force control protocol was applied to the mid-span of the beams. The loading continued up to failure. Using plates under the point load and supports prevented concentration of stresses, and, consequently, local failure.

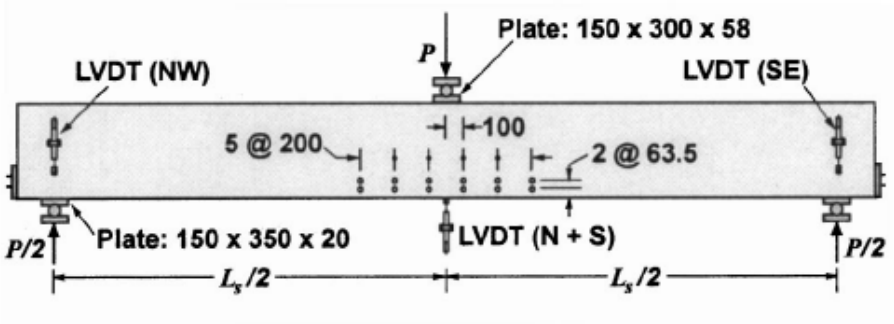

Figure 31. Test setup of the experiment (Unit: mm) [34]

3.2.4. Results

All of the beams failed with diagonal tension failure mode (shear failure). Table 6. This table depicts the total applied load by hydraulic jacks that caused failure and the corresponding deflection of the mid-span at that moment. The shear cracking occurred almost beneath the point load at mid-span.

Table 6. Experimental test results [34]

Beam Name	a/d	P_u (kN)	δ_u (mm)	Failure mode
OA1	4	331	9.1	D-T
OA2	5	320	13.2	D-T
OA3	7	385	32.4	D-T

$1\ kip = 4.45\ kN$; $1\ in. = 25.4\ mm$

3.3. Numerical Modeling

The finite element method and numerical solutions were developed as reliable methods to study the performance of steel and reinforced concrete members [35-39]. The first step of this research was to validate the numerical models with the experimental tests. ABAQUS software [32] was used for the finite element modeling, and the beams were modeled in ABAQUS, with material properties identical to those used in the test setup by Vecchio and Shim [34].

3.3.1. Material Properties

The same concrete material properties described in Table 5 were utilized to mimic the experiments. Similar to that described in Chapter 2, concrete damage plasticity was used to predict cracked concrete in compression and tension. Figure 32 presents the damage parameters (d_c & d_t) for compression and tension. As is shown in the figure, the d_c & d_t parameters are zero before concrete cracks.

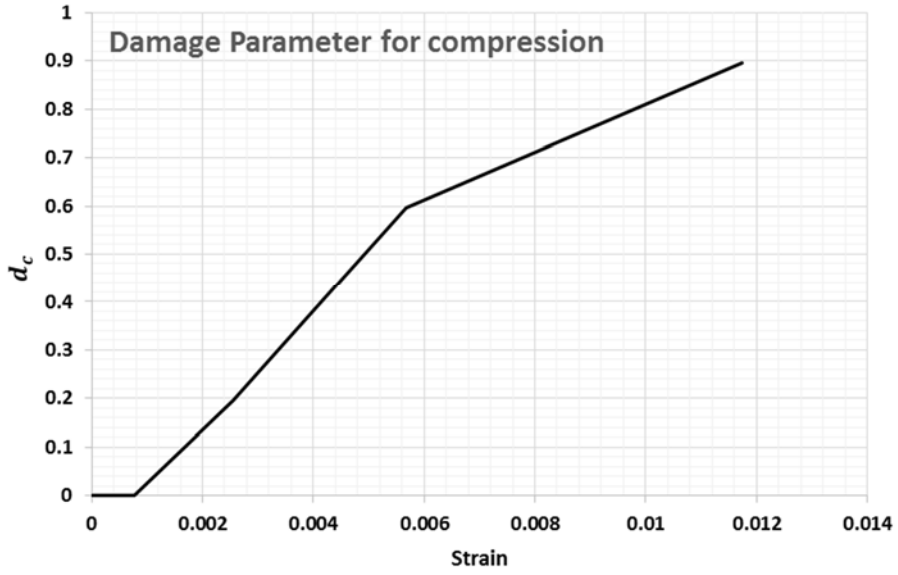

a) $\mathbf{d_c}$

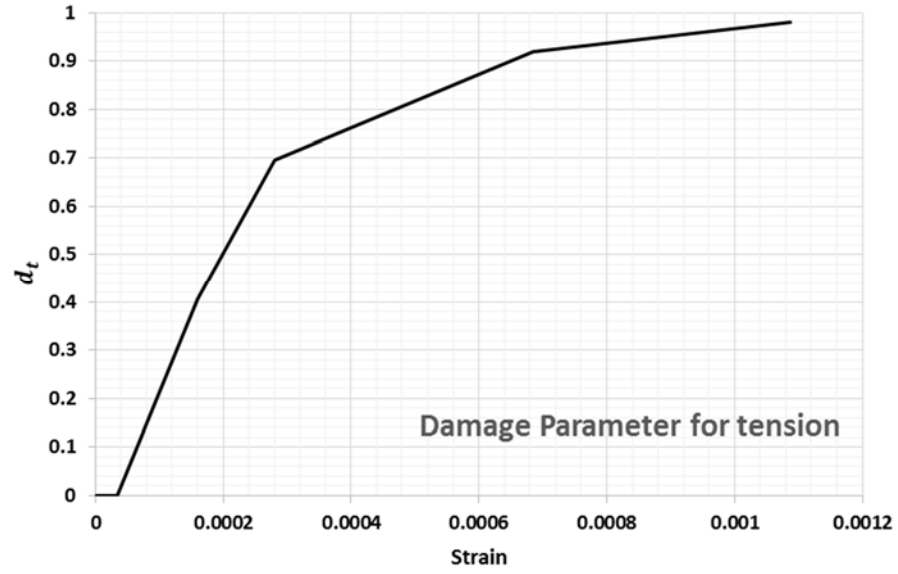

a) $\mathbf{d_t}$

Figure 32. d_c and d_t parameters for used concrete in compression and tension

A linear material with a module of elasticity of 29,000 ksi (200 GPa) was assigned to all of the steel plates in this simulation. A conventional Grade 60 steel rebar, with the behavior shown in Figure 25, was used for longitudinal reinforcement.

3.3.2. Boundary Conditions

Three-dimensional (3D) stress solid elements, C3D8R, were assigned to the concrete beams in the FEM modeling. The C3D8R element is a general purpose linear brick element, with reduced integration (1 integration point), that is located in the middle of the element. One support was defined as pin, and the other as roller. The rebar was embedded in the concrete to ensure that the concrete and steel had the same strain in every section.

3.3.3. Loading and Analysis

General static displacement control load was adopted. The load was applied at a very low rate for a specific duration, with the ramp placed linearly over the step. The loading rate automatically changed between 0.1 and 10×10^{-10} to attain convergence at each increment. The Newton method was used to solve the equations. Observation of the analyses continued after failure behavior of the beams. An automatic stabilization method was employed to avoid local instabilities, such as surface wrinkling, material instability, or local buckling.

3.3.4. Verification of Finite Element Models

Figure 33 shows shear force deflection graphs that compare the experimental tests and FEM modeling. Figure 34 confirms that the crack patterns obtained from the FEM modeling were similar to those obtained from the experimental testing conducted by Vecchio and Shim [34]. As was expected, due to the concentrated load at mid-span, shear cracks converged at the point load.

The proposed framework was applied to the OA1, OA2, and OA3 beams [34] to evaluate their strength under uniformly distributed load, as shown in Figure 35. The total shear force deflection curves were plotted to obtain the ultimate capacity of each beam, as shown in Figure 33. This

figure also shows the comparison between the strength of the beams under point load at mid-span and those under uniformly distributed load.

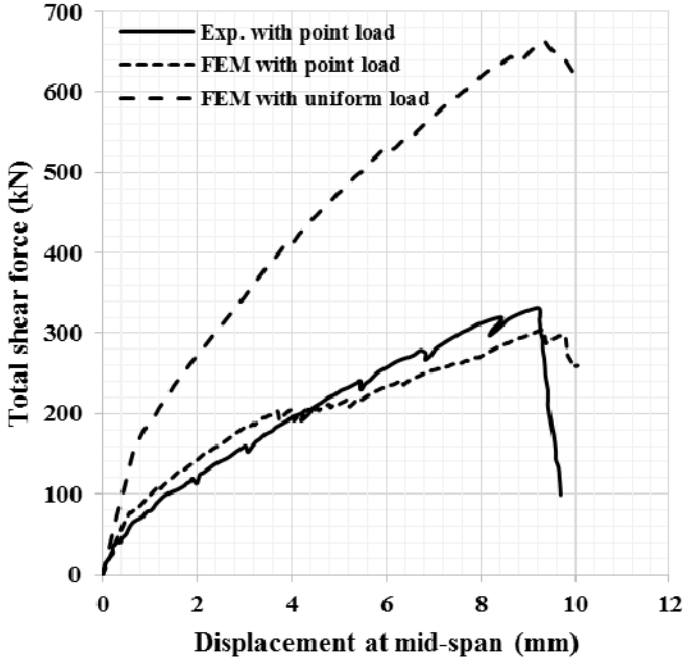

(a) OA1 Beam (a/d = 4)

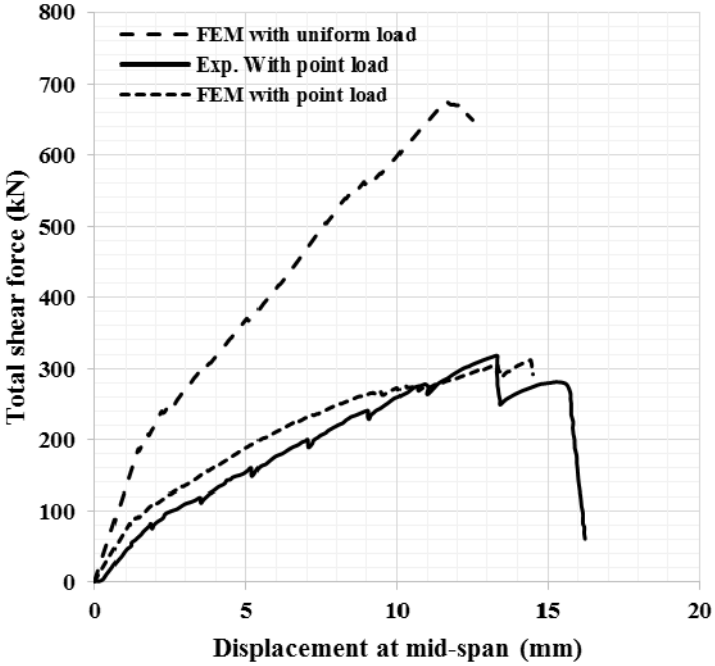

(b) OA2 Beam (a/d = 5)

Figure 33. Comparison of load-deflection curve of the beams for concentrated load and uniformly distributed load (Continued)

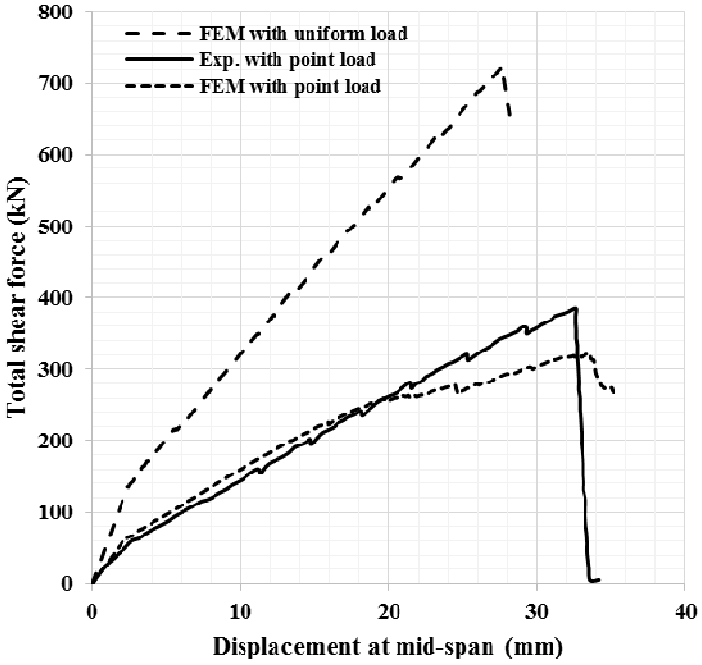

(c) OA3 Beam (a/d = 7)

Figure 33. Comparison of load-deflection curve of the beams for concentrated load and uniformly distributed load

As was expected, the shear-inclined cracks of the uniform load occurred at a distance of effective depth (d) from the supports, while those of the concentrated load occurred under the load. Figure 34 compares the crack patterns of the beams for both concentrated and uniformly distributed loads.

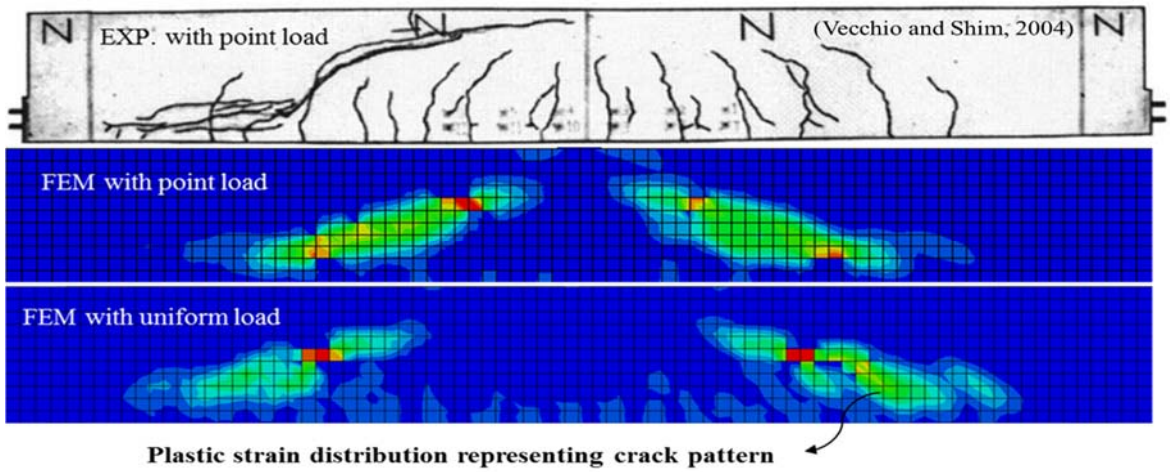

(a) OA1 Beam (a/d = 4)

Figure 34. Crack pattern of the designated beams (Continued)

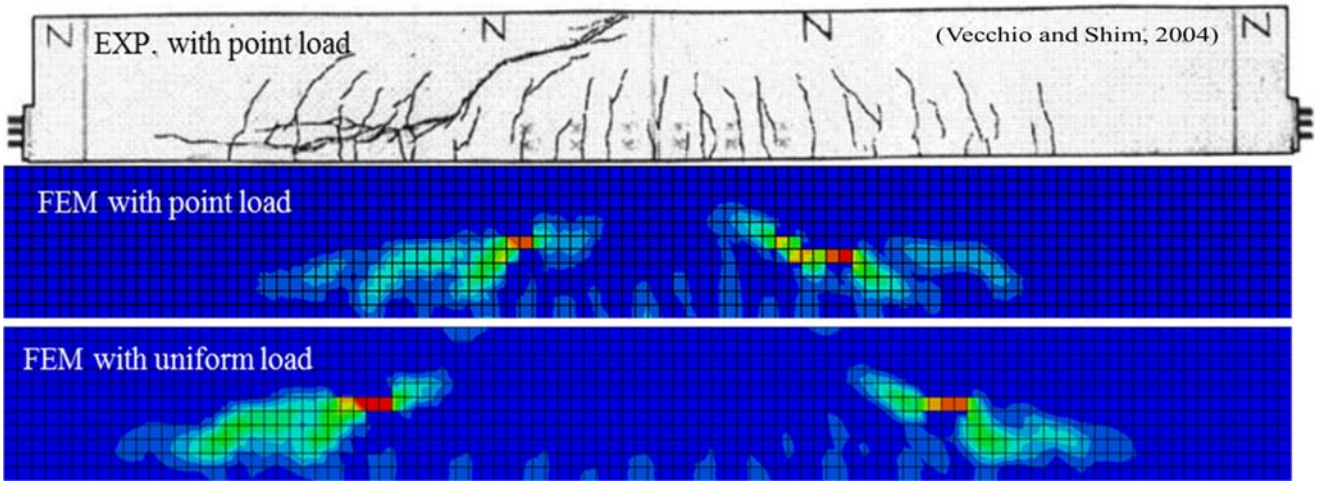

(b) OA2 Beam (a/d = 5)

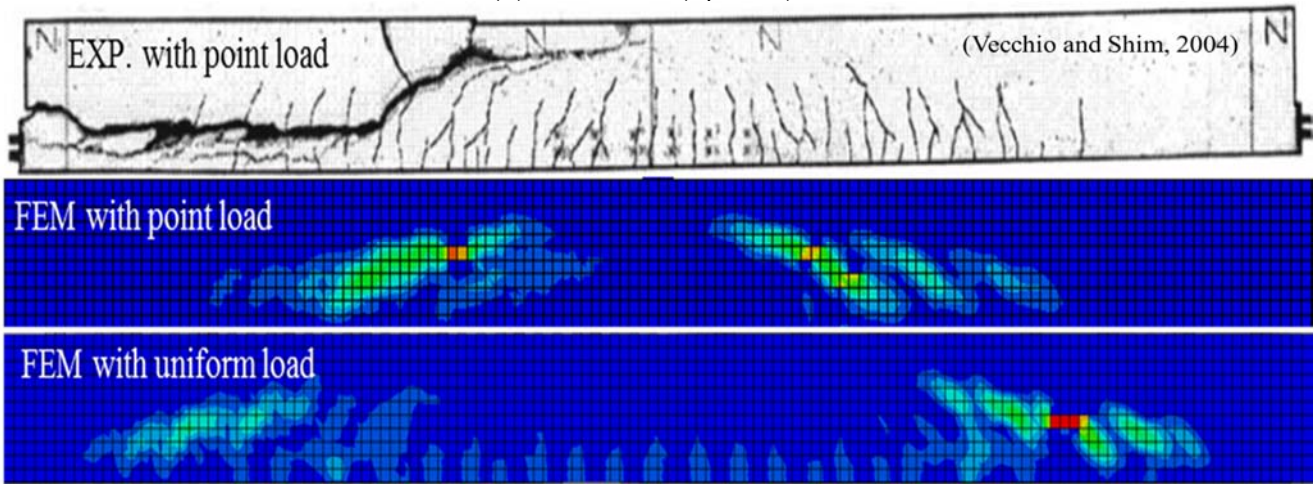

(c) OA3 Beam (a/d = 7)

Figure 34. Crack pattern of the designated beams: (a) OA1 Beam (a/d=4), (b) OA2 Beam (a/d=5), and (c) OA3 Beam (a/d=7)

3.4. Parametric Study

Twenty-four (24) reinforced concrete beams were analyzed to study other parameters which might impact shear strength. Table 7 presents the characteristics of each case study, as well as the beams that were subjected to experimental tests. Four a/d ratios (3, 4, 5, and 7), three different amount of longitudinal reinforcements (1.72%, 2.22%, and 2.72%), and two loading conditions (point and uniform loads) were covered in the parametric study.

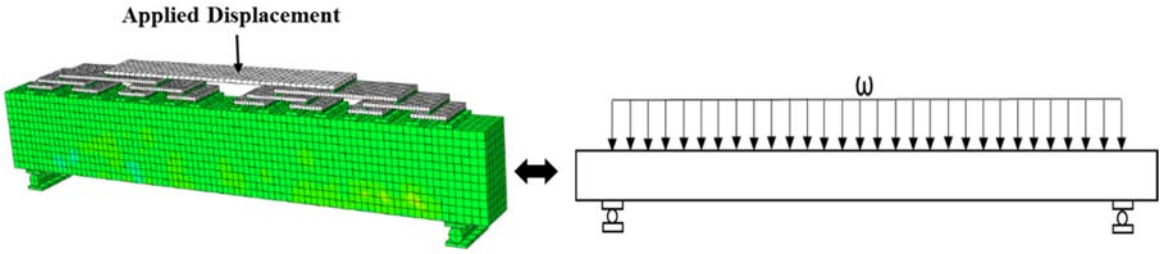

(a) Proposed method for displacement control loading (b) Equivalent distributed load

Figure 35. Finite element model and proposed displacement loading

Table 7. Characteristics of case studies

Beam Name	b (mm)	h (mm)	d (mm)	L (mm)	Span (mm)	Bottom steel (ρ %)	$\frac{a}{d}$	Concrete Material Name	Loading Condition
OA1-P	305	552	457	4,100	3,660	(1.72 %)	4	I	P. L.[*1]
OA1-U	305	552	457	4,100	3,660	(1.72 %)	4	I	U. L.[*2]
OA2-P	305	552	457	5,010	4,570	(2.22 %)	5	II	P.L
OA2-U	305	552	457	5,010	4,570	(2.22 %)	5	II	U. L.
OA3-P	305	552	457	6,840	6,400	(2.72 %)	7	III	P.L
OA3-U	305	552	457	6,840	6,400	(2.72 %)	7	III	U. L.
MA1-P	305	552	457	3183	2743	(1.72 %)	3	I	P.L
MA1-U	305	552	457	3183	2743	(1.72 %)	3	I	U. L.
MA2-P	305	552	457	3183	2743	(2.22 %)	3	I	P.L
MA2-U	305	552	457	3183	2743	(2.22 %)	3	I	U. L.
MA3-P	305	552	457	3183	2743	(2.72 %)	3	I	P.L
MA3-U	305	552	457	3183	2743	(2.72 %)	3	I	U. L.
MA4-P	305	552	457	4,100	3,660	(2.22 %)	4	I	P.L
MA4-U	305	552	457	4,100	3,660	(2.22 %)	4	I	U. L.
MA5-P	305	552	457	4,100	3,660	(2.72 %)	4	I	P.L.
MA5-U	305	552	457	4,100	3,660	(2.72 %)	4	I	U.L.
MA6-P	305	552	457	5,010	4,570	(1.72 %)	5	II	P. L.
MA6-U	305	552	457	5,010	4,570	(1.72 %)	5	II	U. L.
MA7-P	305	552	457	5,010	4,570	(2.72 %)	5	II	P. L.
MA7-U	305	552	457	5,010	4,570	(2.72 %)	5	II	U. L.
MA8-P	305	552	457	6,840	6,400	(1.72 %)	7	III	P. L.
MA8-U	305	552	457	6,840	6,400	(1.72 %)	7	III	U. L.
MA9-P	305	552	457	6,840	6,400	(2.22 %)	7	III	P. L.
MA9-U	305	552	457	6,840	6,400	(2.22 %)	7	III	U. L.

[*1]: Point Load; [*2]: Uniform Load

3.4.1. Results

The second column of Table 8 presents the ultimate shear strength in the critical section, including the results of the experimental tests duplicated by FEM. It should be noted that the critical section of the beams under a concentrated load was at mid-span, and the critical section of the beams, due to the application of a uniformly distributed load, was at distance "d" from supports. The results in Table 8 show that the shear strength of the investigated beams under uniformly distributed load was 1.76 times, on average, greater than the same beams under a concentrated load at mid-span. It also shows that an increase in ρ led to a decrease in the strain of the longitudinal rebar and an increase in the shear strength of the beams, due to dowel action of the longitudinal reinforcements. Additionally, following MCFT [27], the results of the parametric study indicated that a decrease in the strain of the longitudinal rebar, due to higher ρ, led to a decrease in the maximum principal strain and stress, resulting in an increase in the shear strength of the critical section. Since the shear strength of the beams with uniform load was greater than the beams with point load in all three cases, it can be concluded that shear capacity is highly dependent upon loading conditions. Loading conditions impact the internal forces, as well as the strain and stress distributions, of a reinforced concrete component. For instance, if a point load (P) is applied to the mid-span of a simply supported beam, the internal shear force at the mid-span section is $V_{iP} = 0.5P$. The same beam, under a uniformly distributed load with an equivalent intensity ($\omega = \frac{P}{L}$), has an internal shear force of $V_{iu} = P(0.5 - \frac{d}{L})$ in the section that is at a distance "d" from the support. For the case studies in this research, the four $\frac{d}{L}$ values were 0.125, 0.167, 0.1, and 0.071, and the ratios of $V_{ip}/\ V_{iu}$ were 1.33, 1.5, 1.25, and 1.16, respectively. This indicates that the internal shear force in the critical section was an average of 1.31 times greater when a point load (P) was applied at the

mid-span than when the equivalent uniform load ($\omega = \frac{P}{L}$) was applied. Considering only the material properties and sectional characteristics (b, d and ρ) when calculating concrete shear strength (V_c) leads to the same ratio (1.31) for shear capacity of the case-studied beams. Table 8, however, shows a ratio of 1.76, which means that other factors were at play. Based on MCFT [27], a bending moment in the shear critical section, which changed the strain in the longitudinal rebar, accounts for the difference. This interaction is reflected in $\frac{V_u d}{M_u}$ for the shear design in ACI318-14 [26] and also in the β factor for the general shear design in the AASHTO specification. Therefore, it can be concluded that the strain in longitudinal reinforcement, due to a bending moment in reinforced concrete beams, directly impacts concrete shear strength (V_c) [10]. In a simply supported beam with a point load (P) at the mid-span, the internal bending moment at the mid-span section is $M_{iP} = 0.25PL$; while the same beam, under a uniformly distributed load with an equivalent intensity ($\omega = \frac{P}{L}$), has an internal bending moment of $M_{iu} = \frac{Pd}{2}(1 - \frac{d}{L})$ in the section at distance "d" from the support. For the case studies with four $\frac{d}{L}$ values of 0.125, 0.167, 0.1, and 0.071, the ratios of $M_{ip}/\ M_{iu}$ are 4.57, 3.59, 5.55 and 7.58, respectively. Since the strain value in longitudinal reinforcement relates directly to the strength of the bending moment ($\varepsilon = \frac{M/d}{EA_s}$), the ratio of $M_{ip}/\ M_{iu}$ reveals that the strain in the longitudinal rebar in the section at distance "d" from the support, when an equivalent uniform load ($\omega = \frac{P}{L}$) is applied, is significantly less than the strain value in a mid-span section when the point load (P) is applied at the mid-span. For a simply supported beam with point load at mid-span, maximum shear, bending moment, and strain of longitudinal rebar occur at mid-span. Thus, theoretically the critical shear section is about mid-span. In uniformly distributed loads, the maximum shear occurs at supports, while the maximum

bending moment and the strain of the longitudinal rebar are still at mid-span. Therefore, based on structural analysis, the critical section for shear failure is close to the supports.

Table 8. Parametric study results and comparison with AASHTO Specification

Beam Name	Concrete shear strength (Vc) in C.S.* (kN)	Ratio ($\frac{U.L.}{P.L.}$)	Strain in Longitudinal Rebar in C.S.* ($\times 10^{-3}$)		Ratio ($\frac{FEM}{AASHTO}$)	β Value in C.S.*		Ratio ($\frac{FEM}{AASHTO}$)
			FEM	AASHTO		FEM	AASHTO	
OA1-P	152.13	1.64	1.282	1.51	0.849	2.76	2.11	1.31
OA1-U	249.23		0.769	1.071	0.718	4.53	2.5	1.81
OA2-P	156.87	1.72	1.414	1.445	0.978	2.66	2.16	1.23
OA2-U	270.78		0.491	0.883	0.556	4.6	2.71	1.69
OA3-P	161.19	1.92	1.666	1.616	1.031	2.11	2.04	1.03
OA3-U	310.22		0.583	0.809	0.72	4.06	2.81	1.44
MA1-P	187.73	1.59	1.102	1.490	0.739	3.41	2.13	1.6
MA1-U	299.28		0.969	1.336	0.725	5.44	2.25	2.41
MA2-P	200.88	1.56	0.911	1.234	0.737	3.65	2.34	1.56
MA2-U	313.38		0.743	1.083	0.686	5.69	2.49	2.28
MA3-P	220.16	1.56	0.695	1.1	0.629	4	2.96	1.35
MA3-U	343.31		0.787	0.968	0.813	6.24	2.61	2.39
MA4-P	167.21	1.64	1.239	1.285	0.964	3.04	2.29	1.33
MA4-U	274.81		0.762	0.914	0.833	4.99	2.67	1.87
MA5-P	174.81	1.75	1.029	1.096	0.939	3.17	2.47	1.28
MA5-U	306.28		0.631	0.831	0.759	5.56	2.77	2
MA6-P	164.89	1.84	1.862	1.963	0.948	2.8	1.82	1.54
MA6-U	303.98		1.182	1.281	0.922	5.16	2.3	2.24
MA7-P	176.84	1.68	1.327	1.329	1	3	2.26	1.33
MA7-U	297.82		0.593	0.793	0.748	5.06	2.83	1.79
MA8-P	131.79	2.25	2.062	2.092	0.985	1.72	1.75	0.98
MA8-U	296.63		0.653	1.226	0.532	3.88	2.35	1.65
MA9-P	153.57	1.99	1.888	1.887	1	2.01	1.86	1.08
MA9-U	306.15		0.58	0.979	0.592	4.01	2.6	1.54
	Average	**1.76**		**Average**	**0.808**		**Average**	**1.61**

*C.S.: Critical Section

3.5. Comparison with Design Codes

The assessment of design codes and specifications was another purpose of this study. Therefore, the shear methodology of ACI318-14 code [26] and the AASHTO specification [3] were evaluated by the outcomes of the parametric study.

3.5.1. ACI318-14

For every non-prestressed reinforced concrete element, such as a beam, the shear strength is Vc + Vs. The concrete shear strength, Vc, depends on the cross-section dimension, the material properties of the concrete, and the amount of longitudinal rebar. ACI 318-14 [26] suggests using Equation (3-1) in Section 22.5.5 to calculate Vc for non-prestressed members without axial force, such as beams.

The shear strength of concrete (Vc) is obtained by the minimum value of Vc calculated by Equations (3-1a) through (3-1c).

(1a): $V_c = \left(1.9\lambda\sqrt{f_c'} + 2500\rho_w \frac{V_u d}{M_u}\right) b_w d$

(1b): $V_c = \left(1.9\lambda\sqrt{f_c'} + 2500\rho_w\right) b_w d$ Eq. 3-1

(1c): $V_c = 3.5\lambda\sqrt{f_c'} b_w d$

Where f_c' is in psi (1 psi= 0.0069 MPa).

According to Equation (3-1a), the shear strength of concrete (Vc) varies along the span of a beam if the ratio of $\frac{V_u d}{M_u}$ changes. If Equation (3-1a) doesn't govern, regardless of loading condition, using Equations (3-1b) or (3-1c) leads to assigning only one value of Vc to all of the cross sections of a beam.

The shear strength (Vc) of all 24 R.C. beams was compared with ACI318-14's shear design formulation, presented in Table 9. In all of the case-studied beams in this research, Equation (3-1a) governed. According to Table 9, the ACI318-14 prediction of shear strength averaged 1.59 times greater than the FEM results. The ACI prediction was less than the FEM in only one case,

MA8-P, which had the highest a/d ratio and the lowest amount of longitudinal reinforcement (1.72%). Figure 36 illustrates the variation of $V_{FEM}/V_{ACI318-14}$ versus a/d from Table 9. The same procedure described previously was followed to calculate $V_{FEM}/V_{ACI318-14}$ for each a/d in both point and uniformly distributed loads. A similar trend was revealed for the variation of $V_{FEM}/V_{ACI318-14}$ versus a/d with $\beta_{FEM}/\beta_{AASHTO}$ versus a/d. AASHTO's and the ACI's estimates of the shear strength (Vc) of concrete were almost identical for the simply supported beams studied in this research.

Table 9. Parametric study results and comparison with Equation (3-1) in ACI318-14 Code

Beam Name	Total Shear Force (kN)	Concrete shear strength (Vc) in C.S.* from FEM (kN)	Concrete shear strength (Vc) in C.S.* from ACI318-14 (kN)	Ratio $(\frac{FEM}{ACI318-14})$
OA1-P	304.26	152.13	115.71	1.31
OA1-U	664.33	249.23	141.01	1.77
OA2-P	313.74	156.87	123.49	1.27
OA2-U	676.76	270.78	160.50	1.69
OA3-P	322.38	161.19	155.51	1.04
OA3-U	723.6	310.22	206.88	1.50
MA1-P	375.46	187.73	119.19	1.58
MA1-U	897.69	299.28	138.62	2.16
MA2-P	401.77	200.88	126.61	1.59
MA2-U	939.99	313.38	146.05	2.15
MA3-P	440.32	220.16	127.25	1.73
MA3-U	1029.74	343.31	157.98	2.17
MA4-P	334.42	167.21	123.14	1.36
MA4-U	732.56	274.81	148.43	1.85
MA5-P	349.62	174.81	121.76	1.44
MA5-U	816.44	306.28	161.76	1.89
MA6-P	329.78	164.89	121.07	1.36
MA6-U	759.95	303.98	149.74	2.03
MA7-P	353.69	176.84	125.91	1.40
MA7-U	744.54	297.82	171.26	1.74
MA8-P	263.58	131.79	152.06	0.87
MA8-U	692.09	296.63	184.54	1.61
MA9-P	307.14	153.57	153.78	1.00
MA9-U	714.32	306.15	195.71	1.56
			Average	**1.59**

*C.S.: Critical Section

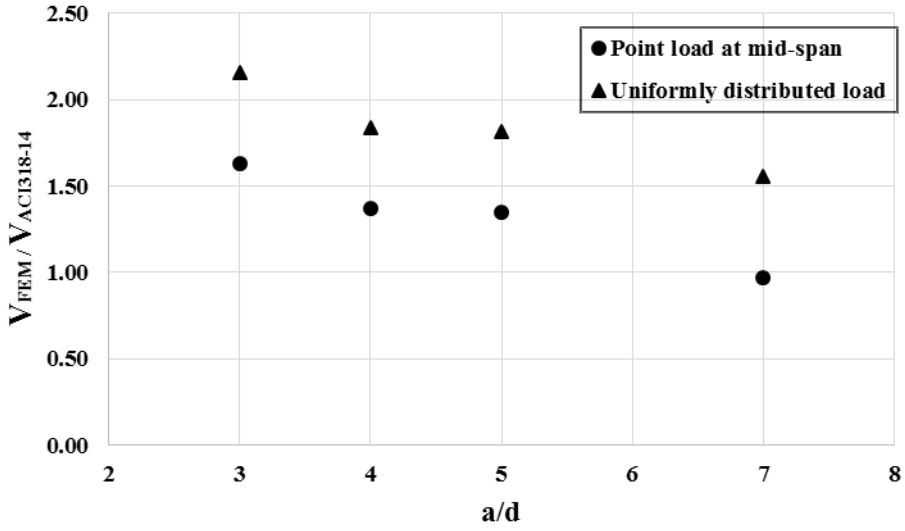

Figure 36. Variation of $V_{FEM}/V_{(ACI318-14)}$ versus a/d

3.5.2. AASHTO Specification

AASHTO's equations for the shear strength of concrete, (Vc), include a β factor, which is calculated $\frac{v_c}{\sqrt{f'_c}}$ when $v_c$and f'_c are in psi (1 psi= 0.0069 MPa). In this study the β factor is obtained directly by the FEM, after identifying the ultimate shear strength of the critical concrete section. AASHTO's equations find the β factor, based on the strain of the longitudinal rebar. Since the cross section and the amount of longitudinal reinforcement along the beam were kept constant for all designated beams in this study, the variations in longitudinal rebar strains were due to the different loading conditions.

Figures 37a, 37b, and 37c show the variations of strain in the longitudinal rebar, along the span of the three beams tested by Vecchio and Shim [34]. a/d ratios of 4, 5, and 7, respectively, were used for the three beams at the ultimate load when concentrated and uniformly distributed loads, obtained from the results of AASHTO's equation and FEM, were applied. According to Figure 37a, the FEM results indicated that the strain of the longitudinal rebar at mid-span for the point

load was 1.282×10^{-3}, and the strain at distance "d" from the supports for the uniform load was approximately0.769×10^{-3}. The decrease in shear strength of the beam subjected to concentrated load was due to the strain in reinforcement being higher than that of the uniformly distributed load. For each loading condition, there is a critical section in the beam, and the strain of the longitudinal rebar of that section affects the shear strength of the entire beam. Thus, to estimate the shear strength of a concrete section, the strain of the longitudinal rebar due to bending moment and axial forces is calculated separately and then added together.

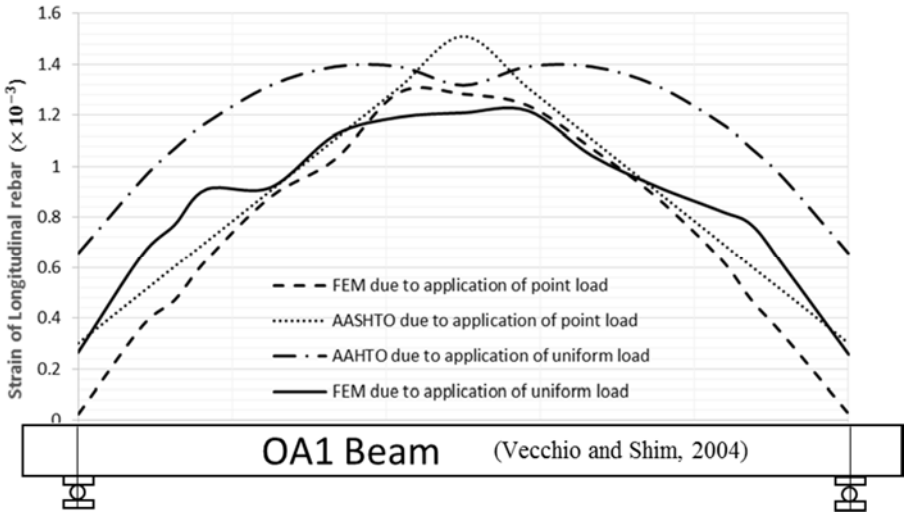

(a) $a/d = 4$

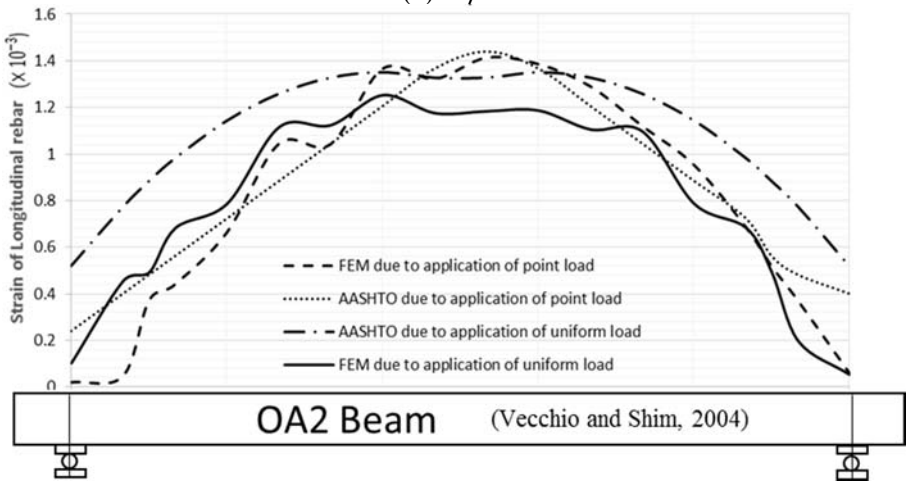

(b) $a/d = 5$

Figure 37. Variation of strain in longitudinal steel along the span (Continued)

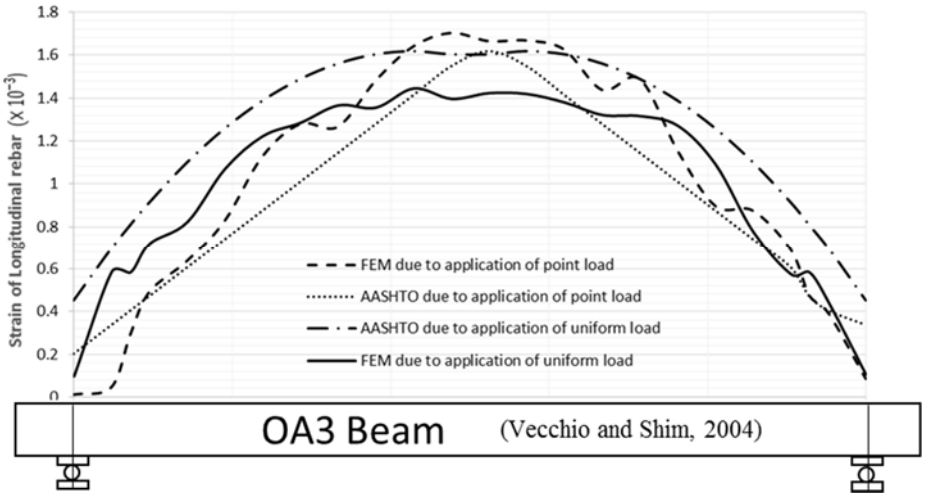

(c) $a/d = 7$

Figure 37. Variation of strain in longitudinal steel along the span: (a) a/d=4, (b) a/d=5, and (c) a/d=7

The comparison of the strains along the span of the OA1, OA2, and OA3 beams indicates that AASHTO's equation reasonably estimates the strain in longitudinal reinforcement in the absence of rebar yielding. The failure mode of the beams studied were diagonal-tension, which means shear failure without rebar yielding. Figures 37a to 37c illustrate that AASHTO's estimation for strain, when applying uniform load, is slightly higher (more conservative) than the FEM results in these case studies; however, it is reasonable when compared with FEM results for applying the concentrated load. The fourth and fifth columns of Table 8 present the strain in longitudinal rebar in the critical section obtained from FEM and AASHTO's equation at ultimate shear strength. The sixth column calculates the ratio of these two quantities and demonstrates that AASHTO's prediction for the strain value differs 19%, on average, from the FEM results of this parametric study. The difference is 10% for the case studies under a point load at mid-span and 28% for those under a uniformly distributed load.

Figures 38a to 38c present the variations of the β value along the span of the tested beams [34] with a/d ratios of 4, 5 and 7, respectively, based on AASHTO's prediction and FEM results for

point load at the mid-span and uniformly distributed load. Due to the application of point load at the mid-span, the shear force is constant along the span. With the FEM, one value for β is reported for every section of each beam; however, with AASHTO, the β factor increases by moving to the supports, where the bending moment is zero. For the designated OA1 beam [34], when a concentrated load is applied at mid-span, AASHTO's equations yield to 2.11 for the β value in the critical section (mid-span section), and FEM's value of β is 2.76, which is about 1.31 times greater than AASHTO's prediction. The sections located at distance "d" from supports are critical sections when applying uniformly distributed load. For the designated OA1 beam under uniformly distributed load, AASHTO's equations yield to β=2.5 and FEM results indicate β=4.53 for the critical section, which is 1.81 times greater than AASHTO's prediction. For the designated OA2 beam [34], the β value, when applying a point load at mid-span in the critical section from FEM, is 2.66, and from AASHTO is 2.16. The AASHTO specification predicts β=2.71 when a uniformly distributed load is applied to the designated OA2 beam in the critical section, and FEM results indicate 4.6 for the β value of the critical section. For the designated OA3 beam [34], which is the longest beam in this study (a / d = 7), the ratio of the β value from FEM to the β value from AASHTO in the critical section, when concentrated load is applied, is 1.03. The value of β from FEM, when applying a uniformly distributed load, is 1.44 times greater than AASHTO's estimation. The seventh and eighth columns of Table 8 express the calculated β values from FEM and AASHTO, respectively, and the ninth column shows the ratio of these values. A comparison of the β factors from AASHTO and FEM results reveals that AASHTO underestimated the shear strength of concrete in the critical section (where the inclined shear crack occurs) of all of the 24 beams tested in this research by an average of 61%. This underestimation, for the case studies

only, under a point load at mid-span was 30%, and for the beams under uniformly distributed load was 92%.

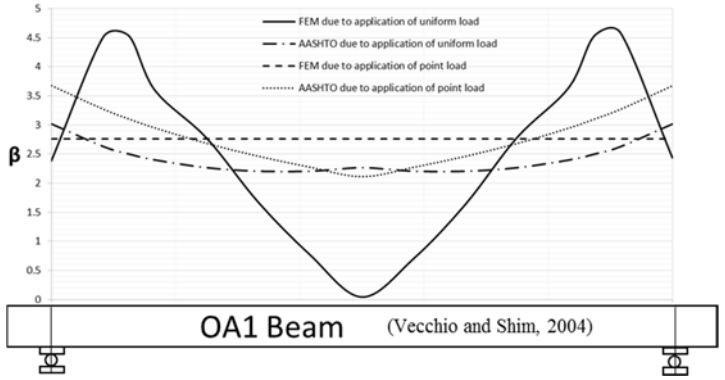

(a) $a/d = 4$

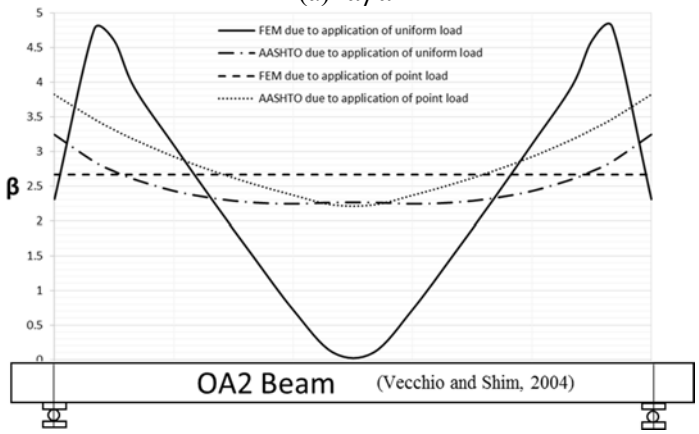

(b) $a/d = 5$

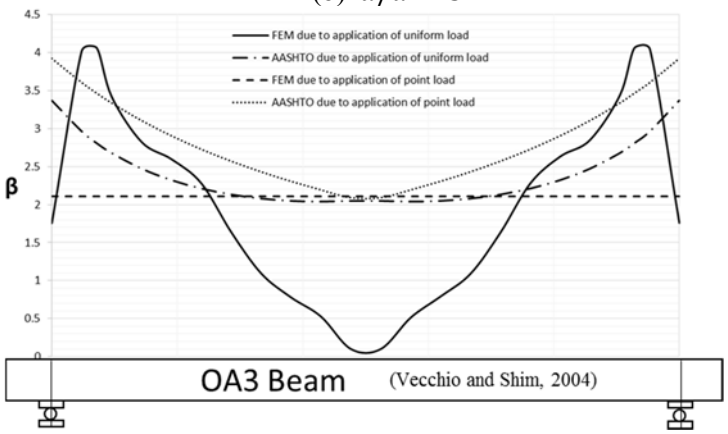

(c) $a/d = 7$

Figure 38. Variation of the β factor along the span: (a) a/d=4, (b) a/d=5, and (c) a/d=7

Thus, the predictions of AASHTO for the β factor and for the strain in longitudinal reinforcement in the critical section were closer to the FEM result when the beams were under a concentrated load at mid-span than when the beams were under uniformly distributed load.

Figure 39 shows the variations of $\beta_{FEM}/\beta_{AASHTO}$ and $\varepsilon_{FEM}/\varepsilon_{AASHTO}$ versus a/d from Table 8. For instance, for a/d of 5 for the point load, the ratio of $\beta_{FEM}/\beta_{AASHTO}$ in this figure was calculated as an average value of the ratio in Table 8 for case studies OA2-P, MA6-P, and MA7-P $(1.23 + 1.54 + 1.33)/3 = 1.37$. Figure 39 indicates that for the highest a/d ratios ($a/d = 7$), AASHTO's prediction for the β factor was very close to the FEM results ($\frac{\beta_{FEM}}{\beta_{AASHTO}} = 1.03$) for the point load. Also, the prediction of strain in the longitudinal rebar, using AASHTO's equation, resulted in the same value obtained from FEM results in the case study ($\frac{\varepsilon_{FEM}}{\varepsilon_{AASHTO}} = 1.005$). According to Figure 39, an increase in the a/d ratio of both point and uniformly distributed loads leads to a decrease in the difference between AASHTO's prediction for the β value and the FEM results. Moreover, when a point load is applied at the mid-span of a simply supported beam, the prediction of the β value, using AASHTO's equations, is closer to the FEM results than when a uniformly distributed load is applied. An increase in the a/d ratio leads to a closer prediction of the strain value between AASHTO's equation and FEM outcomes for point loads; however, this trend is not the same for uniformly distributed loads. It can be concluded that when the strain value is high, which occurs primarily in the mid-span section of a point load, where the maximum bending moment and shear force occur, AASHTO's estimation is similar to the FEM outputs. However, AASHTO's prediction of the strain value of the longitudinal reinforcement is smaller than that of the FEM.

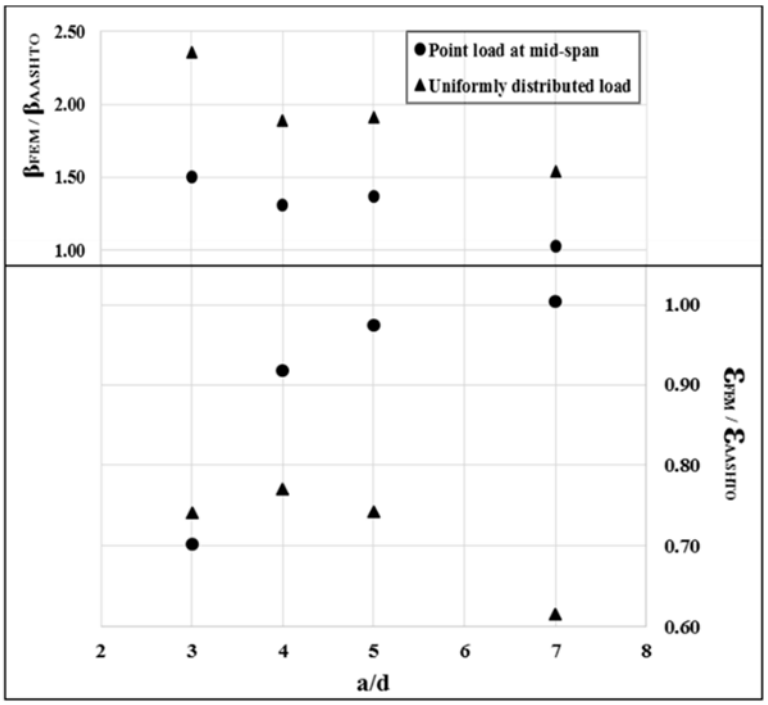

Figure 39. Variation of $\beta_{FEM}/\beta_{AASHTO}$ and $\varepsilon_{FEM}/\varepsilon_{AASHTO}$ versus a/d

CHAPTER 4. EXPERIMENTAL AND NUMERICAL INVESTIGATION OF R.C. BOX CULVERTS

4.1. Overview

After the loading mechanism was validated, the shear strength of the R.C. box culvert's top slab was examined experimentally under the equivalent uniformly distributed load. The experimental tests were performed in the Civil Engineering Laboratory Building (CELB) at the University of Texas at Arlington. Due to the specific configuration of specimens, they were built at CELB by the researcher. The outcomes of the experimental investigation were used to calibrate finite element models. Two sets of reinforced concrete box culverts were built and tested. The first set was made from a high concrete compressive strength, and the second set was made from a low strength concrete, which is commonly used to produce R.C. box culverts.

4.2. Specimens Size

ASTM C1577 [4] recommends 65 reinforced concrete box culverts sizes, with span lengths varying from 3 ft. (914 mm) to 12 ft. (3658 mm). The required reinforcements for different fill heights are defined in the AASHTO LRFD Specification [3], and the results are tabulated in ASTM C1577 [4]. For this research, the smallest box culvert had a 3 ft. (914 mm) span, as recommended by ASTM C1577 [4], and was investigated experimentally. The amount of longitudinal reinforcement was enhanced to 2.22% at the top and bottom of the slabs, and there was no transverse reinforcement to guarantee shear behavior mode. Box culverts were prepared with dimensions of $3' \times 2' \times 4''$ ($914 \times 610 \times 102$ mm) and $3' \times 3' \times 4''$ ($914 \times 914 \times 102$ mm), with identical reinforcement configurations. Three specimens of each size were cast on the same day from the same batch. Figure 40 illustrates the dimensions and rebar arrangements of the specimens. The concrete cover of the rebar of the box culverts with deep fill height was considered

1 in. (25 mm), according to ASTM C1577 [4]. Two of #4 rebar (area = 0.2 in.2) with center-to-center distance of 4 in. (102 mm) were placed as longitudinal reinforcement at the top and bottom of the slabs and walls. The specimens were built with a width of 6 in. (152 mm) to fit within the framework. It should be noted that since a box culvert line, similar to a pipeline, is a plane-strain problem ($\epsilon_{zz} = 0$), the width of the specimens did not affect the results of this study [16].

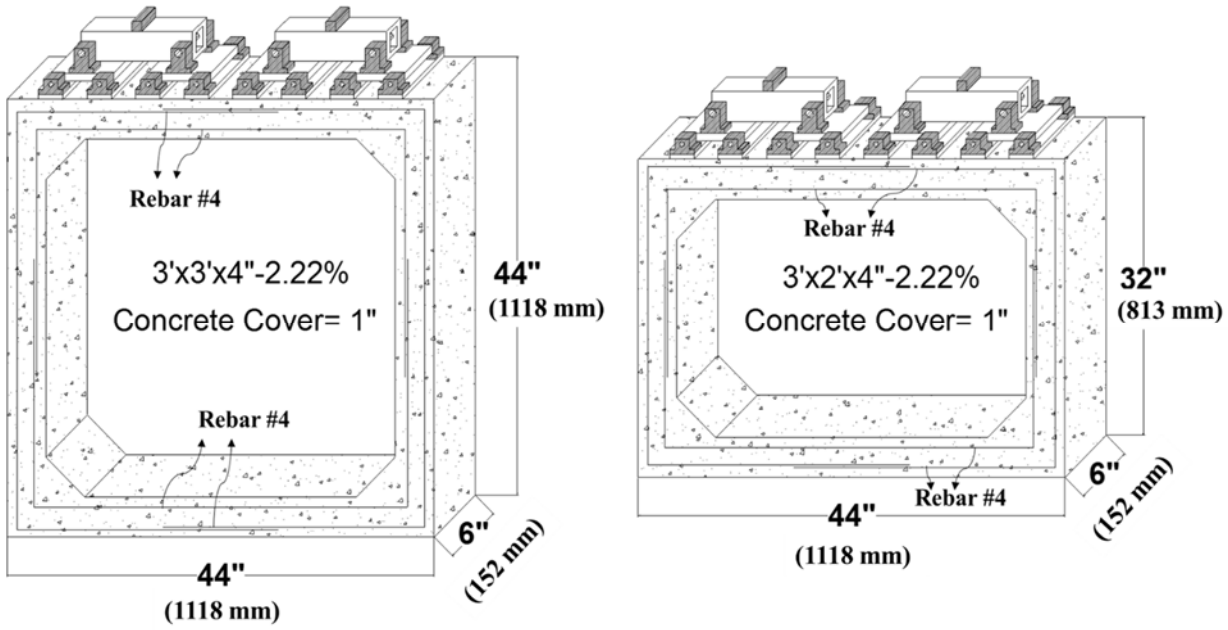

Figure 40. R.C. box culverts' examined characteristics

The material properties of the rebar used in the box culvert specimens were the same as those used for the beam test. Ready-mixed concrete with 6.5 ksi (44.8 MPa) and 4.8 ksi (33.1 MPa) 28-day compressive strength was used to build the specimens. Table 10 presents the concrete properties used in this study. The specimens were cured for 28 days in the open air, and water, required for hydration of the cement, was provided periodically.

Table 10. Concrete properties in the experimental program

f'_c , ksi (MPa)	f_t , ksi (MPa)	Slump, in (mm)	Aggregate size, in (mm)	w/c
4.8 (33.1)	0.45 (3.1)	6 (152)	3/8 (10)	0.5
6.5 (44.8)	0.48 (3.3)	4 (102)	1 (25)	0.4

4.3. Specimens Construction

The first step of specimen construction was to build wooden molds in two different sizes. Making the 45 degree haunch was most difficult part in this step. Figure 41 shows molds built for the experimental program. The next step was preparing the steel reinforcement cages. The rebar was cut and bended by the manufacturer. Cages provided for the box culvert specimens is illustrated in Figure 42. Then, strain gauges were installed on the rebar in three locations. The procedure followed for the strain gauge installation included smoothing, cleaning, and naturalizing the surface, then attaching it, with glue. Figure 43 shows a graphical order for the chemicals used in the strain gauge installation.

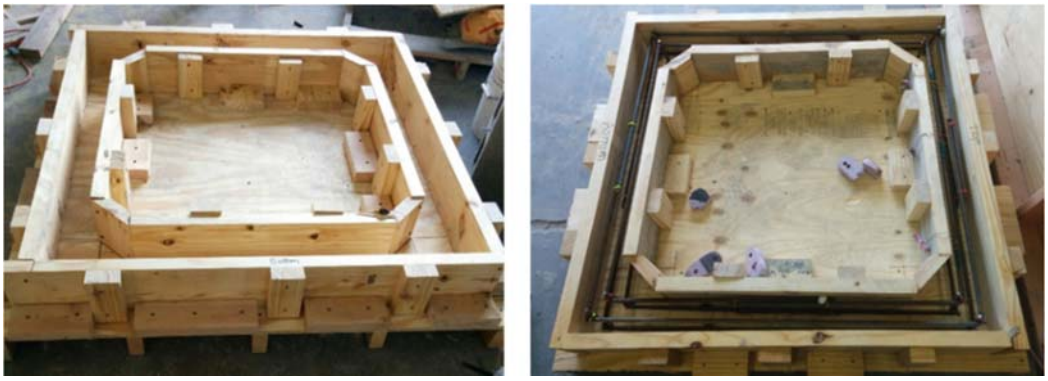

Figure 41. Wooden molds for the box culvert specimens

Figure 42. Reinforcement cages

Figure 43. Chemicals for strain gauge installation

All of the six box culverts were cast from one batch in the same day. An electronic vibrator was used to shake the molds to properly distribute the concrete over the molds. The specimens were left for 28 days for curing. The water needed to complete the hydration action was provided for them periodically. Figure 44 illustrates the box culvert specimens on the casting day and during the curing process.

Figure 44. Box culvert specimens

4.4. Test Setup and Instrumentations

To measure the strain value in the longitudinal rebar during loading, three strain gauges were attached to the rebar before the fresh concrete was poured. One strain gauge at mid-span and two others at distance “d” (3 in. or 76 mm) from the haunch at both sides measured the strain value.

The deflection of the top slab at mid-span, the vertical relative deflection of the slabs at mid-span, and the horizontal relative deflection of the walls at mid-height were recorded by three transducers. The difference between the deflection of the top slab at mid-span and the vertical relative deflection of the slabs at mid-span resulted in the vertical deflection of the bottom slab's mid-span. The test setup and instrumentations of the box culvert tests are provided in Figure 45. The DAQ system continuously recorded the outputs of load, strain, and displacement values during the tests. Similar to the beam test, the test was employed via a displacement control method. The rate of applying displacement was 0.06 in/min (1.5 mm/min), using a 400 kips (1780 kN) hydraulic jack. The box culverts were between the framework for loading, and a rigid steel I-girder was its base, all in one plane.

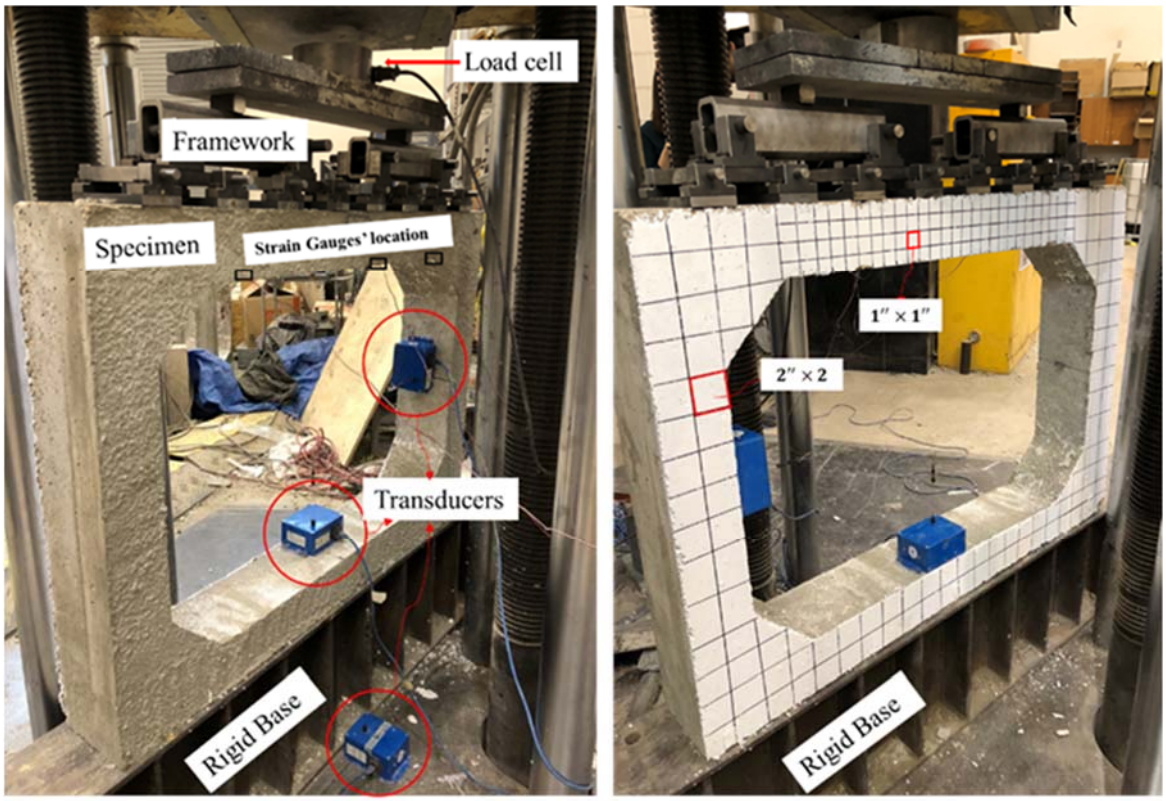

Figure 45. Test setup and instrumentations for the box culvert tests (box culvert size: 3×2×4)

4.5. Results

Table 11 summarizes the measured values of all 12 box culverts examined in the experimental program. It should be noted that the empty cells in Table 11 represent a value that was not measured for that specific test, or was off-scale. The test results demonstrated that an increase in a box culvert's rise does not significantly change the shear strength of its top slab when it has shear behavioral mode. As was expected, higher f_c' led to higher shear strength.

Table 11. The experimental tests outputs

Box Culvert Size ($ft.\times ft.\times in.$)	**f'_c ksi (MPa)**	**Specimen #**	**Total Failure load, kip (kN)**	**Deflection of top slab's mid-span at failure, in. (mm)**	**Deflection of bottom slab's mid-span at failure, in. (mm)**	**Horizontal deflection of walls at mid-height at failure, in. (mm)**	**Strain in the As2 rebar at mid-span at failure, με**	**Strain in the As2 rebar at distance "d" from haunch at failure, με**
$3\times2\times4$	4.8 (33.1)	1	39.9 (177)	0.436 (11)	0.043 (1)	0.216 (5)	-	1654
		2	39.6 (176)	0.438 (11)	0.018 (0.5)	0.225 (6)	-	1584
		3	35.1 (156)	0.366 (9)	0.032 (1)	0.612 (15)	1918	1093
$3\times2\times4$	6.5 (44.8)	1	43.5 (193)	0.317 (8)	-	0.247 (6)	2744	2028
		2	48.4 (215)	0.392 (10)	-	0.237 (6)	2834	2082
		3	48 (214)	0.253 (6)	-	0.151 (4)	1945	1222
$3\times3\times4$	4.8 (33.1)	1	38.4 (171)	0.433 (11)	0.054 (0.5)	0.296 (7)	2472	1285
		2	38.3 (171)	0.461 (12)	0.037 (1)	0.304 (8)	2073	1574
		3	34.6 (154)	0.452 (11)	0.044 (1)	0.299 (8)	2402	1375
$3\times3\times4$	6.5 (44.8)	1	44.6 (198)	0.475 (12)	-	0.201 (5)	-	712
		2	43.1 (192)	0.324 (8)	-	0.359 (9)	2601	884
		3	42.8 (190)	0.244 (6)	-	0.200 (5)	2082	777

As was expected all specimens failed in shear. Diagonal tension cracks occurred about distance "d" from tip of the haunch, and some minor flexural cracks appeared at the mid-span in the maximum positive bending moment region. Since the walls bended, some flexural cracks occurred at the negative moment area. Figure 46 captures the cracking pattern in the specimens. The flexural cracks at mid-span were the first cracks to develop during the early stages of loading. Due to redistribution of stresses caused by indeterminacy of the system, the mid-span cracks did not further propagate. A new series of flexural cracks occurred in the negative moment region in the walls. The shear cracking initiated near the last stage of loading. The crack width of diagonal tension cracks started to increase quickly until the specimens reached their ultimate capacity. The observations of crack development in the experimental investigation demonstrated that several minor flexural cracks initiated first, and the specimens eventually failed due to a major shear crack at distance "d" from haunch. It should be noted that there were no major cracks in the bottom slab. The reinforced concrete box culverts in this study failed from the top slab.

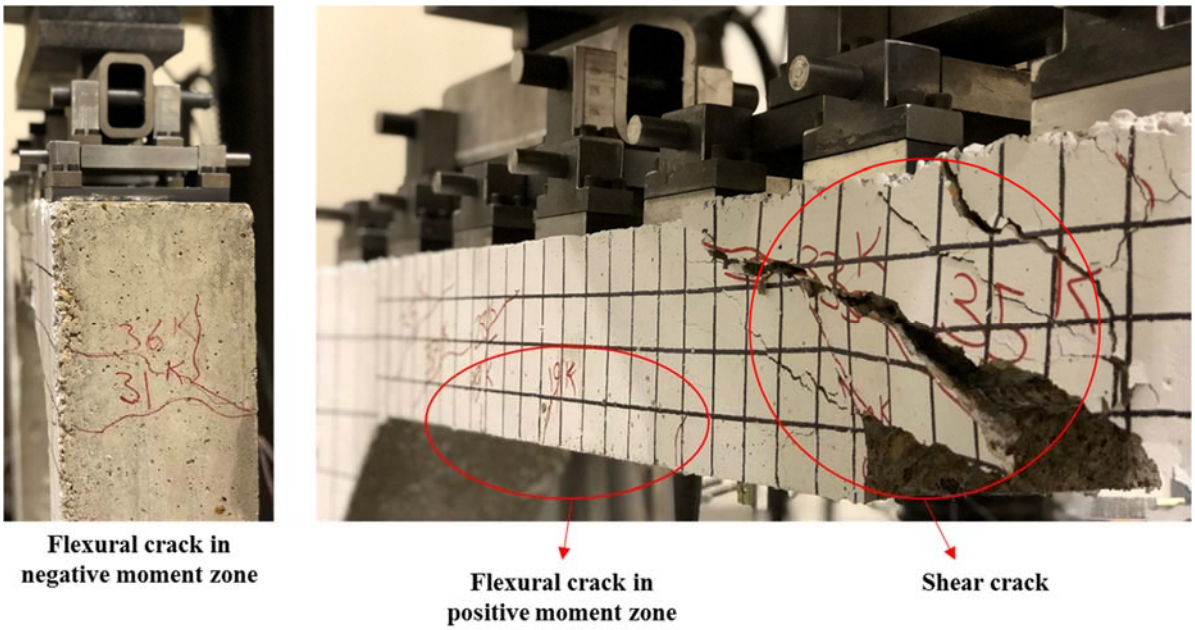

Figure 46. Crack patterns (box culvert size: 3 × 3 × 4)

The outcomes of the experimental investigation indicated that although the failure mode of the specimens was shear, the longitudinal rebar in the most of cases yielded at the mid-span in the positive bending moment region.

4.6. Finite Element Modeling

The finite element method (FEM) was used to mimic the experimental tests of many studies on the shear strength of reinforced concrete members [40, 41]. Numerical models of the specimens tested were developed by using the FEM performed by the ABAQUS software [32]. The numerical models allowed other outputs which could not be derived directly from the experimental tests, such as sectional shear force, bending moment, and strain value. The numerical models built by the ABAQUS software [32] are shown in Figure 47. All of the assumptions that were used to mimic the tests are described below.

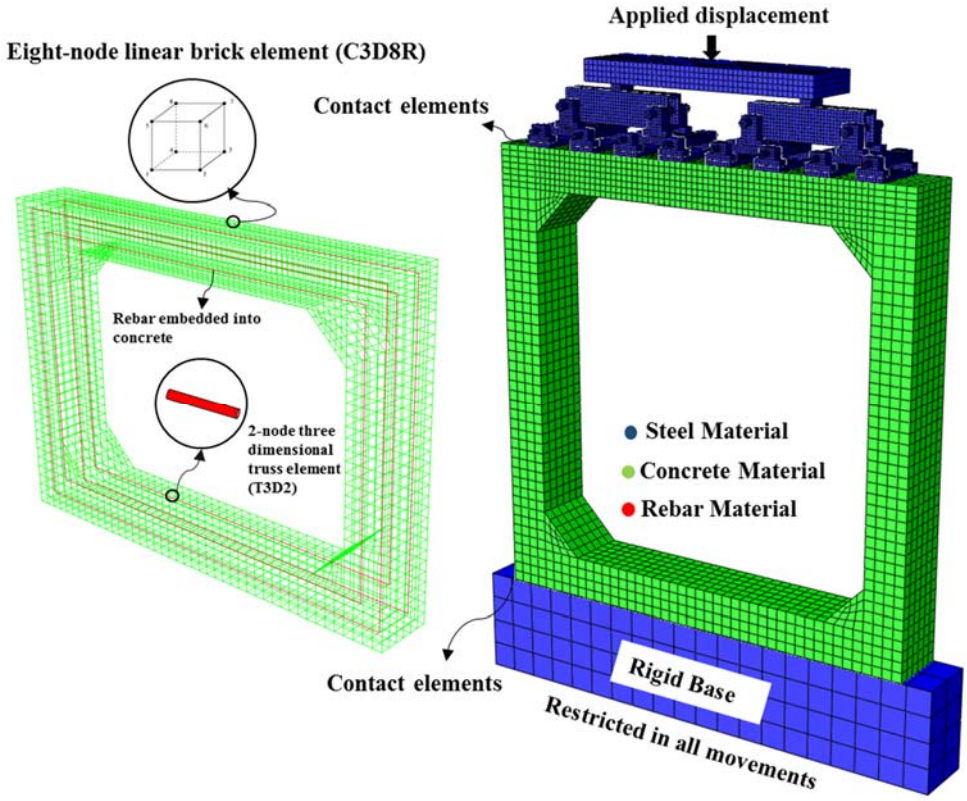

Figure 47. Finite element model and assumptions

4.7. Material Properties

Three different materials were used in this numerical modeling. The behavior of concrete and steel for the rebar included linear and nonlinear parts; however, a linear steel was assigned to the framework's material.

4.7.1. Concrete

Figure 48 plots the stress-strain curves of compression and tension in both of the concretes used to simulate the experimental tests. A concrete damage plasticity (CDP) model [33, 43] was used to observe the after-damage compression and tension behavior of the concrete. This type of model provides a general capability for modeling concrete and other quasi-brittle materials for all types of structures. It employs the concepts of isotropic-damaged elasticity, in combination with isotropic tensile and compressive plasticity, to represent the inelastic behavior of concrete. It is designed for applications in which the concrete is subjected to arbitrary loading conditions, including cyclic loading [32]. The model considers the degradation of the elastic stiffness induced by plastic straining, both in tension and compression [32].

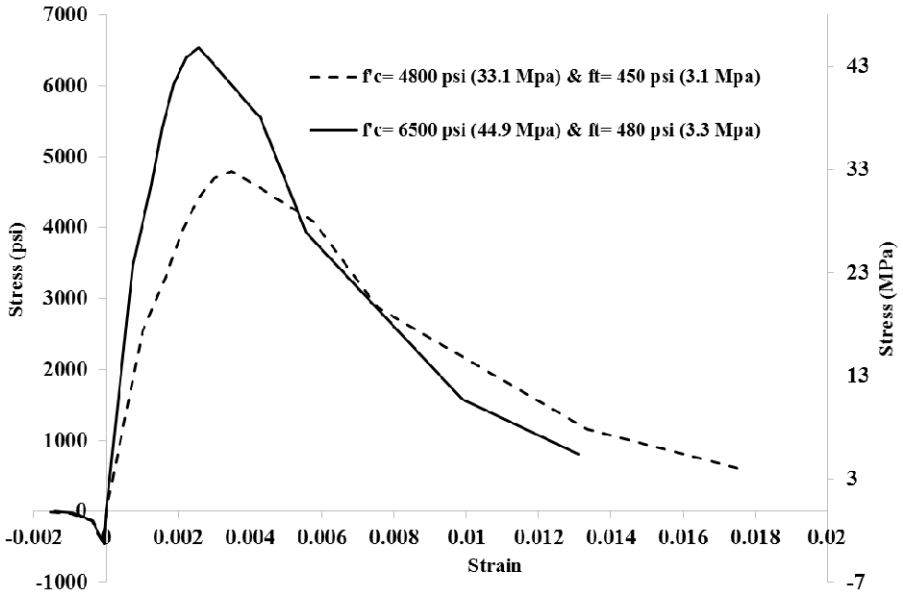

Figure 48. Stress-strain curve for concrete material in compression and tension

4.7.2. Rebar

A conventional Grade 60 ($E = 29000\ ksi$, 200 GPa) rebar with elastic-perfectly plastic behavior was used for the numerical model for this research.

4.7.3. Steel

A linear material with module of elasticity of 29,000 ksi (200 GPa) was defined for those parts made from steel.

4.8. Element Type

The concrete and framework were modeled using 3D element, and a 2D truss element was utilized for the longitudinal reinforcement.

4.8.1. Solid Element

Three-dimensional stress solid elements, C3D8R, were assigned to the models for the concrete and steel meshes. The C3D8R element is a general purpose linear brick element, with reduced integration (1 integration point). The node numbering followed the convention of Figure 47. The integration point of the C3D8R element was located in the middle of the element [32]

4.8.2. Truss Element

A 2-node three-dimensional truss element, T3D2, was used to model the rebar [32]. It should be noted that these elements were also used in the numerical modeling of the beam test in this research.

4.9. Boundary Conditions

The hard-contact elements for normal behavior were defined between the bottom layer of the framework and the top of the specimens. There was no friction, nor any restrictions for tangential movement of the framework. These assumptions were used only for transferring the normal forces

to the top of the specimens. It should be noted that since structural components deform under load, if the bottom plates of the framework cannot slide easily, the normal applied point loads cannot be identical.

The box culverts were put on a rigid mat that was constrained in all degrees of freedom. With this boundary condition, the bottom slab could move up, due to applied bending moment, and the side walls could bend in-plane. The walls of the box section were free to deflect in-plane. The rebar was embedded in the concrete to assure that every section of the concrete and steel had the same strain, for both the beam simulation and the box culverts.

4.10. Loading and Analysis

A general static analysis was performed, using the displacement control procedure. The displacement was applied at a very low rate during a specific time, with the ramp placed linearly over the step to prevent dynamic effects of the corresponding applied load. The loading rate automatically changed between 10E-2 and 10E-10 to attain convergence at each increment. The Newton method was used to solve the equations. Observation of the analyses continued post-failure.

4.11. Finite Element Model Verifications

Figure 49 shows a comparison of the total shear load-deflection curves of the FEM results and those obtained from the experimental data, indicating that the numerical models predicted the shear behavior of the examined box culverts satisfactorily. The agreements between the FEM results and experimental data for crack patterns and strain values of the longitudinal rebar are shown in Figures 50 and 51, respectively.

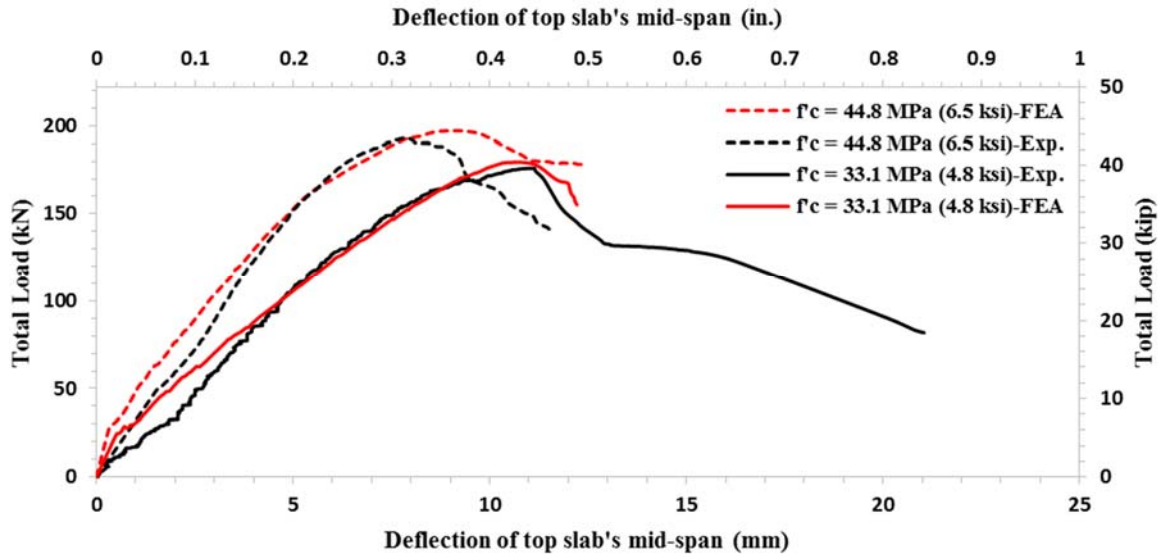

a) Box culvert 3 × 2 × 4- ρ = 2.22%

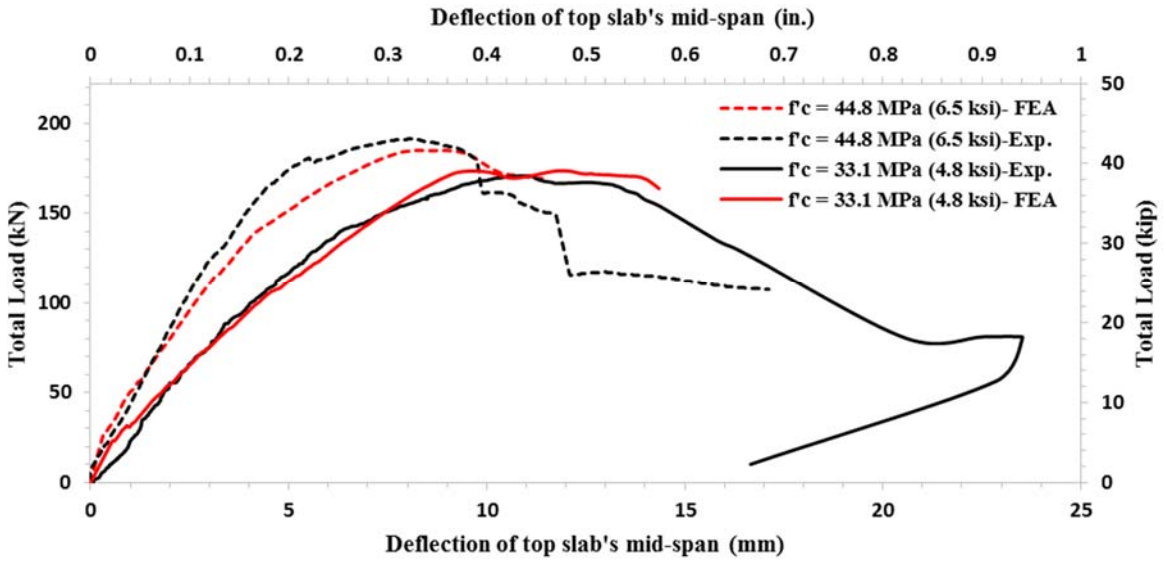

b) Box culvert 3 × 3 × 4- ρ = 2.22%

Figure 49. Comparison of numerical results with experimental data, a) for box culvert 3×2×4; b) for box culvert 3×3×4

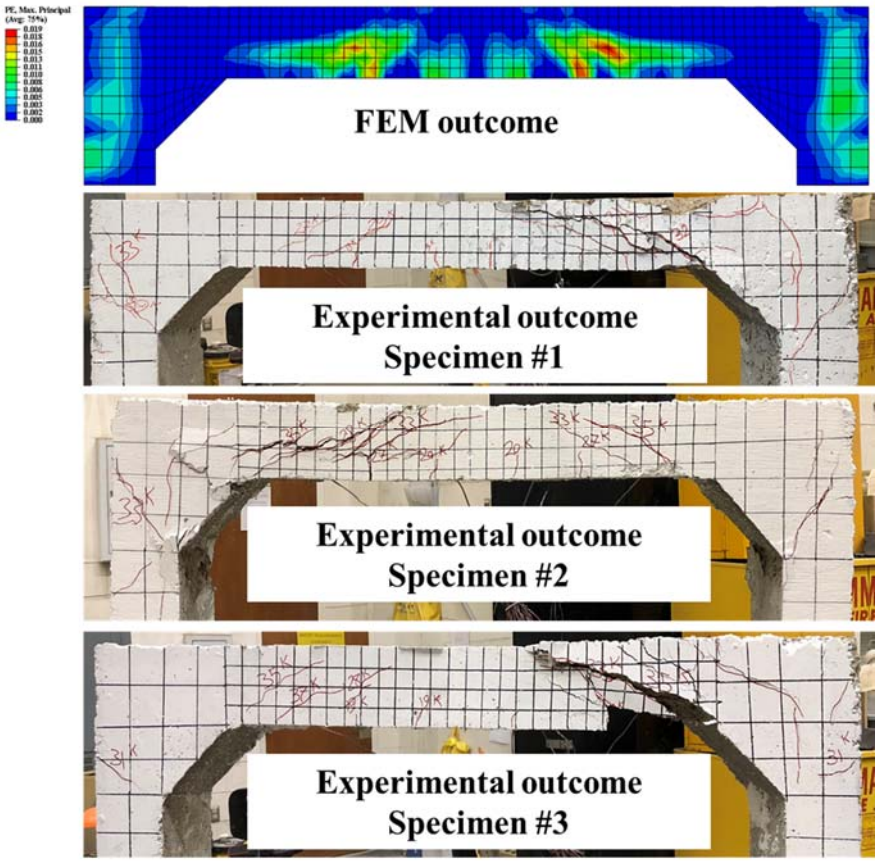

Figure 50. Validation of numerical model's crack pattern via experimental data for box culvert examined 3×3×4- ρ=2.22%- f_c^'=4.8 ksi (33.1 MPa)

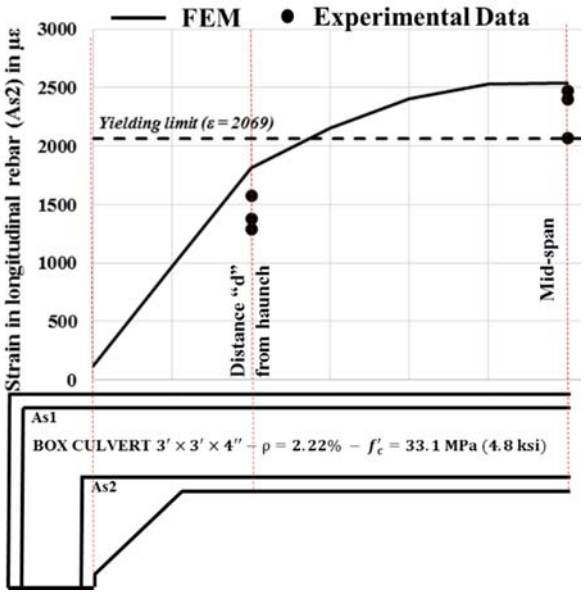

Figure 51. Comparison of numerical results with experimental data to predict the stain value in longitudinal rebar at failure

4.11. Effects of Box Culverts' Width

According to previous studies [16] and also considering the box culvert line as a plane-strain problem, the width of the member does not influence the shear strength of top slab to any appreciable degree. To check this conclusion, a reinforced concrete box culvert was investigated numerically, once with a 6 in. (152 mm) width, similar to the tested specimens; and then, the same box culvert with 144 in. (3658 mm) width. Except for the width, the material properties, boundary conditions, loading, analysis, etc. were identical in both models. Figure 52 illustrates finite element models of $12' \times 12' \times 16''$ box culverts with different widths. The amount of longitudinal reinforcement was 2.3%. The failure mode of both culverts was the same, and they failed in shear. The shear cracking occurred about distance "d" from haunch in both models. In order to have a quantity comparison, the shear stress in the section at distance "d" from haunch was plotted versus the deflection of the top slab's mid-span, as shown in Figure 53. This graph shows increasing the shear stress in the section up to failure. It should be noted that, in both models, the loading was a uniform pressure at the top slab that was applied following force control analysis. Thus, post-failure behavior of the members was not available. A slight difference in shear stress in the designated section was recorded when the width of member changed. This difference maximized at the failure by 13%. It can be concluded that a change in the box culvert width did not change the failure mode and only slightly affected the shear stress of the top slab.

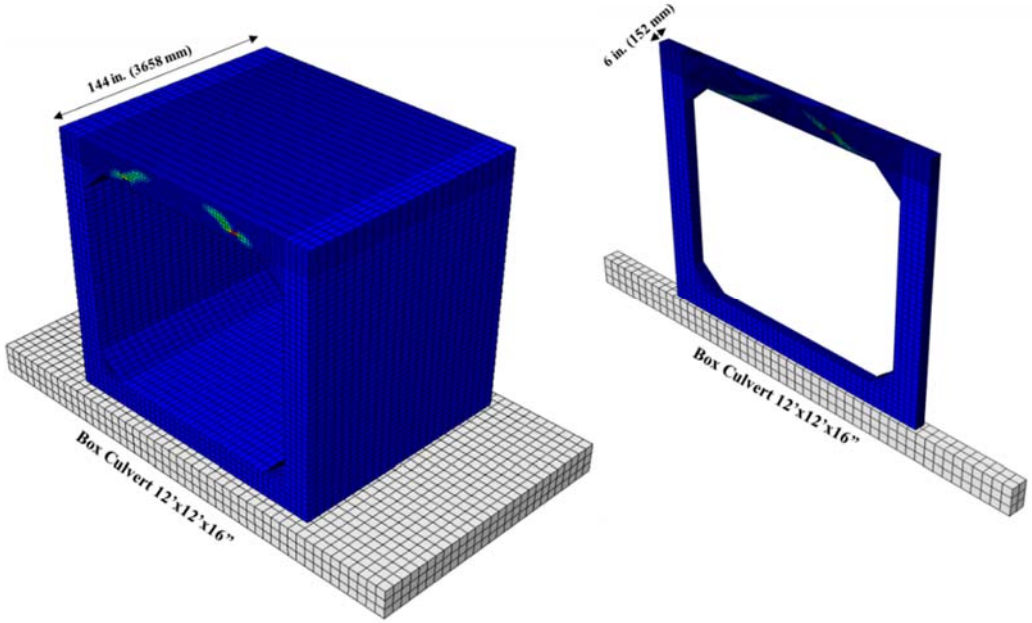

Figure 52. Comparison of box culvert's width in failure mode

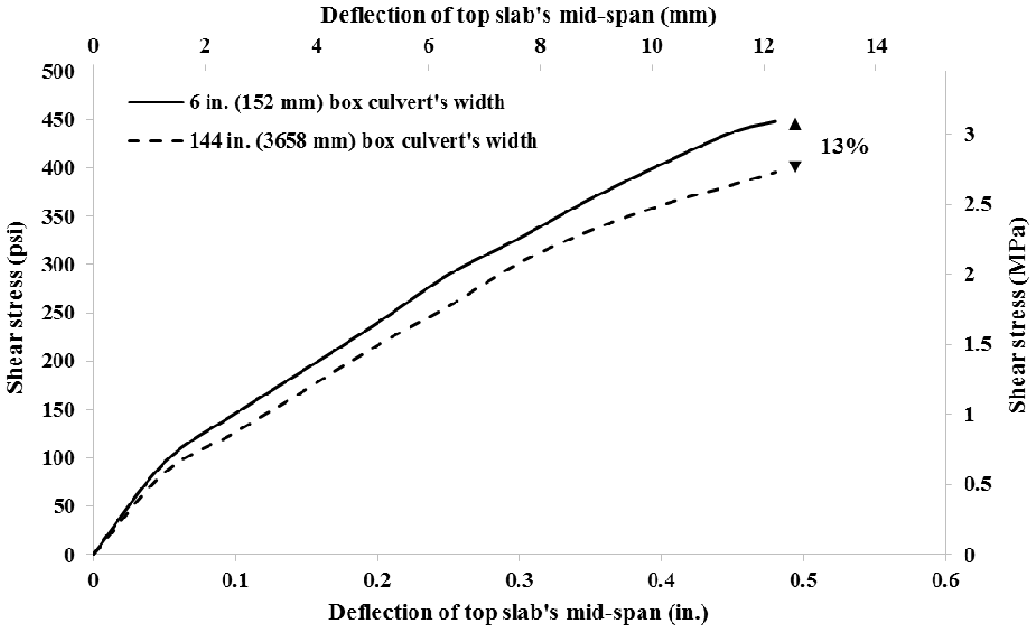

Figure 53. Shear stress at distance "d" from haunch versus deflection of top slab's mid-span up to failure

4.12. Size Effects in Shear Strength

An et al. [42] investigated the ability of numerical simulations to consider the effect of size on the shear strength of reinforced concrete beams. They concluded that the softening of tension and shear in concrete material, based on fracture energy, is one of the important factors to consider when assessing the effect of size on R.C. elements. To validate the ability of the numerical modeling in this research, a series of tested beams by Shioya et al. [8] was simulated using the finite element method. The experimental data indicated that an increase in the effective depth (d) of R.C. beams leads to a decrease in the shear stress. Figure 54 presents the results of a comparison between finite element analysis and experimental data. As was expected the finite element analysis successfully considers the size effect in reinforced concrete members.

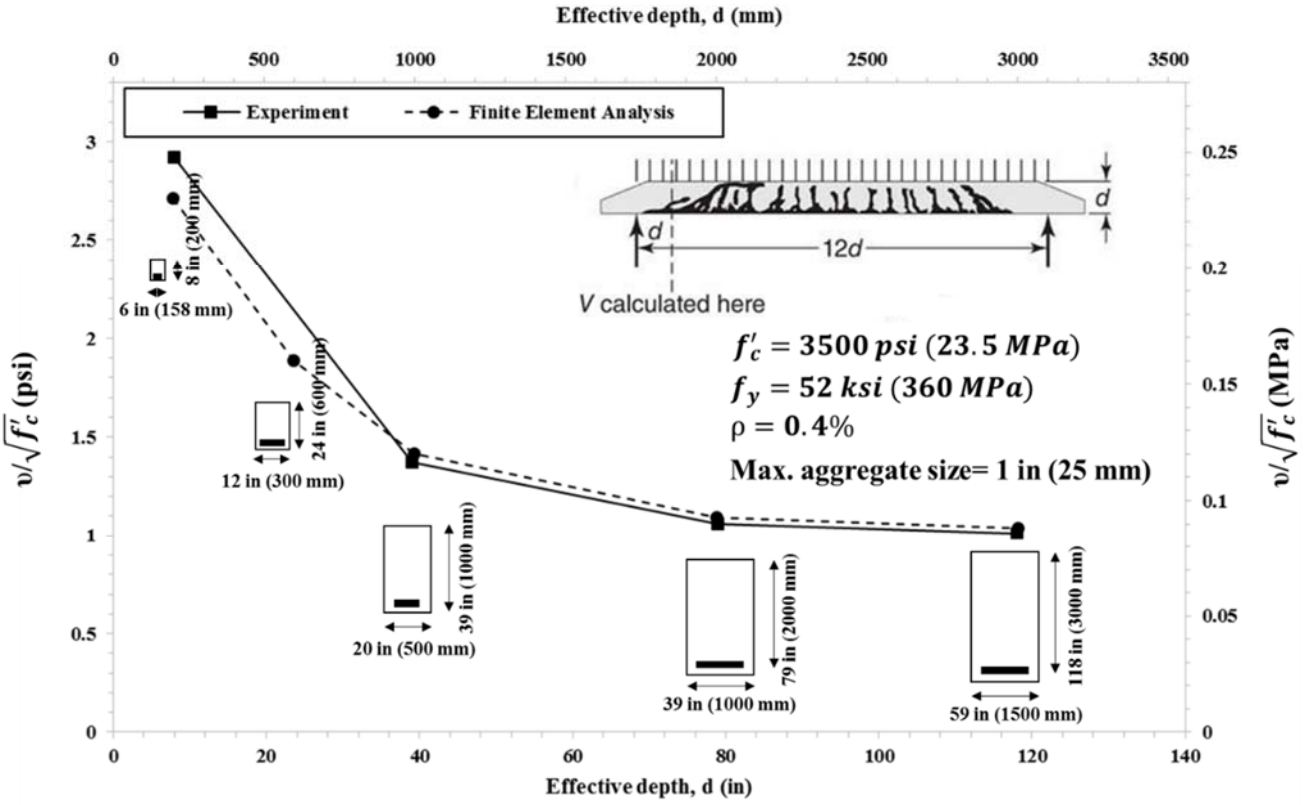

Figure 54. Validity of finite element method to consider size effect

4.12. Effects of Indeterminacy

In order to investigate the effects of indeterminacy in box culverts, a series of box culverts was analyzed and outcomes were compared with equivalent simply supported beams. To this end, six thickness of 4, 8, 12, 16, 20 and 24 inches (102, 204, 306, 408, 510 and 612 mm) for top slabs of box culverts were selected. All the six cases had span/thickness of 9 and span/rise of 1. Concrete with 5000 psi (34.5 MPa) compressive strength and Grade 60 ksi (420 MPa) steel rebar were assigned to the models. The ratio of longitudinal reinforcement was 2.3%. The shear stress at failure was calculated in a section at distance "d" from haunch for box culverts and in a section at distance "d" from support for beams. Figure 55 compares the shear stress of box culverts at failure with their equivalent simply supported beams. The results demonstrated that the shear strength of the top slabs of box culverts were much higher than that of the beams. For instance, for the case with a top slab thickness of 4 inches (102 mm), the maximum shear-stress/$\sqrt{f_c'}$ in the designated section was 7.3. This ratio was 4.8, if a similar section (section A-A in Figure 55) served in a simply supported beam. It should be noted that span/thickness in all beams was 9. The descending trend that appeared for the both box culverts and beams in this figure revealed the validity of finite element analysis in considering the size effect.

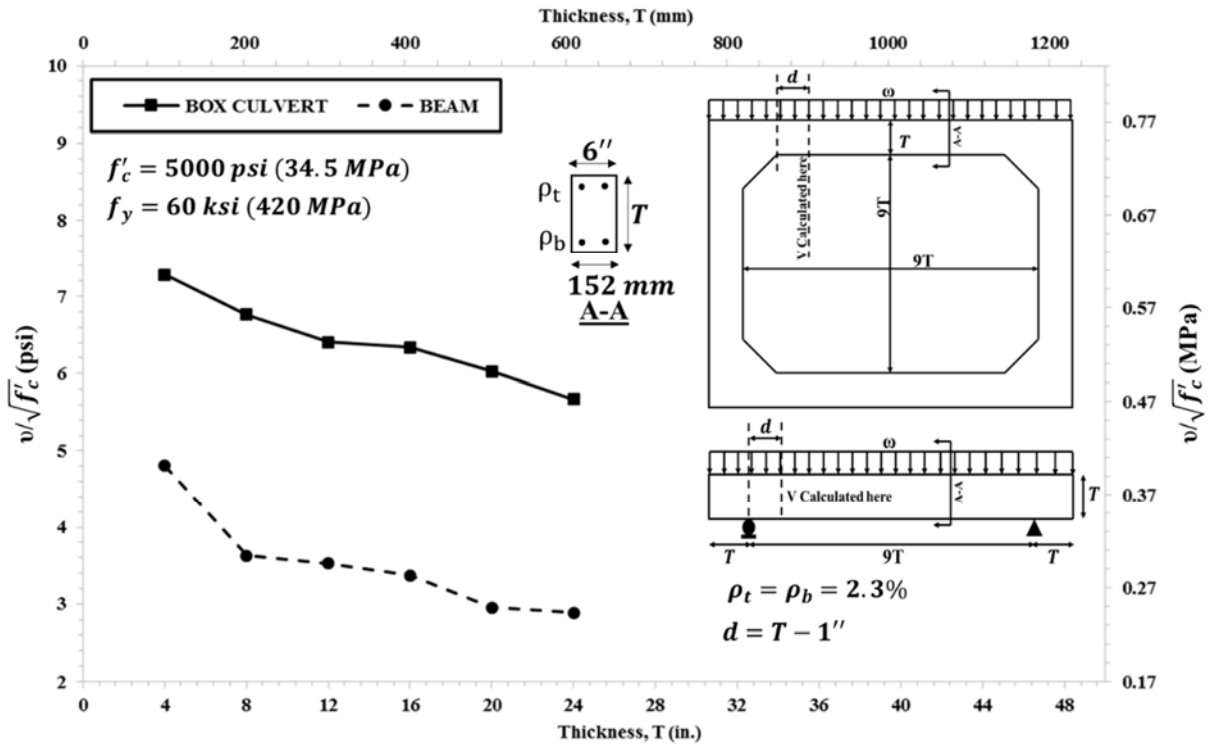

Figure 55. Comparison of the shear strength for box culverts and simply supported beams

Table 12 presents the failure load for each case. It also shows the shear force and bending moment in the designated sections at failure. A comparison of the results from finite element analysis and ACI318-14 [26] is presented in Table 12. The finite element analysis (FEA) agreed with ACI318-14 [26] in prediction of the shear strength of investigated R.C. beams; however, the FEA predicted on average 83% higher shear strength rather than ACI318-14 [26] for box culverts. According to these six cases, the failure load of box culverts was, on average 2.6 times, greater than that of the equivalent simply supported beams. Additionally, the shear strength in the critical section at the failure in box culverts averaged 1.85 times greater than that of the equivalent simply supported beams.

Table 12. Results of comparison of box culverts with simply supported beam

Thickness, in. (mm)	Element	Failure Load, kip/ft. (kN/m)	Ratio $\frac{\omega_{Box}}{\omega_{Beam}}$	Shear force at failure*, kip (kN)	Ratio	Bending moment at failure*, kip.ft. (kN.m)	ACI 318-14, kip (kN)	$\frac{V_{FEA}}{V_{ACI}}$
4 (102)	Beam	4.93 (71.9)	2.07	6.1 (27.1)	1.52	0.53 (0.72)	4.45 (19.8)	1.37
	Box	10.21 (148.9)		9.3 (41.4)		0.59 (0.8)	4.45 (19.8)	2.08
8 (204)	Beam	4.31 (62.9)	2.63	10.8 (48.1)	1.86	1.43 (1.94)	10.4 (46.2)	1.04
	Box	11.33 (165.3)		20.1 (89.4)		1.58 (2.14)	10.4 (46.2)	1.93
12 (306)	Beam	4.6 (67.1)	2.52	16.4 (73)	1.82	3.62 (4.91)	16.3 (72.7)	1
	Box	11.59 (169.1)		29.9 (133.1)		4.17 (5.66)	16.3 (72.7)	1.83
16 (408)	Beam	4.52 (65.9)	2.61	21.5 (95.7)	1.87	5.59 (7.58)	22.3 (99.1)	0.96
	Box	11.82 (172.4)		40.3 (179.3)		2.57 (3.48)	22.3 (99.1)	1.8
20 (510)	Beam	4.06 (59.2)	2.84	23.8 (105.9)	2.04	15.08 (20.47)	27.4 (121.9)	0.87
	Box	11.53 (168.2)		48.6 (216.3)		2.57 (3.49)	28.2 (125.5)	1.72
24 (612)	Beam	3.97 (57.9)	2.89	28.1 (125.1)	1.97	13.92 (18.9)	32.3 (143.9)	0.87
	Box	11.47 (167.3)		55.3 (246.1)		9.58 (13)	34.1 (152)	1.62
		Mean	**2.6**	**Mean**	**1.85**	**Average of beams**		**1.02**
						Average of boxes		**1.83**

* Shear force and bending moment were calculated in a section at distance "d" from haunch for box culverts and in a section at distance "d" from support for beams.

To better understand the differences in the behavior of box culverts and simply supported beams, shear force and bending moment diagrams were plotted for a culvert with a thickness of 4 inches (102 mm), as shown in Figure 56.

A difference in the failure modes of box culverts and beams could be the reason for higher shear strength. The propagation of cracks for a $12' \times 12' \times 16''$ box culvert and $12' \times 16''$ beam is illustrated in Figure 57. The failure mode of the beam, as a slender element, was flexural-shear mode; however, the box culvert failed in shear. The crack propagation in the beam indicated that the flexural cracks initiated, and then they became shear cracks (diagonal tension cracking). For box culverts, the crack propagation revealed that, unlike the beam, the shear cracks initiated at the early stages of loading, even before total development of flexural cracking. Redistribution of internal strains and stresses, due to indeterminacy, caused the locations of stress concentration to vary along the element. This action limited the development of flexural cracks.

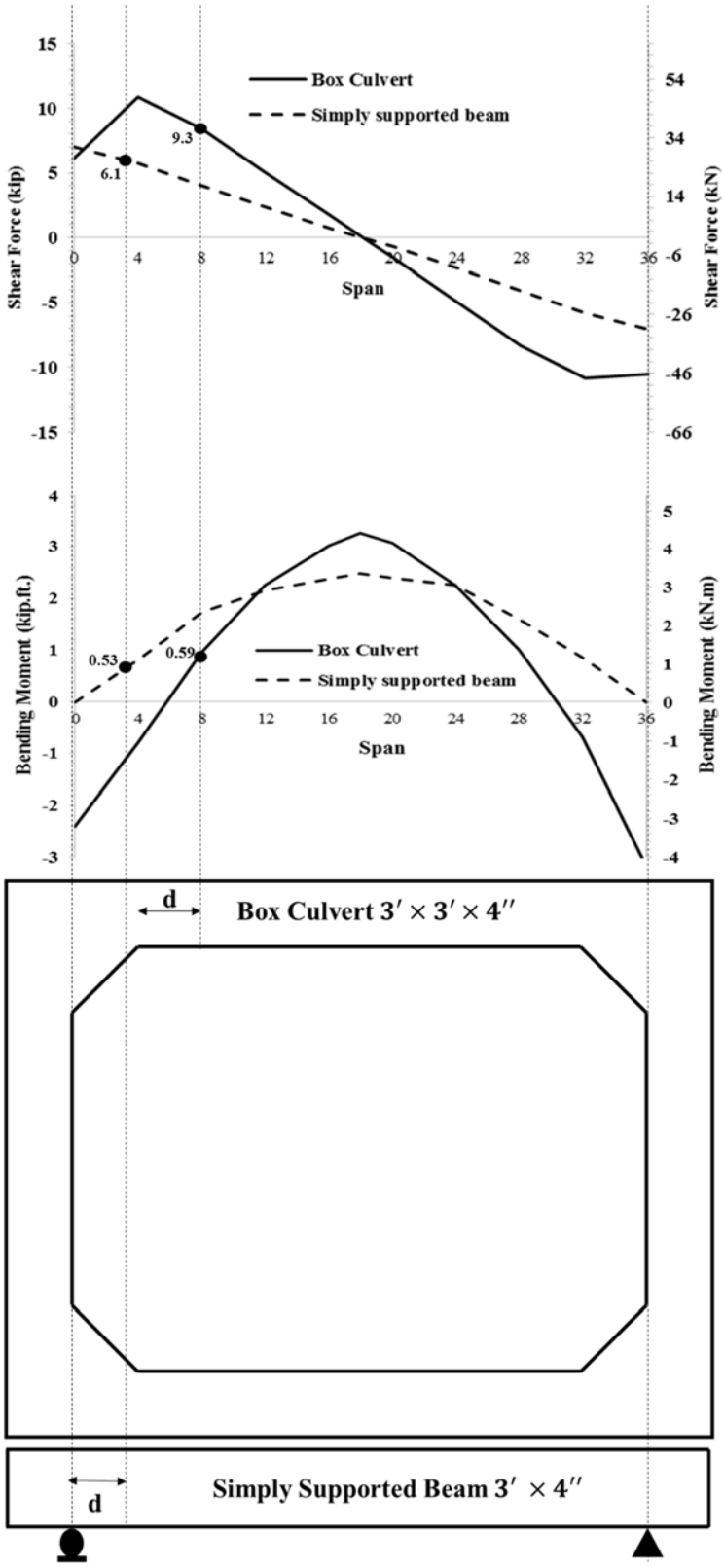

Figure 56. Shear force and bending moment diagrams for box culvert 3 × 3 × 4 and beam 3 × 4

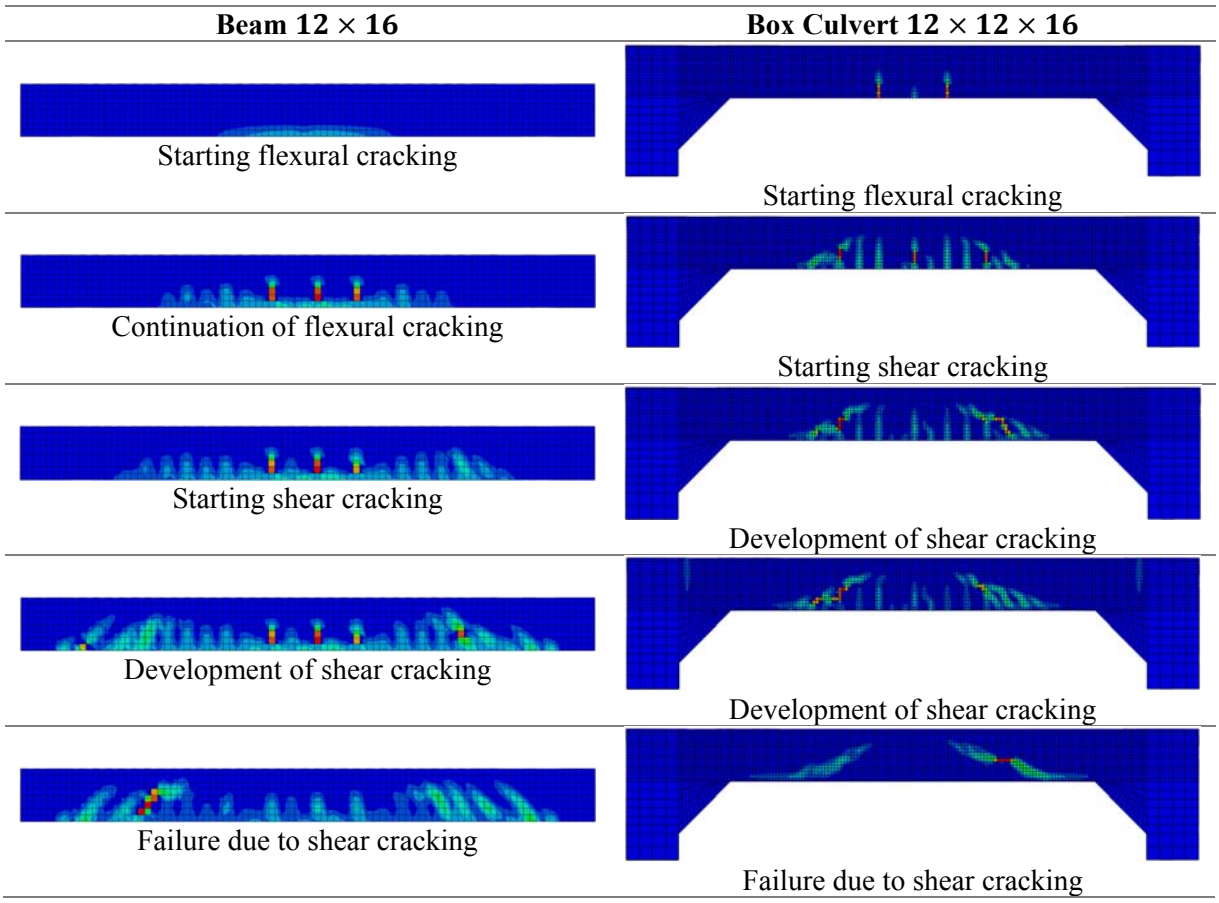

Figure 57. Comparison of crack propagation in box culverts and simply supported beams

4.13. Effects of Bedding

In the experimental investigation, as well as numerical modeling, the box culverts were placed on rigid bedding. The boundary conditions applied to a deformed shape of a box culvert under a uniformly distributed load at the top slab were similar to those applied to a box culvert placed on two roller supports, as illustrated in Figure 58a and 58b. A schematic bending moment and shear force diagrams for these boundary conditions and loading are given in Figure 58c and 58d. While the maximum shear force in the top slab was $\omega l/2$, the shear force in the walls was negligible and in the bottom slab was zero. If the bedding is not assumed rigid, depending on its module of

elasticity, a uniform load applies to the bottom slab. The worst scenario is when a uniform load with the same intensity (ω) applies to the bottom slab upward. In this case, the support reactions are zero. Figure 59 illustrates the loading, along with the bending moment and shear force diagrams. It indicates that variations in the rigidity of the bedding do not significantly affect the shear force and bending moment of the top slab; it only changes the internal stresses of the bottom slab. Therefore, considering a soil bedding with any module of elasticity results in less internal shear and fewer flexural stresses in the bottom slab than in the top one.

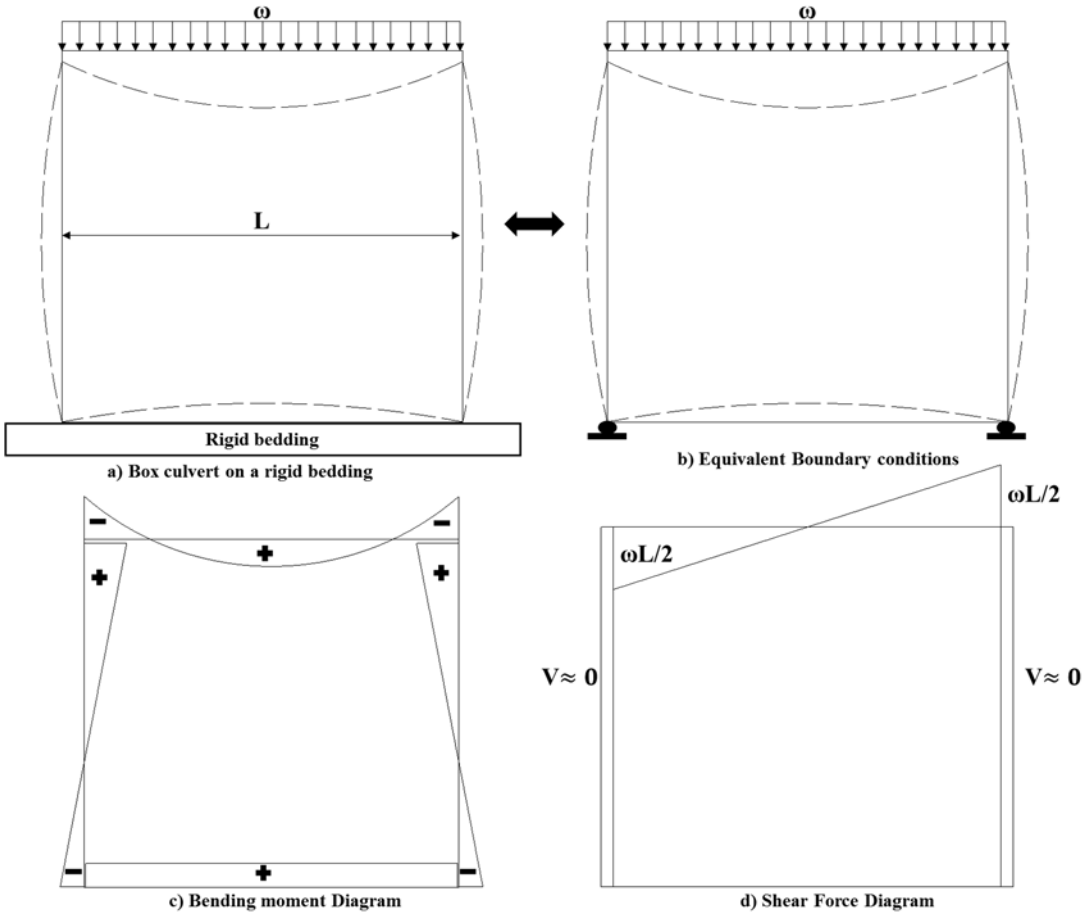

Figure 58. Box culvert on a rigid bedding: a) on a rigid bedding; b) equivalent boundary condition; c) bending moment diagram; d) shear force diagram

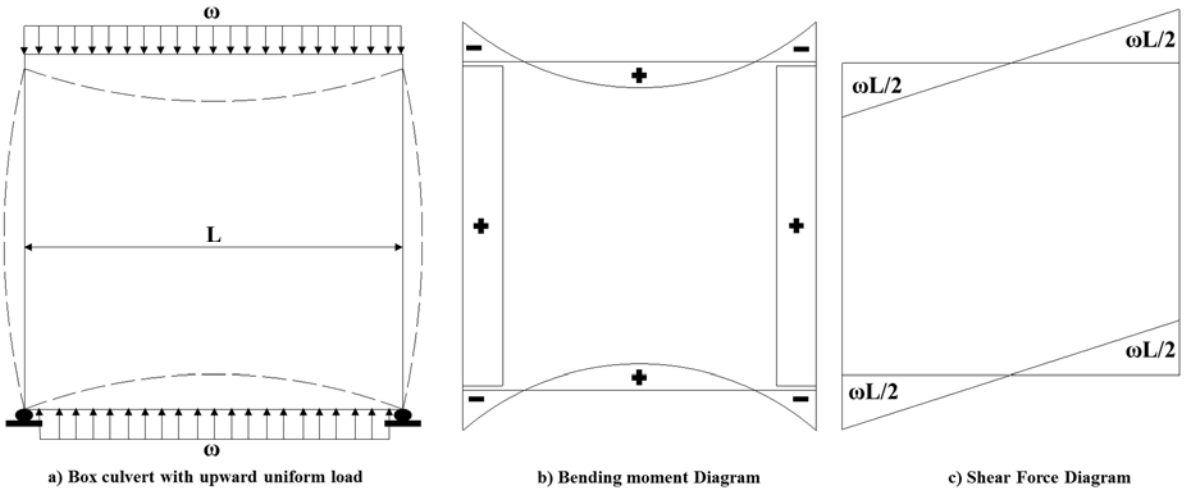

Figure 59. Box culvert with upward loading: a) a uniform load applies to the bottom slab; b) bending moment diagram; c) shear force diagram

CHAPTER 5. PARAMETRIC STUDY AND DESIGN CODES ASSESSMENTS

5.1. Overview

The parameters that impact the ultimate strength of the top slabs of R.C. box culverts were investigated, using the verified finite element models. The proposed framework was utilized to apply the equivalent uniformly distributed load, as illustrated in Figure 60. As it has already been concluded in this research that the width of box culverts does not influence the failure mode or maximum shear stress, all of the case studies were modeled with a width of 6 inches (102 mm). The ACI318-14 [26] shear design was evaluated for 108 cases. All of the cases with shear failure mode were used to assess the AASHTO specification. The purpose of the parametric study was to utilize the verified finite element models to investigate several sizes and concrete material properties of box culverts, thereby obtaining a wide range of results that would be helpful in extending the conclusion of this study to more cases in practice. It should be noted that the sizes studied in this parametric study were box culverts customized for fill heights up to 100 ft. (31,000 mm) and were beyond those of the tabulated sizes in ASTM C1577 [4]. The initial target was to have shear failure in every case, which is why the amount of longitudinal reinforcement selected was at least 1.3%.

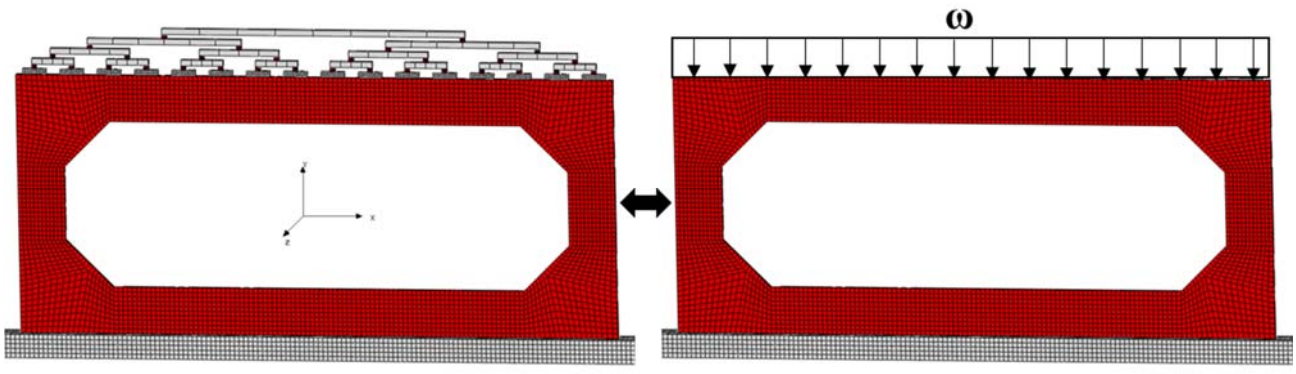

a) Proposed method for loading b) Equivalent distributed load

Figure 60.Finite element model and proposed framework for loading

5.2. Case Studies

Forty-eight (48) sizes of box culverts were studied, with spans (S) of 1830, 3660, 5490, and 7315 mm (6, 12, 18, and 24 ft.); rises (R) of 1830, 3660, and 4572 mm (6, 12, and 15 ft.); and top slab thicknesses (T) of 305, 406, 508, and 610 mm (12, 16, 20, and 24 in.). Longitudinal reinforcements (ρ) of 1.3% and 2.3% and three specified concrete compressive strengths (f_c') of 20.7, 34.5, and 48.3 MPa (3, 5, and 7 ksi) were applied. Thus, a total of 288 case studies were analyzed: $4(S) \times 3(R) \times 4(T) \times 2(\rho) \times 3(f_c') = 288$. The results of the parametric study are revealed in APPENDIX 3. Table 13 presents the characteristics of the case studies. The selected sizes were customized for deeply buried box culverts and were in shear behavioral mode; they are not tabulated in ASTM C1577 [4].

Table 13. The characteristics of case studies

No.	Size ($ft.\times ft.\times in.$)	ρ (%)		f_c' (MPa)			No.	Size($ft.\times ft.\times in.$)	ρ (%)		f_c' (MPa)		
1	$6\times6\times12$	1.3	2.3	20.7	34.5	48.3	**25**	$18\times6\times12$	1.3	2.3	20.7	34.5	48.3
2	$6\times6\times16$	1.3	2.3	20.7	34.5	48.3	**26**	$18\times6\times16$	1.3	2.3	20.7	34.5	48.3
3	$6\times6\times20$	1.3	2.3	20.7	34.5	48.3	**27**	$18\times6\times20$	1.3	2.3	20.7	34.5	48.3
4	$6\times6\times24$	1.3	2.3	20.7	34.5	48.3	**28**	$18\times6\times24$	1.3	2.3	20.7	34.5	48.3
5	$6\times12\times12$	1.3	2.3	20.7	34.5	48.3	**29**	$18\times12\times12$	1.3	2.3	20.7	34.5	48.3
6	$6\times12\times16$	1.3	2.3	20.7	34.5	48.3	**30**	$18\times12\times16$	1.3	2.3	20.7	34.5	48.3
7	$6\times12\times20$	1.3	2.3	20.7	34.5	48.3	**31**	$18\times12\times20$	1.3	2.3	20.7	34.5	48.3
8	$6\times12\times24$	1.3	2.3	20.7	34.5	48.3	**32**	$18\times12\times24$	1.3	2.3	20.7	34.5	48.3
9	$6\times15\times12$	1.3	2.3	20.7	34.5	48.3	**33**	$18\times15\times12$	1.3	2.3	20.7	34.5	48.3
10	$6\times15\times16$	1.3	2.3	20.7	34.5	48.3	**34**	$18\times15\times16$	1.3	2.3	20.7	34.5	48.3
11	$6\times15\times20$	1.3	2.3	20.7	34.5	48.3	**35**	$18\times15\times20$	1.3	2.3	20.7	34.5	48.3
12	$6\times15\times24$	1.3	2.3	20.7	34.5	48.3	**36**	$18\times15\times24$	1.3	2.3	20.7	34.5	48.3
13	$12\times6\times12$	1.3	2.3	20.7	34.5	48.3	**37**	$24\times6\times12$	1.3	2.3	20.7	34.5	48.3
14	$12\times6\times16$	1.3	2.3	20.7	34.5	48.3	**38**	$24\times6\times16$	1.3	2.3	20.7	34.5	48.3
15	$12\times6\times20$	1.3	2.3	20.7	34.5	48.3	**39**	$24\times6\times20$	1.3	2.3	20.7	34.5	48.3
16	$12\times6\times24$	1.3	2.3	20.7	34.5	48.3	**40**	$24\times6\times24$	1.3	2.3	20.7	34.5	48.3
17	$12\times12\times12$	1.3	2.3	20.7	34.5	48.3	**41**	$24\times12\times12$	1.3	2.3	20.7	34.5	48.3
18	$12\times12\times16$	1.3	2.3	20.7	34.5	48.3	**42**	$24\times12\times16$	1.3	2.3	20.7	34.5	48.3
19	$12\times12\times20$	1.3	2.3	20.7	34.5	48.3	**43**	$24\times12\times20$	1.3	2.3	20.7	34.5	48.3
20	$12\times12\times24$	1.3	2.3	20.7	34.5	48.3	**44**	$24\times12\times24$	1.3	2.3	20.7	34.5	48.3
21	$12\times15\times12$	1.3	2.3	20.7	34.5	48.3	**45**	$24\times15\times12$	1.3	2.3	20.7	34.5	48.3
22	$12\times15\times16$	1.3	2.3	20.7	34.5	48.3	**46**	$24\times15\times16$	1.3	2.3	20.7	34.5	48.3
23	$12\times15\times20$	1.3	2.3	20.7	34.5	48.3	**47**	$24\times15\times20$	1.3	2.3	20.7	34.5	48.3
24	$12\times15\times24$	1.3	2.3	20.7	34.5	48.3	**48**	$24\times15\times24$	1.3	2.3	20.7	34.5	48.3

Figure 61 shows the strain-stress curve for the concrete material in compression and tension that was used in the parametric study. A steel rebar with 420 MPa (60 ksi) yielding stress and 200 GPa (29,000 ksi) module of elasticity associated with elastic and plastic behavior was used to model the longitudinal reinforcement.

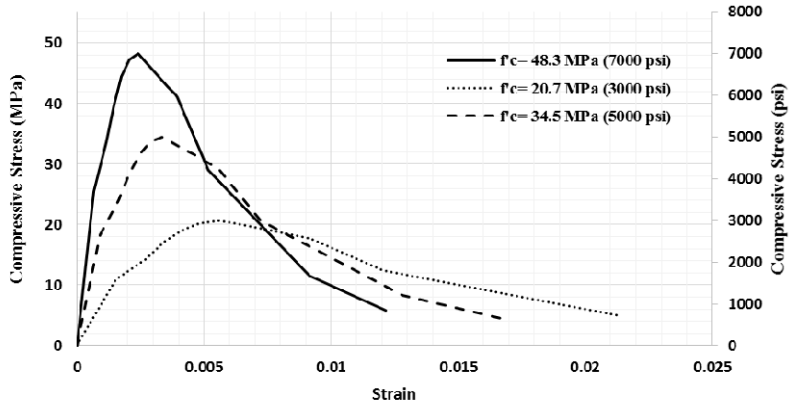

a) Compression

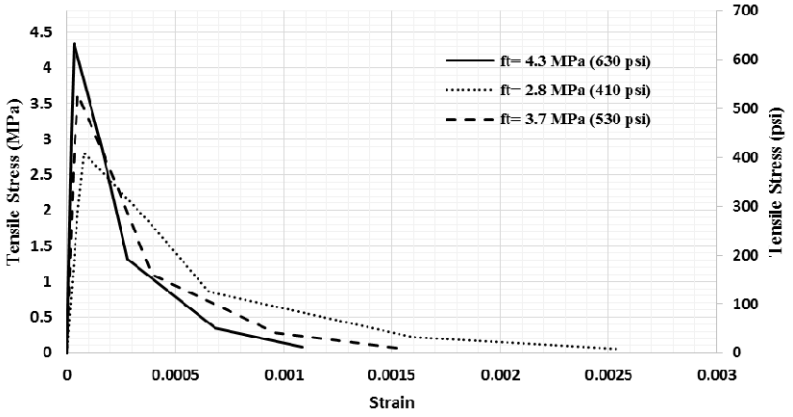

b) Tension

Figure 61.Strain-stress curve for concrete material; a) in compression; b) in tension

The cracking pattern was one of the indicators used in this study to determine the failure mode of each case. The box culverts failed with flexural cracking, primarily in both end zones of the top slab, where the maximum negative moment occurred. The cases with diagonal tension cracks (inclined cracking) in the top slabs were detected as shear failure mode. Some cases had combined shear and flexural failure mode, with both shear cracks in the top slab and flexural cracks at the

end of the slab, where the slab and wall connected. Figure 62 compares cracking patterns for different failure modes in the top slab. It should be noted that the cracks shown in Figure 62 are the major cracks. There were also some minor cracks in different locations, but they do not appear in this figure.

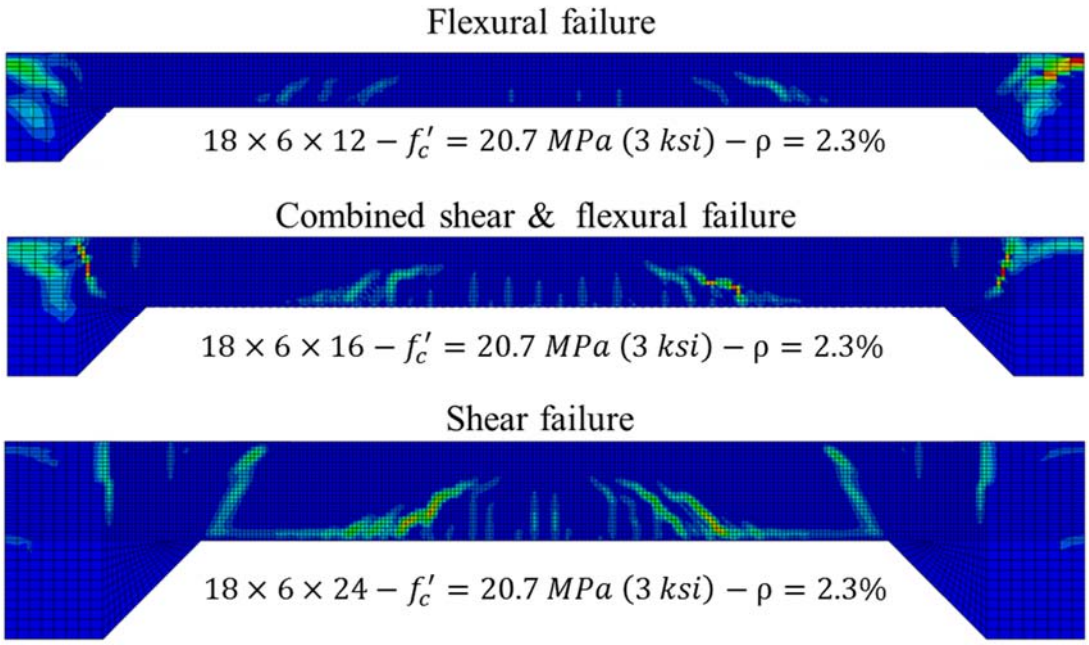

Figure 62. Indication of failure mode based on cracking pattern

5.3. Results and Discussions

The first step of the study was to determine the failure load of each box culvert. Figure 63 exhibits the total failure load and failure mode for all of the case studies. The total failure load is the length of the span times the uniform load ($span\ (mm) \times\ \omega\ (N/mm)$). A total of 54 cases studies had flexural failure mode, and 24 cases had a combination of the shear and flexural failure modes. The rest of case studies, as was expected, had shear failure mode. The shear force, bending moment, and the strain in the longitudinal rebar in the section at distance "d" from haunch were obtained from finite element analysis at failure.

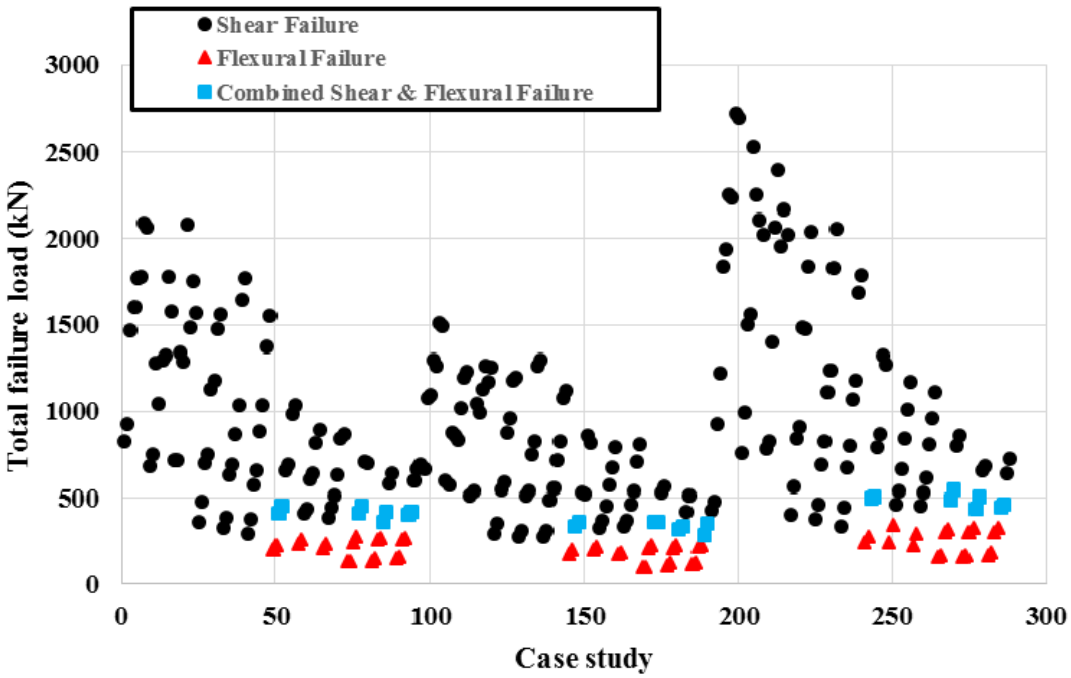

Figure 63. Total failure load and failure mode for each case study

As was anticipated, an increase in ρ, f_c' or T led to an increase in the ultimate strength of the top slab of the R.C. box culverts. Figures 64 and 65 show the variations of the strength of the top slab of the investigated box culverts when the S/R and S/T ratios varied. An increase in the S/R ratio led to a slight decrease in the total failure load; however, an increase in S/T led to a significant decrease in the total failure load. The cases with flexural failure mode had the highest S/T ratios (18 and 24). Thus, as was expected, the higher S/T ratio for the top slab of the R.C. box culverts imposed the flexural behavioral mode, and the lower S/T ratio imposed the shear failure mode associated with the highest total failure load.

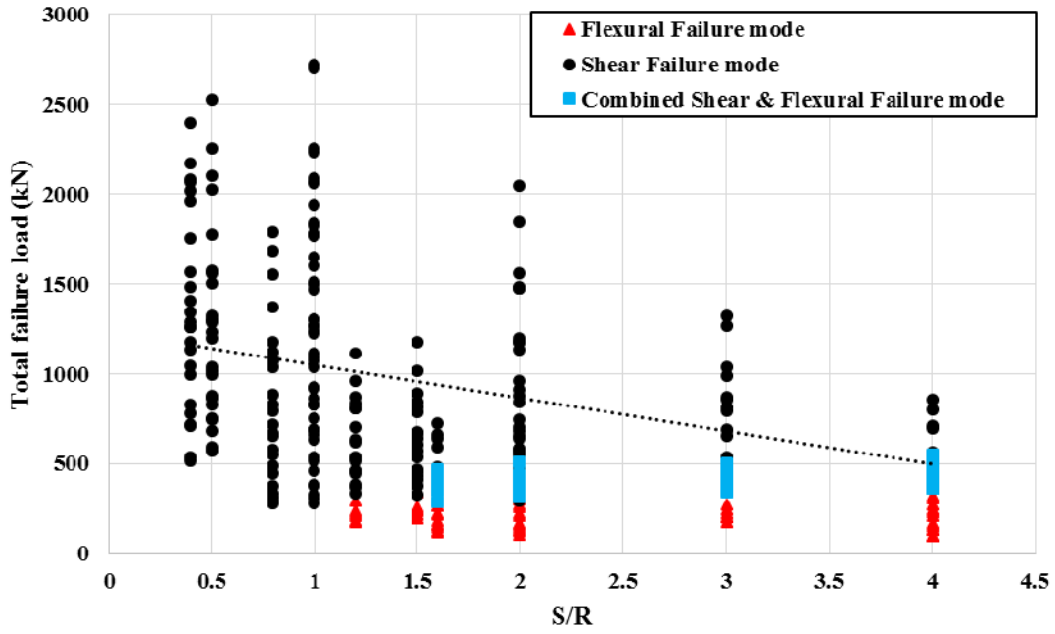

Figure 64. Variations of the total failure load vs change in S/R

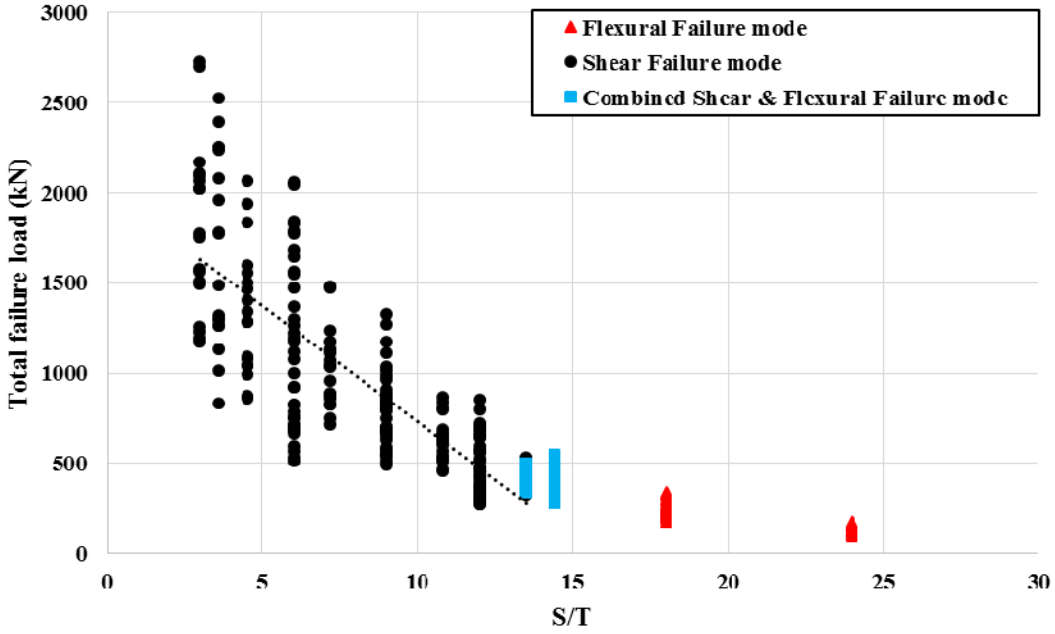

Figure 65. Variations of the total failure load vs change in S/T

The case studies associated with shear behavioral mode in the parametric study were filtered in order to assess the formulation of design codes. Among 288 case studies, 210 cases had shear failure mode. The total shear load carried by box culverts at failure versus the shear force in section at distance "d" from haunch was plotted and is shown in Figure 66. The total shear load represents

all forces transferred though the box culvert to the rigid base. Since a uniformly distributed load was applied at the top slab, a portion of the applied load was transferred axially by the walls. Thus, in the shear critical section in the top slab, the total shear force was much higher than two times the shear force. Since the shear failure of the box culverts was a local failure in the top slab, the shear strength of the top slab was considered in evaluating the shear design methodology of codes and specifications.

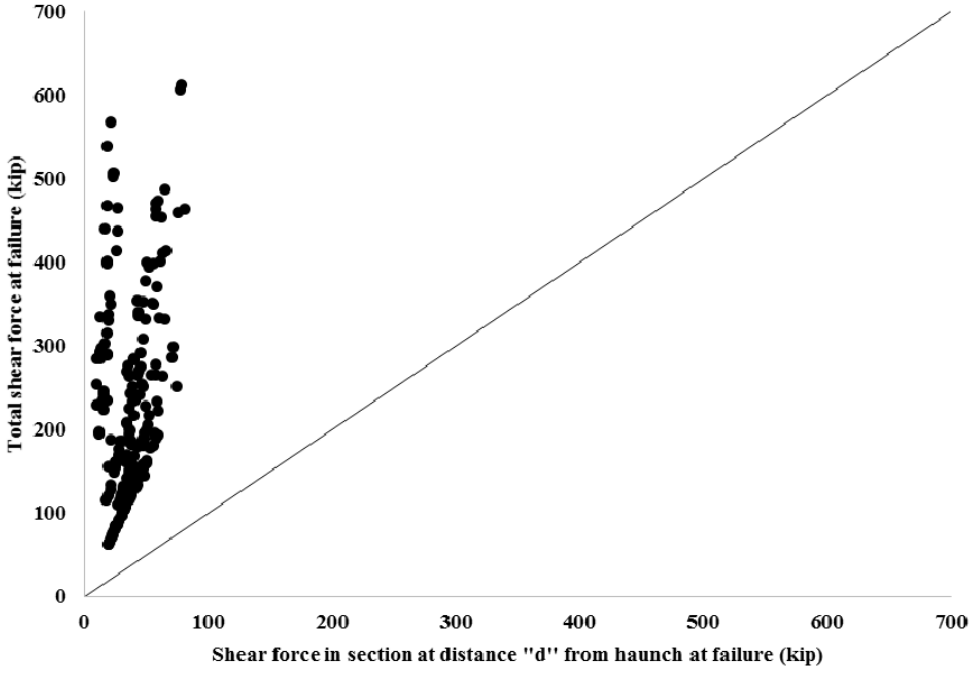

Figure 66. Comparison of total shear force and the shear force at the critical section in top slab

Depending on the geometry of box culverts, mostly S/T, the location of shear cracking varies along the span of the box culverts. For S/T<6, the shear cracking happened close to the haunch and even, in some cases, before the tip of the haunch. Although these case failed in shear, diagonal tension cracks occurred in cases with S/T>6, and shear cracking occurred, due to compressive stresses, for cases associated with S/T<6. Figure 67 illustrates the location of the shear cracking along the span

of the top slab. Most of the shear cracking occurred close to distance “d” from haunch and toward the mid-span.

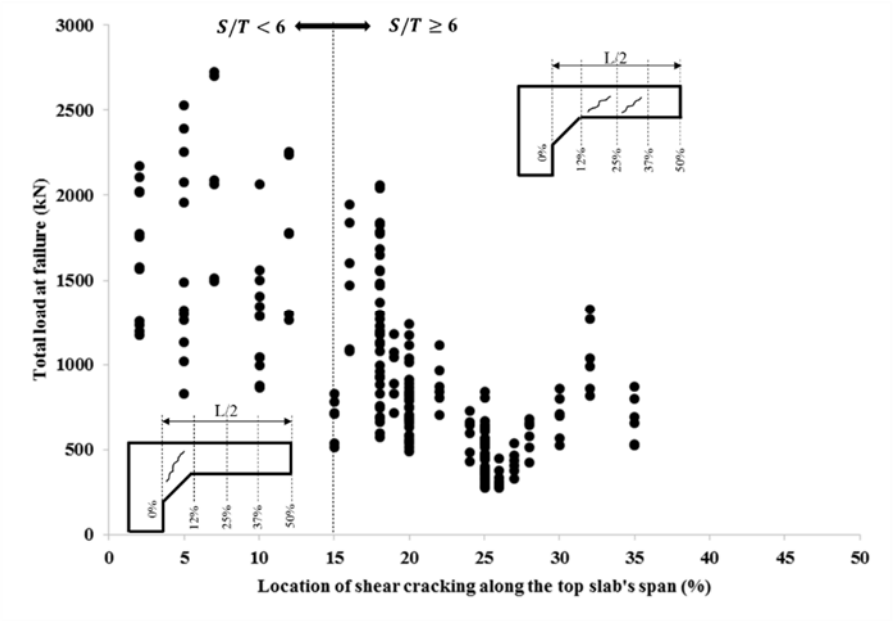

Figure 67. Shear cracking location for case studies with shear failure mode

There were two different shear failure modes: diagonal tension failure for cases with $S/T \geq 6$ and shear compression failure for cases with $S/T < 6$. Figure 68 illustrates these two shear failure modes.

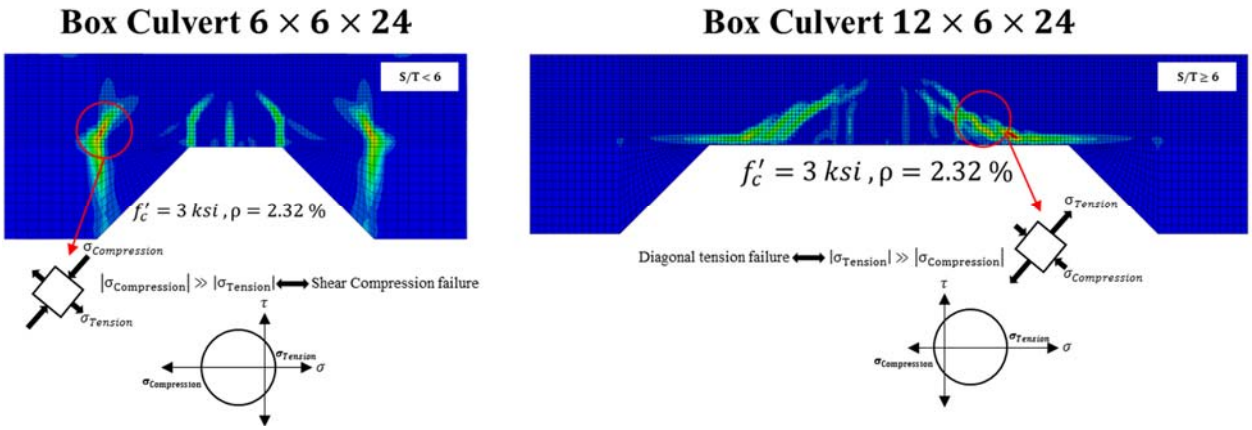

Figure 68. Different types of shear failure

More shear compression failures occurred in cases with a thick top slab than due to the length of the spans. The applied load was transferred to the top slab with virtually no bending in the top slab. Cases with $S/T < 6$ were not practical and were induced during the development of the parametric cases by varying different independent parameters. For example, box culverts buried in deep fill with a span of 6 ft. and thickness values between 16 in. and 24 in., as shown in Table 14, are outside of common design procedures. Tables 14 presents the characteristics of those cases with $S/T < 6$. It should be noted that three concrete compressive strengths (f_c') were analyzed for each size; thus there were 36 cases.

Table 14. Characteristics of cases with S/T<6

No.	Size ($ft.\times ft.\times in.$)	ρ%	Span ft.	Rise ft.	Thickness in.	S/R	S/T
1	$6\times6\times16$	1.3	6	6	16	1	4.5
2	$6\times6\times16$	2.3	6	6	16	1	4.5
3	$6\times6\times20$	1.3	6	6	20	1	3.6
4	$6\times6\times20$	2.3	6	6	20	1	3.6
5	$6\times6\times24$	1.3	6	6	24	1	3
6	$6\times6\times24$	2.3	6	6	24	1	3
7	$6\times12\times16$	1.3	6	12	16	0.5	4.5
8	$6\times12\times16$	2.3	6	12	16	0.5	4.5
9	$6\times12\times20$	1.3	6	12	20	0.5	3.6
10	$6\times12\times20$	2.3	6	12	20	0.5	3.6
11	$6\times12\times24$	1.3	6	12	24	0.5	3
12	$6\times12\times24$	2.3	6	12	24	0.5	3
13	$6\times15\times16$	1.3	6	15	16	0.4	4.5
14	$6\times15\times16$	2.3	6	15	16	0.4	4.5
15	$6\times15\times20$	1.3	6	15	20	0.4	3.6
16	$6\times15\times20$	2.3	6	15	20	0.4	3.6
17	$6\times15\times24$	1.3	6	15	24	0.4	3
18	$6\times12\times24$	2.3	6	15	24	0.4	3

5.4. ACI318-14

A total of 108 case studies were investigated to evaluate the ACI318-14 [26] shear design methodology. This parametric study included four different values for each box culvert's span: three for the rise, four for the top slab's thickness, two for the amount of longitudinal reinforcement, and three for the concrete compressive strength. All of these cases were larger than those tabulated in ASTM C1577 [4] that were associated with shear failure mode in the top slab. Table 15 depicts the characteristics of the case studies for evaluating the ACI318-14 [26] code. The chosen sizes represent deeply buried R.C. box culverts for which the designer had to increase the thickness of the top slab to meet the requirements for flexural loads, since the increase in the amount of longitudinal reinforcement was restricted by design codes. The shear strength of the top slab, as well as the critical shear section of each case study, was determined by finite element analysis. It should be noted that the critical shear section contained a diagonal shear crack. The internal shear force in the critical shear section at the failure (peak load) was the concrete shear strength of the top slab. The analysis results were compared with ACI318-14's formulation.

5.4.1. Methodology

ACI318-14 methodology is described in Section 3.5.1.

5.4.2. Assessment

Figure 69 illustrates the internal shear force and bending moment of the peak load in a section of the top slab where shear failure occurred in all four tested reinforced concrete box culverts in the experimental program. The shear force of the section at the failure represented the shear strength of the box culvert's top slab. Table 16 compares using Equation (3-1) with the obtained shear capacity from the FEM outputs for the four tested R.C. box culverts. This comparison reveals that the verified finite element analysis determined higher shear strength for the investigated R.C. box

culverts' top slab than ACI318-14's shear design methodology. It also indicates that an increase in the span/rise ratio led to a decrease in the difference between the analysis results and ACI318-14's prediction.

Table 15. Case study characteristics for evaluation of ACI318-14

No.	Box Culvert Size ($ft.\times ft.\times in.$)	ρ^* (%)	f'_c ksi (MPa)		
1	6 × 6 × 12	1.33	3 (21)	5 (34)	7 (48)
2	6 × 6 × 12	2.27	3 (21)	5 (34)	7 (48)
3	6 × 6 × 16	1.33	3 (21)	5 (34)	7 (48)
4	6 × 6 × 16	2.31	3 (21)	5 (34)	7 (48)
5	12 × 6 × 12	1.33	3 (21)	5 (34)	7 (48)
6	12 × 6 × 12	2.27	3 (21)	5 (34)	7 (48)
7	12 × 6 × 16	1.33	3 (21)	5 (34)	7 (48)
8	12 × 6 × 16	2.31	3 (21)	5 (34)	7 (48)
9	12 × 6 × 20	1.38	3 (21)	5 (34)	7 (48)
10	12 × 6 × 20	2.44	3 (21)	5 (34)	7 (48)
11	12 × 12 × 12	1.33	3 (21)	5 (34)	7 (48)
12	12 × 12 × 12	2.27	3 (21)	5 (34)	7 (48)
13	12 × 12 × 16	1.33	3 (21)	5 (34)	7 (48)
14	12 × 12 × 16	2.31	3 (21)	5 (34)	7 (48)
15	12 × 12 × 20	1.38	3 (21)	5 (34)	7 (48)
16	12 × 12 × 20	2.44	3 (21)	5 (34)	7 (48)
17	18 × 6 × 20	1.38	3 (21)	5 (34)	7 (48)
18	18 × 6 × 20	2.44	3 (21)	5 (34)	7 (48)
19	18 × 6 × 24	1.45	3 (21)	5 (34)	7 (48)
20	18 × 6 × 24	2.32	3 (21)	5 (34)	7 (48)
21	18 × 12 × 20	1.38	3 (21)	5 (34)	7 (48)
22	18 × 12 × 20	2.44	3 (21)	5 (34)	7 (48)
23	18 × 12 × 24	1.45	3 (21)	5 (34)	7 (48)
24	18 × 12 × 24	2.32	3 (21)	5 (34)	7 (48)
25	18 × 15 × 20	1.38	3 (21)	5 (34)	7 (48)
26	18 × 15 × 20	2.44	3 (21)	5 (34)	7 (48)
27	18 × 15 × 24	1.45	3 (21)	5 (34)	7 (48)
28	18 × 15 × 24	2.32	3 (21)	5 (34)	7 (48)
29	24 × 12 × 20	1.38	3 (21)	5 (34)	7 (48)
30	24 × 12 × 20	2.44	3 (21)	5 (34)	7 (48)
31	24 × 12 × 24	1.45	3 (21)	5 (34)	7 (48)
32	24 × 12 × 24	2.32	3 (21)	5 (34)	7 (48)
33	24 × 15 × 20	1.38	3 (21)	5 (34)	7 (48)
34	24 × 15 × 20	2.44	3 (21)	5 (34)	7 (48)
35	24 × 15 × 24	1.45	3 (21)	5 (34)	7 (48)
36	24 × 15 × 24	2.32	3 (21)	5 (34)	7 (48)

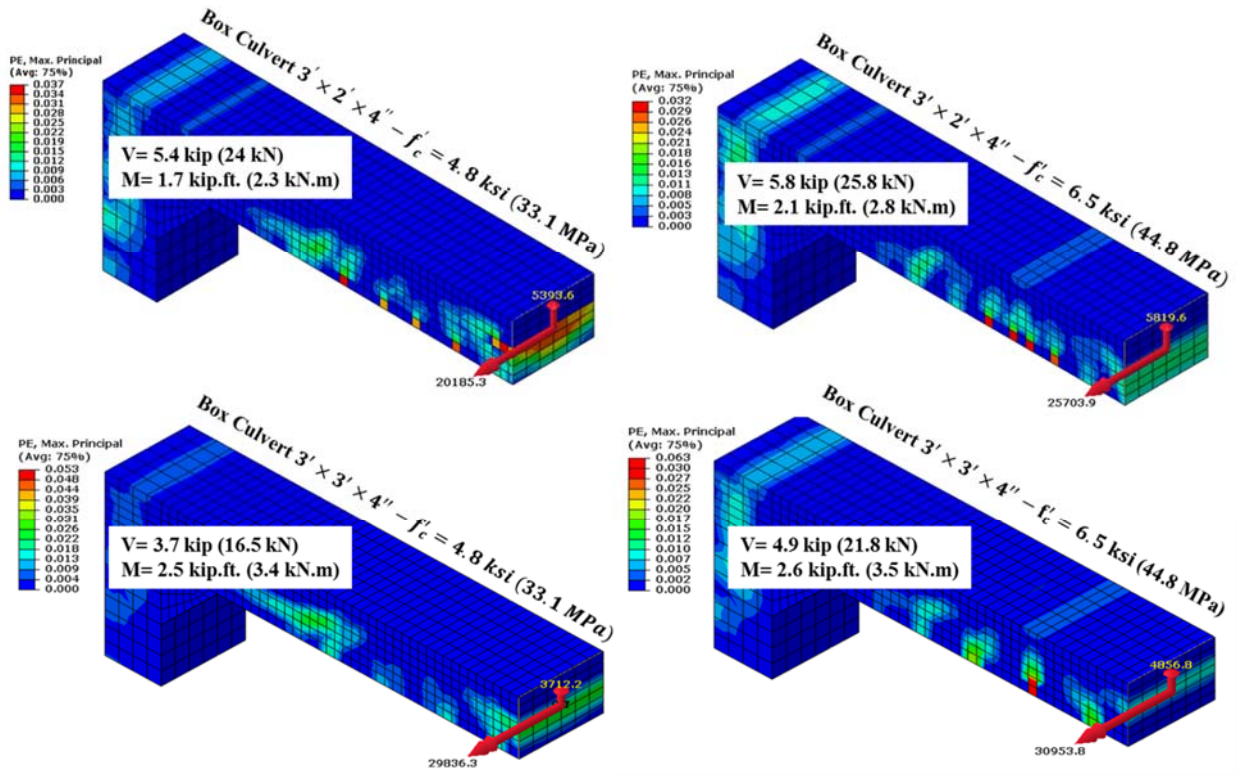

Figure 69. The shear strength and bending moment of the critical shear section in top slab at failure from FEA for the examined box culverts

Table 16. Comparison of the examined R.C. box culverts with ACI318-14

Box Culvert Size ($ft.\times ft.\times in.$)	f'_c, ksi (MPa)	Shear strength in *C.S from FEM, kip (kN)	Bending moment in *C.S from FEM, kip.ft. (kN.m)	Shear strength in *C.S from ACI318-14, kip (kN)	$\frac{V_{FEM}}{V_{ACI318-14}}$
$3\times2\times4$	4.8 (33.1)	5.4 (24)	1.7 (2.3)	3.2(14)	1.69
$3\times2\times4$	6.5 (44.8)	5.8 (26)	2.1 (2.8)	3.5 (16)	1.66
$3\times3\times4$	4.8 (33.1)	3.7 (16)	2.5 (3.4)	2.8 (12)	1.32
$3\times3\times4$	6.5 (44.8)	4.9 (22)	2.6 (3.5)	3.3 (15)	1.48

APPENDIX 3 shows the shear force and the bending moment in the critical section, and ACI318-14's prediction for shear strength. The results indicated that the shear strength of the box culvert's top slab was predicted by numerical analysis to be, on average, 66% greater than that predicted by ACI318-14's shear design methodology. Equation (3-1c) didn't govern in any of the cases studied. In 71 cases, Equation (3-1a) governed; and in 37 cases, Equation (3-1b) governed to determine

Vc. In 15 cases studied, all of which had the longest span length (24 ft.) and a ratio of $\frac{V_{FEM}}{V_{ACI318-14}}$ greater than 0.8, the shear strength predicted by FEA was less than the code's estimation. Figure 70 shows a comparison of the shear strength of the R.C. box culverts' top slab obtained from the analyses outputs of Equations (3-1a) to (3-1c) and ACI318-14's prediction (minimum of Equations (3-1a) to (3-1c)). The points below the 45 degree dashed line in these figures indicate the cases for which the proposed shear strength was lower, according to the FEM, than per the equation. Using Equation (3-1a) resulted in the prediction of shear strength, on average, 78% lower than that of the FEM outcomes, and 25 cases were below the dashed line. The ratios of Equations (3-1b) and (3-1c) to the proposed shear strength were 0.62 and 0.84, respectively. There were 21 and 55 cases below the dashed line for Equations (3-1b) and (3-1c), respectively. The variations of the proposed shear strength of ACI318-14's prediction ratio versus the span/rise ratio was plotted and is shown in Figure 71. An increase in the span/rise ratio led to a slight decrease in the difference between the analysis results and the ACI318-14 formulation. There were cases with span/rise ratios of 1.6 and 2 with $\frac{V_{FEM}}{V_{ACI318-14}}$ less than 1. Figure 72 describes the variations of the proposed shear strength of ACI318-14's prediction ratio versus the span/top slab's thickness ratio. This figure reveals that an increase in the span/top slab's thickness ratio led to a significant decrease in the difference between the analysis results and ACI318-14's formulation. The ratio of $\frac{V_{FEM}}{V_{ACI318-14}}$ was less than 1 for some cases with a span/top slab's thickness ratio of 12 and almost all cases with a ratio of 14.4.

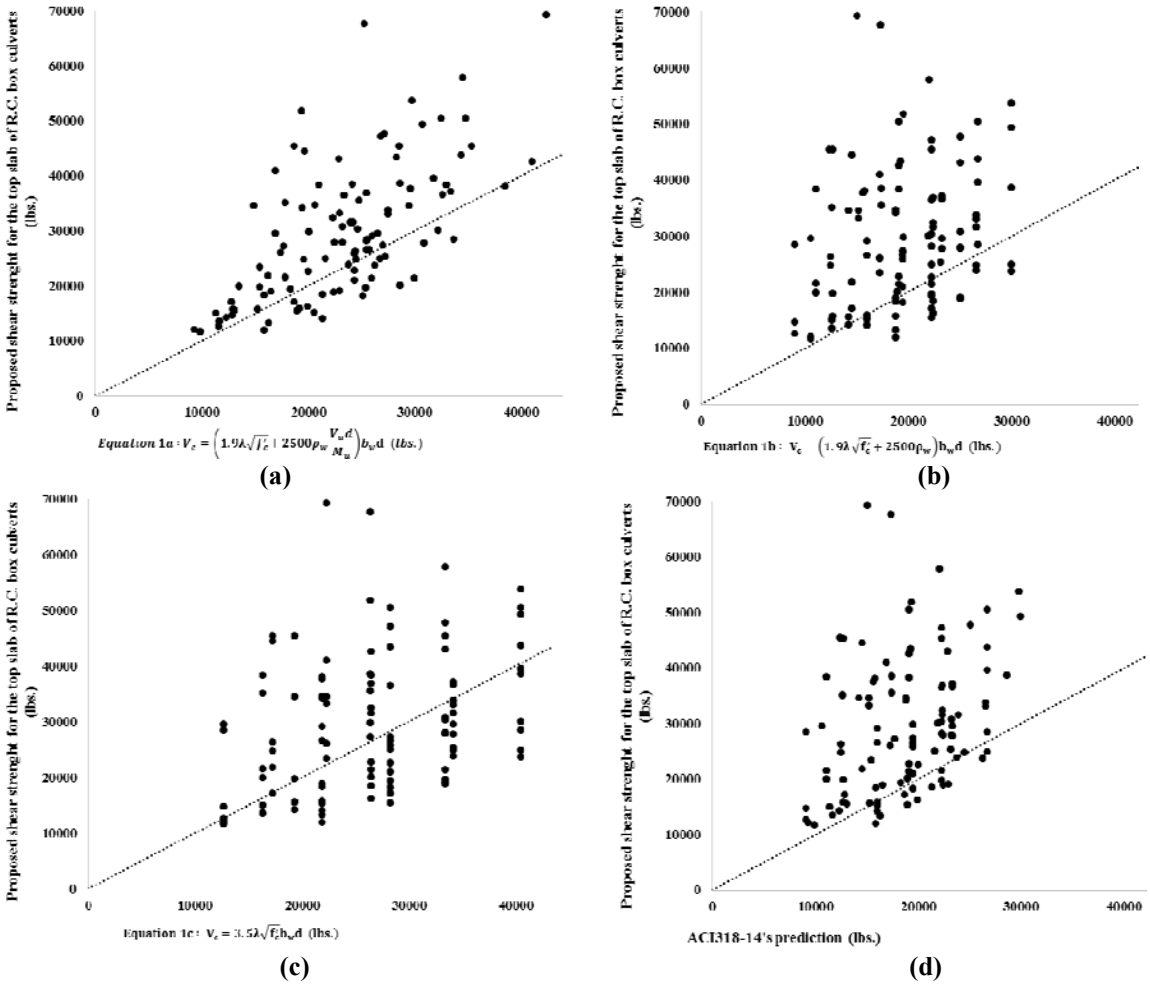

Figure 70. Comparison of analysis outcomes with ACI318-14's shear formulations: a) comparison with Equation 3-1a, b) comparison with Equation 3-1b, c) comparison with Equation 3-1c, d) comparison with ACI318-14's prediction (1 lbs. = 0.00445 kN)

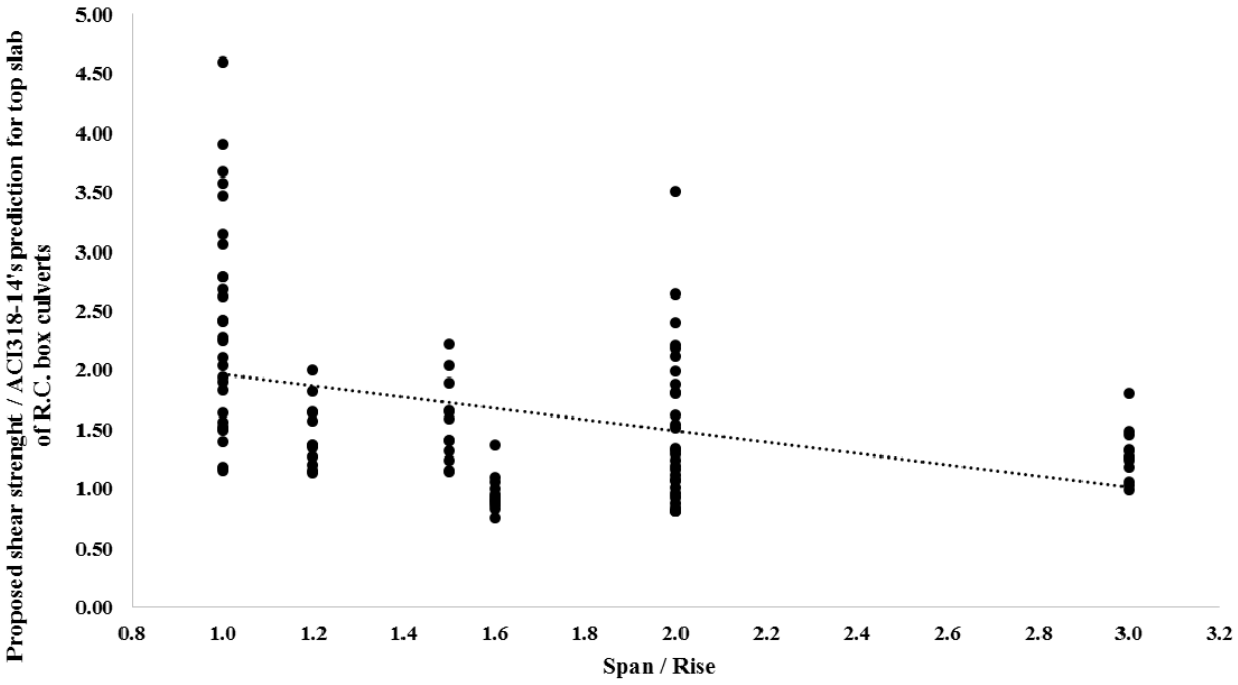

Figure 71. Variations of $V_{FEM}/V_{(ACI318-14)}$ versus span/rise for R.C. box culverts' top slab under uniformly distributed loads

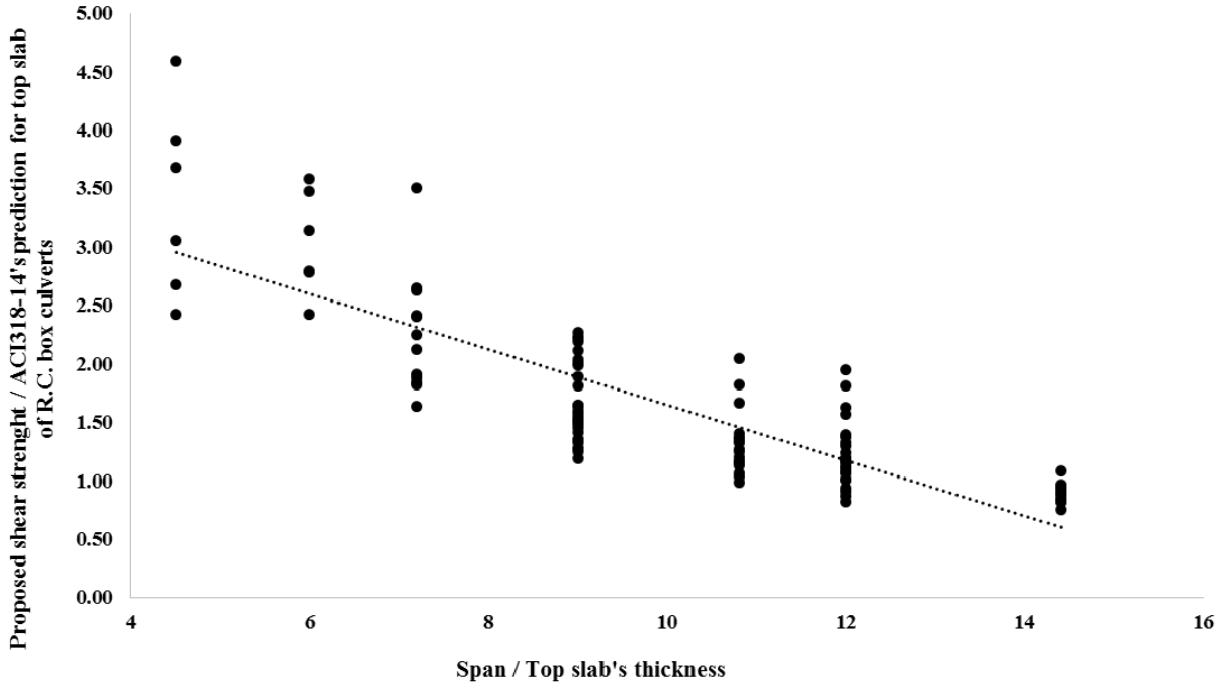

Figure 72. Variations of $V_{FEM}/V_{(ACI318-14)}$ versus span/top slab's thickness for R.C. box culverts' top slab under uniformly distributed loads

5.5. AASHTO Specification

Box culvert designers follow the requirements of codes and specifications to design the top slabs of R.C. box culverts against flexure loads, and then control the thickness of the slab against the shear load in the critical shear section, which is located at distance "d" from haunch. In order to assess AASHTO's shear design formulations for the case studies having shear failure mode, the β factor in the critical shear section was obtained from the analysis results and from AASHTO's equations at the failure load.

5.5.1. Methodology

According to codes and specifications [3], both live loads, from the wheels of vehicles, and dead loads should be applied to box culverts with shallow covers. The effects of the live loads are more critical than those of the dead loads. Soil pressure is the only design load that is considered for box culverts that are buried deep (up to 100 feet). The slabs are designed for bending moment and then are checked for shear. The equation specified by AASHTO [3] for estimating the shear strength (Vc) of concrete slabs of box culverts can be found in Section 5.14.5.3 and is expressed by Equation 5-1.

$$V_c = \left(0.0676\sqrt{f_c'} + 4.6\frac{A_s}{bd_e}\frac{V_u d_e}{M_u}\right) bd_e \qquad \text{Eq. 5-1}$$

Where f_c' is 28-day specified concrete compressive strength, ksi; A_s is area of non-prestressed longitudinal tension reinforcement, $in.^2$; b is web width or diameter of circular section, in.; d_e is distance from extreme compression fiber to centroid of longitudinal tension reinforcement, in.; M_u is factored moment at section, in.-lb.; V_u is factored shear force at section, lb.

The AASHTO specification [3] stipulates that V_c shall not exceed $0.126\sqrt{f_c'}bd_e$, the V_c of single-cell box culverts with monolithic slabs with walls need not be less than $0.0948\sqrt{f_c'}bd_e$, and the

V_c of simply supported slabs need not be less than $0.0791\sqrt{f_c'}bd_e$. Sections 5.8.3.3 and 5.8.3.4 contain formulations for general shear design, where the shear strength of concrete (V_c) is calculated by Equation 5-2.

$$V_c = 0.0316\beta\sqrt{f_c'}b_v d_v \qquad \text{Eq. 5-2}$$

Where β is the factor indicating the ability of diagonally cracked concrete to transmit tension and shear, f_c' is in ksi, d_v is effective shear depth, and b_v is effective web width taken as the minimum web width within the depth d_v.

According to the AASHTO, the β value varies with the changing of the longitudinal rebar strain, and is expressed by Equation 5-3.

$$\begin{cases} \text{For sections containing at least the minimum amount of transverse reinforcement:} \\ \beta = \frac{4.8}{1+750\varepsilon_s} \\ \text{When sections do not contain at least the minimum amount of transverse reinforcement:} \\ \beta = \frac{4.8}{1+750\varepsilon_s}\frac{51}{39+S_{xe}} \end{cases} \qquad \text{Eq. 5-3}$$

ε_s is strain of longitudinal rebar which AASHTO calculates for non-prestressed members without axial load, by Equation 5-4.

$$\varepsilon_s = \frac{\frac{|M_u|}{d_v}+|V_u|}{E_s A_s} \qquad \text{Eq. 5-4}$$

And $S_{xe}$is the crack-spacing parameter that is determined by Equation 5-5.

$$S_{xe} = S_x\frac{1.38}{a_g+0.63} \qquad (12\ in. \le S_{xe} \le 80\ in.) \qquad \text{Eq. 5-5}$$

Where S_x is the lesser of either d_v or the maximum distance between layers of longitudinal crack control reinforcement, and a_g is maximum aggregate size (in.).

These formulations are based on a general method for shear design that was suggested by Collins et al. [10] and was based upon the modified compression field theory (MCFT) developed by Vecchio and Collins [27]. MCFT indicates that concrete can carry more shear stress after cracking by aggregates interlock. This shear stress across the cracked interface is expressed by Equation 5-6.

$$v_{ci} = \frac{2.16\sqrt{f'_c}}{0.3+\frac{24w}{a+0.63}} \quad \text{Eq. 5-6}$$

Where f'_c is in psi, w is crack width in inches, and a is aggregate size in inches.

According to this theory, the shear strength of the reinforced concrete sections depends on the strain of the longitudinal rebar. The maximum principal strain of the crack section is calculated in terms of the longitudinal rebar strain, according to Equation 5-7.

$$\varepsilon_1 = \varepsilon_x + (\varepsilon_x - \varepsilon_2)\,(\cot\theta)^2 \quad \text{Eq. 5-7}$$

Where $\varepsilon_1$and ε_2 are maximum and minimum principal strains, respectively; ε_x is strain of longitudinal rebar; and the θ is angle of crack inclination.

Maximum principal stress (f_1) is expressed in the term of v_{ci} in Equation 5-8.

$$f_1 = v_{ci} \tan\theta \quad \text{Eq. 5-8}$$

Thus, the shear strength of concrete in vertical section is:

$$V_c = f_1 b_v d_v \cot\theta \quad \text{Eq. 5-9}$$

The β is defined $\frac{v}{\sqrt{f'_c}}$ and by substituting Eq. 5-8 for Eq. 5-9, we have:

$$V_c = \beta\sqrt{f'_c} b_v d_v \quad \text{Eq. 5-10}$$

Considering AASHTO's general equation for shear design and the designated limitation for concrete shear strength in the design of the top slab of a box culvert leads to the conclusion that the β factor should be between 3 and 4 when the slabs are monolithic with walls, and between 2.5 and 4 when slabs are simply supported.

5.5.2. Assessment

Box culvert designers follow the requirements of codes and specifications to design the top slab of R.C. box culverts against flexure loads, and then control the thickness of the slab against the shear load in a section located at distance "d" from haunch, which is the critical shear section. In order to assess AASHTO's shear design formulations for the case studies having shear failure mode, the β factor was obtained in the critical shear section from the analysis results and from AASHTO's equations at the failure load. A comparison indicated that the analysis results predicted the β factor an average of 1.89 times greater than the AASHTO's equations in the section at distance "d" from haunch. The strain value in the longitudinal rebar in the same section was also investigated, and it was revealed that the finite element analysis determined the value an average of 1.19 times greater than the AASHTO's equation. The difference seems to be reasonable in the prediction of strain value; however, the underestimation of the prediction of the concrete shear strength (the β factor) is considerable. Figure 73 plots a comparison between the proposed β factors versus the one calculated via AASHTO's equations. The case studies below the 45 degree line demonstrated that employing the AASHTO equations resulted in predicting a higher β factor than that predicted by the analysis Based upon 210 studies with the shear failure mode, AASHTO's prediction was higher than the analysis results in only 26 case studies. The dots closest to the inclined line indicate the case studies with very similar β factors from both approaches. The figure shows that the most of the case studies were above the line, and the analysis determined a greater

β factor than AASHTO's equations. Figure 74 compares the prediction of the strain from the finite element method (FEM) with AASHTO's equation.

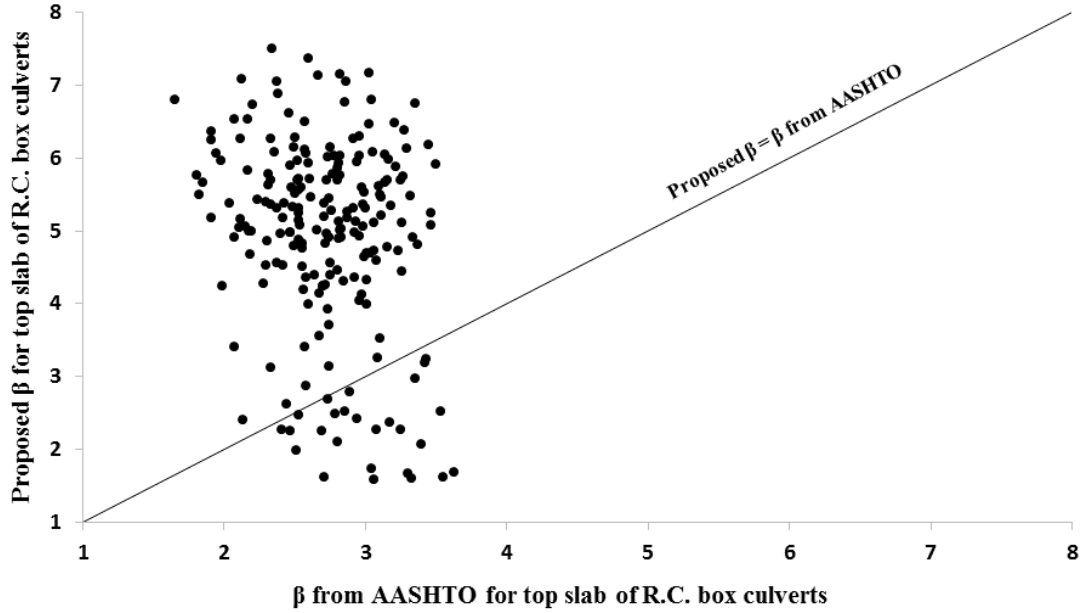

Figure 73. Comparison of the obtained β factor from FEA and AASHTO in the section at distance "d" from haunch

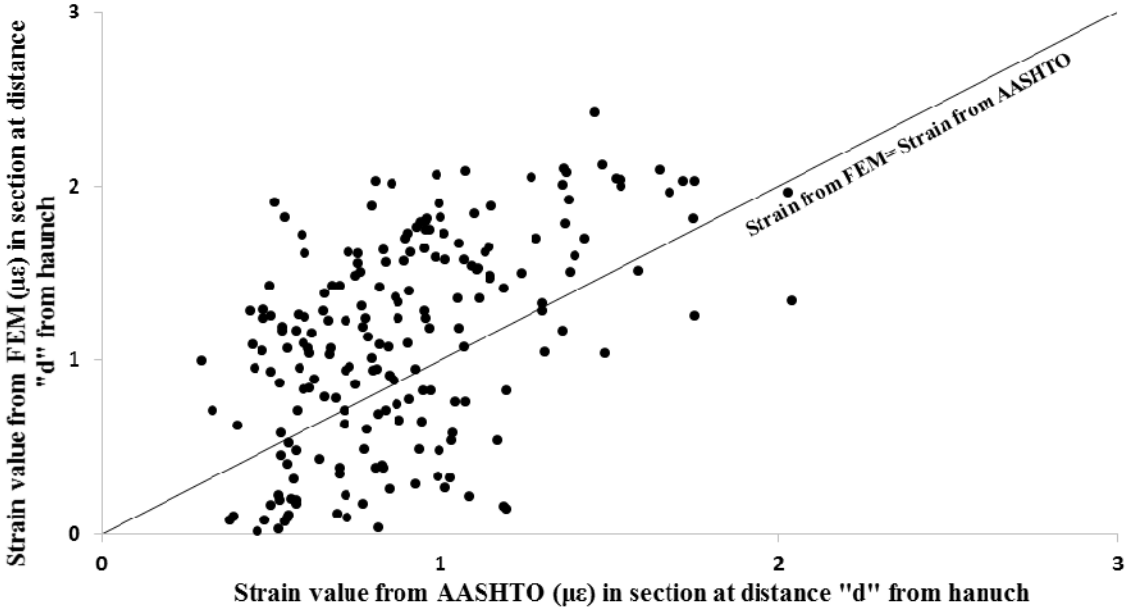

Figure 74. Comparison of the obtained strain value in longitudinal rebar from FEA and AASHTO in the section at distance "d" from haunch

The variations of the $\frac{\beta_{AASHTO}}{\beta_{FEA}}$ ratio, if R/S and T vary, are plotted in Figure 75, which contains six contour plats for three values of f_c' and two values of ρ. They indicate that using AASHTO's approach to calculating the β factor led to higher values than using finite element analysis for the cases associated with R/S greater than 2 and the thickness of top slab between 406 to 610 mm (16 to 24 in.). AASHTO significantly underestimated the β factor when the R/S was low (less than 1) and the top slab was thicker. The contour plots demonstrate that a change in f_c' does not influence $\frac{\beta_{AASHTO}}{\beta_{FEA}}$.

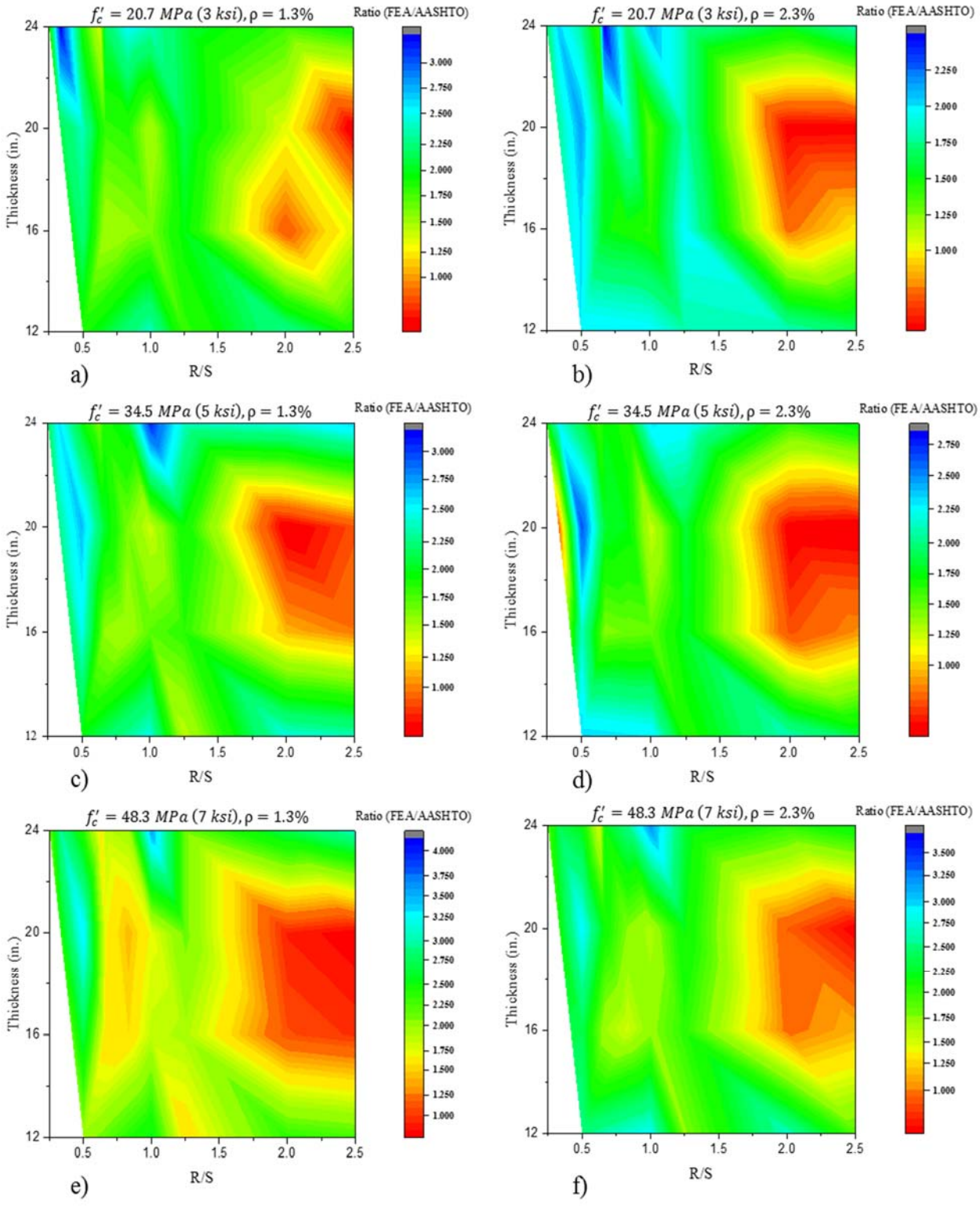

Figure 75. Variations of $\beta_{AASHTO}/\beta_{FEA}$ ratio versus changing top slab's thickness and R/S in the section at distance "d" from haunch: a) when f_c'=20.7 MPa & ρ=1.3%, b) when f_c'=20.7 MPa & ρ=2.3%, c) when f c'=34.5 MPa & ρ=1.3%, d) when f_c'=34.5 MPa & ρ=2

CHAPTER 6. REGRESSION ANALYSIS

6.1. Overview

A summary of the nonlinear regression analysis concept, quoted from a reference book entitled "Nonlinear Regression Analysis and Its Applications" by Bates and Watts [43], is presented below.

"Linear regression is a powerful method for analyzing data described by models which are linear in the parameters. Often, however, a researcher has a mathematical expression which relates the response to the predictor variables, and these models are usually nonlinear in the parameters. In such cases, linear regression techniques must be extended, which introduces considerable complexity.

A nonlinear regression model can be written:

$$Y_n = f(X_n, \theta) + Zn \qquad \text{Eq. 6-1}$$

where f is the expectation function and X_n is a vector of associated regressor variables or independent variables for the n^{th} case. This model is of exactly the same form as the linear regression model, except that the expected responses are nonlinear functions of the parameters. That is, for nonlinear models, at least one of the derivatives of the expectation function with respect to the parameters, depends on at least one of the parameters.

To emphasize the distinction between linear and nonlinear models, we used θ for the parameters of a nonlinear model and P for the number of parameters.

When analyzing a particular set of data, we considered the vectors X_n, n = 1, 2,…., N, as fixed and concentrated on the dependence of the expected responses of θ. We created the N-vector η (θ) with n^{th} element.

$\eta n\ (\theta) = f\ (X_n\ ,\ \theta)\ ,\ n = 1, 2,\ldots,N$ Eq. 6-2

And wrote the nonlinear regression model as

$Y = \eta\ (\theta) + Z$ Eq. 6-3

With Z assumed to have a spherical normal distribution. That is,

$E\ [Z] = 0$ Eq. 6-4

$Var\ (Z) = E\ [ZZ^T] = \sigma^2 I$ Eq. 6-5

As in the linear model.

The problem of finding the least squares estimates can be stated very simply geometrically, given a data vector y, an expectation function $f\ (X_n\ ,\ \theta)$, and a set of design vectors X_n, n = 1, 2,….,N.

(1) Find the point $\hat{\eta}$ on the expectation surface which is closest to y, and then (2) determine the parameter vector $\hat{\theta}$ which corresponds to the point $\hat{\eta}$.

For a linear model, step (1) is straightforward because the expectation surface is a plane of infinite extent, and we may write down an explicit expression for the point on that plane which is closest to y,

$\hat{\eta} = Q_1 Q^T_1 y$ Eq. 6-6

For a linear model, step (2) is also straightforward because the P-dimensional parameter plane maps linearly and invertidly to the expectation plane, so once we know where we are on one plane, we can easily find the corresponding point on the other. Thus

$\hat{\beta} = R_1^{-1} Q_1^T \hat{\eta}$ Eq. 6-7

In the nonlinear case, however, the two steps are very difficult: the first because the expectation surface is curved and often of finite extent (or at least has edges) so that it is difficult even to find $\hat{\eta}$, and the second because we can map points easily only in one direction - from the parameter plane to the expectation surface. Even if we know $\hat{\eta}$, it is extremely difficult to determine the parameter plane coordinates $\hat{\theta}$ corresponding to that point. To overcome these difficulties, we used iterative methods to determine the least squares estimates."

6.2. Assumptions

Since there was no trend between the proposed β factor and AASHTO's prediction, as shown in Figure 73, using a single regression analysis was not an option. Therefore, multiple linear and nonlinear regression analyses [44] were utilized to develop an equation that would predict the concrete shear strength (V_{c-top}), based on the data set of the 156 case studies that exhibited shear failure mode and $S/T \geq 6$. The parameters investigated were the span (S), rise (R), thickness of the top slab (T), amount of longitudinal reinforcement (ρ), and concrete compressive strength (f_c'). For the regression analysis, parameters of T, R/S, f_c' and the strain in the longitudinal rebar times the rebar area ($A_s\varepsilon$) were considered as variables. Figure 76 shows the scatter plot of the concrete shear strength if each of the variables changes independently. As was expected, an increase in f_c' and the thickness of the top slab led to an increase in the shear strength. Since higher A_s causes lower ε, Figure 76c shows scatter dots without any specific trend. Also, the variable of $A_s\varepsilon$ indirectly represents the tension force in longitudinal reinforcement. There was a descending trend when R/S increased.

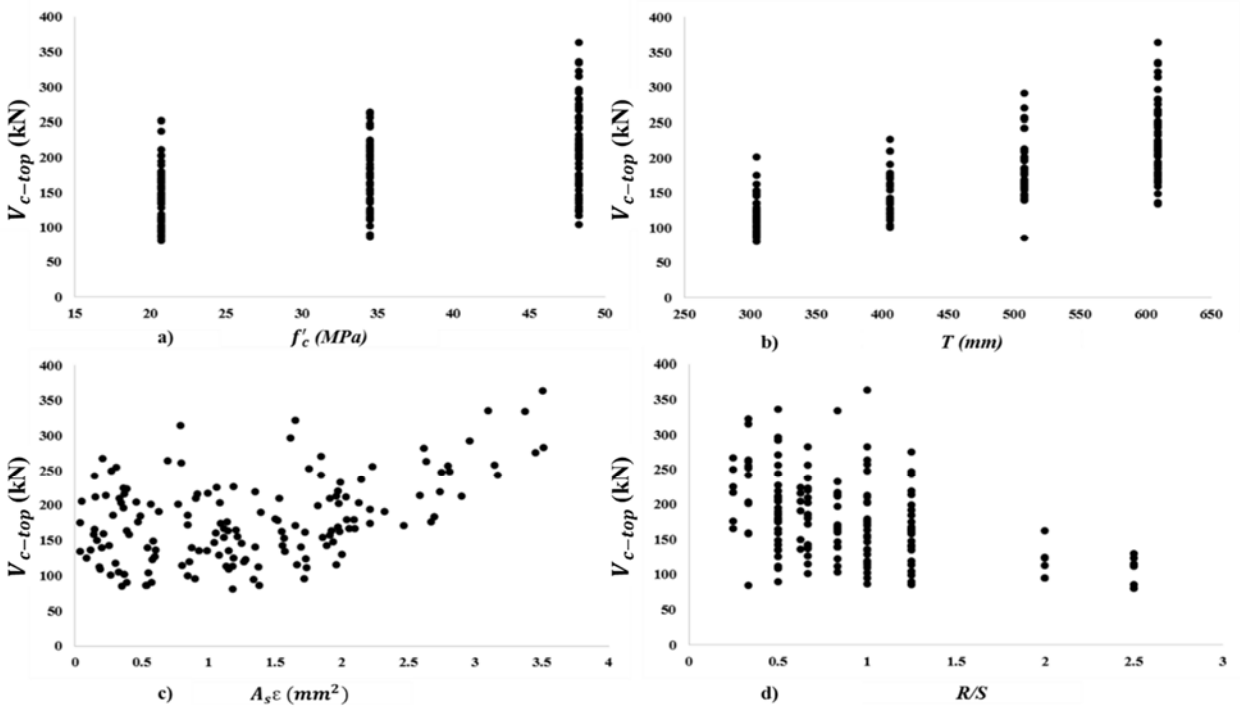

Figure 76. Change in the shear strength in the critical section versus a) f_c'', b) Top slab's thickness (T), c) area of longitudinal rebar in tension times the strain value ($A_s\varepsilon$) where *As* is in mm^2 ; d) R/S

No significant correlation was found between the variables. Table 17 presents the correlation matrix. The variance inflation factor indicated the validity of keeping all of the variables in the regression model. Ten cases from the data set of 156 were randomly selected to validate the developed model, and the remaining 146 were used to train the model. The valid data set was obtained from the FEM for various sizes and material properties. Although the statistical tests showed some outliers, both in variables and response values, no data set was removed as an outlier. A statistical summary of the data sets used to train and validate the model is presented in Table 18.

Table 17. Correlation matrix

Variables	f'_c	$A_s\varepsilon$	T	R/S	V_c
f'_c	1.000				
$A_s\varepsilon$	0.124	1.000			
T	-3E-17	0.205	1.000		
R/S	6E-17	0.293	-0.509	1.000	
V_{c-top}	0.479	0.443	0.714	-0.412	1.000

Table 18. Summary statistics

	Data set for training					Data set for validation				
Variable	**Obs.**	**Min.**	**Max.**	**Mean**	**Std. deviation**	**Obs.**	**Min.**	**Max.**	**Mean**	**Std. deviation**
V_{c-top} **(kN)**	146	80.57	363.82	177.95	59.07	10	116.95	296.52	187.47	60.21
f'_c **(MPa)**	146	20.7	48.3	34.31	11.23	10	20.700	48.3	37.26	12.68
$A_s\varepsilon$	146	0.039	3.51	1.32	0.88	10	0.09	2.23	1.00	0.86
T (mm)	146	304.8	609.6	475.99	119.77	10	304.8	609.6	487.68	115.34
R/S	146	0.25	2.5	0.91	0.506	10	0.25	2.5	0.583	0.236

6.3. Shear Strength of Top Slab of Box Culverts using MLR

A multiple linear regression model is in the form of $Y_i=\beta_0+\beta_1X_{i1}+\beta_2X_{i2}+\beta_3X_{i3}+\beta_4X_{i4}+\varepsilon_i$, where Y_i represents the mean value of the shear strength of the R.C. box culverts' top slab, and X_{i1} to X_{i4} are independent variables. The multiple linear regression estimates coefficients of β_0 to β_4 to provide the best fit. The residual analysis showed that a transformation of both dependent variables (Y) and independent variables (X_{i1}… X_{i4}) was necessary. Therefore, they were transformed via a logarithmic function of natural logarithm (Ln). The correlation between transformed variables, using variance inflation factor (VIF), was checked to avoid any multicollinearity. Table 19 exhibits the VIF for the transformed independent variables. The ANOVA table for the multiple linear regression is presented in Table 20. The regression analysis found that all of the independent variables were significant. No interaction term was added in order to keep the equation as simple as possible. Considering a confidence level of 95% ($\alpha = 0.05$), Table 21 presents coefficients resulting from multiple linear regression. The results indicated that f'_c contributed to the shear strength in terms of $\sqrt{f'_c}$.

Table 19. Variance inflation factor

	Ln(f'_c)	**Ln(T)**	**Ln($A_s\varepsilon$)**	**Ln(R/S)**
Tolerance	0.996	0.728	0.661	0.544
VIF	1.004	1.374	1.514	1.838

Table 20. ANOVA for training data sets

Source	DF	Sum of squares	Mean squares	F	Pr > F
Model	4	14.441	3.610	317.492	**< 0.0001**
Error	141	1.603	0.011		
Corrected Total	145	16.044			

Table 21. Model parameters

Source	Value	Standard error	t	Pr > |t|	Lower bound (95%)	Upper bound (95%)
Intercept	-0.851	0.258	-3.297	0.001	-1.361	-0.341
Ln(f'_c)	0.428	0.025	16.949	< 0.0001	0.378	0.478
Ln(T)	0.119	0.011	10.910	< 0.0001	0.097	0.140
Ln($A_s\varepsilon$)	0.727	0.040	18.262	< 0.0001	0.648	0.805
Ln(R/S)	-0.190	0.023	-8.441	< 0.0001	-0.235	-0.146

The multiple regression analysis resulted in Equations 6-8 associated with R-square of 0.9.

$$Ln(V_{c-top}) = -0.851 + 0.428\,Ln(f_c') + 0.119\,Ln(T) + 0.727\,Ln(A_s\varepsilon) - 0.190\,Ln(\frac{R}{S}) \quad \text{Eq. 6-8}$$

Therefore, it can be obtained:

$$V_{c-top} = 0.43(f_c')^{0.43}(T)^{0.12}(A_s\varepsilon)^{0.73}(\frac{S}{R})^{0.19} \quad \text{Eq. 6-9}$$

To obtain the shear strength of top slab of 1000 mm wide R.C. box culverts, this equation must be multiplied by $1000/152 = 6.58$. Therefore:

$$V_{c-top} = 2.8(f_c')^{0.43}(T)^{0.12}(A_s\varepsilon)^{0.73}(\frac{S}{R})^{0.19} \quad \text{Eq.6-10a}$$

Where the shear strength of top slab of box culvert in section at distance "d" from haunch (V_{c-top}) is in kN per m, concrete compressive strength (f_c') is in MPa, area of longitudinal reinforcement (A_s) is in mm^2, and, thickness of top slab (T) is in mm.

$$V_{c-top} = 9.24(f_c')^{0.43}(T)^{0.12}(A_s\varepsilon)^{0.73}(\frac{S}{R})^{0.19} \quad \text{Eq. 6-10b}$$

Where the shear strength of top slab of box culvert in section at distance "d" from haunch (V_{c-top}) is in kip per ft., concrete compressive strength (f_c') is in ksi, area of longitudinal reinforcement (A_s) is in in^{-2}, and, thickness of top slab (T) is in inches.

Figure 77 plots the shear strength of the top slabs of R.C. box culverts (V_{c-top}) obtained from finite element analysis versus the predicted value, using multiple linear regression analysis. It should be noted that this equation is valid for f_c' between 20.7 and 48.3 MPa (3 and 7 ksi), top slab's thickness between 304.8 and 609.6 mm (12 and 24 in.), strain in longitudinal rebar between 200 με and 1500 με, and R/S between 0.25 and 2.5. The multiple linear regression model is not valid if the input variables are not within these ranges.

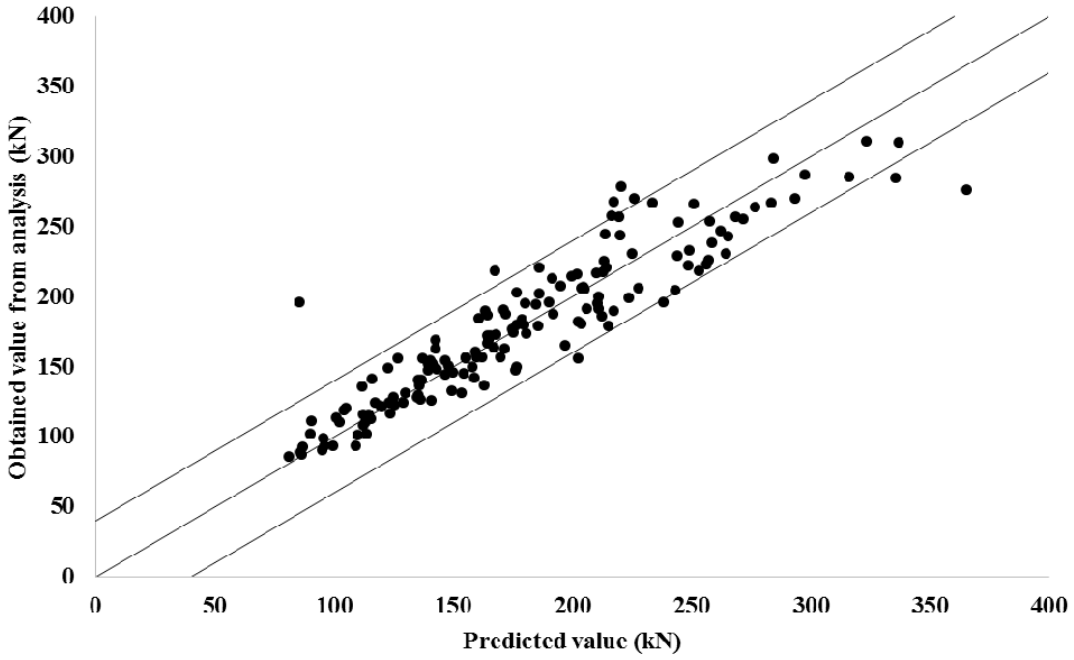

Figure 77. Evaluation of multiple linear regression model

6.4. Proposed AASHTO Shear Design Equation for Top Slab

The format of the equation in the AASHTO specification (Eq. 5-1) was introduced to the nonlinear regression analysis. Equation 6-11 is the proposed formulation for the calculation of the shear strength of the top slab of a reinforced concrete box culvert associated with 0.87 R-square and based on case studies in this research. It should be noted that this equation is only valid for box culverts in the specific range of those in the case studies, and no extrapolation is allowed. Figure 78 compares the prediction of the regression model with the outcomes obtained through finite element analysis and demonstrates that the model is reasonably able to predict the shear strength of top slabs.

$$V_{c-top} = [6.44\sqrt{f_c'} + 0.1(A_s\varepsilon)^{1.1}(T^{0.65})](T^{0.52})(\frac{S}{R})^{0.22} \quad \text{Eq. 6-11a}$$

Where the shear strength of top slab of box culvert in section at distance "d" from haunch (V_{c-top}) is in kN per m, concrete compressive strength (f_c') is in MPa, area of longitudinal reinforcement (A_s) is in mm^2, and, thickness of top slab (T) is in mm.

$$V_{c-top} = [5.8\sqrt{f_c'} + 15.2(A_s\varepsilon)^{0.74}(T^{1.08})](T^{0.5})(\frac{S}{R})^{0.19} \quad \text{Eq. 6-11b}$$

Where the shear strength of top slab of box culvert in section at distance "d" from haunch (V_{c-top}) is in kip per ft., concrete compressive strength (f_c') is in ksi, area of longitudinal reinforcement (A_s) is in in.^{2}, and, thickness of top slab (T) is in inches.

The proposed equation is in the same format as AASHTO's equation. It is not unique, and other formats may exist that are a better fit for data with a higher R-square. This equation is valid for f_c' between 20.7 and 48.3 MPa (3 and 7 ksi), top slab's thickness between 304.8 and 609.6 mm (12

and 24 in.), strain in longitudinal rebar between 200 με and 1500 με, and R/S between 0.25 and 2.5.

This equation presents the shear force in the section at distance "d" from haunch when a box culvert under uniformly distributed load reaches its failure load. Since the top slabs of box culverts are designed for flexural loads and are controlled for shear strength, the equation has been derived for that section. The diagonal tension cracks did not occur exactly in the designated section in any of the cases. The location of the cracked section in the top slab changed, depending on the S/T ratio. The exact location of the shear cracked section could not be determined using conventional structural analysis (frame analysis); however, considering the section at distance "d" from haunch could be a reasonable section for the shear design.

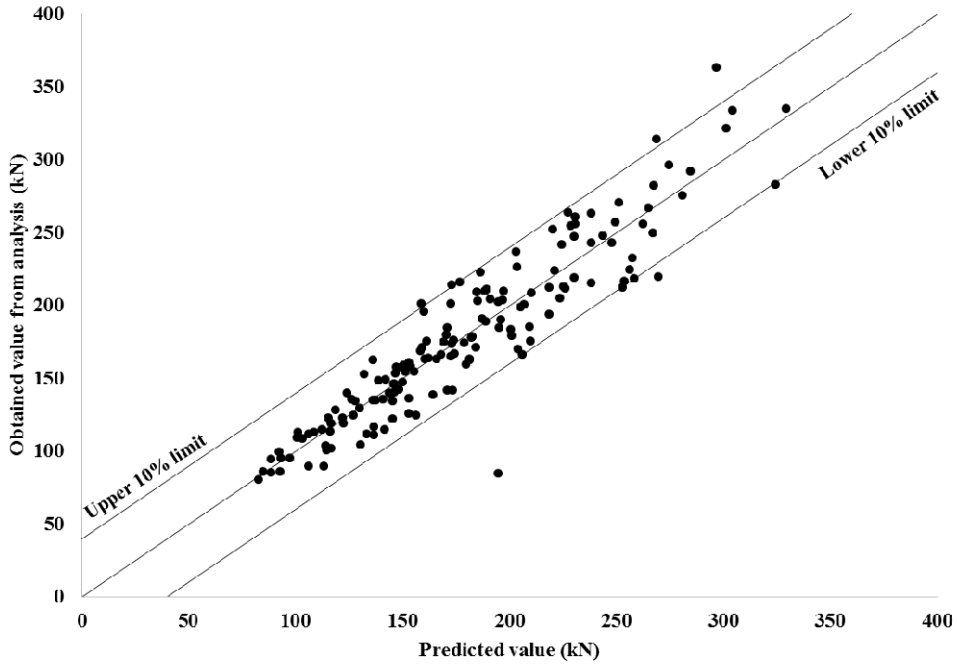

Figure 78. Evaluation of nonlinear regression model

6.5. An Equation Independent of the Strain Value (Shear Capacity of Box Culvert)

An equation, based upon 156 case studies and using multiple linear regression analysis, was developed for the total load carried by box culverts with shear failure mode and $S/T \geq 6$. The shear strength (P_{total}) in the equation is *not* the shear strength of the top slab of the box culvert; it is the total load that was uniformly distributed on the top slab of the box culvert at failure. The strain value in the longitudinal rebar was removed from this equation, because the shear force represented the shear capacity of the entire system, and a specific section could not be selected for reading the strain value. Table 22 presents the ANOVA table for the regression analysis. The equation predicts the total load (the shear strength of the whole box culvert) associated with R-square of 0.52.

Table 22. ANOVA table

	df	*SS*	*MS*	*F*	*Significance F*
Regression	4	16.81	4.20	41.44	2.06E-23
Residual	151	15.31	0.10		
Total	155	32.13			

The coefficient calculated for each transformed variable is presented in Table 23.

Table 23. Model Parameters

	Coefficients	*Standard Error*	*t Stat*	*P-value*	*Lower 95%*	*Upper 95%*
Intercept	1.51	0.42	3.55	0.000505	0.67	2.35
Ln(S/R)	-0.27	0.05	-4.94	2.04E-06	-0.38	-0.16
Ln(T)	0.96	0.16	6.11	7.9E-09	0.65	1.27
Ln(As)	0.22	0.09	2.23	0.026762	0.02	0.41
Ln(fc)	0.46	0.07	6.31	2.91E-09	0.31	0.60

The multiple regression analysis resulted in Equation 6-12:

$$Ln(P_{total}) = 1.51 + 0.46\,Ln(f_c') + 0.96\,Ln(T) + 0.22\,Ln(A_s) + 0.27\,Ln(\frac{R}{S}) \qquad \text{Eq. 6-12}$$

Therefore, it can be obtained:

$$P_{total} = 4.53(f_c')^{0.46}(T)^{0.96}(A_s)^{0.22}(\frac{R}{S})^{0.27}$$ Eq. 6-13

To obtain the shear strength of entire R.C. box culverts with one-foot width, the equation must be multiplied by 2. Therefore:

$$P_{total} = 9(f_c')^{0.46}(T)^{0.96}(A_s)^{0.22}(\frac{R}{S})^{0.27}$$ Eq.6-14a

Where the shear capacity of entire box culvert (P_{total}) is in kip per ft., concrete compressive strength (f_c') is in ksi, area of longitudinal reinforcement (A_s) is in in^2, and, thickness of slabs and walls (T) is in inches.

$$P_{total} = 0.6(f_c')^{0.46}(T)^{0.96}(A_s)^{0.22}(\frac{R}{S})^{0.27}$$ Eq. 6-14b

Where the shear capacity of entire box culvert (P_{total}) is in kN per m, concrete compressive strength (f_c') is in MPa, area of longitudinal reinforcement (A_s) is in mm^2, and, thickness of slabs and walls (T) is in mm.

CHAPTER 7. SUMMARY AND CONCLUSIONS

7.1. Summary and Conclusions

This research resulted in the development of statistical equations that predict the shear strength of reinforced concrete box culverts associated with shear behavioral mode, and also independently, an equation for the shear strength of top slabs. Comprehensive experimental and numerical investigations were conducted to determine the shear capacity of R.C. box culverts under uniformly distributed load. A finite element model was developed and verified to extend the variations of geometrical parameters that influence the shear capacity of R.C. box culverts. The outcomes of the parametric study were compared with the shear equation in the AASHTO specification and ACI318-14 code, and a significant difference was observed. Therefore, an equation was developed, based on 288 data sets obtained from multiple linear and nonlinear regression analysis, to predict the shear capacity for both the entire box culvert and its top slab.

A framework was developed to perform displacement-controlled analysis of uniformly distributed loads on beams. This framework served as a loading mechanism to estimate the ultimate shear strength of beams under uniformly distributed load by employing the coupled nonlinear finite element method. A FEM model was developed to mimic the shear behavior of the three beams tested by Vecchio and Shim [34]. The verified FEM analysis was used to obtain the strain values and the concrete shear strength (the β factor) of 24 reinforced concrete beams analyzed under concentrated load at mid-span and the equivalent uniformly distributed load. A comparison of the experimental test total shear force-deflection curves with FEM results shows an agreement between them, with 9.4%, 2.4%, and 19.9% differences in ultimate loads for beams OA1, OA2, and OA3, respectively. Similar crack patterns obtained from the results of both experimental tests and finite element modeling of OA1, OA2 and OA3 beams were due to a concentrated load at mid-

span. It should be noted that the proposed framework system was used to convert a single displacement control load to a uniformly distributed load on the beam.

As was expected, the analysis results showed that beams subjected to uniformly distributed loads exhibited greater shear strength than those with single concentrated loads applied at mid-span. This is attributed to the difference in the rebar strain value of beams subjected to different loadings; namely, a larger strain value in the critical section for beams under concentrated load. For instance, for the OA1 beam, the strain value in the longitudinal rebar in the critical section, due to a concentrated load at mid-span, was 67% greater than the strain value of a uniformly distributed load.

The AASHTO's estimation for strain in longitudinal rebar, for beams subjected to uniformly distributed and concentrated loads, agrees reasonably with FEM results under both loading conditions. However, the AASHTO's prediction for the β value is significantly different from the results obtained from FEM. This is attributed to the difference in the shear strength of beams resulting from experimental tests and AASHTO's approach. Moreover, an increase in the a/d ratio leads to a decrease in the difference between the FEM results and AASHTO's approach to predicting the concrete shear strength (the β factor).

The ACI318-14's shear design approach (Equation 3-1) was compared with analysis results. It showed that following the ACI code formulation results in underestimating the prediction of the concrete shear strength (V_{c-top}).

The framework was built for experimental investigation. The constructed framework converted a single applied displacement to eight identical point loads along the span of the specimens. The load-transferring mechanism was validated through experimental and numerical investigations.

Two R.C. box culverts were continuously examined in the laboratory to determine the shear strength of the top slab under the proposed framework. The finite element method was utilized to mimic the experiments. The analysis results of the shear strength of a box culvert's top slab in the critical section was compared with the shear design approach in ACI318-14. The comparison indicated that using the code methodology resulted in an underestimation of the shear strength of the top slab. Taking advantage of the verified numerical models, a parametric study was conducted to assess the code's prediction for determining the concrete shear strength (V_{c-top}) in R.C. box culverts. According to 108 case studies, the ACI318-14's prediction for the shear strength of the top slab of the studied box culverts differed, on average, 66% from the value obtained from the FEM results. Additionally, this difference decreased slightly if the span/rise ratio changed; however, the $\frac{V_{FEM}}{V_{ACI318-14}}$ ratio decreased considerably if the span/top slab's thickness ratio increased.

Various geometrical and material property parameters that affect the concrete shear strength of top slabs (V_{c-top}) of reinforced concrete box culverts were investigated in this research, using the verified finite element method. The numerical models were calibrated via experimental data obtained from testing R.C. box culverts under equivalent uniformly distributed loads in the laboratory at the University of Texas at Arlington. A total of 288 case studies were analyzed to determine the shear strength of the top slab, as well as the failure mode. The results indicated that an increase in the span/rise ratio and the span/top slab's thickness ratio led to a decrease in the total failure load of R.C. box culverts. The results of the case studies with shear failure mode in the parametric study assessed the AASHTO methodology for predicting the concrete shear strength (V_c) and strain value in the longitudinal reinforcement (ε). The assessment revealed that the AASHTO equations underestimate the concrete shear strength (V_{c-top}); however, their

prediction of the strain value is reasonably acceptable. Based on the cases associated with shear behavioral mode studied in this research, the AASHTO method predicted the β factor, on average, 1.89 times greater than analysis outcomes. For box culverts with R/S ratios higher than 2, which are rarely-used sizes, the AASHTO's prediction for the β factor was greater than the analysis results. Regression analyses proposed Equations 6-10 and 6-11 for predicting the concrete shear strength of top slabs (V_{c-top}) of reinforced concrete box culverts under uniformly distributed loads with $S/T \geq 6$. It should be noted that these equations only work for the range of parameters studied in this research, meaning that no extrapolation is permitted.

7.2. Recommendations for further investigations

Some aspects of this research project merit further investigation. The following bullet points are recommended for future studies:

1- Considering the lateral pressure of soil in buried box culverts;

2- Investigation of more box culvert sizes, including those tabulated in ASTM C1577 [4]; and

3- Investigation of effects of using high-strength steel rebar on the shear strength of the top slab of reinforced concrete box culverts,

APPENDIX 1. LOAD-DEFLECTION CURVES

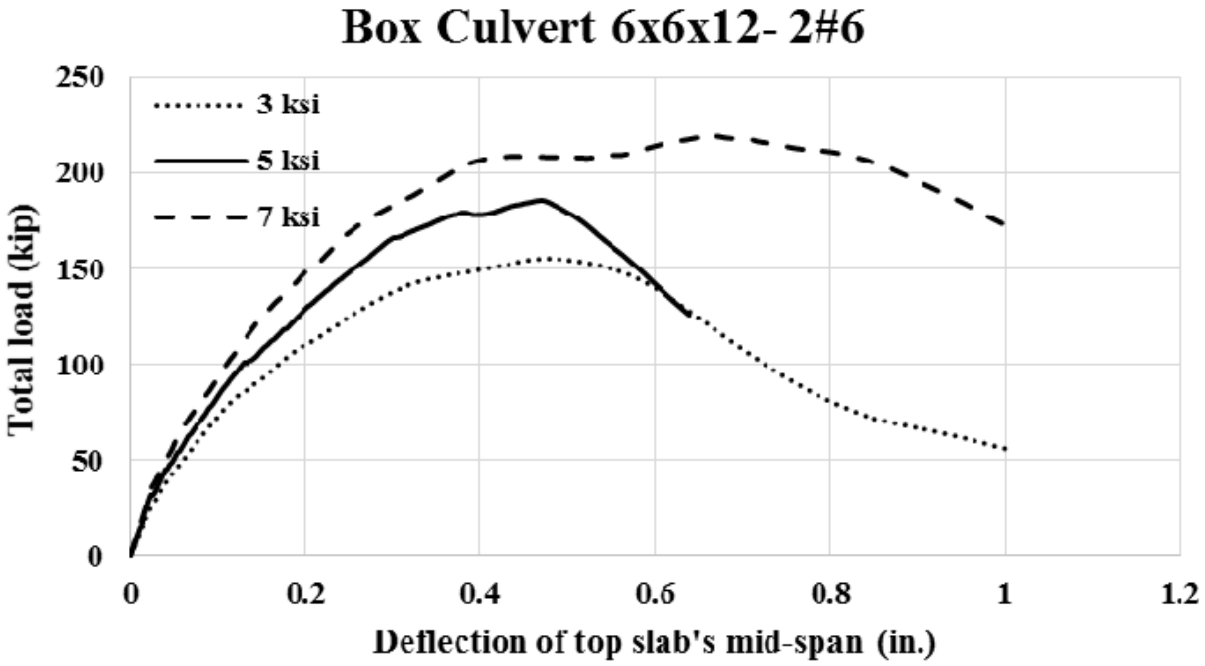
Box Culvert 6x6x12- 2#6
3 ksi
5 ksi
7 ksi
Total load (kip)
250
200
150
100
50
0
0
0.2
0.4
0.6
0.8
1
1.2
Deflection of top slab's mid-span (in.)

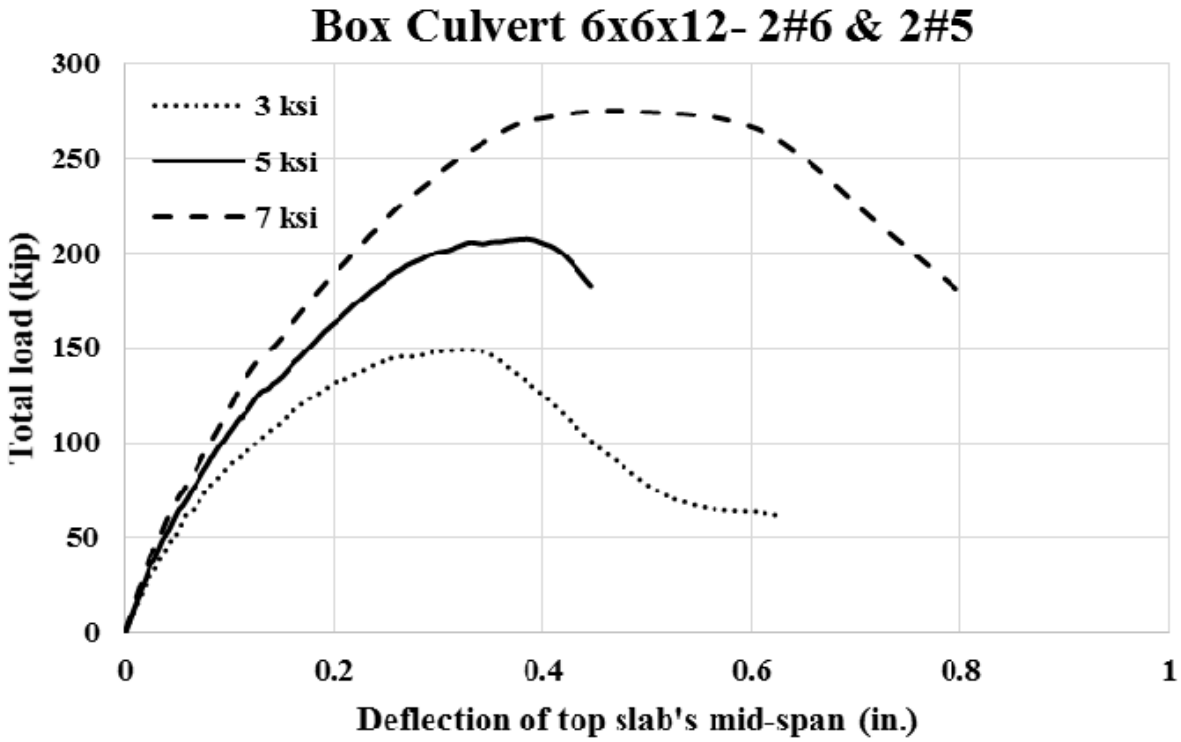
Box Culvert 6x6x12- 2#6 & 2#5
3 ksi
5 ksi
7 ksi
Total load (kip)
300
250
200
150
100
50
0
0
0.2
0.4
0.6
0.8
1
Deflection of top slab's mid-span (in.)

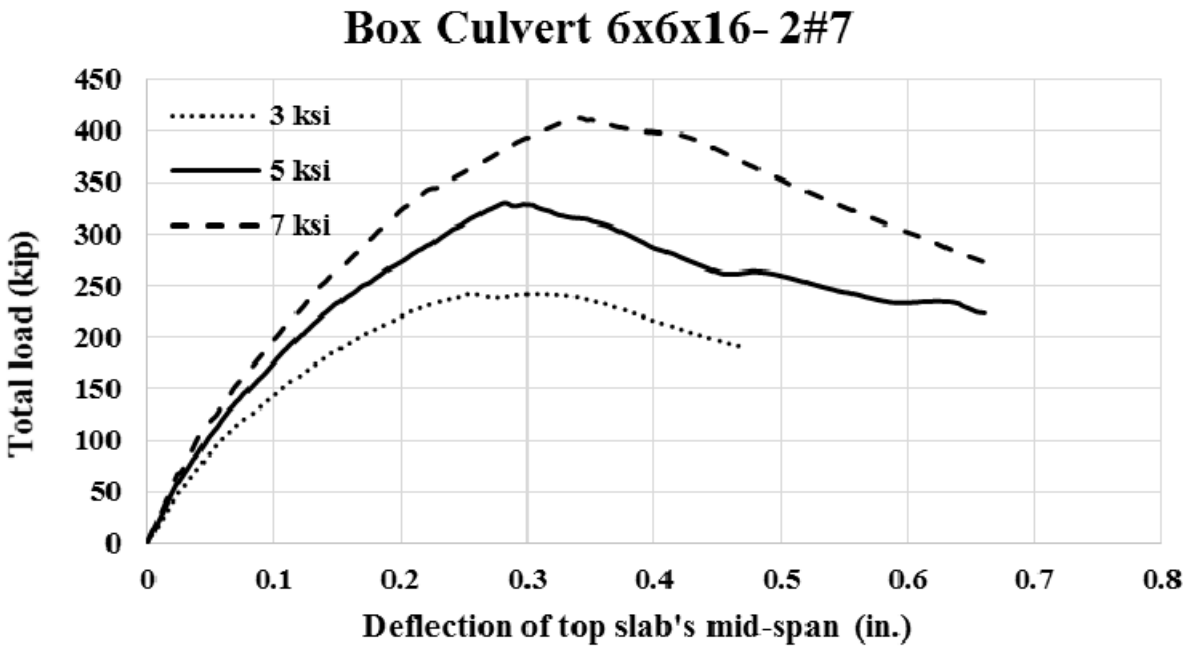
Box Culvert 6x6x16- 2#7
3 ksi
5 ksi
7 ksi
Total load (kip)
450
400
350
300
250
200
150
100
50
0
0
0.1
0.2
0.3
0.4
0.5
0.6
0.7
0.8
Deflection of top slab's mid-span (in.)

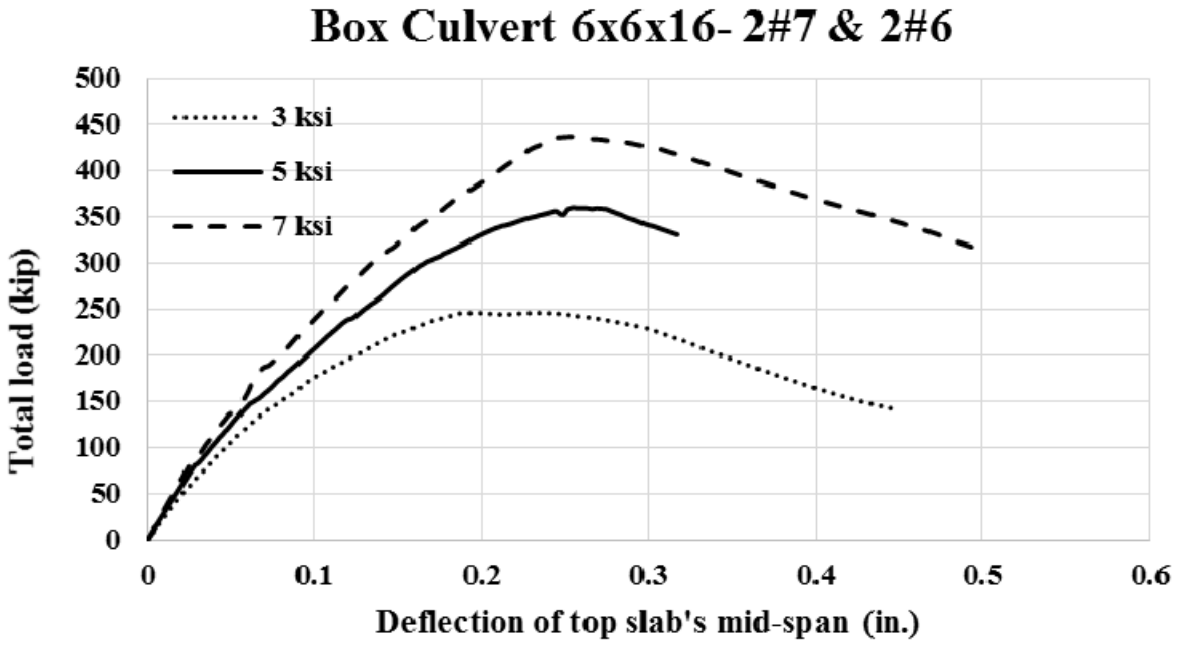
Box Culvert 6x6x16- 2#7 & 2#6
3 ksi
5 ksi
7 ksi
Total load (kip)
500
450
400
350
300
250
200
150
100
50
0
0
0.1
0.2
0.3
0.4
0.5
0.6
Deflection of top slab's mid-span (in.)

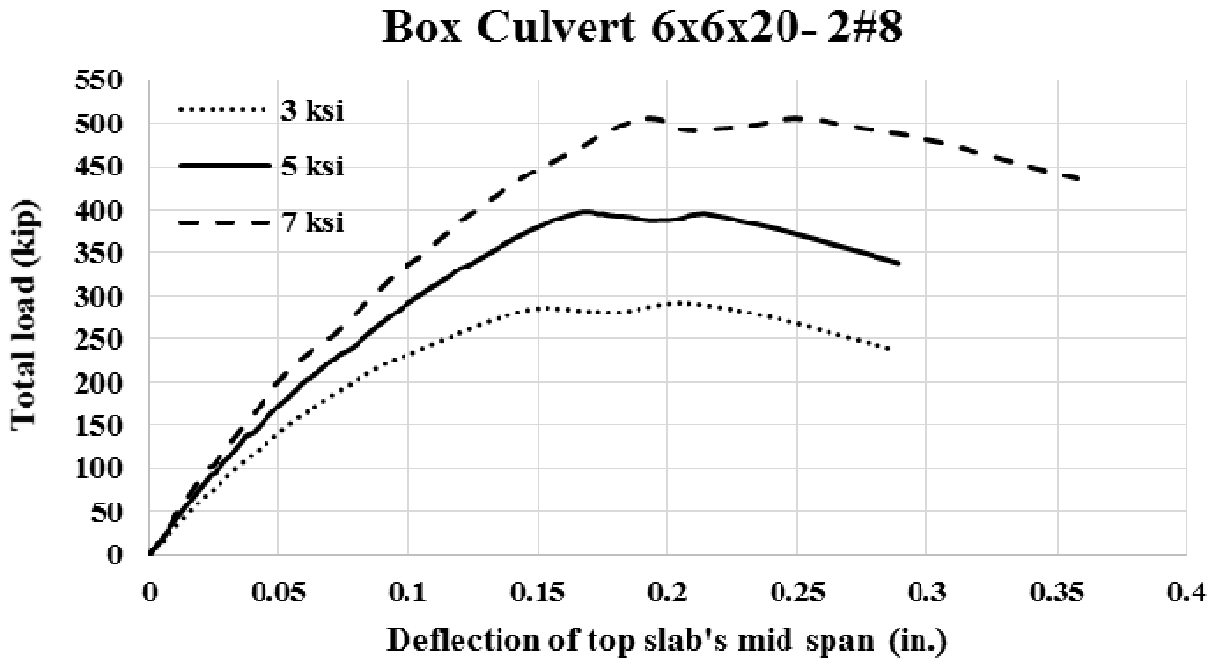
Box Culvert 6x6x20- 2#8
3 ksi
5 ksi
7 ksi
Total load (kip)
550
500
450
400
350
300
250
200
150
100
50
0
0
0.05
0.1
0.15
0.2
0.25
0.3
0.35
0.4
Deflection of top slab's mid span (in.)

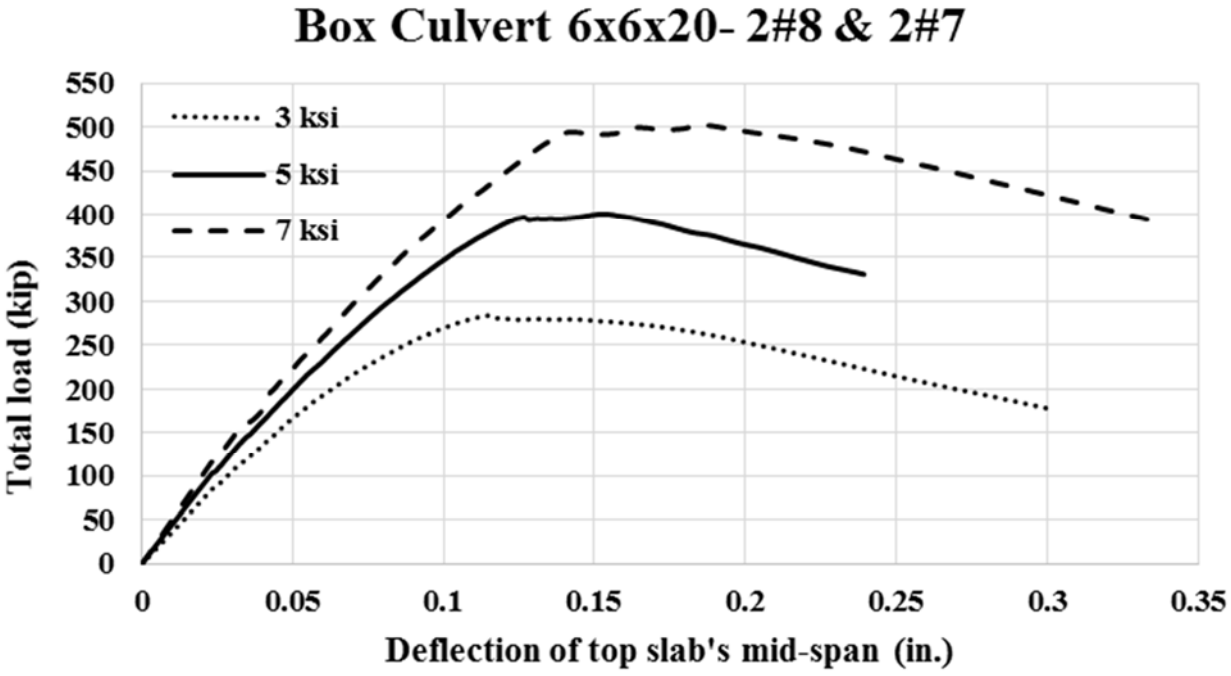
Box Culvert 6x6x20- 2#8 & 2#7
3 ksi
5 ksi
7 ksi
Total load (kip)
550
500
450
400
350
300
250
200
150
100
50
0
0
0.05
0.1
0.15
0.2
0.25
0.3
0.35
Deflection of top slab's mid-span (in.)

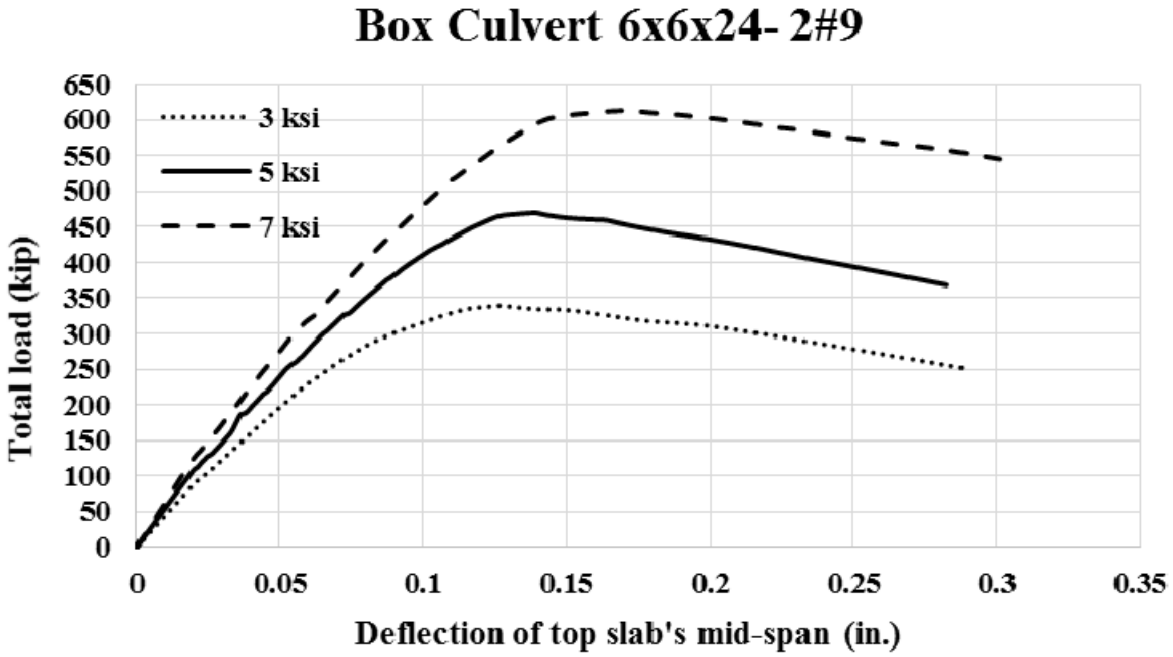
Box Culvert 6x6x24- 2#9
3 ksi
5 ksi
7 ksi
Total load (kip)
650
600
550
500
450
400
350
300
250
200
150
100
50
0
0
0.05
0.1
0.15
0.2
0.25
0.3
0.35
Deflection of top slab's mid-span (in.)

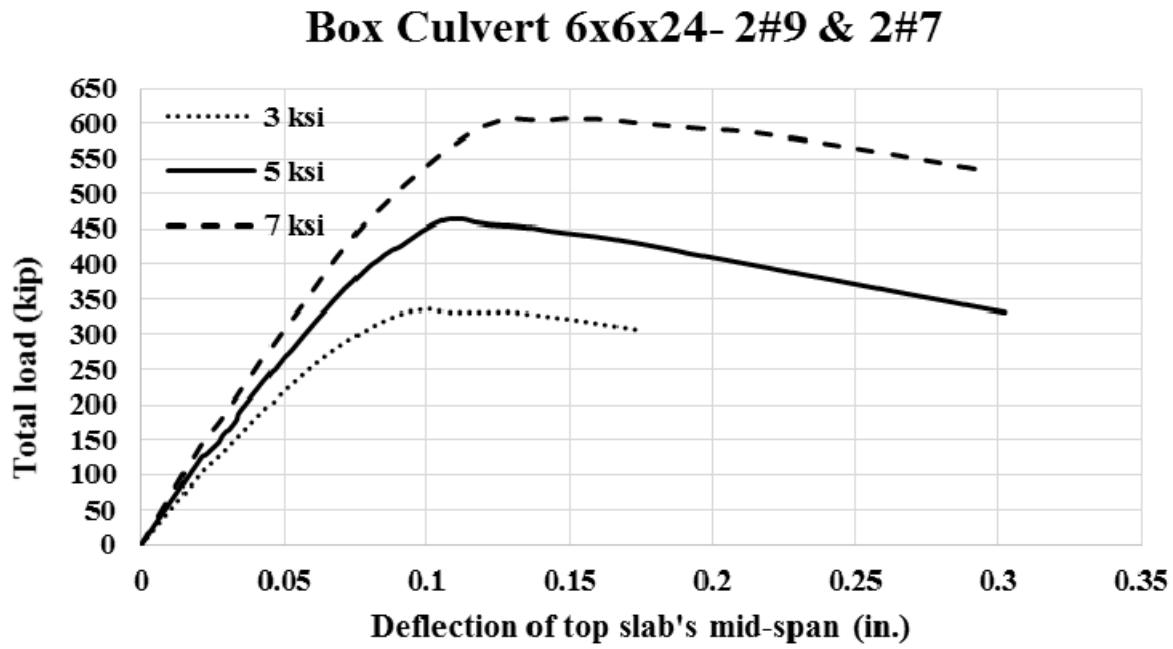
Box Culvert 6x6x24- 2#9 & 2#7
3 ksi
5 ksi
7 ksi
Total load (kip)
650
600
550
500
450
400
350
300
250
200
150
100
50
0
0
0.05
0.1
0.15
0.2
0.25
0.3
0.35
Deflection of top slab's mid-span (in.)

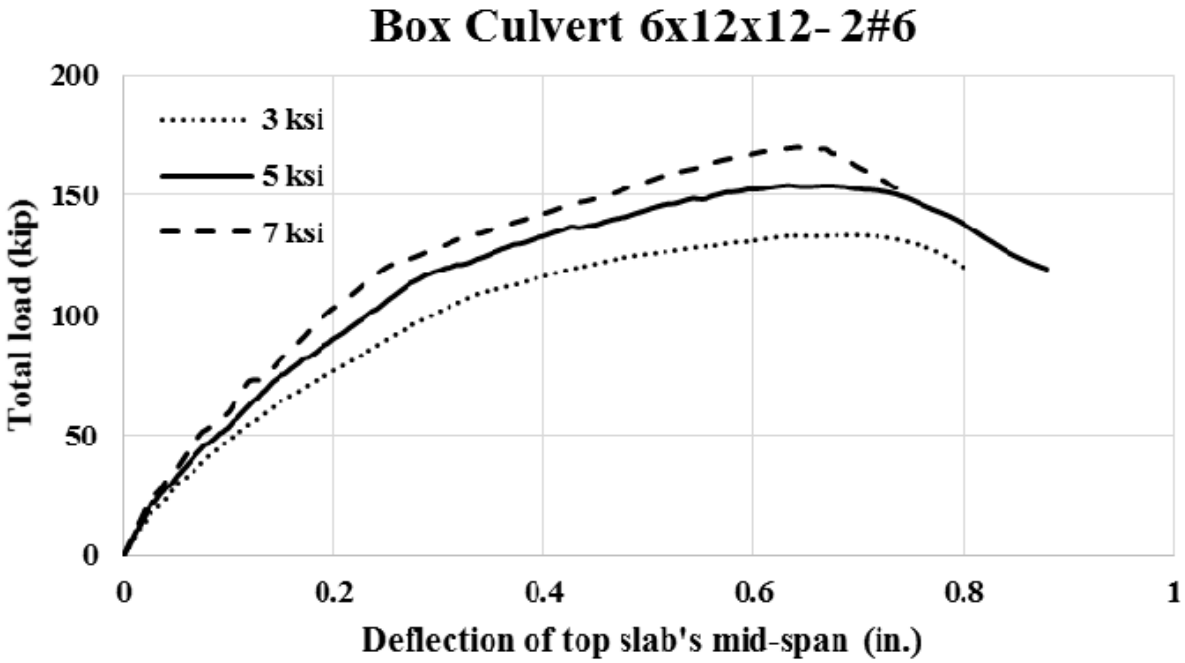
Box Culvert 6x12x12- 2#6
3 ksi
5 ksi
7 ksi
Total load (kip)
200
150
100
50
0
0
0.2
0.4
0.6
0.8
1
Deflection of top slab's mid-span (in.)

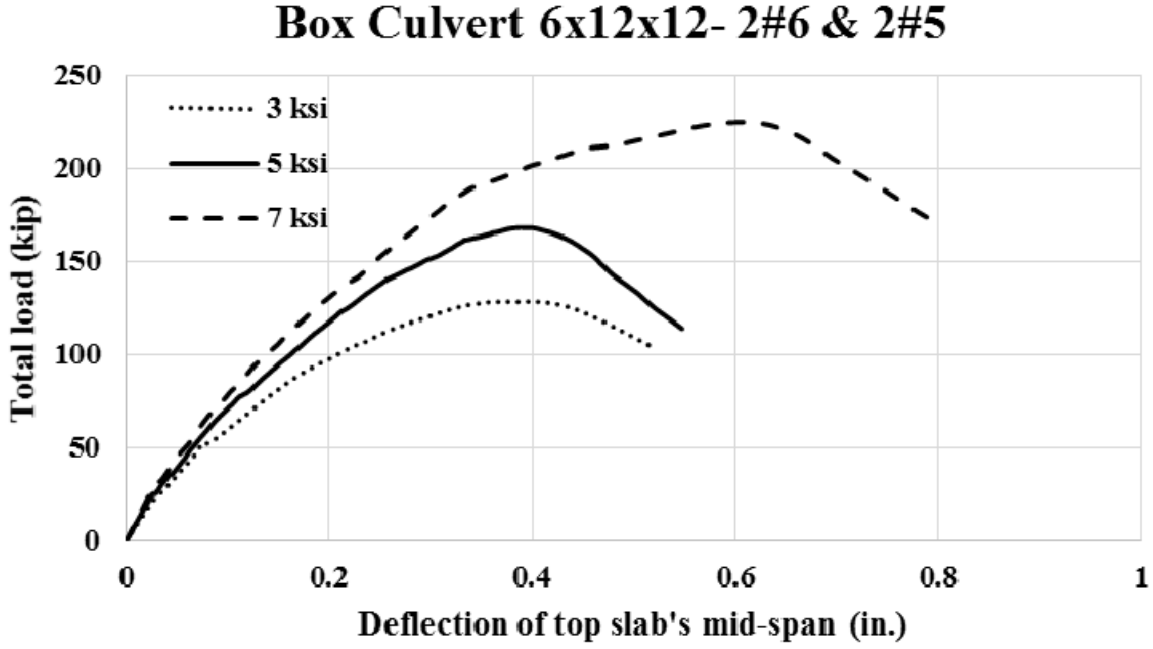
Box Culvert 6x12x12- 2#6 & 2#5
3 ksi
5 ksi
7 ksi
Total load (kip)
250
200
150
100
50
0
0
0.2
0.4
0.6
0.8
1
Deflection of top slab's mid-span (in.)

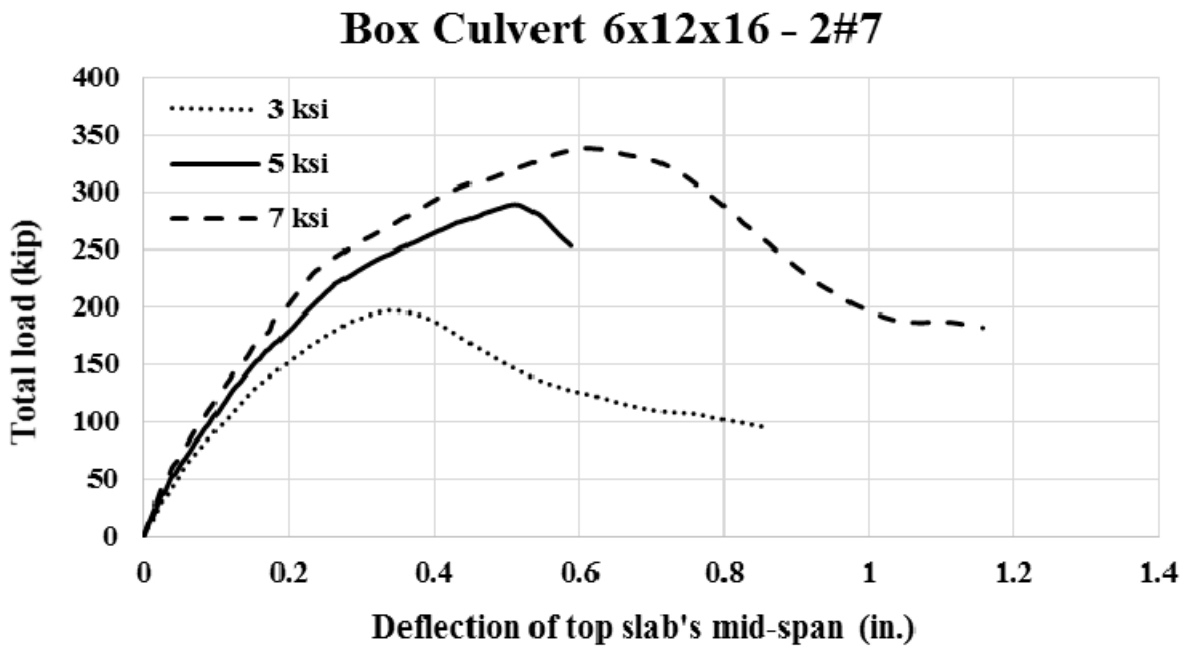
Box Culvert 6x12x16 - 2#7
3 ksi
5 ksi
7 ksi
Total load (kip)
400
350
300
250
200
150
100
50
0
0
0.2
0.4
0.6
0.8
1
1.2
1.4
Deflection of top slab's mid-span (in.)

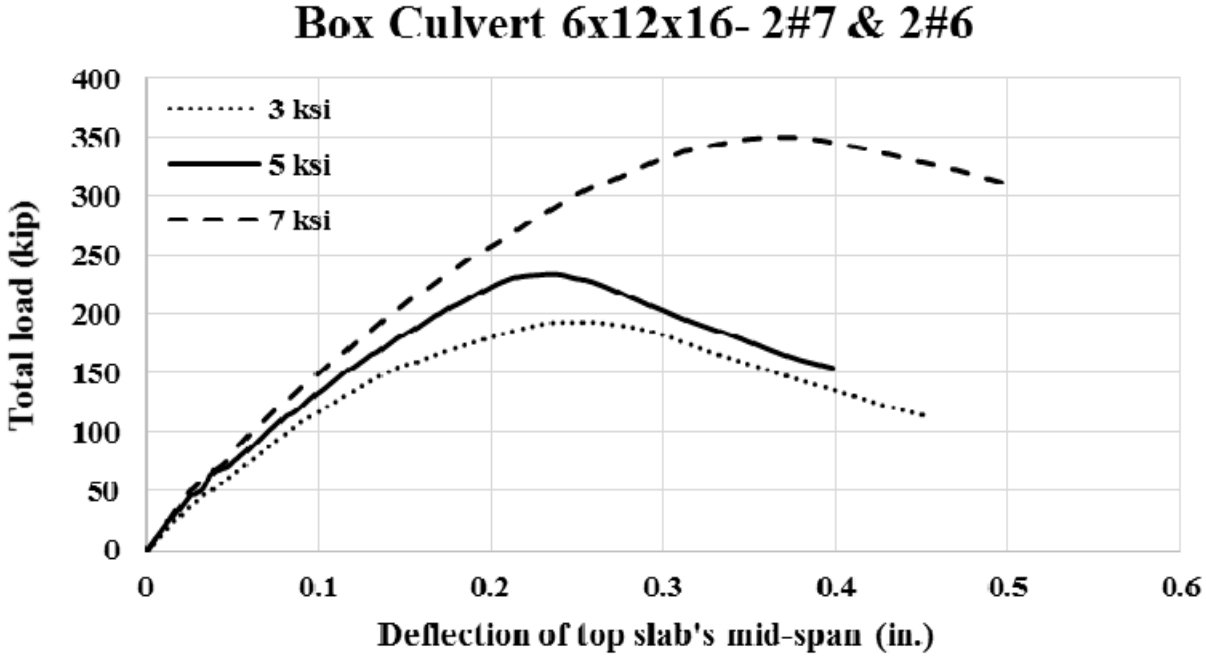
Box Culvert 6x12x16- 2#7 & 2#6
3 ksi
5 ksi
7 ksi
Total load (kip)
400
350
300
250
200
150
100
50
0
0
0.1
0.2
0.3
0.4
0.5
0.6
Deflection of top slab's mid-span (in.)

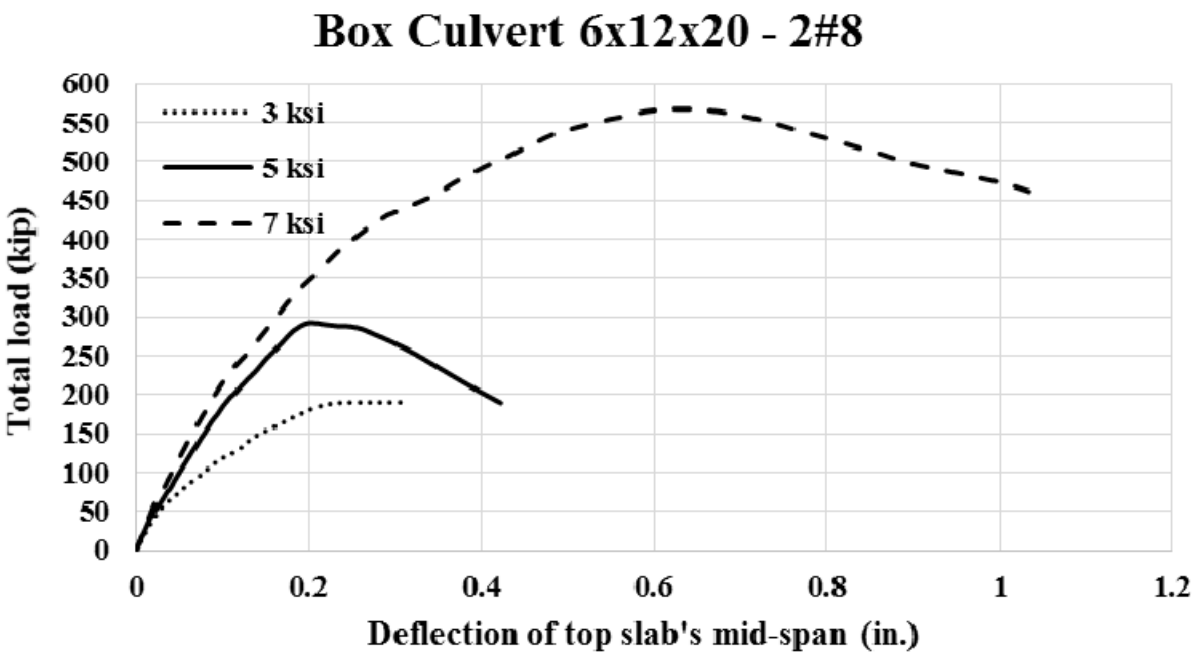
Box Culvert 6x12x20 - 2#8
3 ksi
5 ksi
7 ksi
Total load (kip)
600
550
500
450
400
350
300
250
200
150
100
50
0
0
0.2
0.4
0.6
0.8
1
1.2
Deflection of top slab's mid-span (in.)

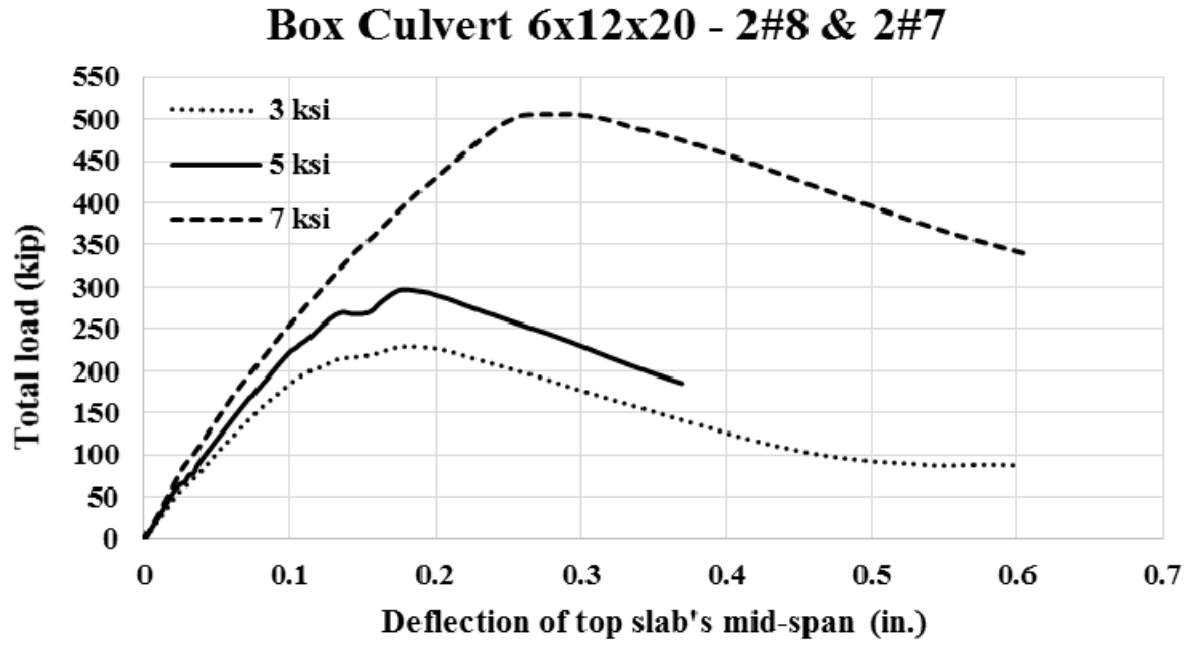
Box Culvert 6x12x20 - 2#8 & 2#7
3 ksi
5 ksi
7 ksi
Total load (kip)
550
500
450
400
350
300
250
200
150
100
50
0
0
0.1
0.2
0.3
0.4
0.5
0.6
0.7
Deflection of top slab's mid-span (in.)

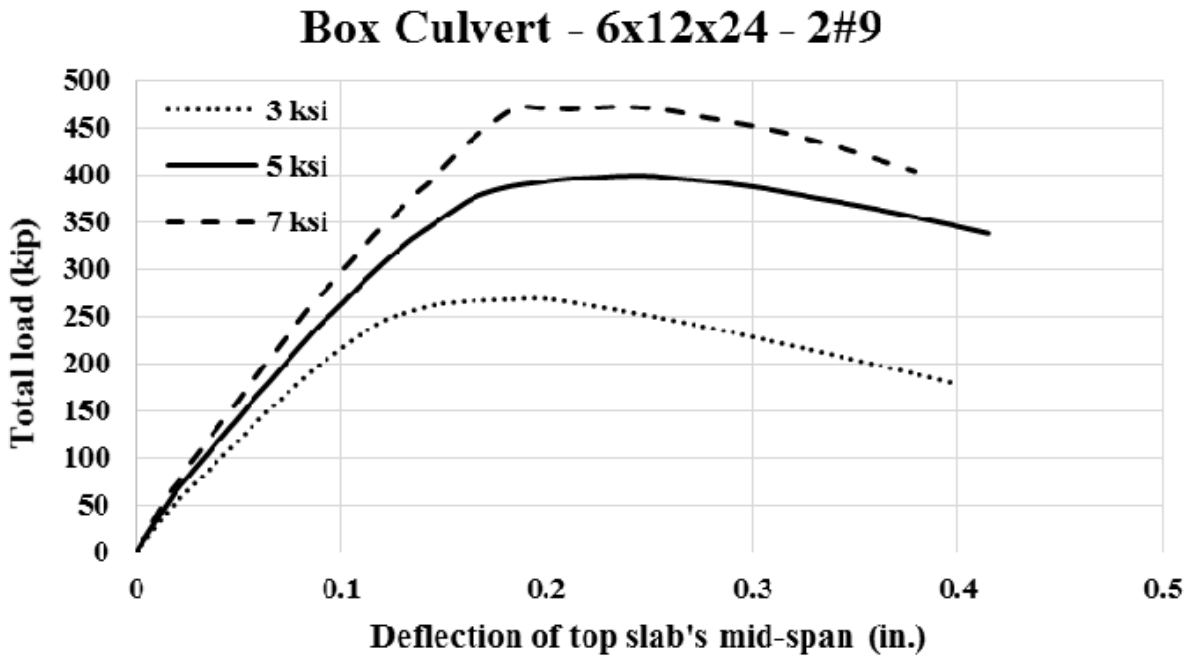
Box Culvert - 6x12x24 - 2#9
3 ksi
5 ksi
7 ksi
Total load (kip)
500
450
400
350
300
250
200
150
100
50
0
0
0.1
0.2
0.3
0.4
0.5
Deflection of top slab's mid-span (in.)

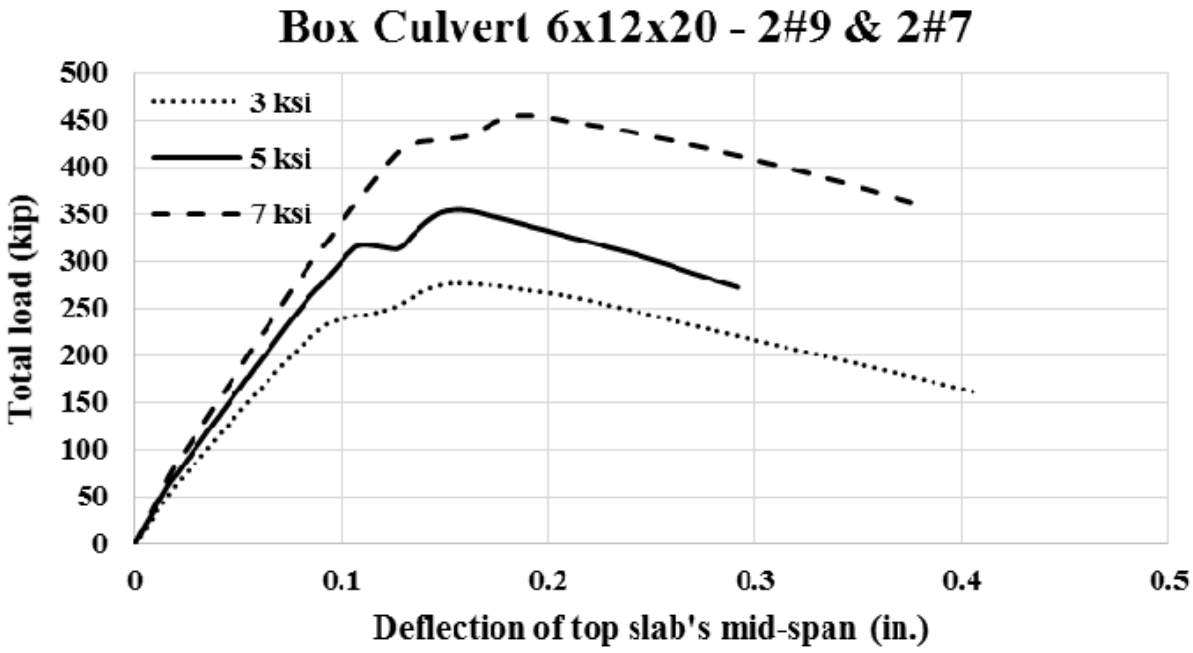
Box Culvert 6x12x20 - 2#9 & 2#7
3 ksi
5 ksi
7 ksi
Total load (kip)
500
450
400
350
300
250
200
150
100
50
0
0
0.1
0.2
0.3
0.4
0.5
Deflection of top slab's mid-span (in.)

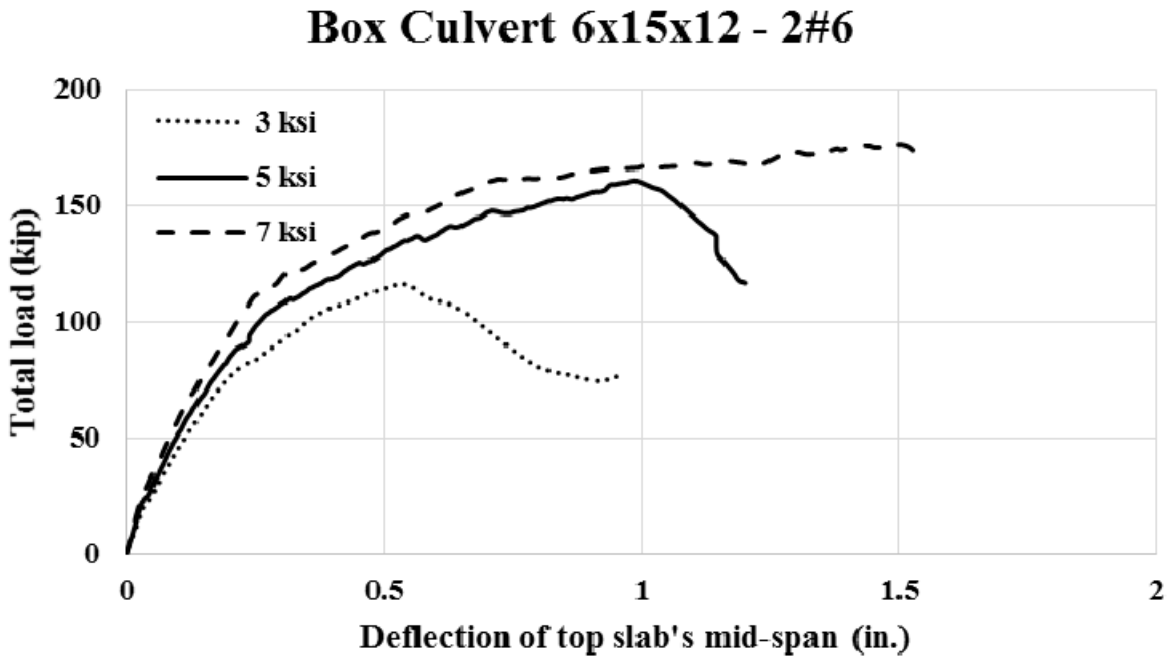
Box Culvert 6x15x12 - 2#6
3 ksi
5 ksi
7 ksi
Total load (kip)
200
150
100
50
0
0
0.5
1
1.5
2
Deflection of top slab's mid-span (in.)

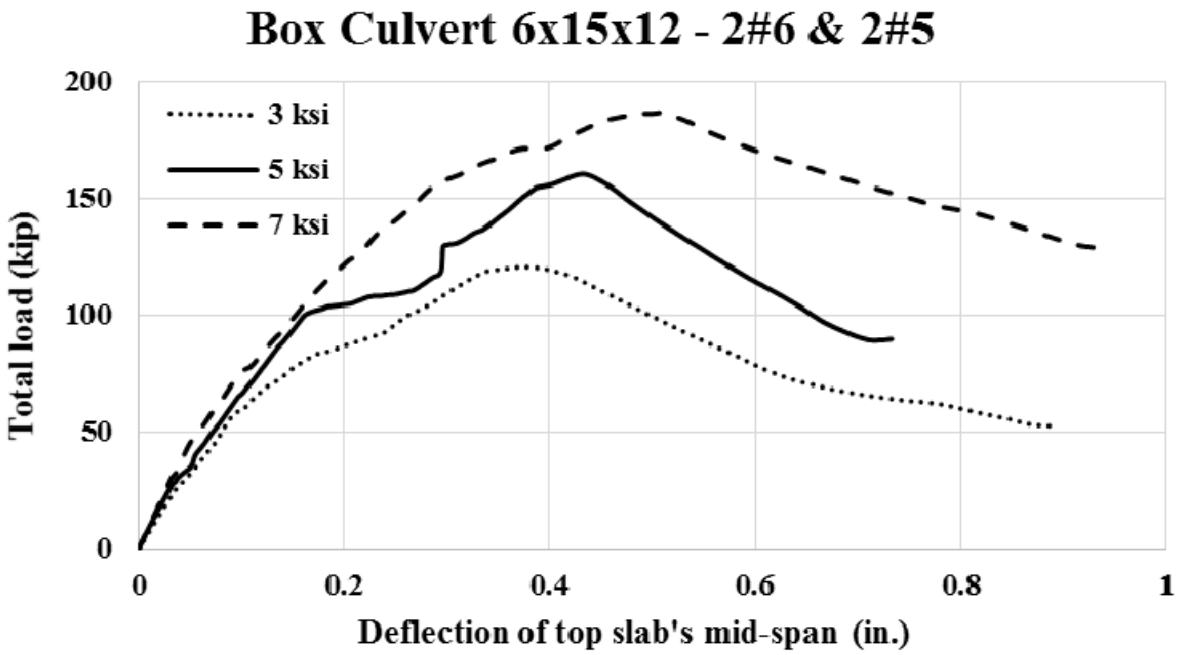
Box Culvert 6x15x12 - 2#6 & 2#5
3 ksi
5 ksi
7 ksi
Total load (kip)
200
150
100
50
0
0
0.2
0.4
0.6
0.8
1
Deflection of top slab's mid-span (in.)

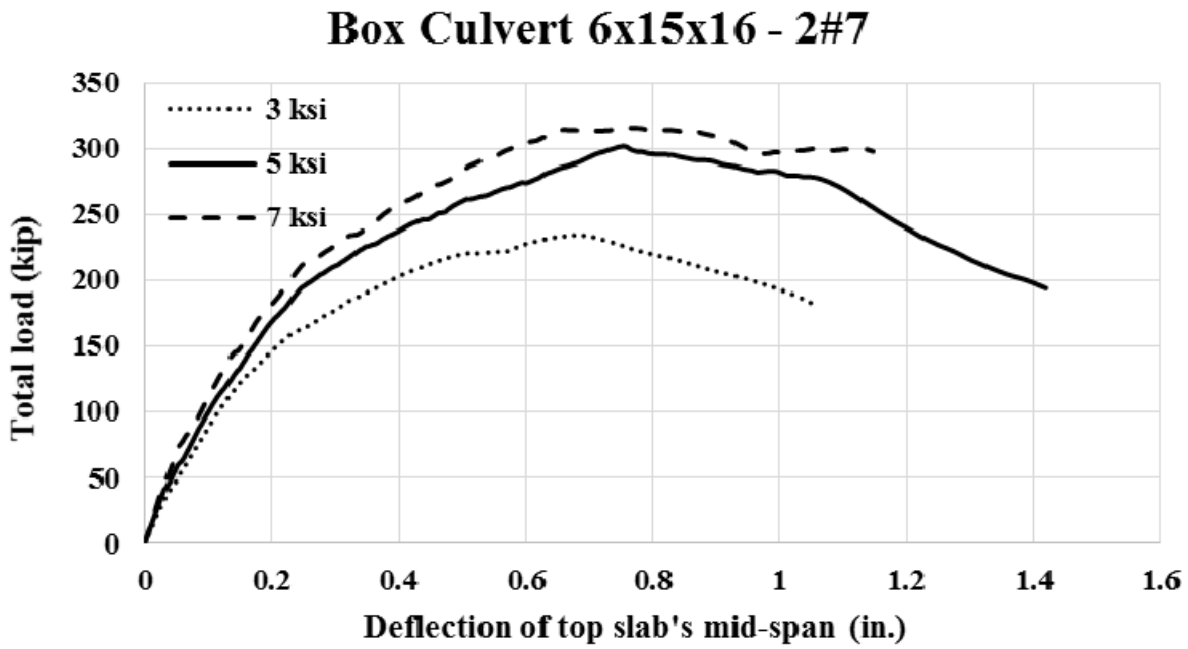
Box Culvert 6x15x16 - 2#7
3 ksi
5 ksi
7 ksi
Total load (kip)
350
300
250
200
150
100
50
0
0
0.2
0.4
0.6
0.8
1
1.2
1.4
1.6
Deflection of top slab's mid-span (in.)

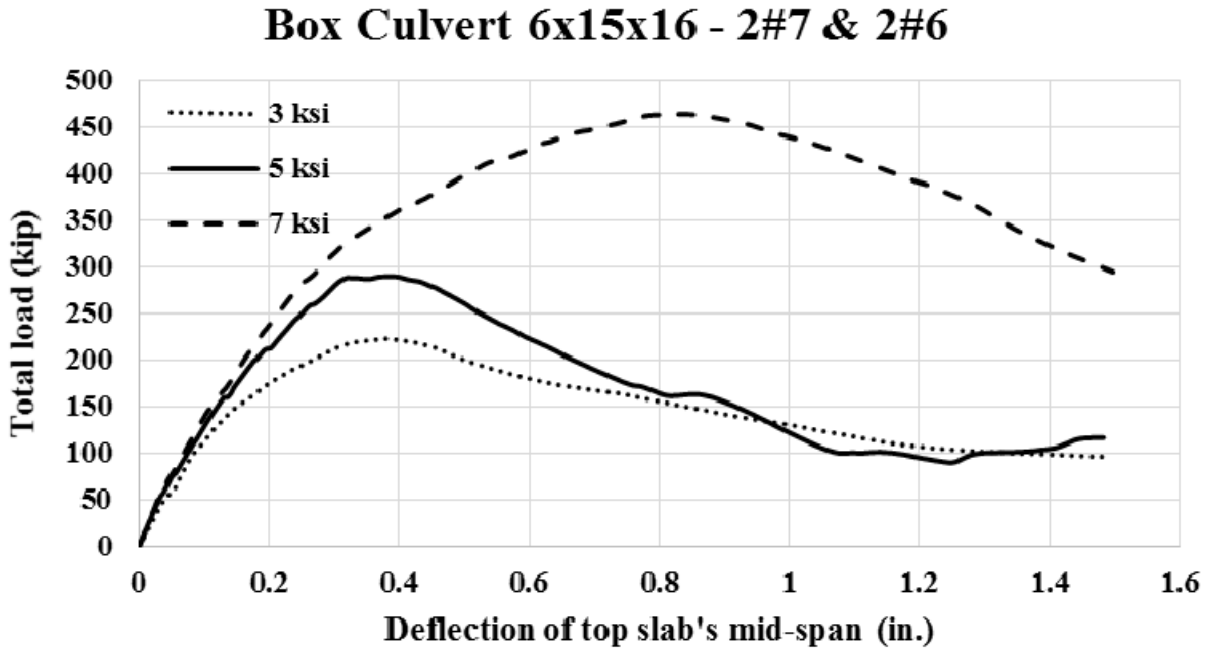
Box Culvert 6x15x16 - 2#7 & 2#6
3 ksi
5 ksi
7 ksi
Total load (kip)
500
450
400
350
300
250
200
150
100
50
0
0
0.2
0.4
0.6
0.8
1
1.2
1.4
1.6
Deflection of top slab's mid-span (in.)

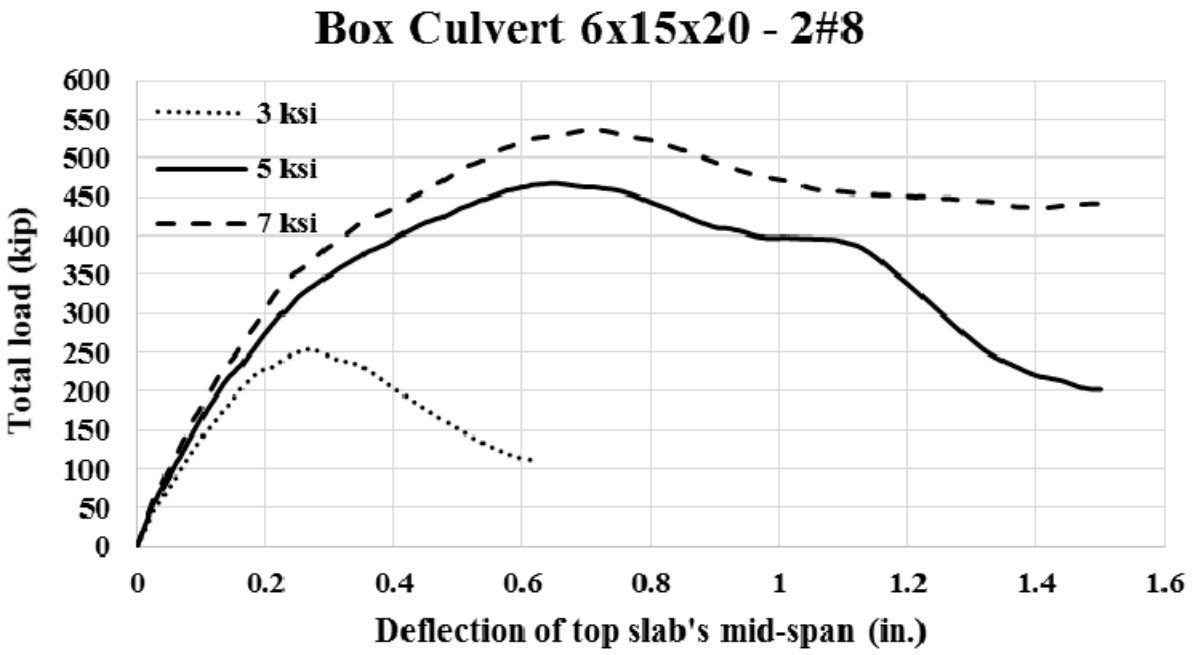
Box Culvert 6x15x20 - 2#8
3 ksi
5 ksi
7 ksi
Total load (kip)
600
550
500
450
400
350
300
250
200
150
100
50
0
0
0.2
0.4
0.6
0.8
1
1.2
1.4
1.6
Deflection of top slab's mid-span (in.)

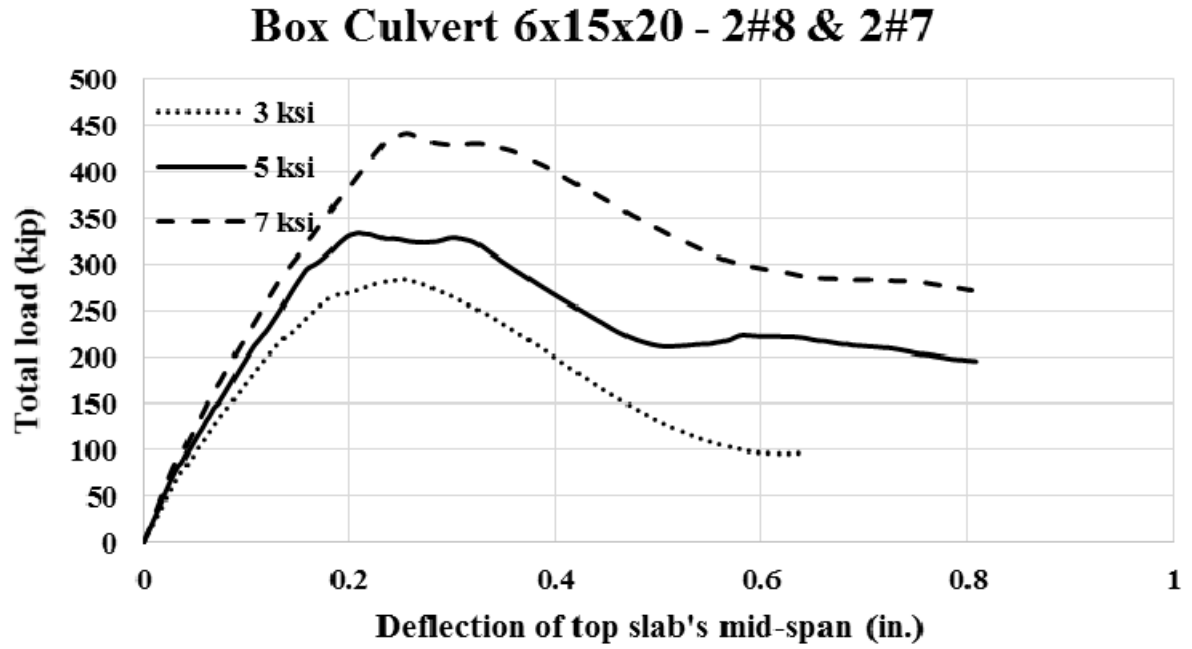
Box Culvert 6x15x20 - 2#8 & 2#7
3 ksi
5 ksi
7 ksi
Total load (kip)
500
450
400
350
300
250
200
150
100
50
0
0
0.2
0.4
0.6
0.8
1
Deflection of top slab's mid-span (in.)

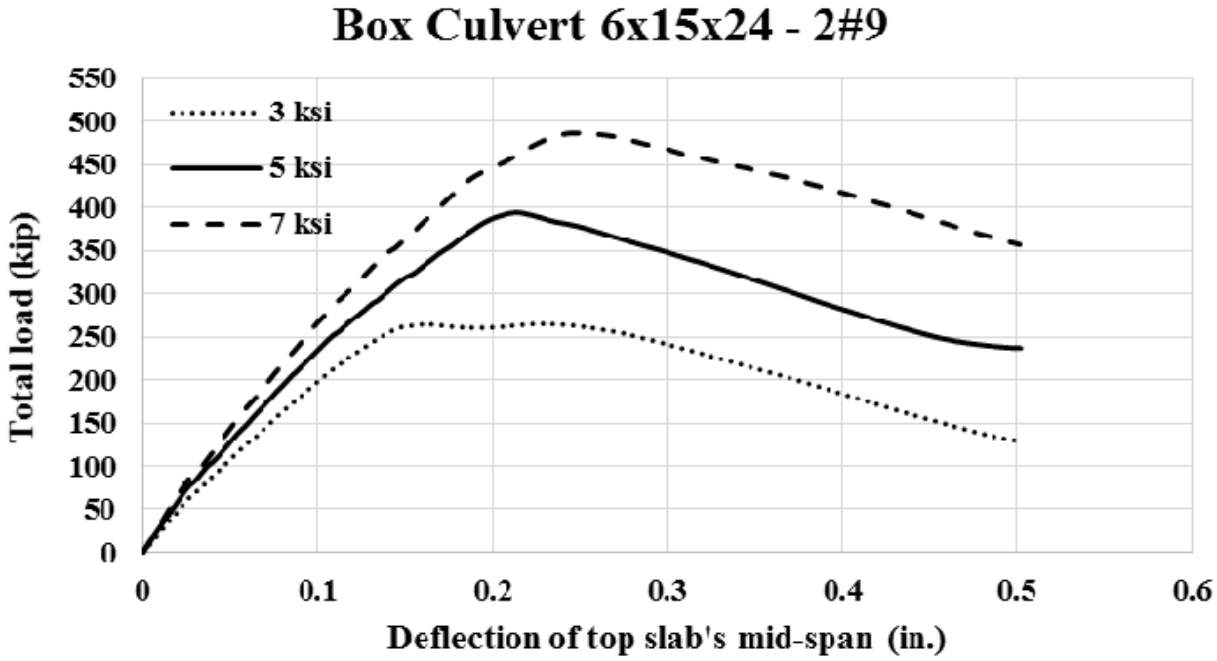
Box Culvert 6x15x24 - 2#9
3 ksi
5 ksi
7 ksi
Total load (kip)
550
500
450
400
350
300
250
200
150
100
50
0
0
0.1
0.2
0.3
0.4
0.5
0.6
Deflection of top slab's mid-span (in.)

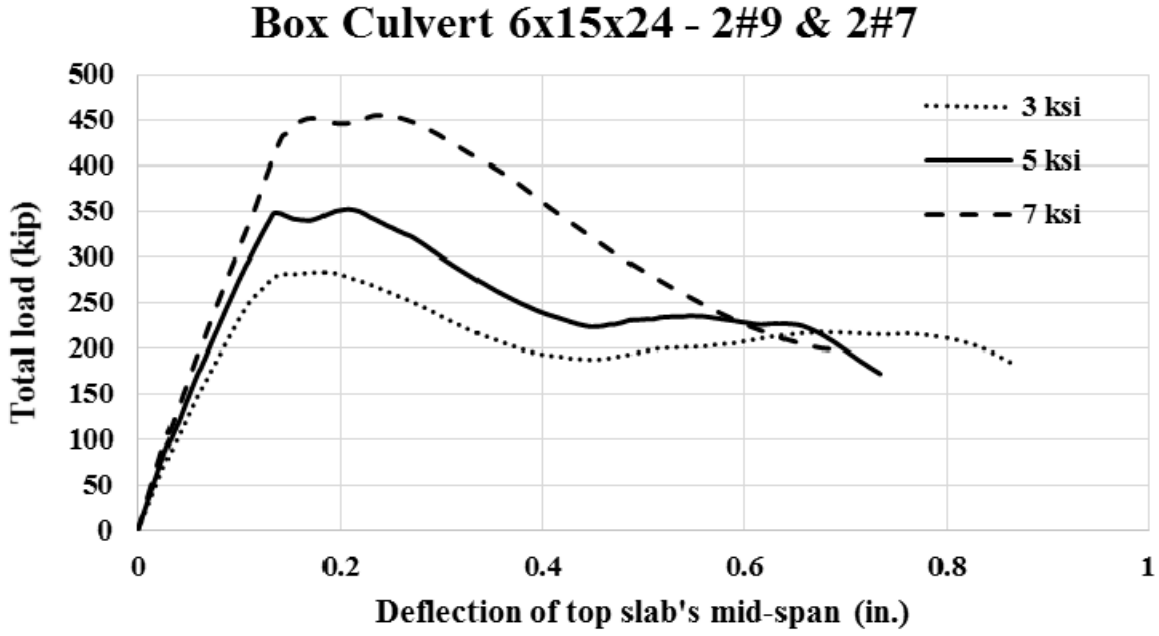
Box Culvert 6x15x24 - 2#9 & 2#7
3 ksi
5 ksi
7 ksi
Total load (kip)
500
450
400
350
300
250
200
150
100
50
0
0
0.2
0.4
0.6
0.8
1
Deflection of top slab's mid-span (in.)

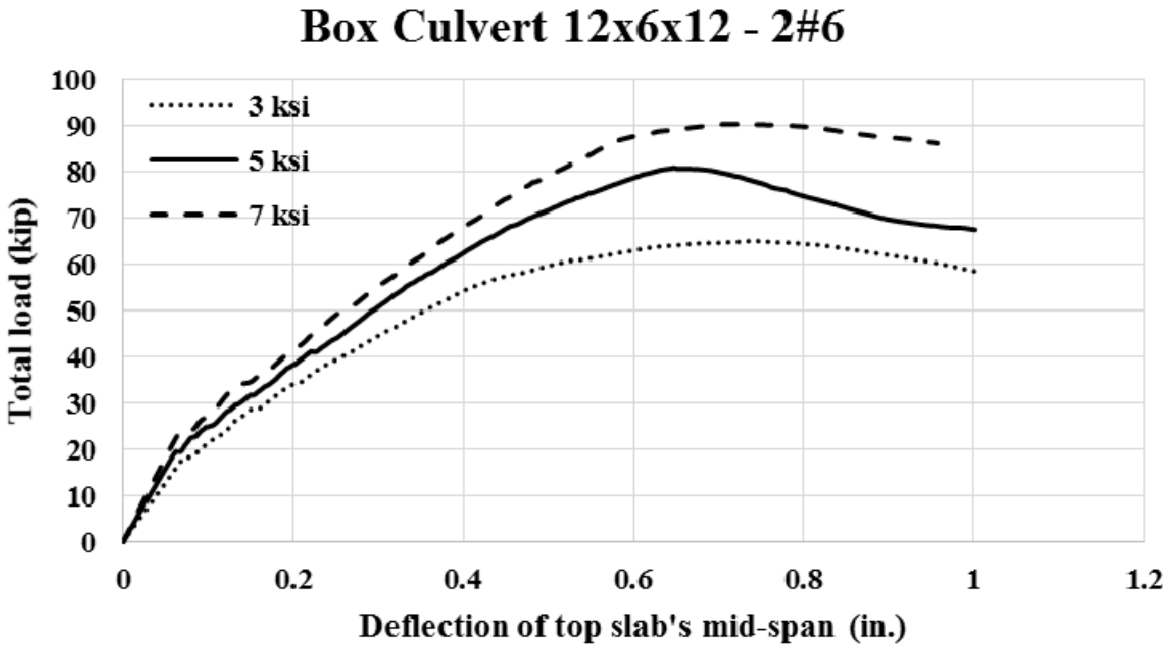
Box Culvert 12x6x12 - 2#6
3 ksi
5 ksi
7 ksi
Total load (kip)
100
90
80
70
60
50
40
30
20
10
0
0
0.2
0.4
0.6
0.8
1
1.2
Deflection of top slab's mid-span (in.)

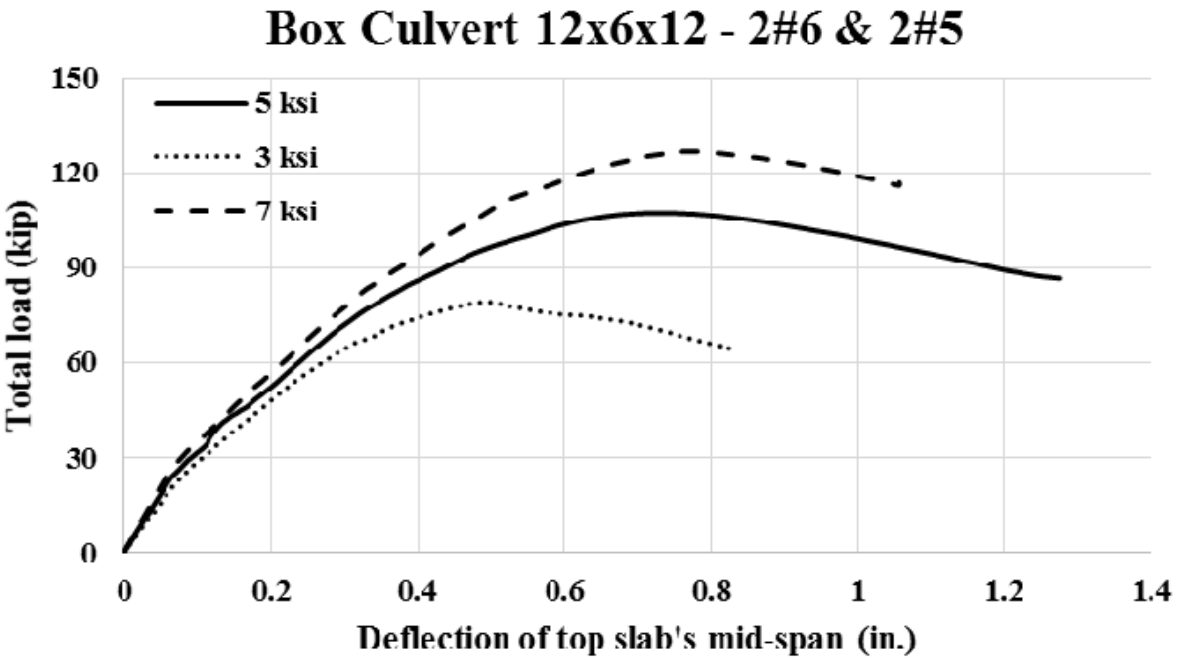
Box Culvert 12x6x12 - 2#6 & 2#5
5 ksi
3 ksi
7 ksi
Total load (kip)
150
120
90
60
30
0
0
0.2
0.4
0.6
0.8
1
1.2
1.4
Deflection of top slab's mid-span (in.)

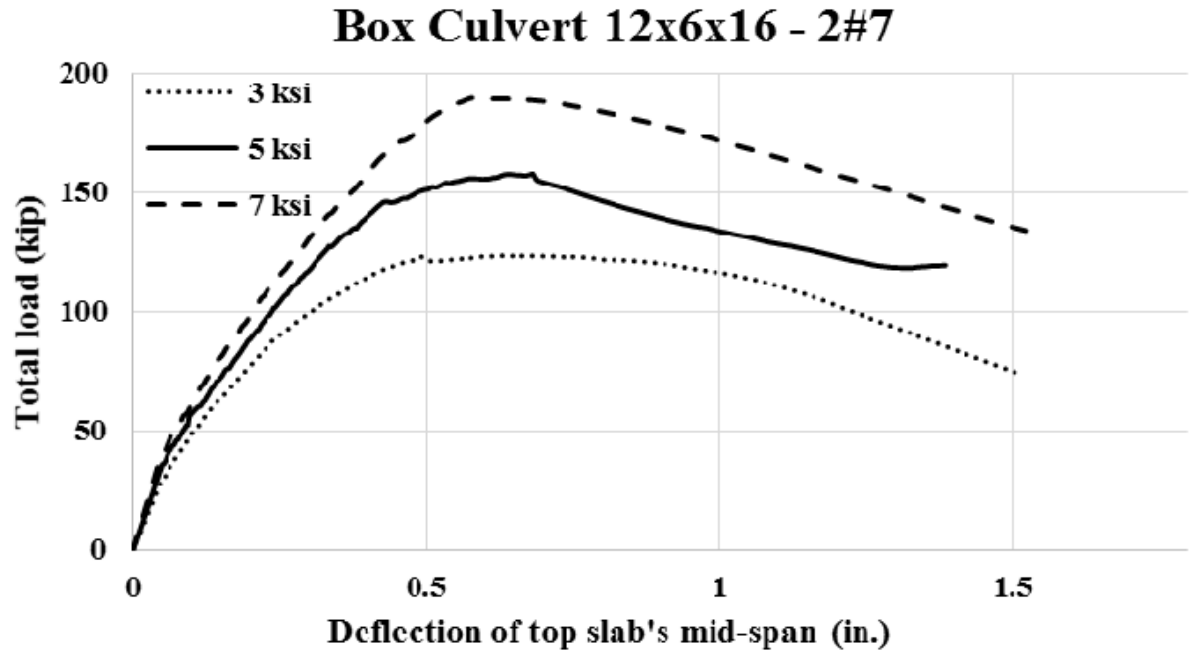
Box Culvert 12x6x16 - 2#7
3 ksi
5 ksi
7 ksi
Total load (kip)
200
150
100
50
0
0
0.5
1
1.5
Deflection of top slab's mid-span (in.)

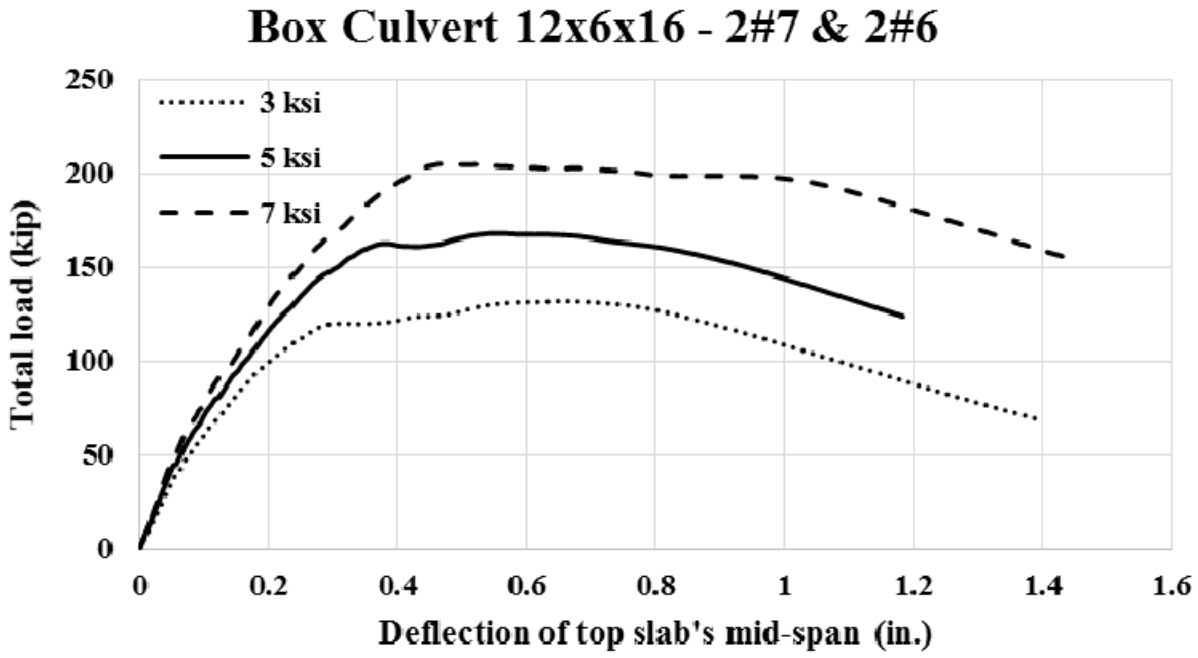
Box Culvert 12x6x16 - 2#7 & 2#6
3 ksi
5 ksi
7 ksi
Total load (kip)
250
200
150
100
50
0
0
0.2
0.4
0.6
0.8
1
1.2
1.4
1.6
Deflection of top slab's mid-span (in.)

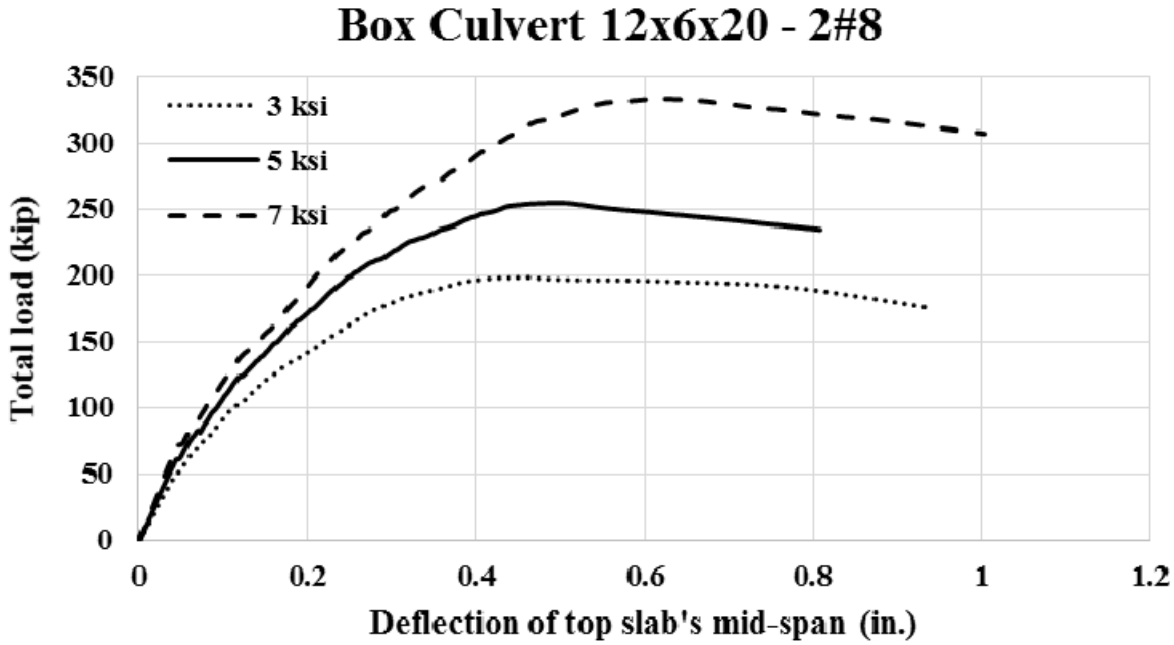
Box Culvert 12x6x20 - 2#8
3 ksi
5 ksi
7 ksi
Total load (kip)
350
300
250
200
150
100
50
0
0
0.2
0.4
0.6
0.8
1
1.2
Deflection of top slab's mid-span (in.)

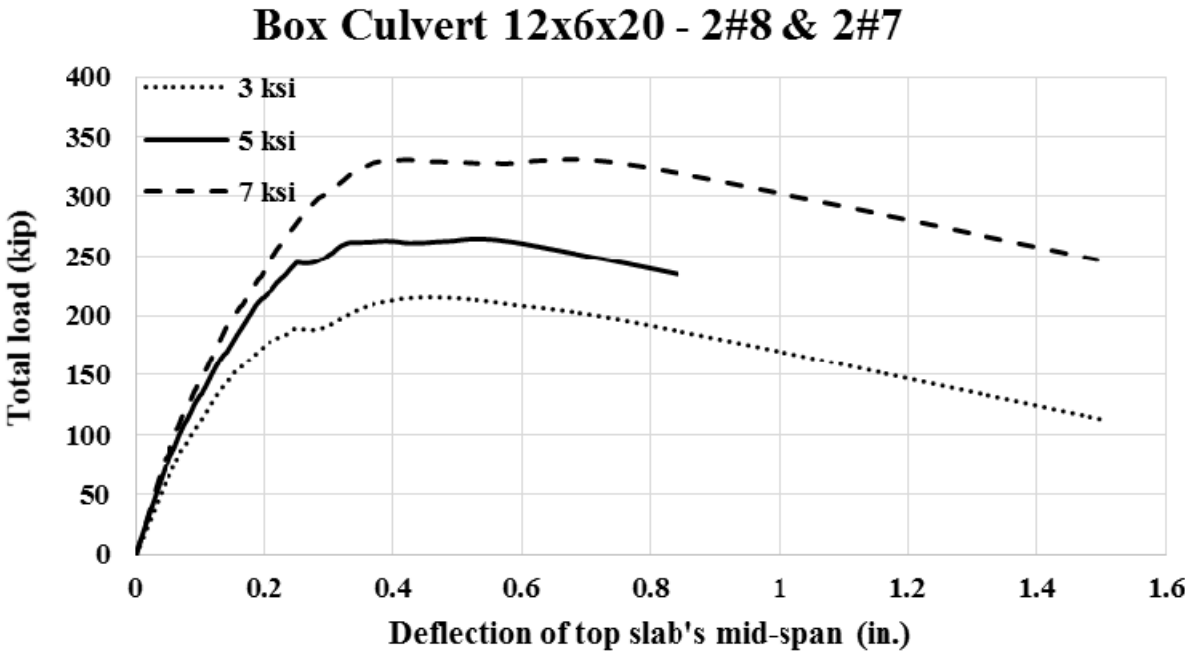
Box Culvert 12x6x20 - 2#8 & 2#7
3 ksi
5 ksi
7 ksi
Total load (kip)
400
350
300
250
200
150
100
50
0
0
0.2
0.4
0.6
0.8
1
1.2
1.4
1.6
Deflection of top slab's mid-span (in.)

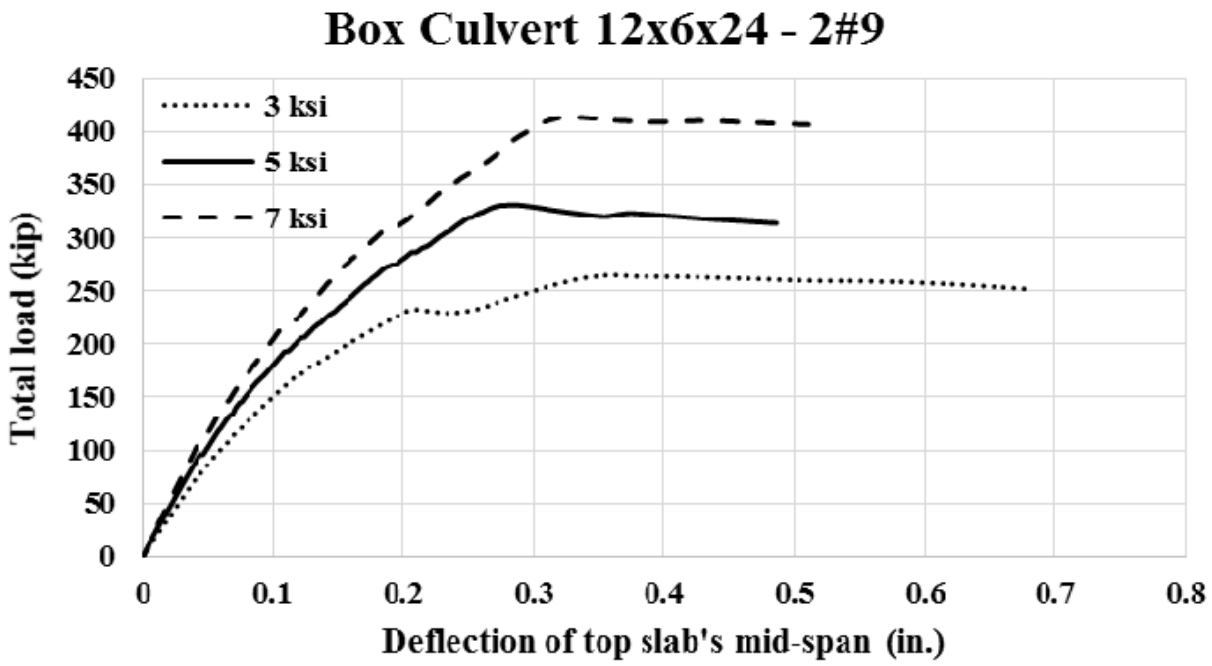
Box Culvert 12x6x24 - 2#9
3 ksi
5 ksi
7 ksi
Total load (kip)
450
400
350
300
250
200
150
100
50
0
0
0.1
0.2
0.3
0.4
0.5
0.6
0.7
0.8
Deflection of top slab's mid-span (in.)

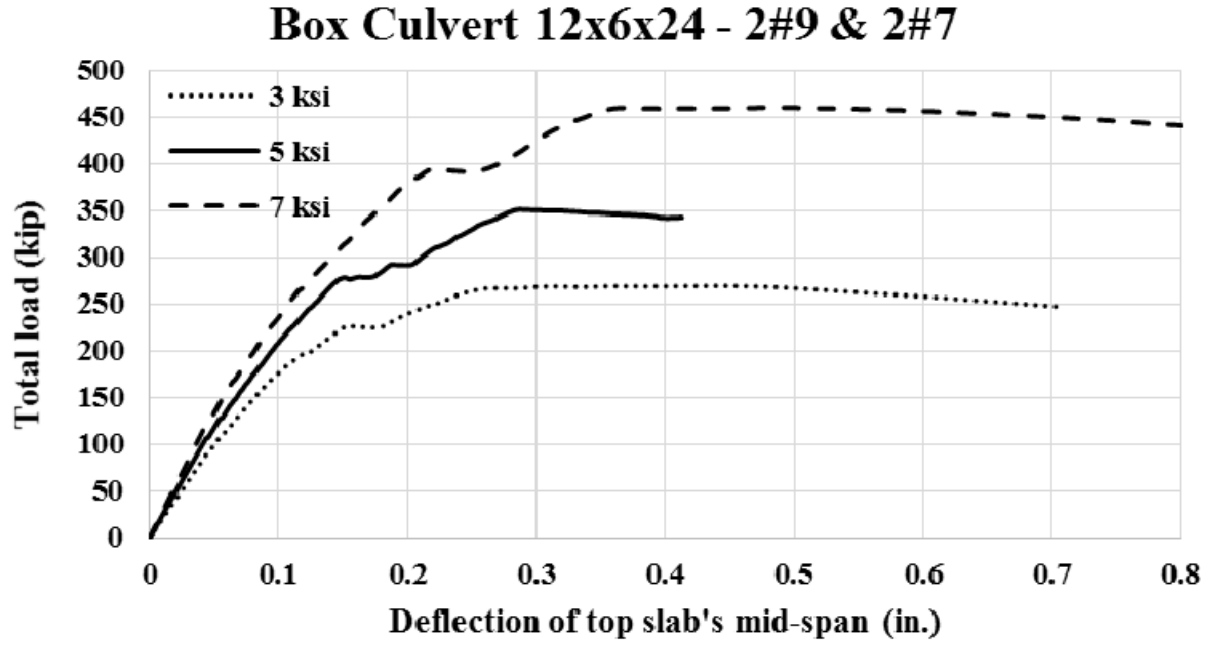
Box Culvert 12x6x24 - 2#9 & 2#7
3 ksi
5 ksi
7 ksi
Total load (kip)
500
450
400
350
300
250
200
150
100
50
0
0
0.1
0.2
0.3
0.4
0.5
0.6
0.7
0.8
Deflection of top slab's mid-span (in.)

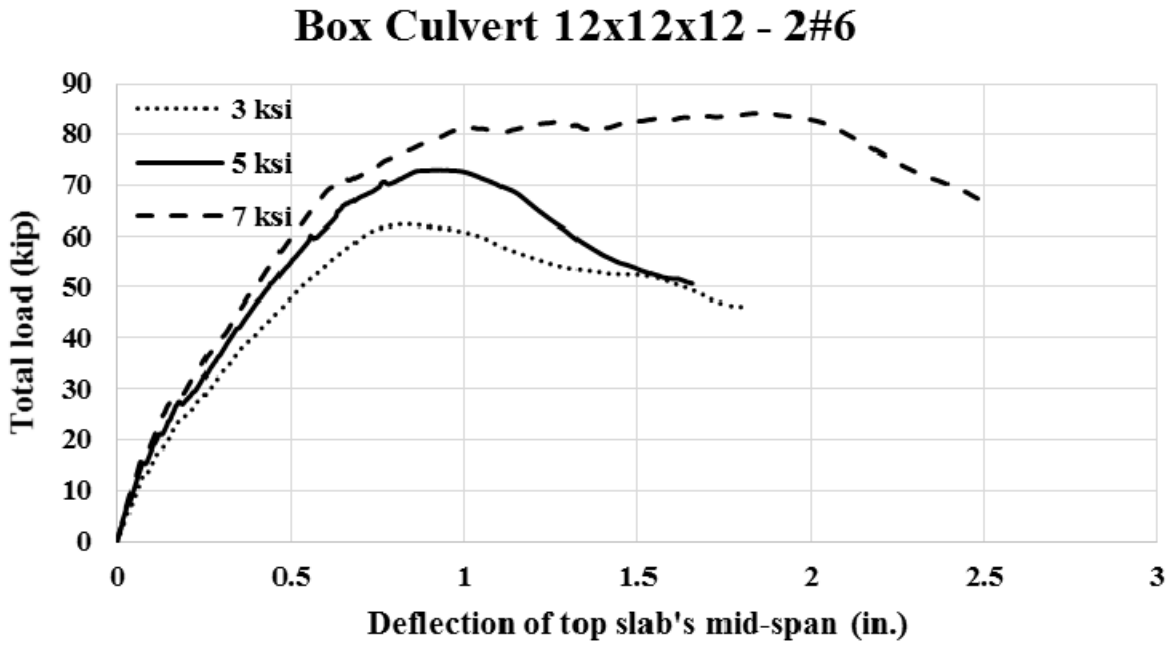
Box Culvert 12x12x12 - 2#6
3 ksi
5 ksi
7 ksi
Total load (kip)
0
10
20
30
40
50
60
70
80
90
0
0.5
1
1.5
2
2.5
3
Deflection of top slab's mid-span (in.)

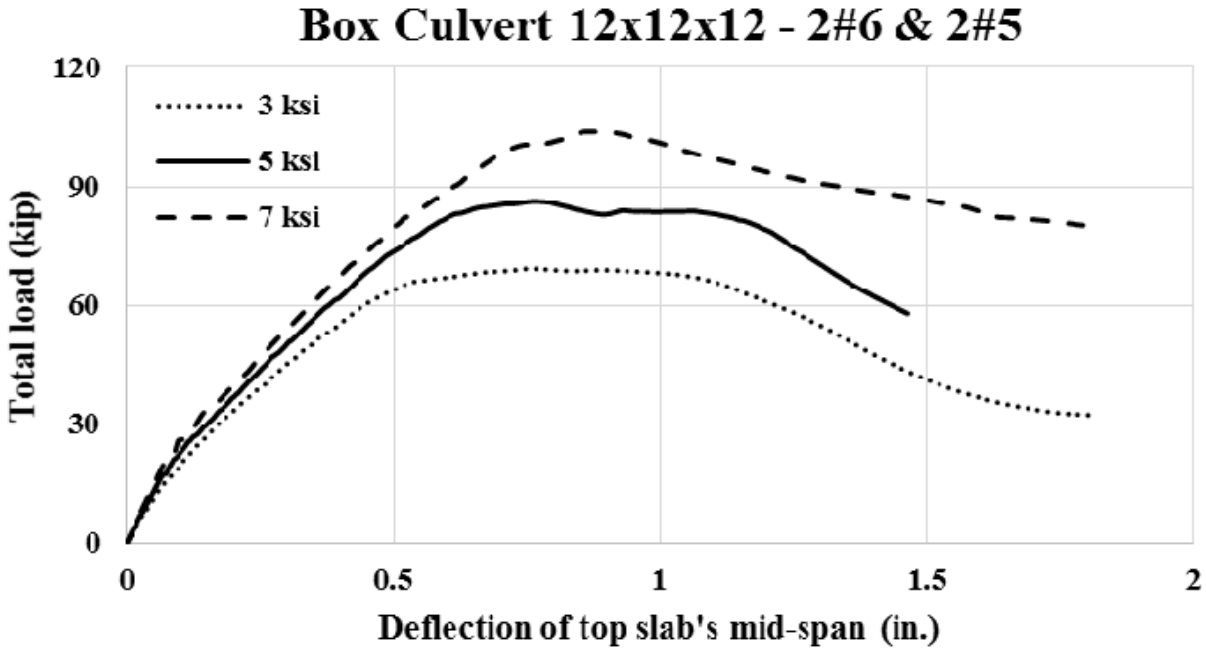
Box Culvert 12x12x12 - 2#6 & 2#5
3 ksi
5 ksi
7 ksi
Total load (kip)
0
30
60
90
120
0
0.5
1
1.5
2
Deflection of top slab's mid-span (in.)

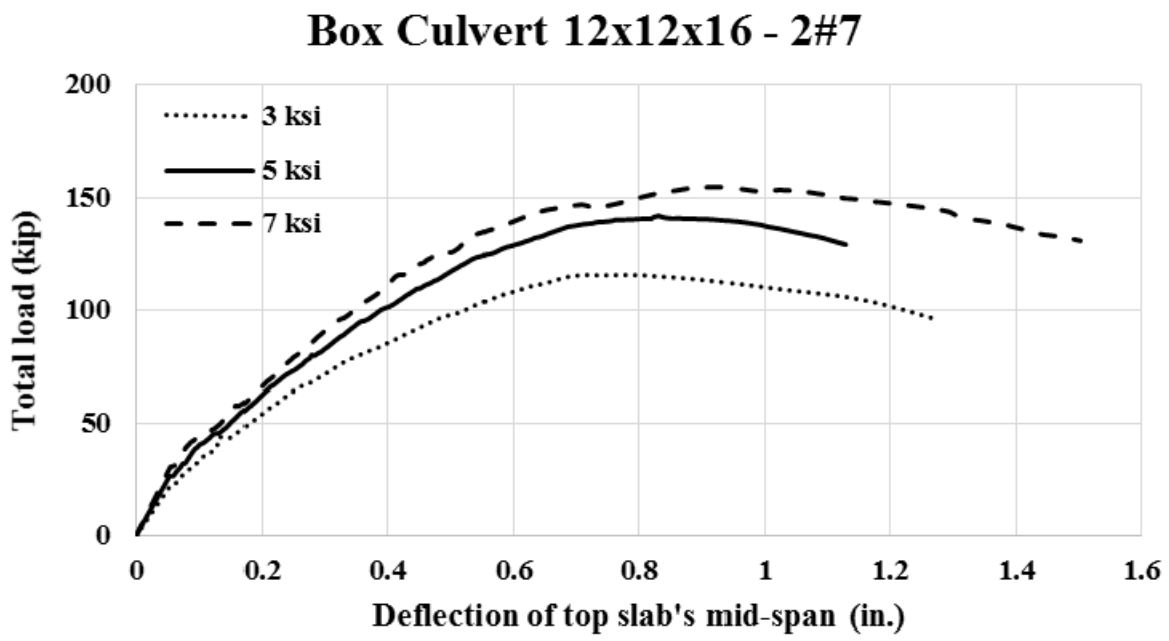
Box Culvert 12x12x16 - 2#7
3 ksi
5 ksi
7 ksi
Total load (kip)
200
150
100
50
0
0
0.2
0.4
0.6
0.8
1
1.2
1.4
1.6
Deflection of top slab's mid-span (in.)

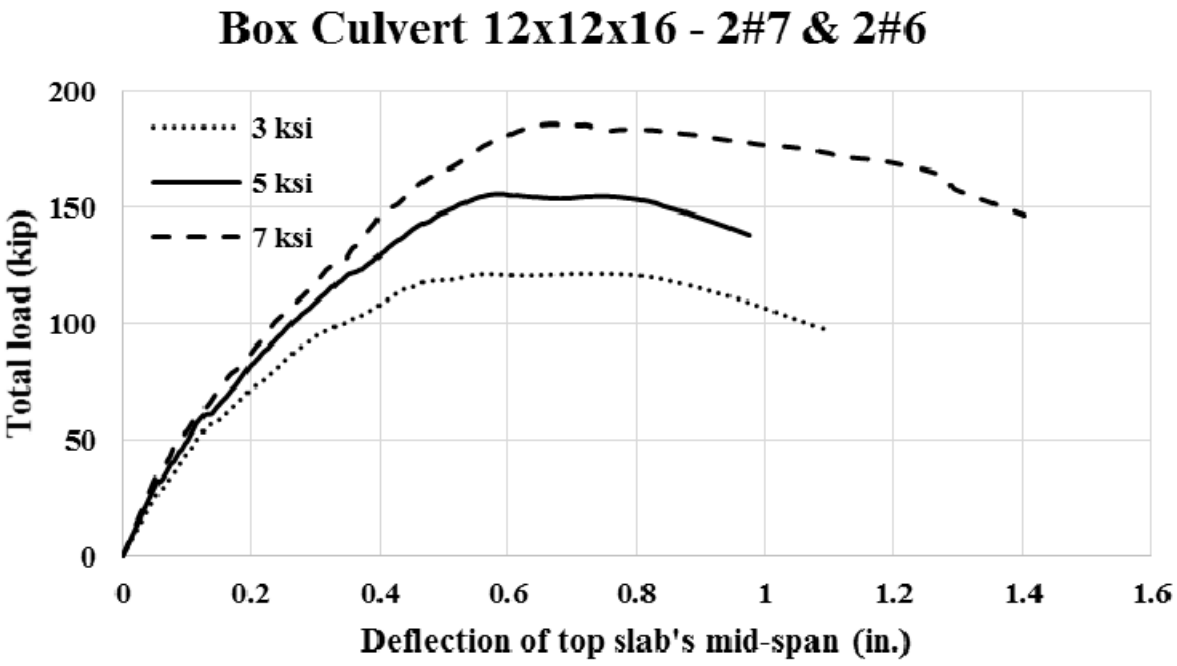
Box Culvert 12x12x16 - 2#7 & 2#6
3 ksi
5 ksi
7 ksi
Total load (kip)
200
150
100
50
0
0
0.2
0.4
0.6
0.8
1
1.2
1.4
1.6
Deflection of top slab's mid-span (in.)

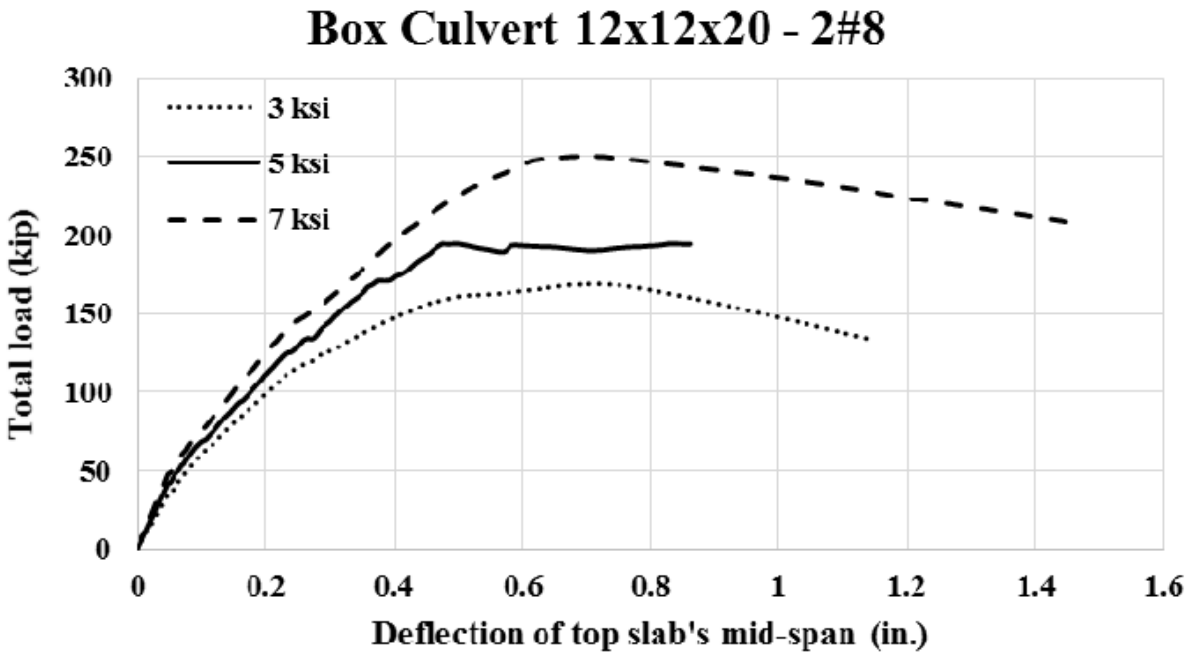
Box Culvert 12x12x20 - 2#8
3 ksi
5 ksi
7 ksi
Total load (kip)
300
250
200
150
100
50
0
0
0.2
0.4
0.6
0.8
1
1.2
1.4
1.6
Deflection of top slab's mid-span (in.)

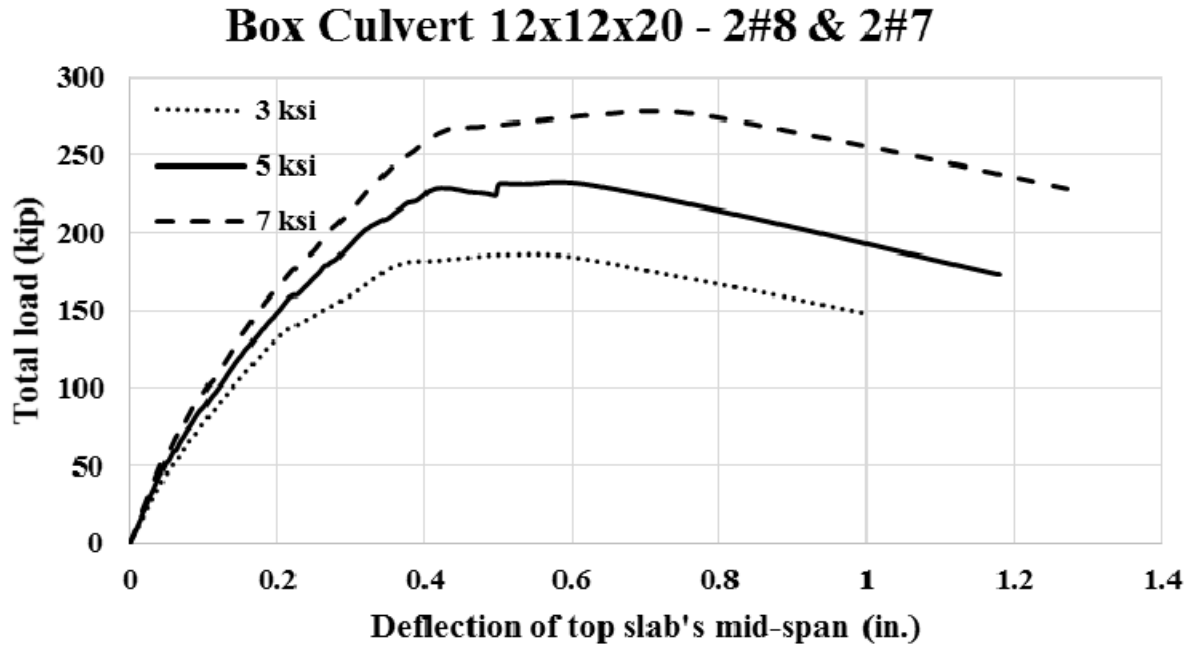
Box Culvert 12x12x20 - 2#8 & 2#7
3 ksi
5 ksi
7 ksi
Total load (kip)
300
250
200
150
100
50
0
0
0.2
0.4
0.6
0.8
1
1.2
1.4
Deflection of top slab's mid-span (in.)

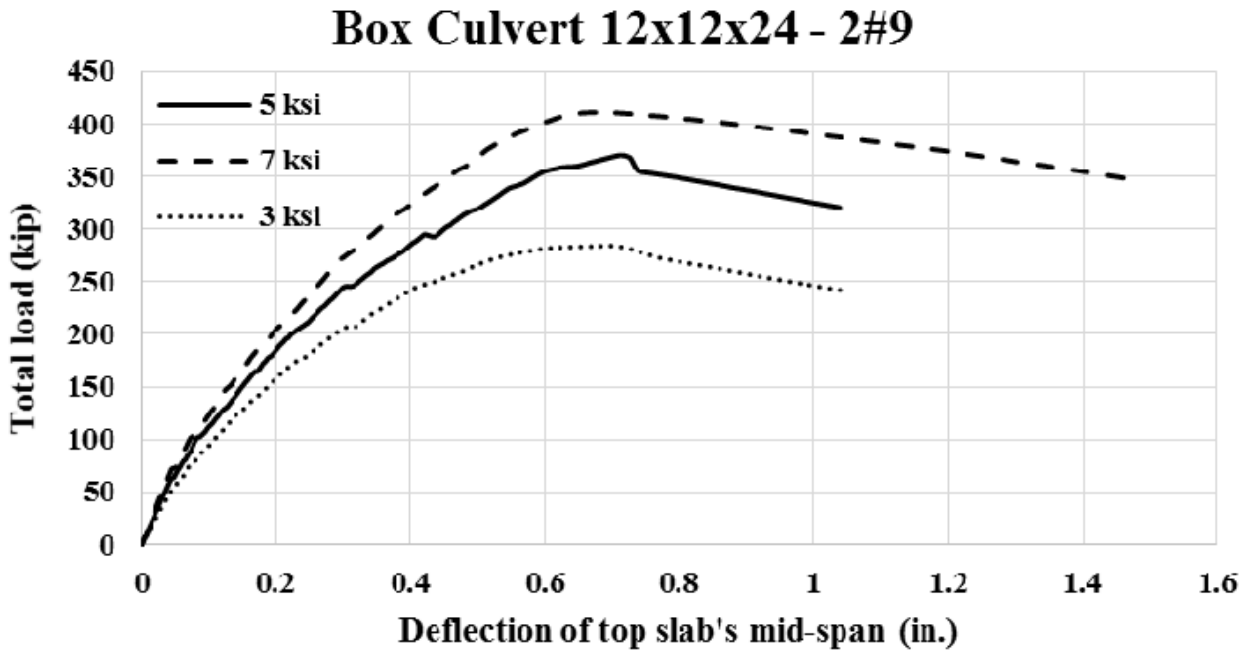
Box Culvert 12x12x24 - 2#9
5 ksi
7 ksi
3 ksi
Total load (kip)
450
400
350
300
250
200
150
100
50
0
0
0.2
0.4
0.6
0.8
1
1.2
1.4
1.6
Deflection of top slab's mid-span (in.)

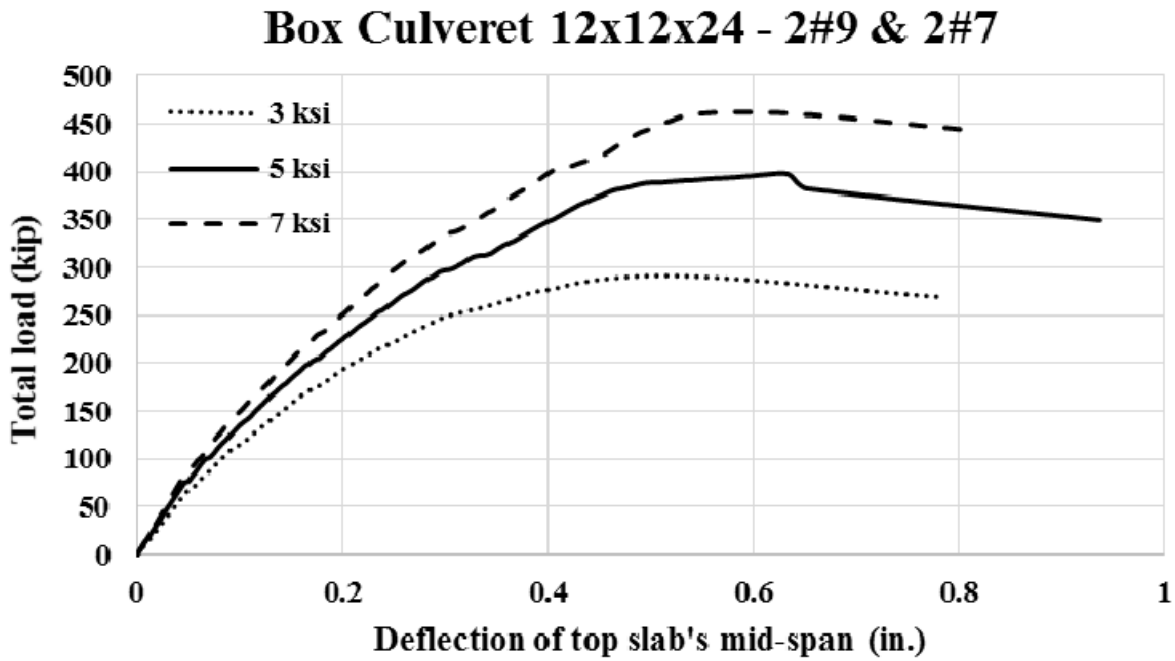
Box Culveret 12x12x24 - 2#9 & 2#7
3 ksi
5 ksi
7 ksi
Total load (kip)
500
450
400
350
300
250
200
150
100
50
0
0
0.2
0.4
0.6
0.8
1
Deflection of top slab's mid-span (in.)

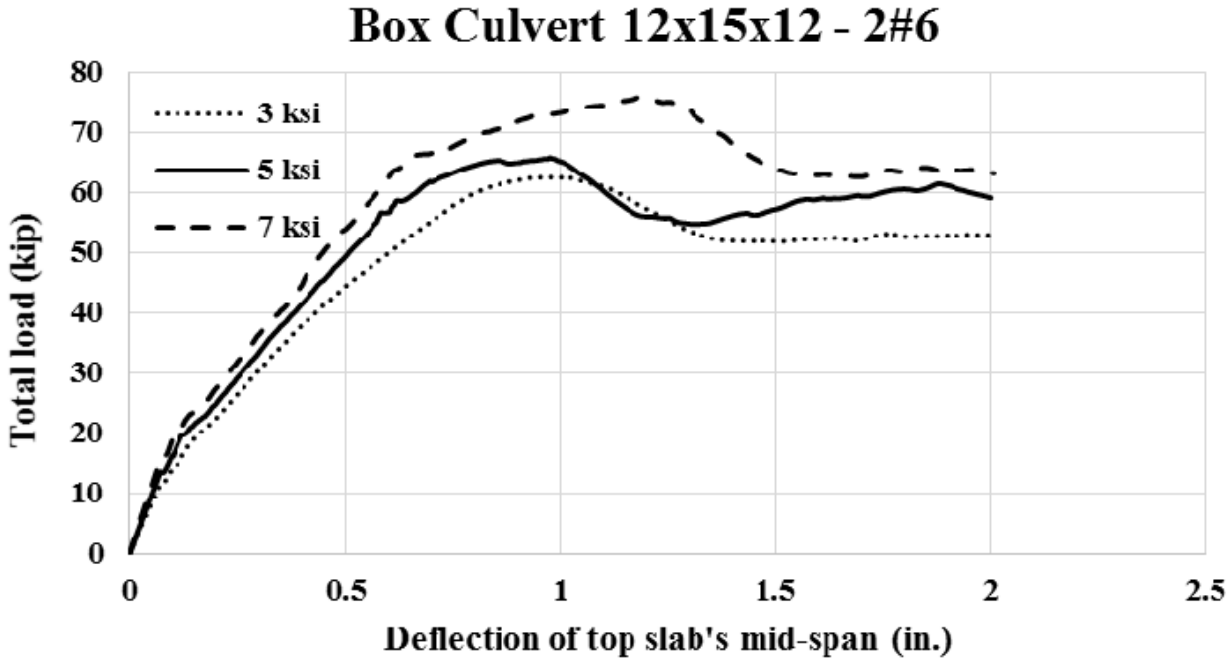
Box Culvert 12x15x12 - 2#6
3 ksi
5 ksi
7 ksi
Total load (kip)
Deflection of top slab's mid-span (in.)
0
10
20
30
40
50
60
70
80
0
0.5
1
1.5
2
2.5

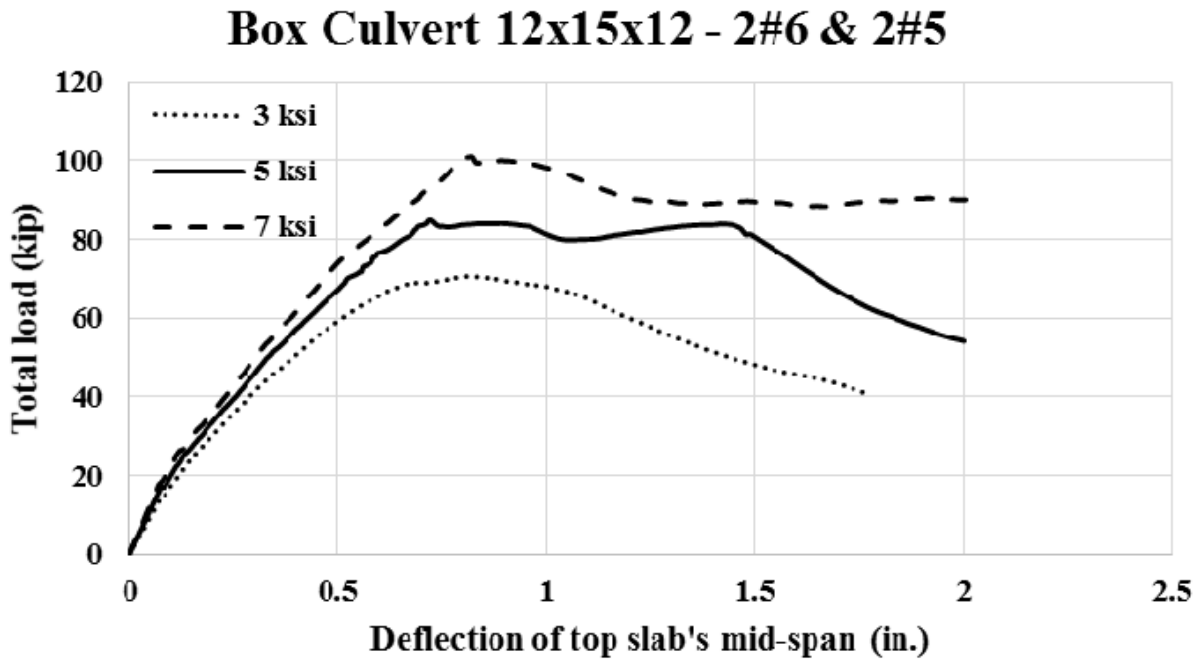
Box Culvert 12x15x12 - 2#6 & 2#5
3 ksi
5 ksi
7 ksi
Total load (kip)
Deflection of top slab's mid-span (in.)
0
20
40
60
80
100
120
0
0.5
1
1.5
2
2.5

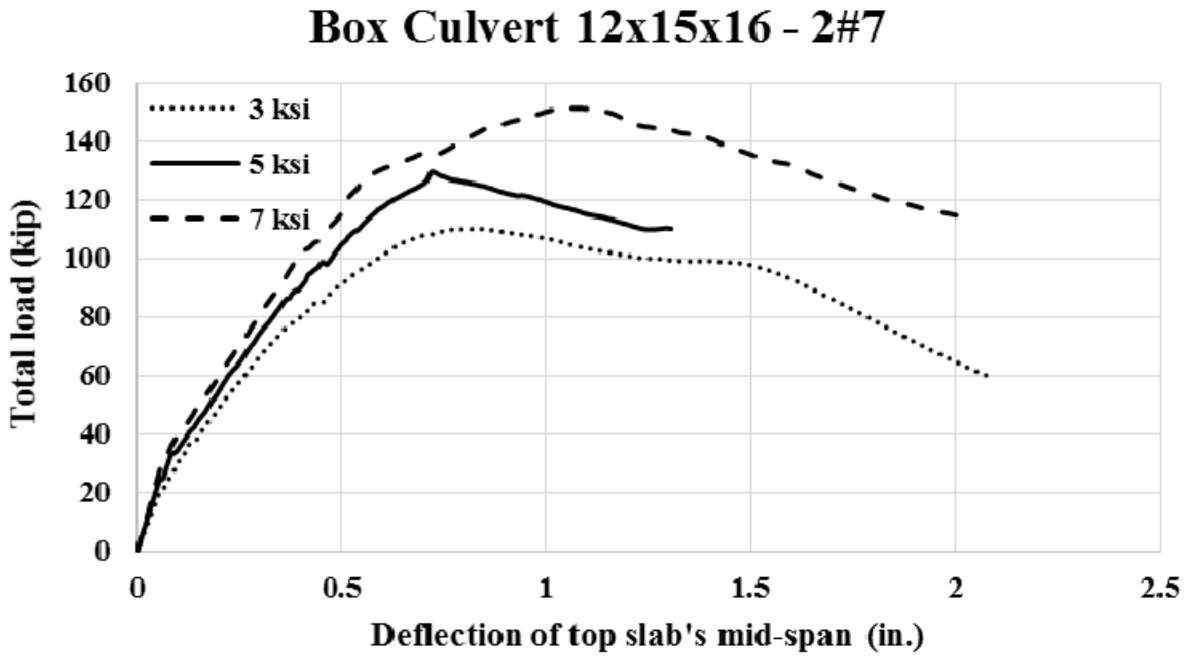
Box Culvert 12x15x16 - 2#7
3 ksi
5 ksi
7 ksi
Total load (kip)
0
20
40
60
80
100
120
140
160
0
0.5
1
1.5
2
2.5
Deflection of top slab's mid-span (in.)

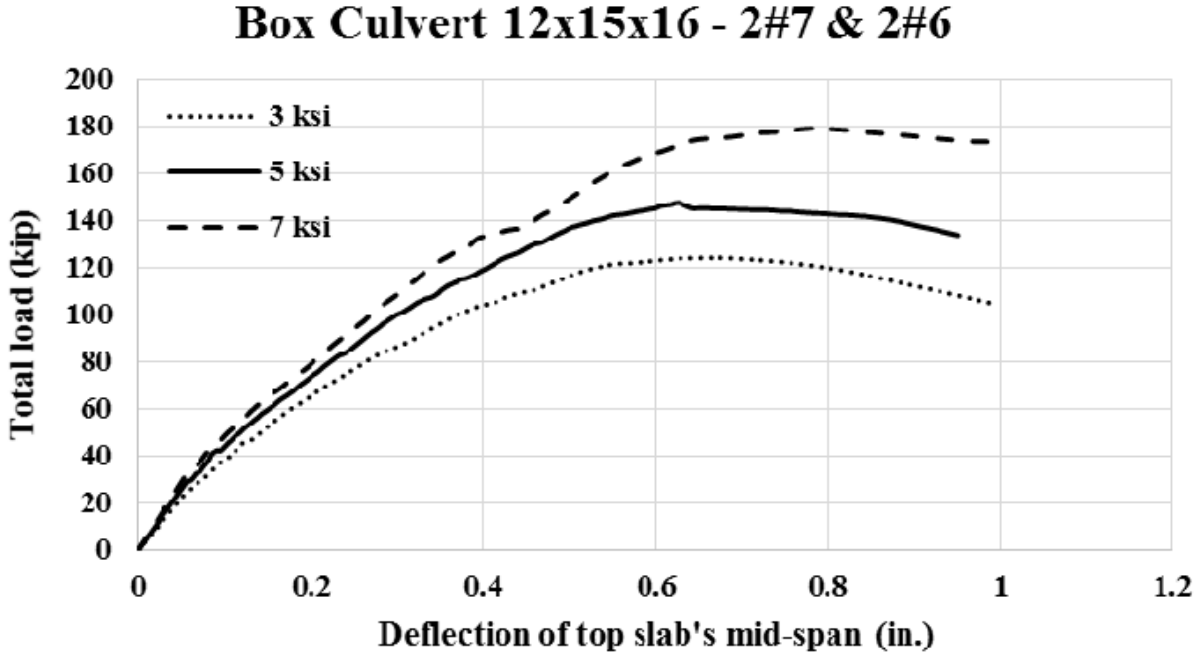
Box Culvert 12x15x16 - 2#7 & 2#6
3 ksi
5 ksi
7 ksi
Total load (kip)
0
20
40
60
80
100
120
140
160
180
200
0
0.2
0.4
0.6
0.8
1
1.2
Deflection of top slab's mid-span (in.)

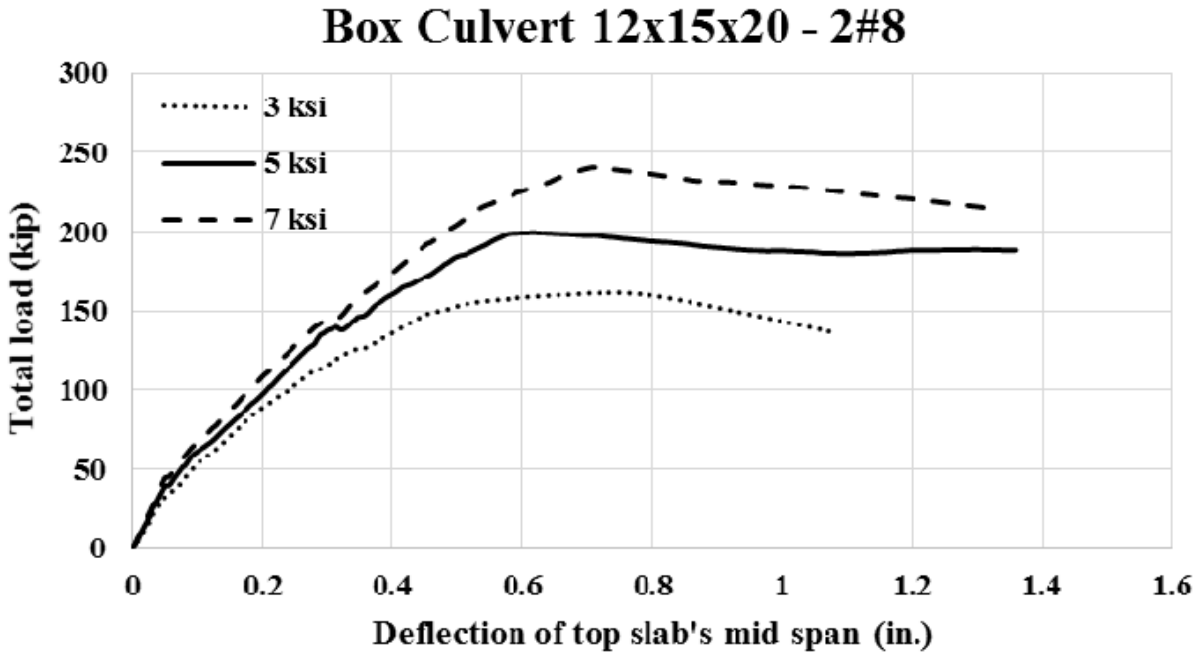
Box Culvert 12x15x20 - 2#8
3 ksi
5 ksi
7 ksi
Total load (kip)
300
250
200
150
100
50
0
0
0.2
0.4
0.6
0.8
1
1.2
1.4
1.6
Deflection of top slab's mid span (in.)

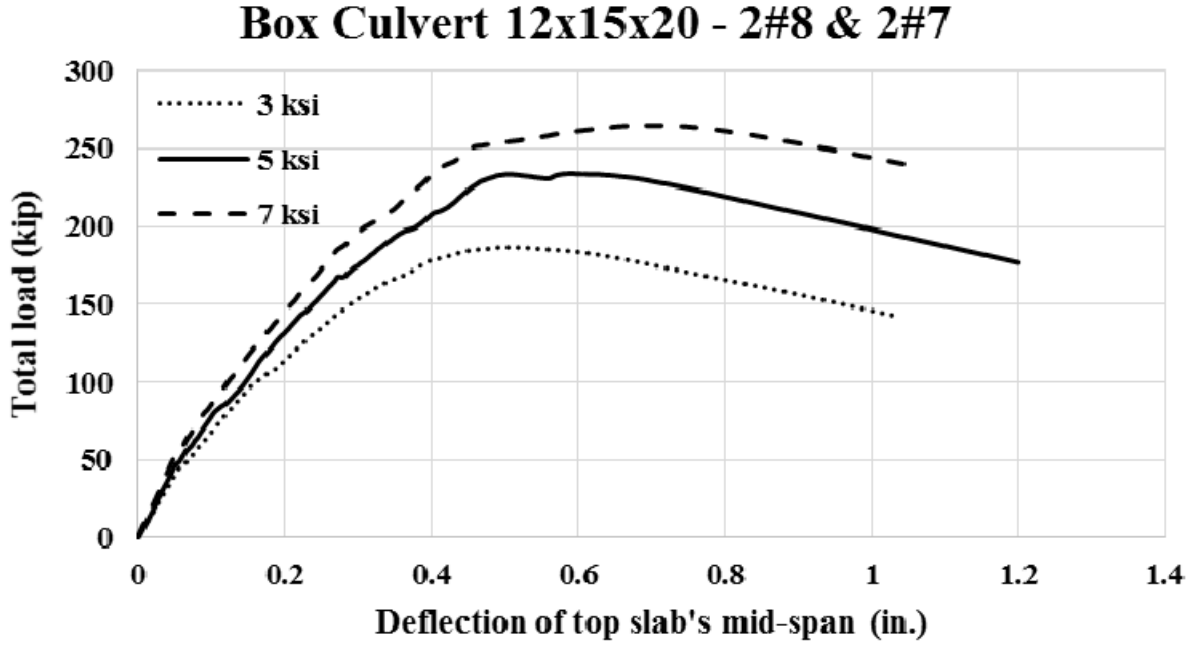
Box Culvert 12x15x20 - 2#8 & 2#7
3 ksi
5 ksi
7 ksi
Total load (kip)
300
250
200
150
100
50
0
0
0.2
0.4
0.6
0.8
1
1.2
1.4
Deflection of top slab's mid-span (in.)

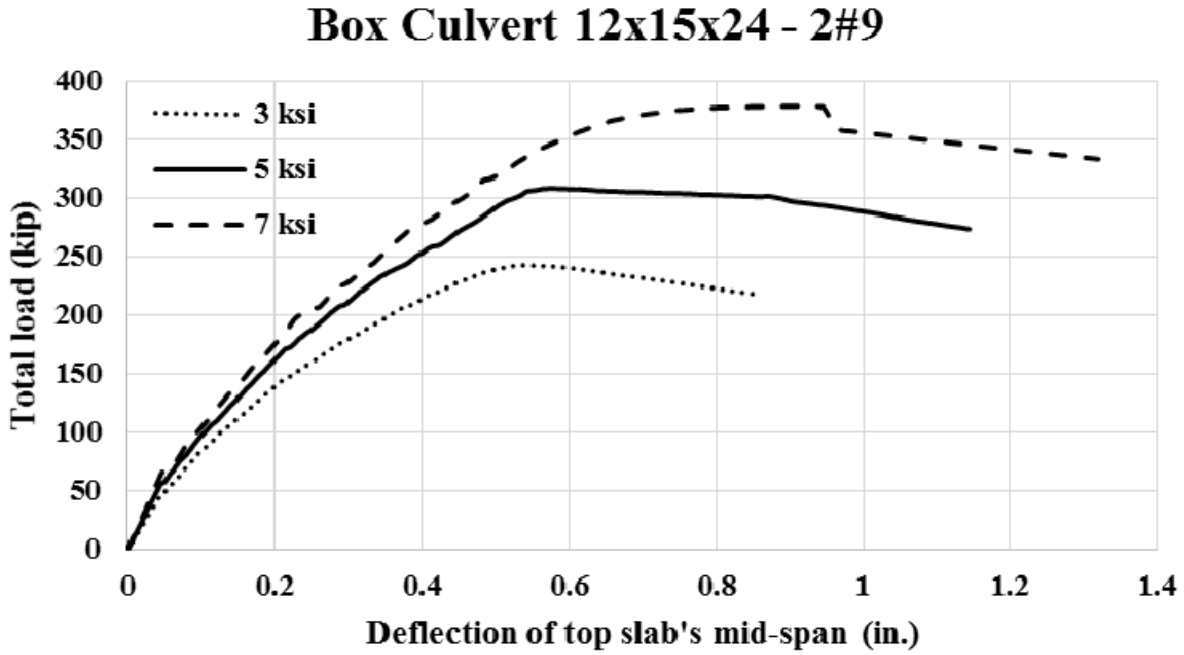
Box Culvert 12x15x24 - 2#9
3 ksi
5 ksi
7 ksi
Total load (kip)
400
350
300
250
200
150
100
50
0
0
0.2
0.4
0.6
0.8
1
1.2
1.4
Deflection of top slab's mid-span (in.)

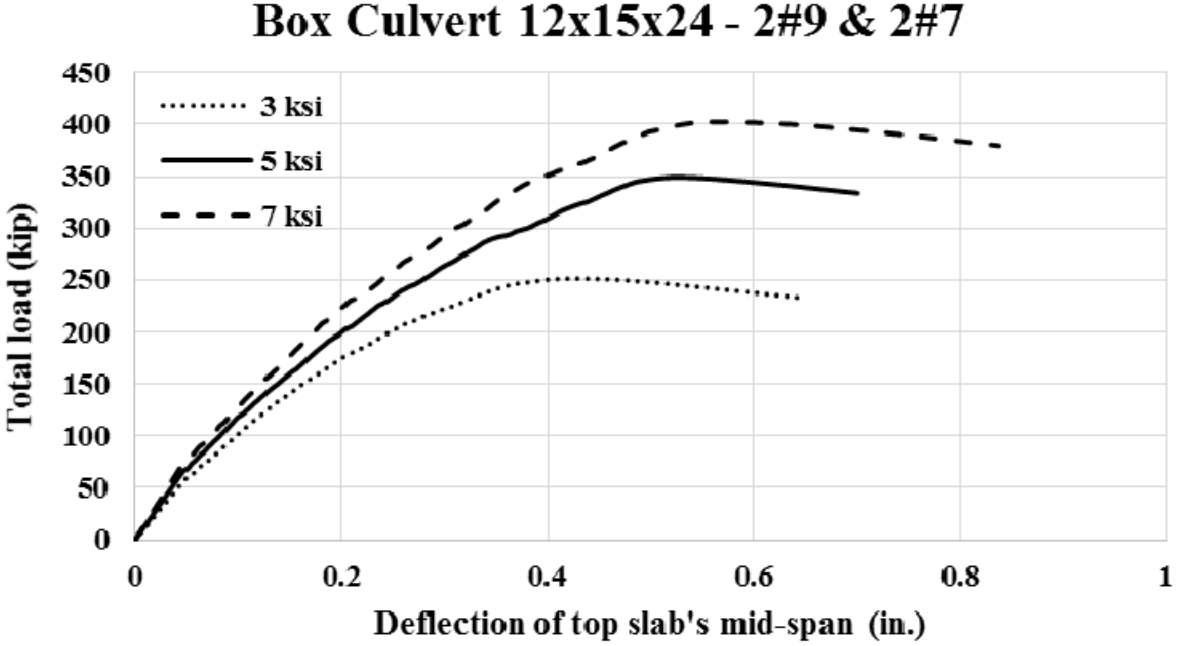
Box Culvert 12x15x24 - 2#9 & 2#7
3 ksi
5 ksi
7 ksi
Total load (kip)
450
400
350
300
250
200
150
100
50
0
0
0.2
0.4
0.6
0.8
1
Deflection of top slab's mid-span (in.)

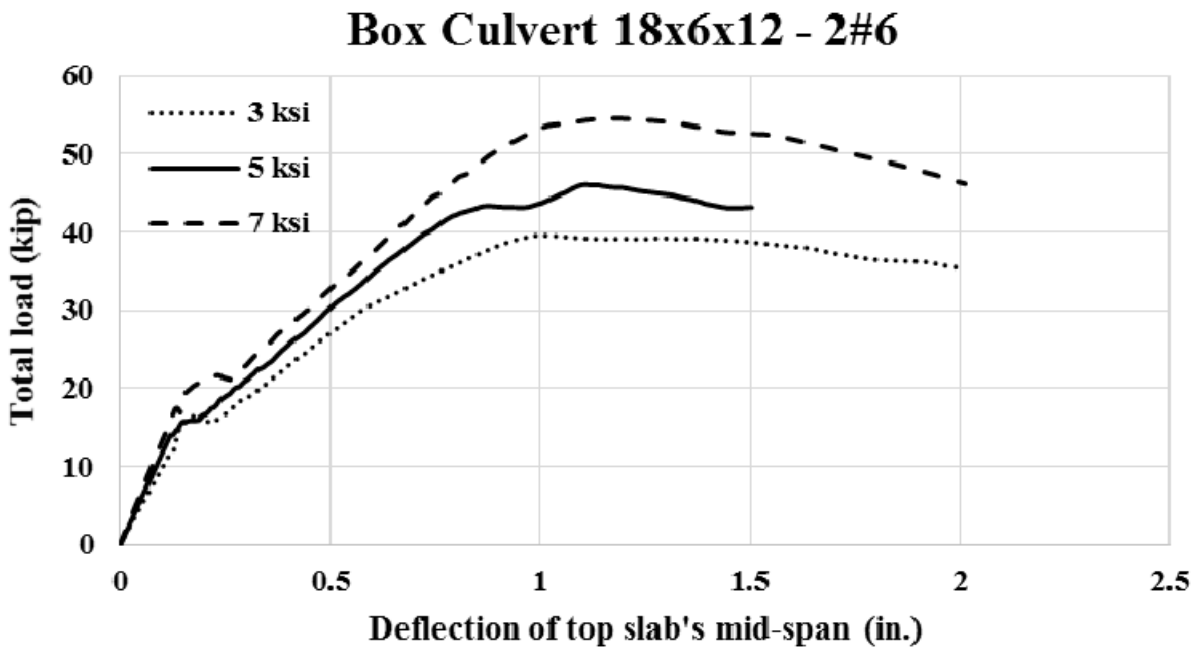
Box Culvert 18x6x12 - 2#6
3 ksi
5 ksi
7 ksi
Total load (kip)
Deflection of top slab's mid-span (in.)
0
10
20
30
40
50
60
0
0.5
1
1.5
2
2.5

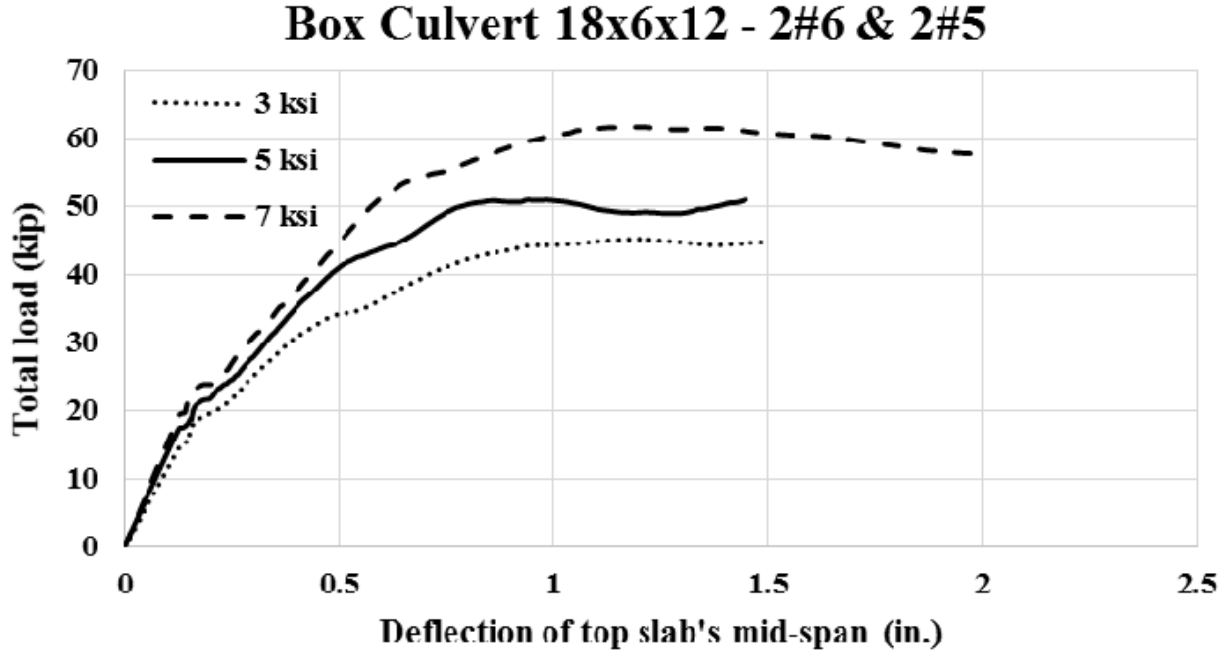
Box Culvert 18x6x12 - 2#6 & 2#5
3 ksi
5 ksi
7 ksi
Total load (kip)
Deflection of top slab's mid-span (in.)
0
10
20
30
40
50
60
70
0
0.5
1
1.5
2
2.5

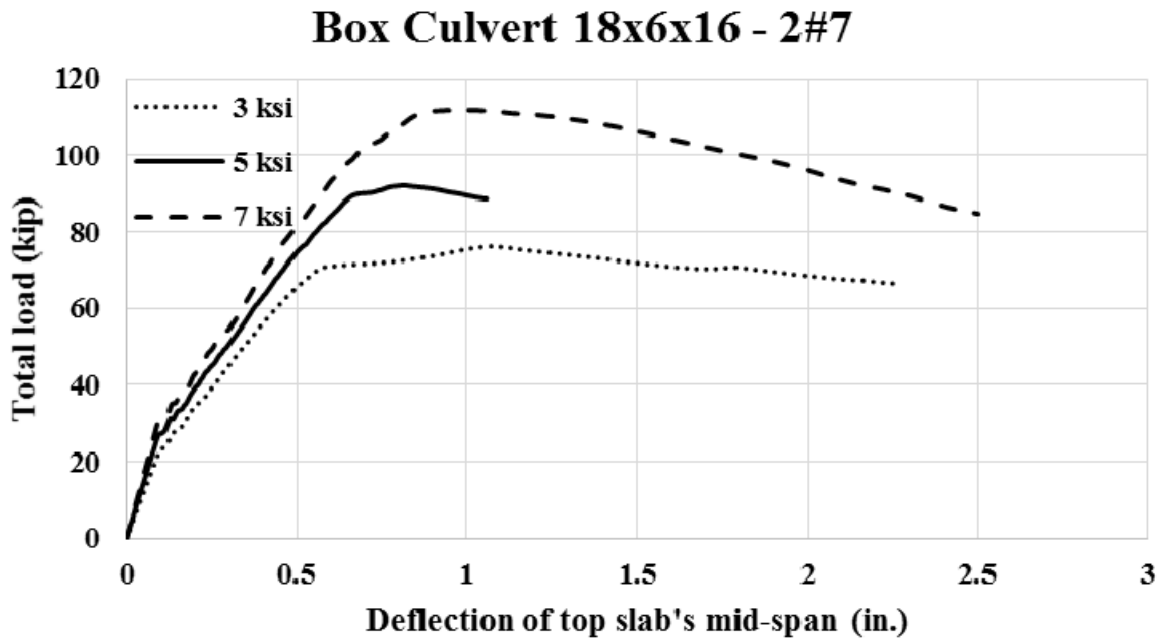
Box Culvert 18x6x16 - 2#7
3 ksi
5 ksi
7 ksi
Total load (kip)
120
100
80
60
40
20
0
0
0.5
1
1.5
2
2.5
3
Deflection of top slab's mid-span (in.)

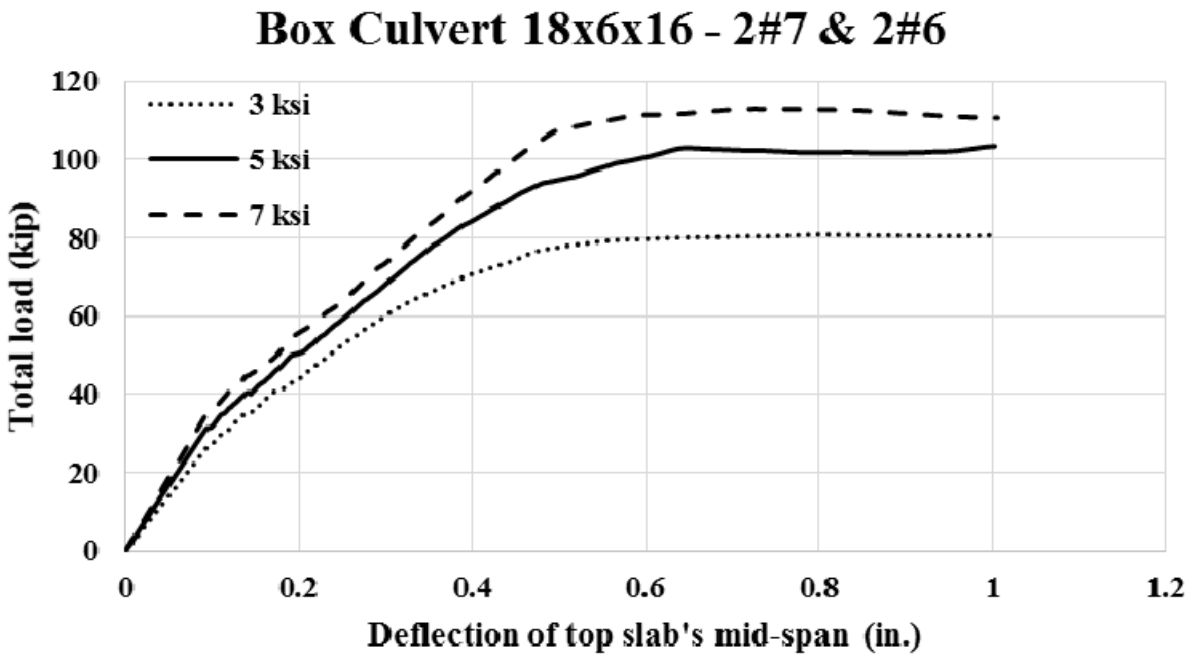
Box Culvert 18x6x16 - 2#7 & 2#6
3 ksi
5 ksi
7 ksi
Total load (kip)
120
100
80
60
40
20
0
0
0.2
0.4
0.6
0.8
1
1.2
Deflection of top slab's mid-span (in.)

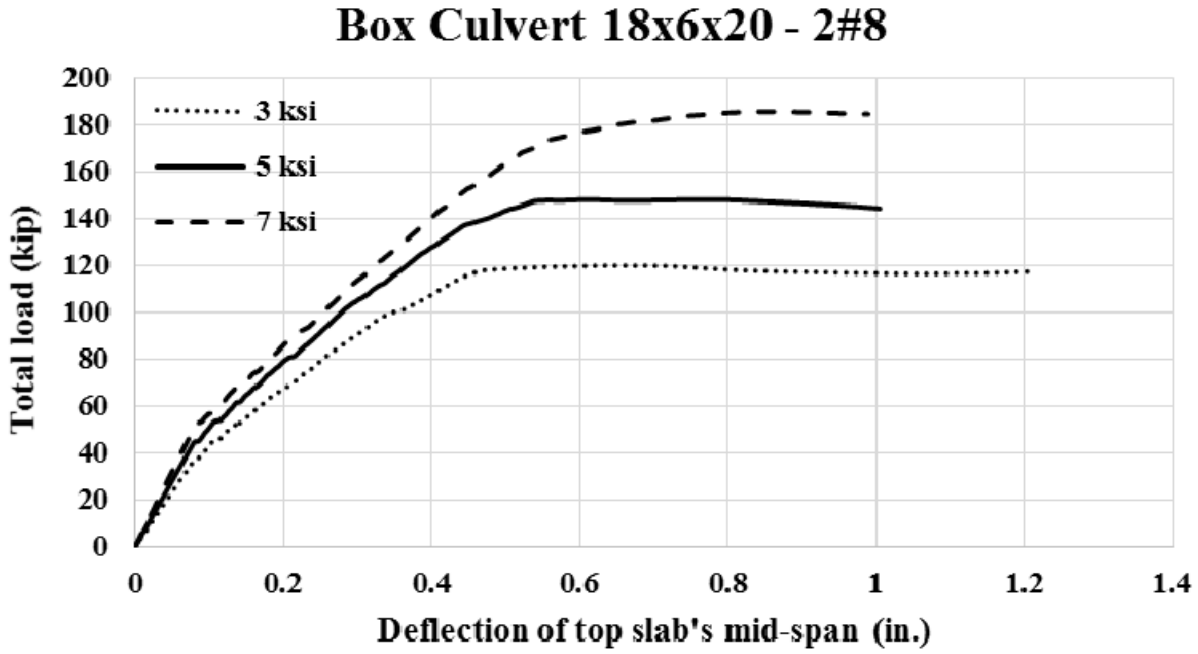
Box Culvert 18x6x20 - 2#8
3 ksi
5 ksi
7 ksi
Total load (kip)
200
180
160
140
120
100
80
60
40
20
0
0
0.2
0.4
0.6
0.8
1
1.2
1.4
Deflection of top slab's mid-span (in.)

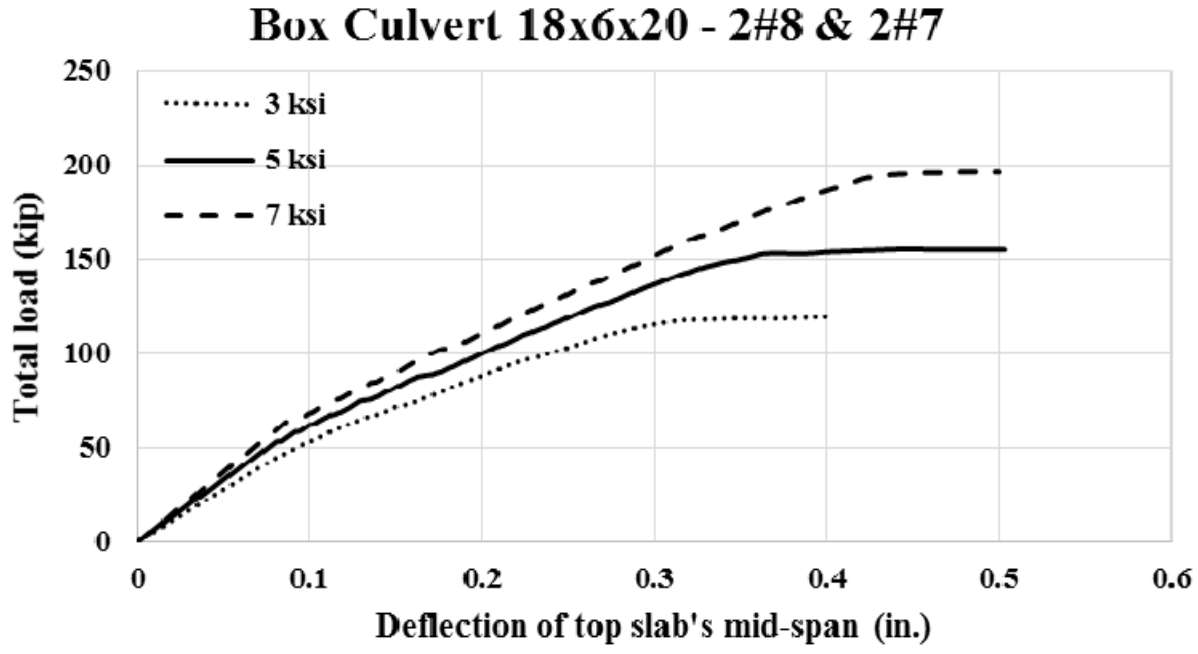
Box Culvert 18x6x20 - 2#8 & 2#7
3 ksi
5 ksi
7 ksi
Total load (kip)
250
200
150
100
50
0
0
0.1
0.2
0.3
0.4
0.5
0.6
Deflection of top slab's mid-span (in.)

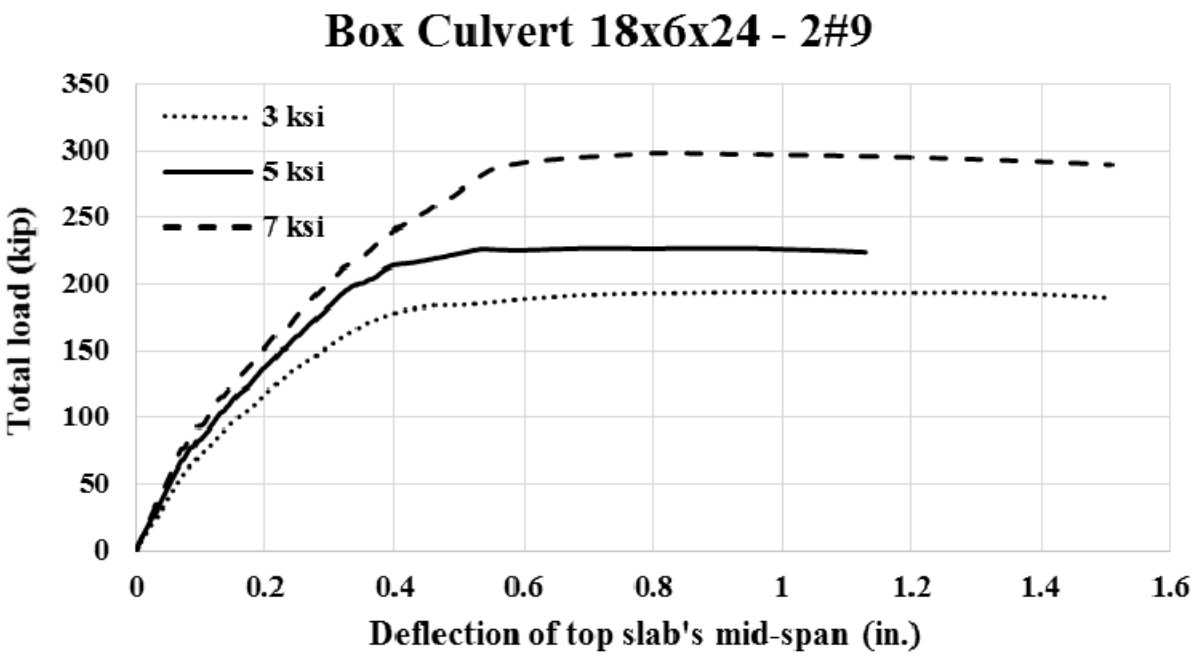
Box Culvert 18x6x24 - 2#9
3 ksi
5 ksi
7 ksi
Total load (kip)
350
300
250
200
150
100
50
0
0
0.2
0.4
0.6
0.8
1
1.2
1.4
1.6
Deflection of top slab's mid-span (in.)

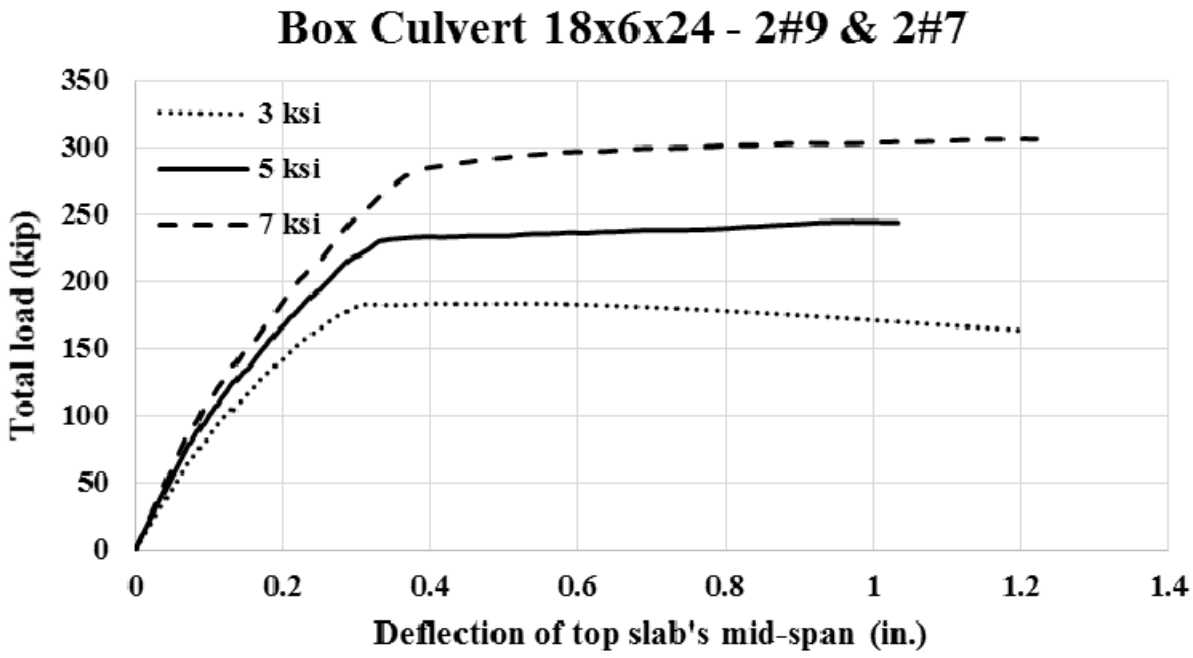
Box Culvert 18x6x24 - 2#9 & 2#7
3 ksi
5 ksi
7 ksi
Total load (kip)
350
300
250
200
150
100
50
0
0
0.2
0.4
0.6
0.8
1
1.2
1.4
Deflection of top slab's mid-span (in.)

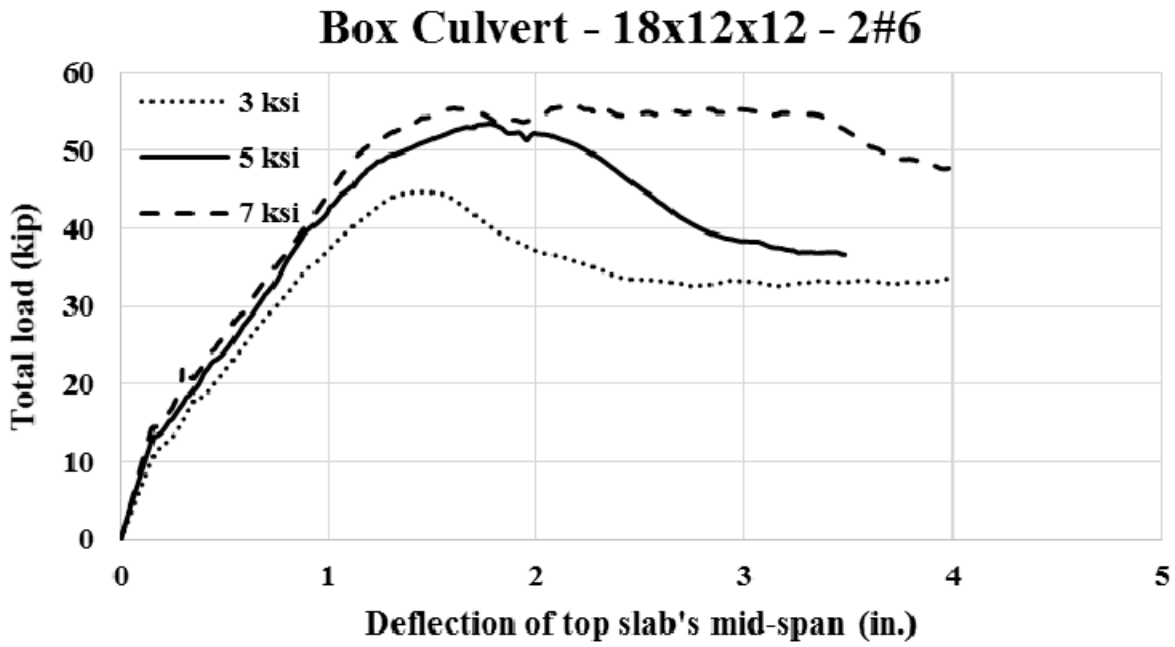
Box Culvert - 18x12x12 - 2#6
3 ksi
5 ksi
7 ksi
Total load (kip)
0
10
20
30
40
50
60
0
1
2
3
4
5
Deflection of top slab's mid-span (in.)

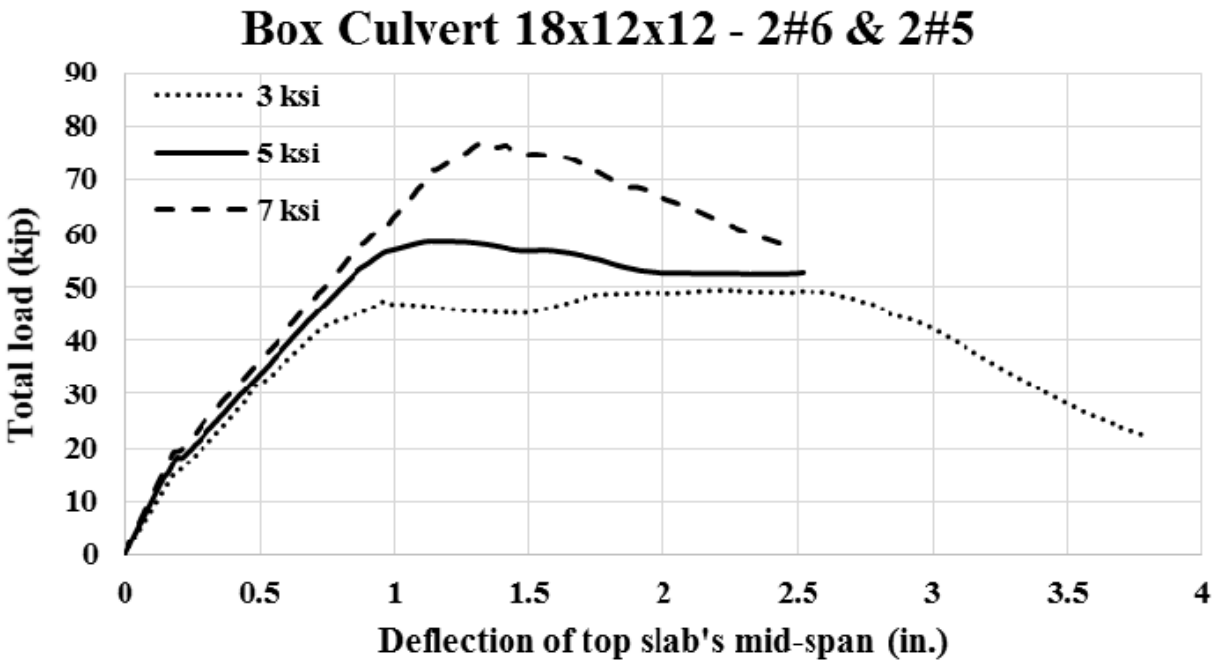
Box Culvert 18x12x12 - 2#6 & 2#5
3 ksi
5 ksi
7 ksi
Total load (kip)
0
10
20
30
40
50
60
70
80
90
0
0.5
1
1.5
2
2.5
3
3.5
4
Deflection of top slab's mid-span (in.)

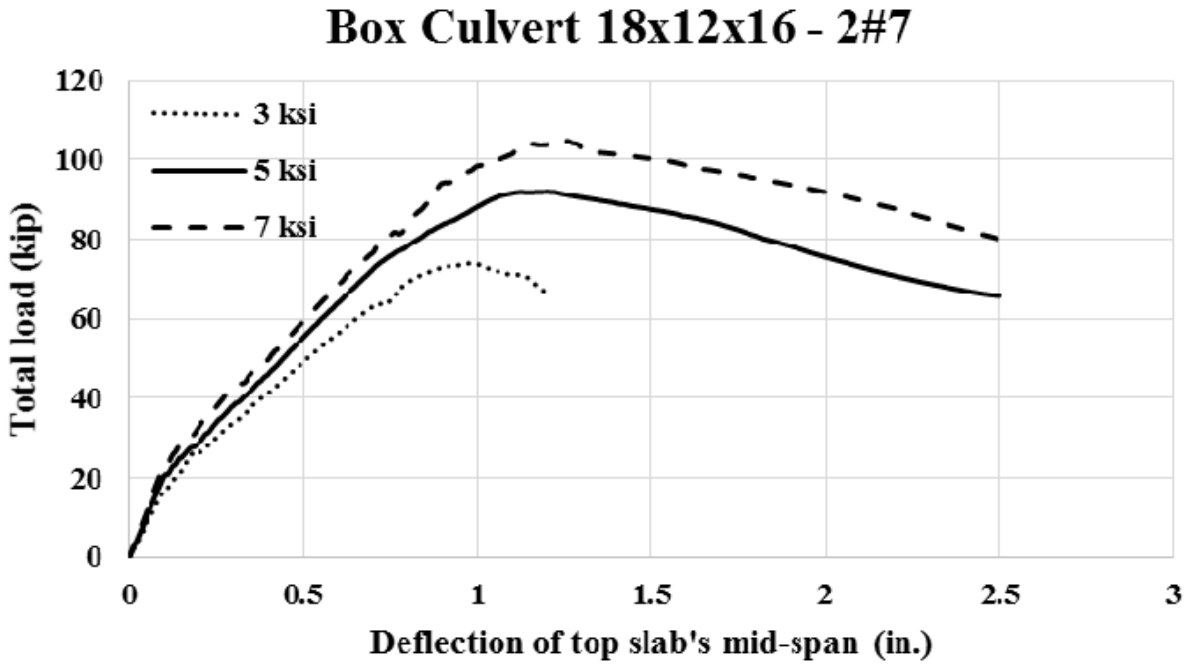
Box Culvert 18x12x16 - 2#7
3 ksi
5 ksi
7 ksi
Total load (kip)
Deflection of top slab's mid-span (in.)
0
20
40
60
80
100
120
0
0.5
1
1.5
2
2.5
3

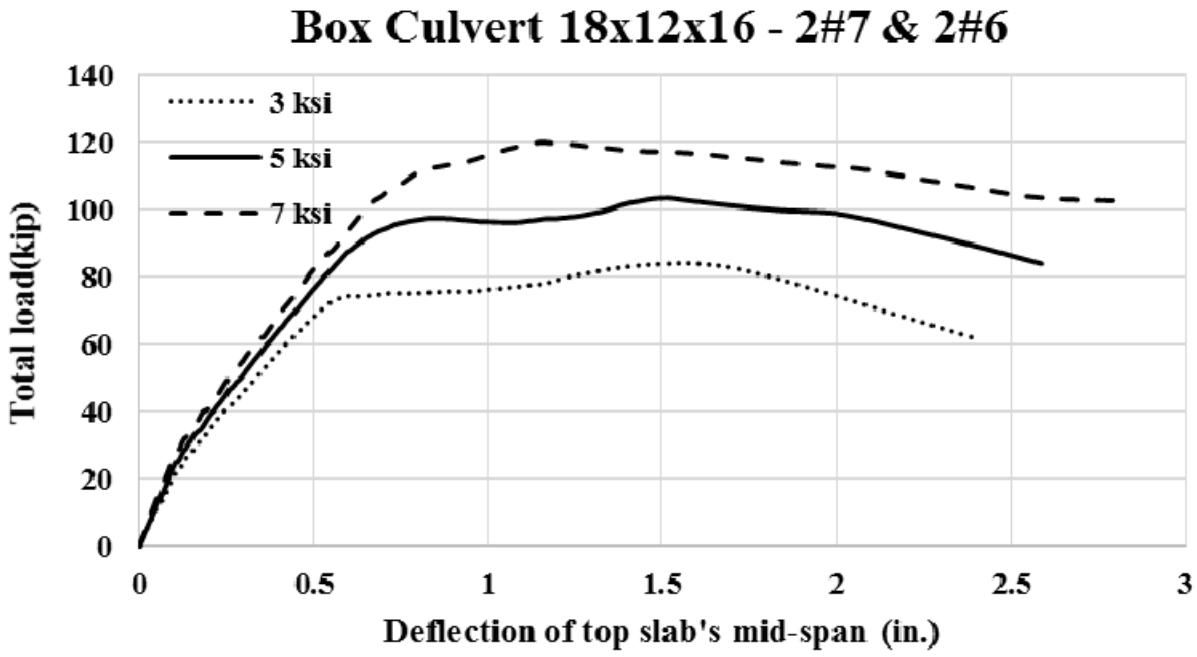
Box Culvert 18x12x16 - 2#7 & 2#6
3 ksi
5 ksi
7 ksi
Total load(kip)
Deflection of top slab's mid-span (in.)
0
20
40
60
80
100
120
140
0
0.5
1
1.5
2
2.5
3

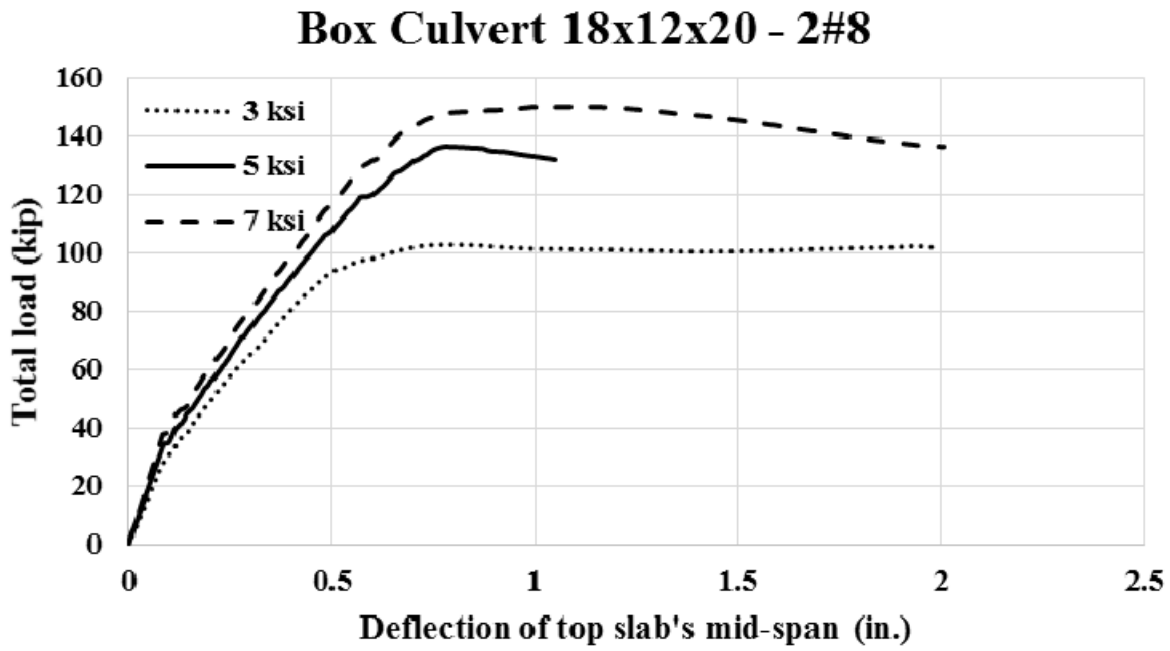
Box Culvert 18x12x20 - 2#8
3 ksi
5 ksi
7 ksi
Total load (kip)
0
20
40
60
80
100
120
140
160
0
0.5
1
1.5
2
2.5
Deflection of top slab's mid-span (in.)

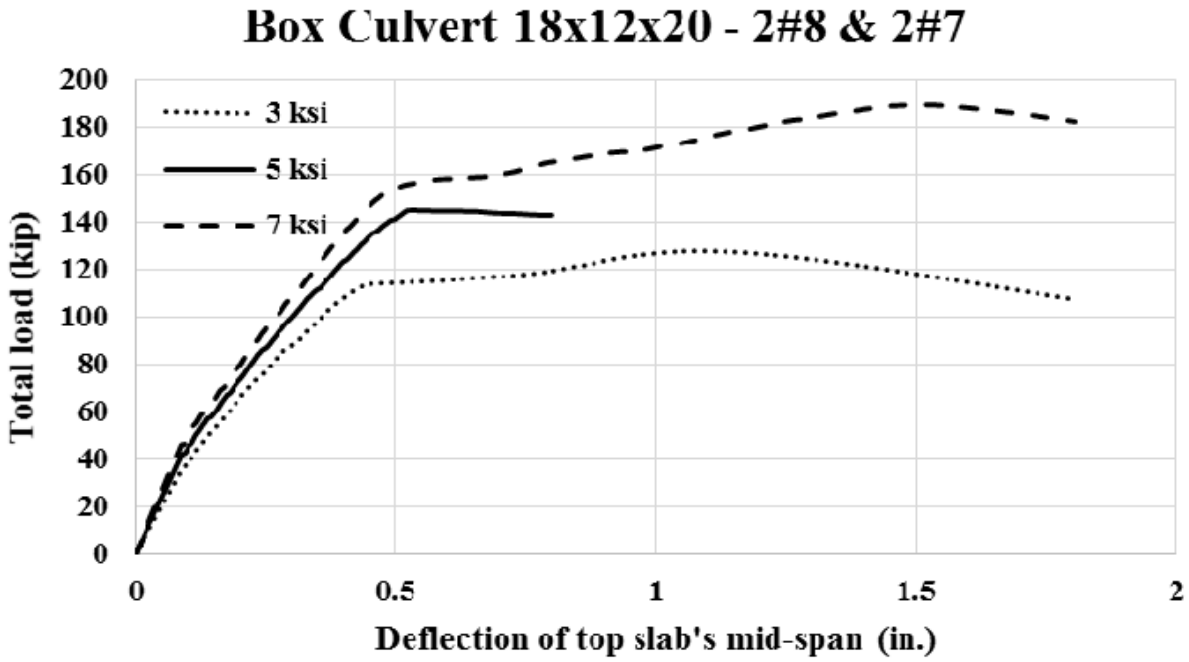
Box Culvert 18x12x20 - 2#8 & 2#7
3 ksi
5 ksi
7 ksi
Total load (kip)
0
20
40
60
80
100
120
140
160
180
200
0
0.5
1
1.5
2
Deflection of top slab's mid-span (in.)

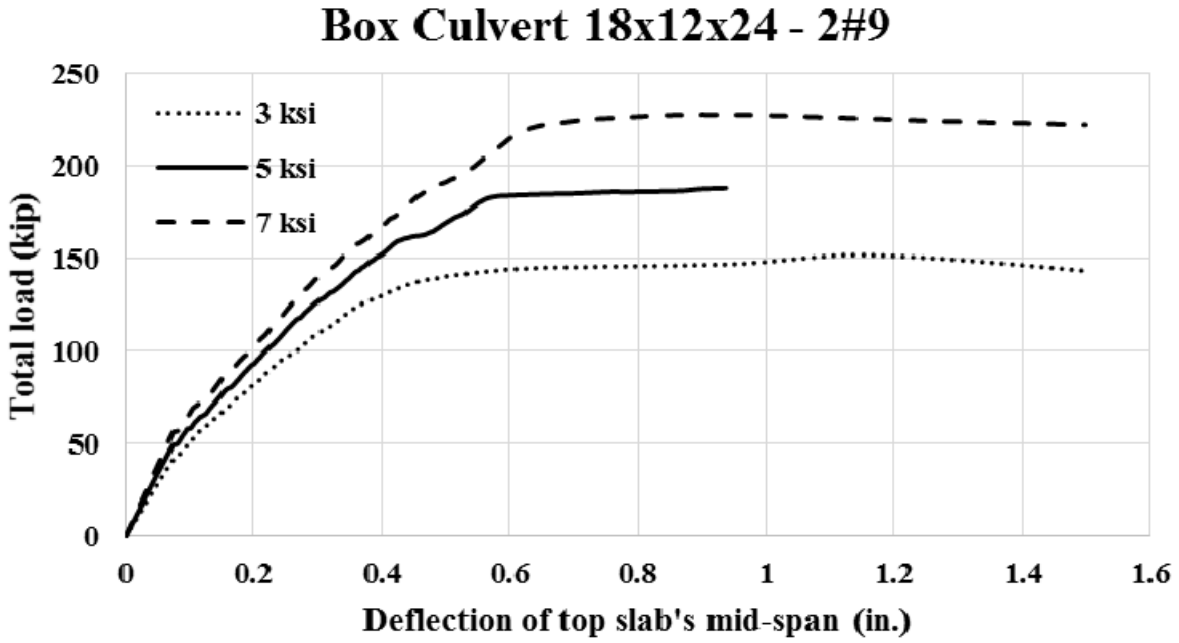
Box Culvert 18x12x24 - 2#9
3 ksi
5 ksi
7 ksi
Total load (kip)
250
200
150
100
50
0
0
0.2
0.4
0.6
0.8
1
1.2
1.4
1.6
Deflection of top slab's mid-span (in.)

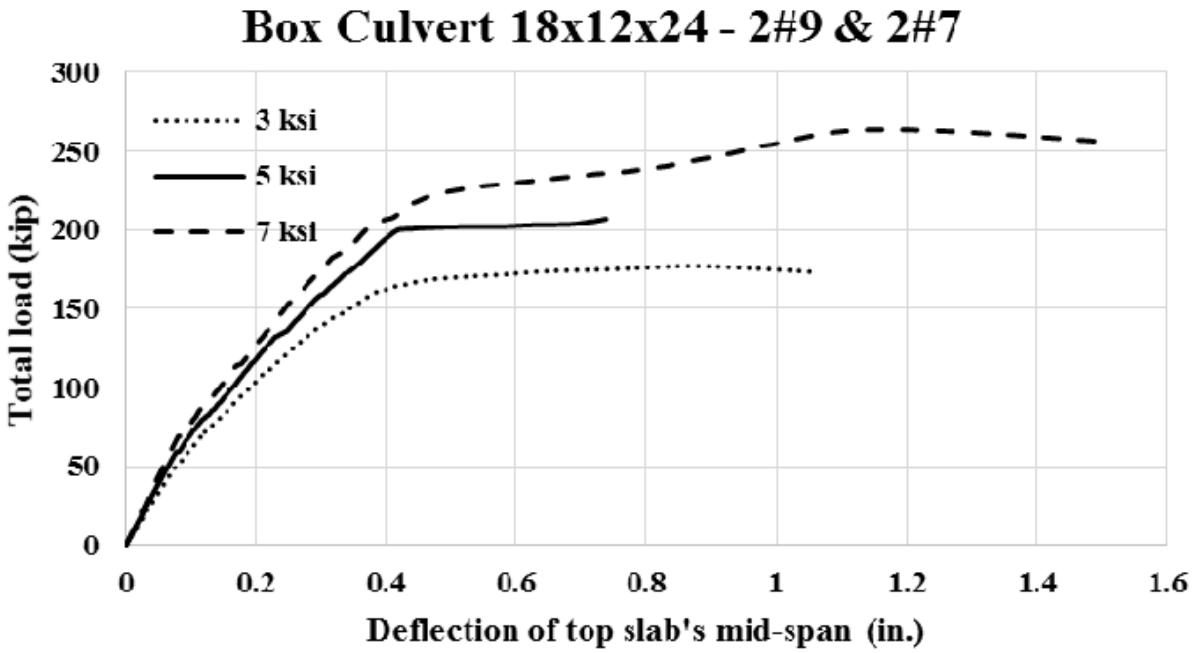
Box Culvert 18x12x24 - 2#9 & 2#7
3 ksi
5 ksi
7 ksi
Total load (kip)
300
250
200
150
100
50
0
0
0.2
0.4
0.6
0.8
1
1.2
1.4
1.6
Deflection of top slab's mid-span (in.)

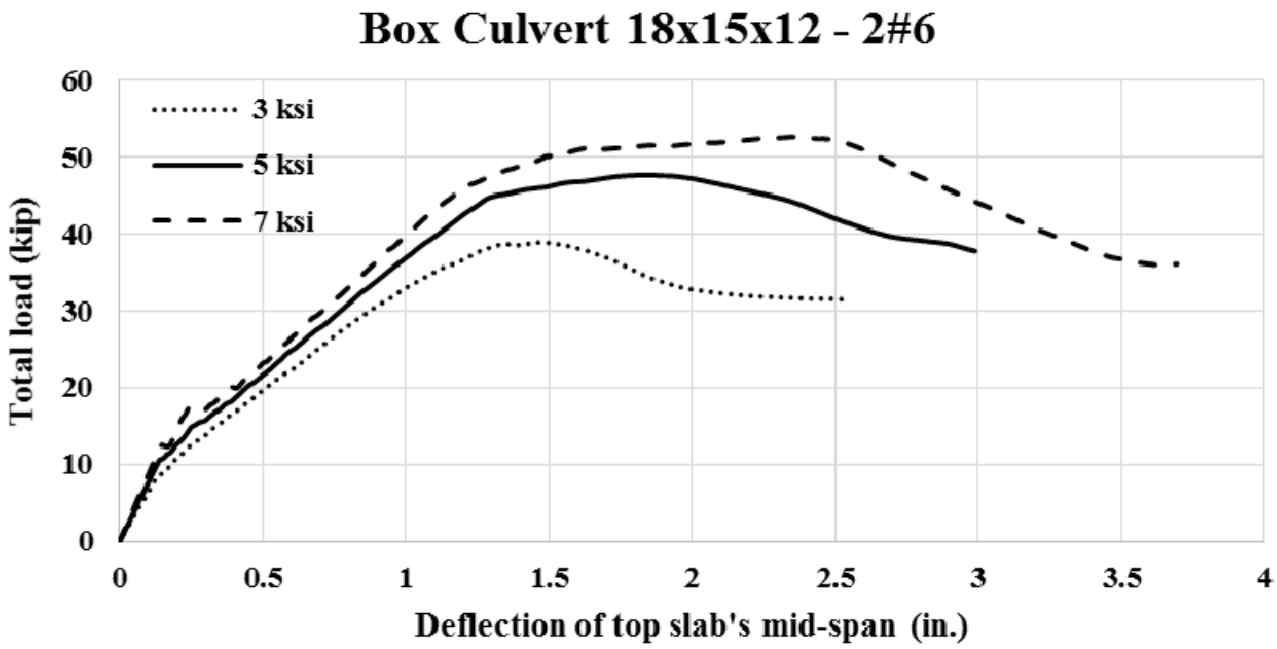
Box Culvert 18x15x12 - 2#6
3 ksi
5 ksi
7 ksi
Total load (kip)
0
10
20
30
40
50
60
0
0.5
1
1.5
2
2.5
3
3.5
4
Deflection of top slab's mid-span (in.)

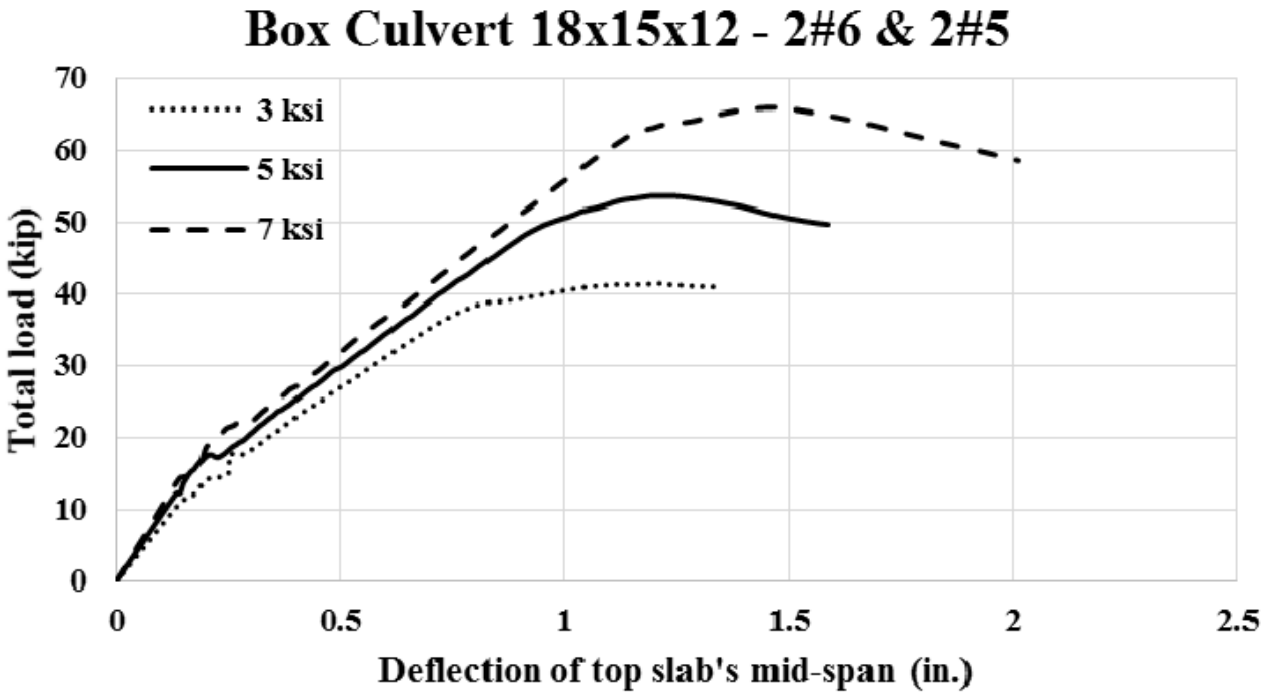
Box Culvert 18x15x12 - 2#6 & 2#5
3 ksi
5 ksi
7 ksi
Total load (kip)
0
10
20
30
40
50
60
70
0
0.5
1
1.5
2
2.5
Deflection of top slab's mid-span (in.)

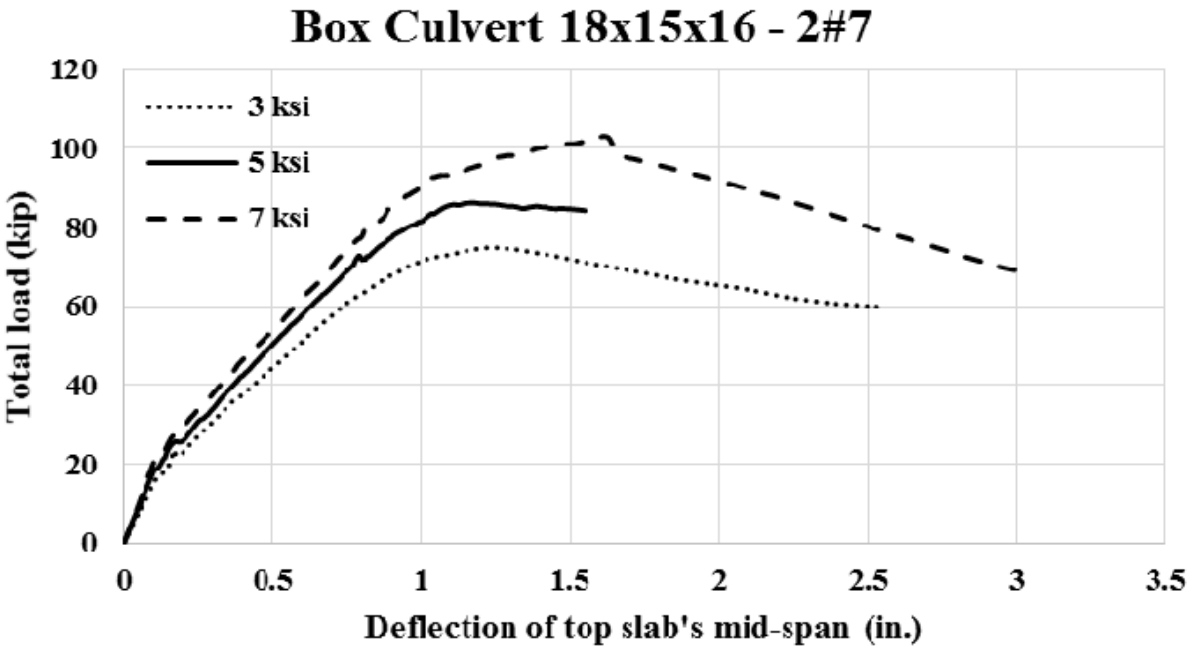
Box Culvert 18x15x16 - 2#7
3 ksi
5 ksi
7 ksi
Total load (kip)
120
100
80
60
40
20
0
0
0.5
1
1.5
2
2.5
3
3.5
Deflection of top slab's mid-span (in.)

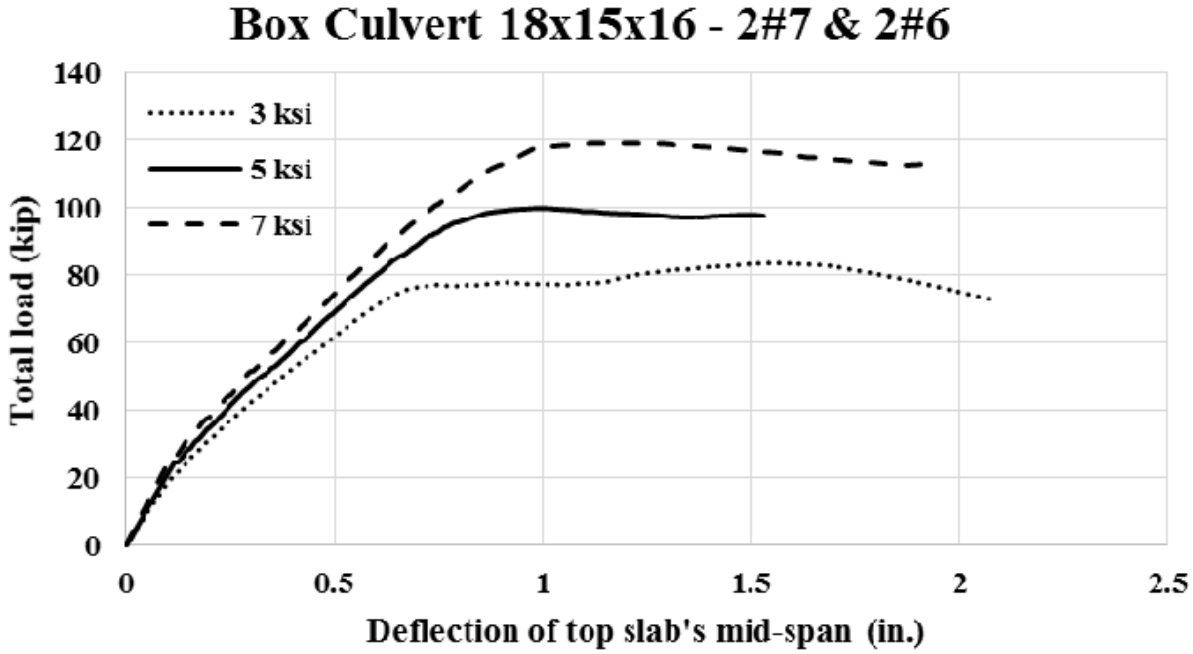
Box Culvert 18x15x16 - 2#7 & 2#6
3 ksi
5 ksi
7 ksi
Total load (kip)
140
120
100
80
60
40
20
0
0
0.5
1
1.5
2
2.5
Deflection of top slab's mid-span (in.)

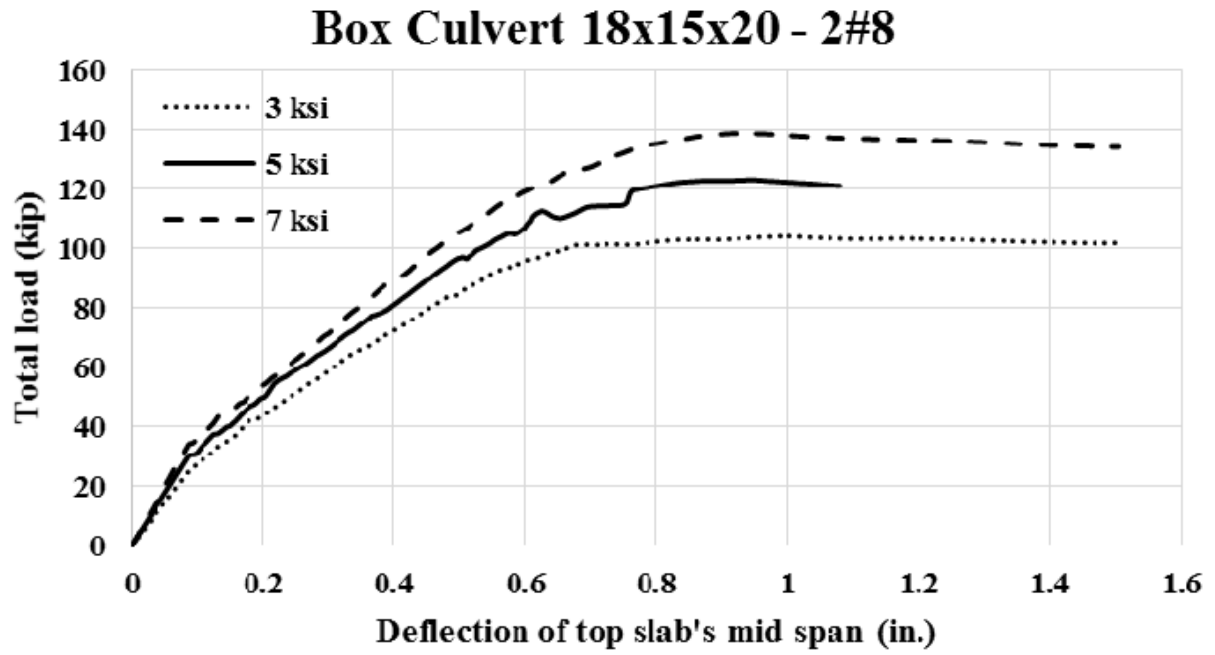
Box Culvert 18x15x20 - 2#8
3 ksi
5 ksi
7 ksi
Total load (kip)
160
140
120
100
80
60
40
20
0
0
0.2
0.4
0.6
0.8
1
1.2
1.4
1.6
Deflection of top slab's mid span (in.)

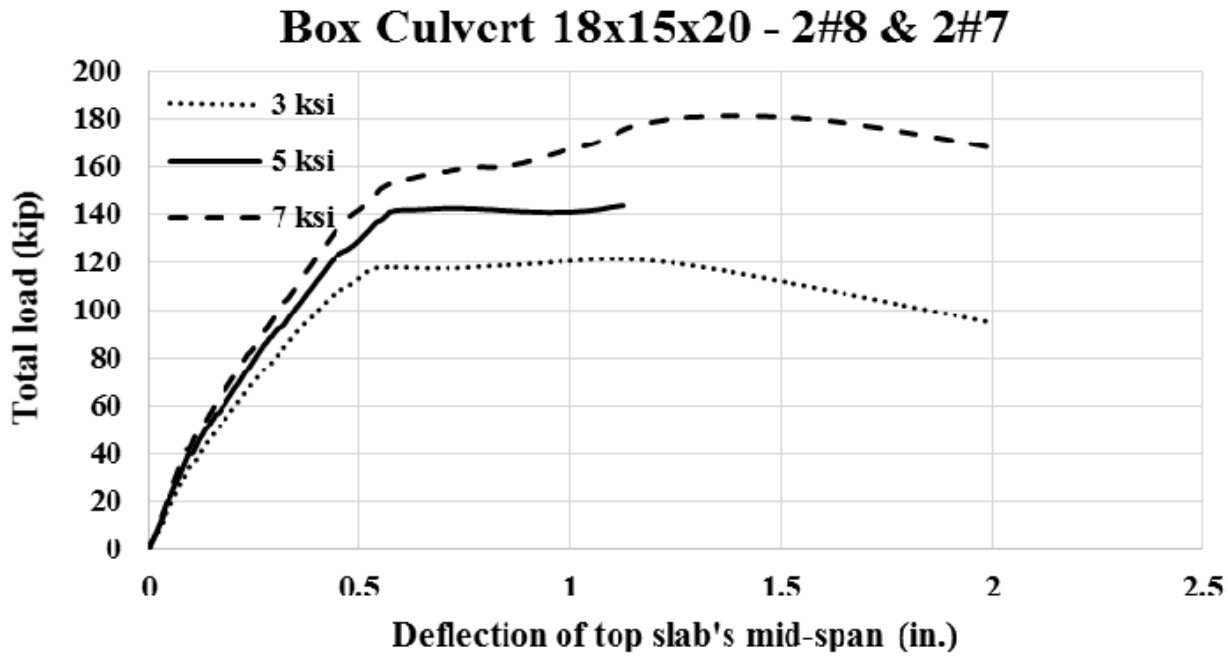
Box Culvert 18x15x20 - 2#8 & 2#7
3 ksi
5 ksi
7 ksi
Total load (kip)
200
180
160
140
120
100
80
60
40
20
0
0
0.5
1
1.5
2
2.5
Deflection of top slab's mid-span (in.)

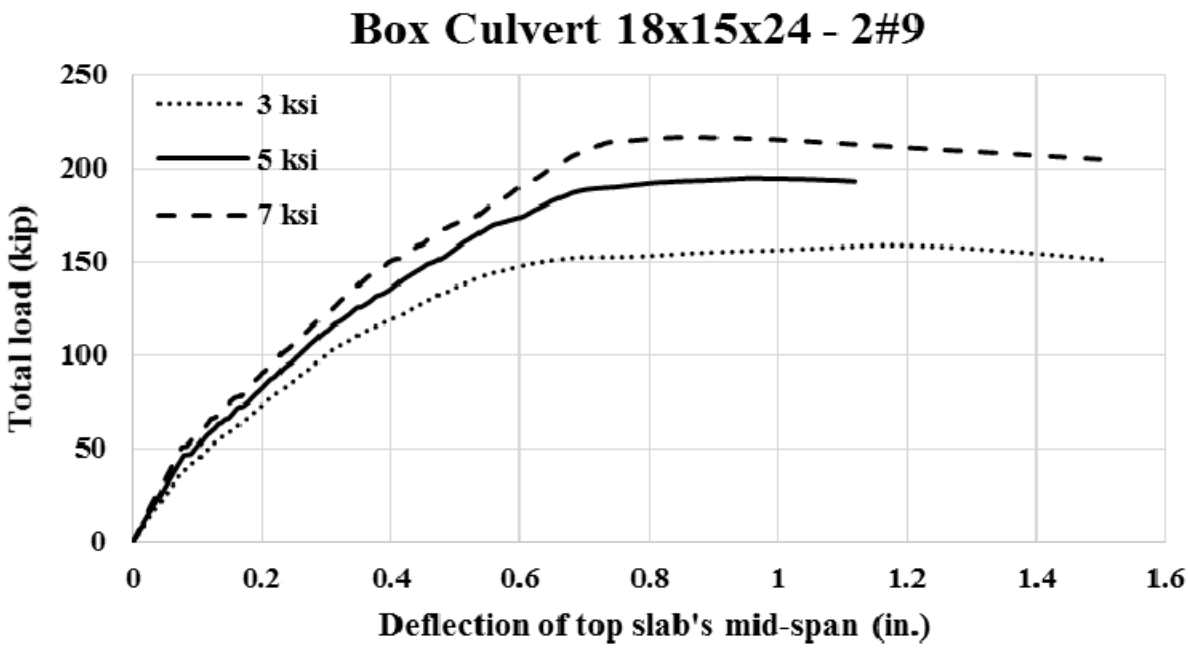
Box Culvert 18x15x24 - 2#9
3 ksi
5 ksi
7 ksi
Total load (kip)
250
200
150
100
50
0
0
0.2
0.4
0.6
0.8
1
1.2
1.4
1.6
Deflection of top slab's mid-span (in.)

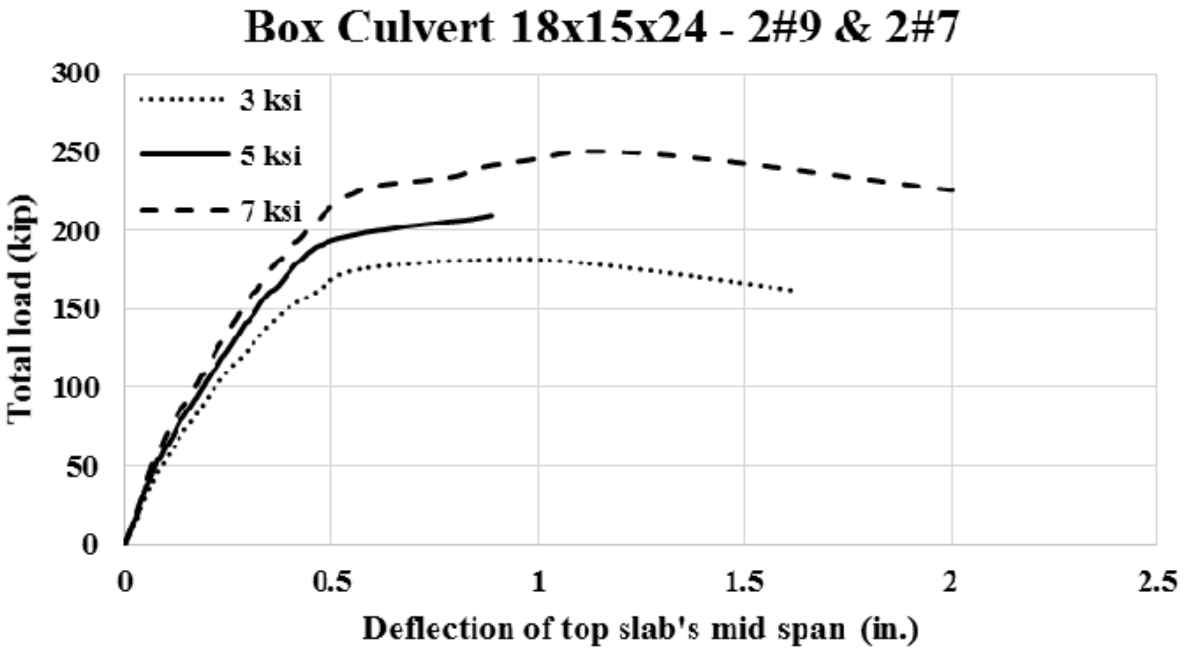
Box Culvert 18x15x24 - 2#9 & 2#7
3 ksi
5 ksi
7 ksi
Total load (kip)
300
250
200
150
100
50
0
0
0.5
1
1.5
2
2.5
Deflection of top slab's mid span (in.)

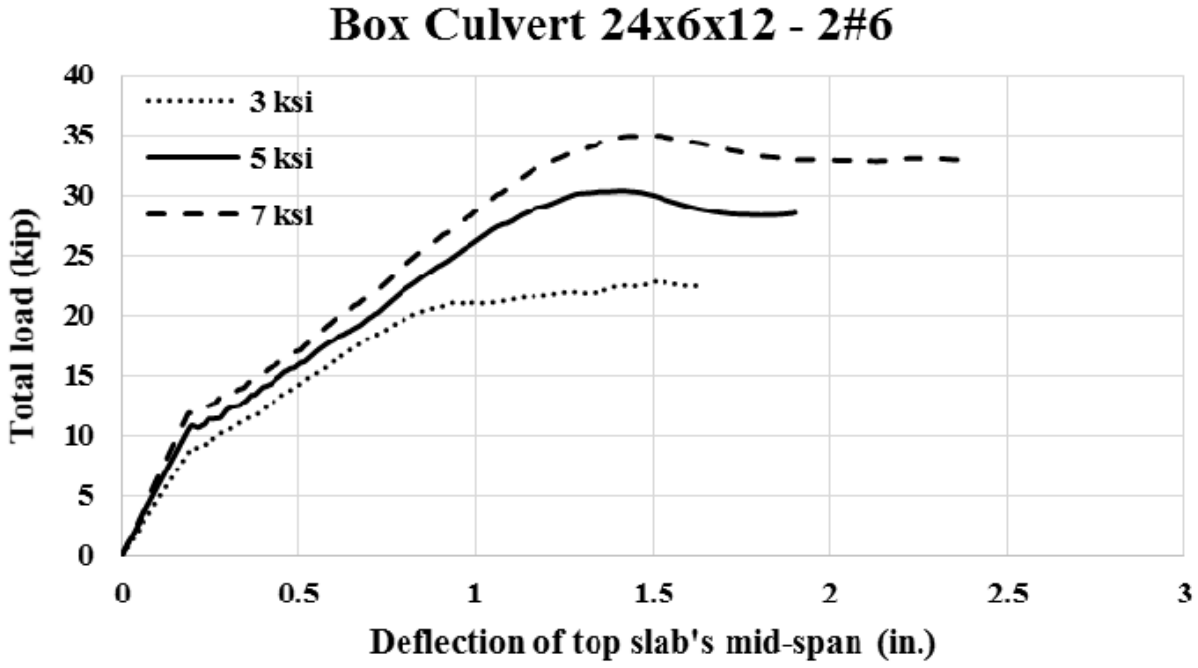
Box Culvert 24x6x12 - 2#6
3 ksi
5 ksi
7 ksi
Total load (kip)
0
5
10
15
20
25
30
35
40
0
0.5
1
1.5
2
2.5
3
Deflection of top slab's mid-span (in.)

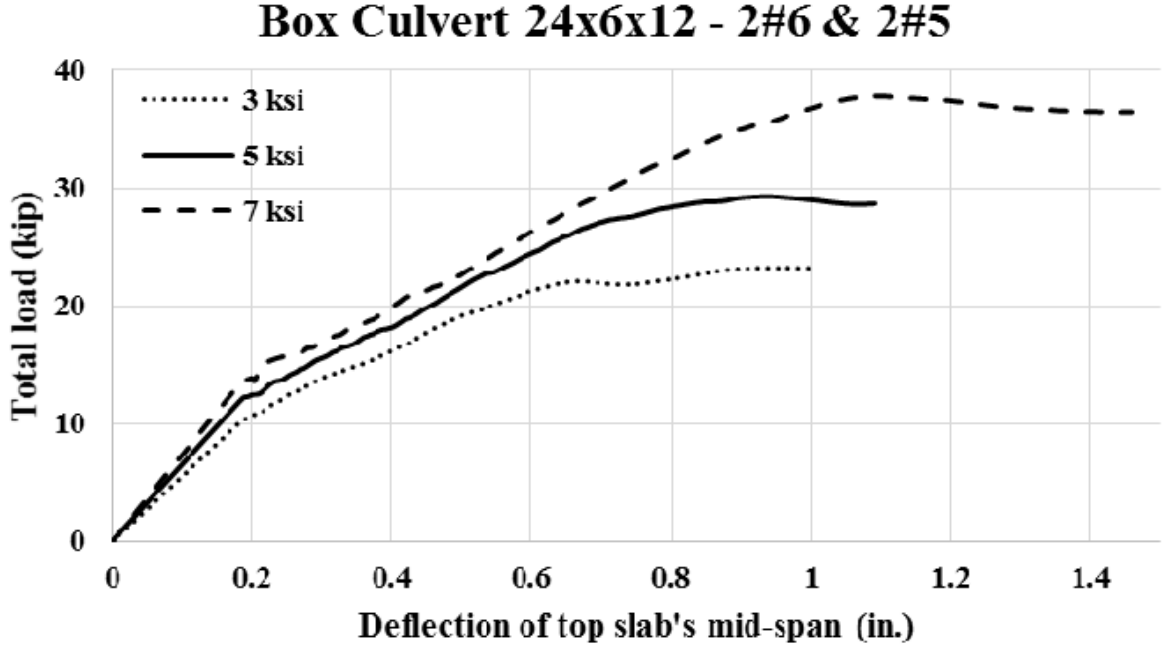
Box Culvert 24x6x12 - 2#6 & 2#5
3 ksi
5 ksi
7 ksi
Total load (kip)
0
10
20
30
40
0
0.2
0.4
0.6
0.8
1
1.2
1.4
Deflection of top slab's mid-span (in.)

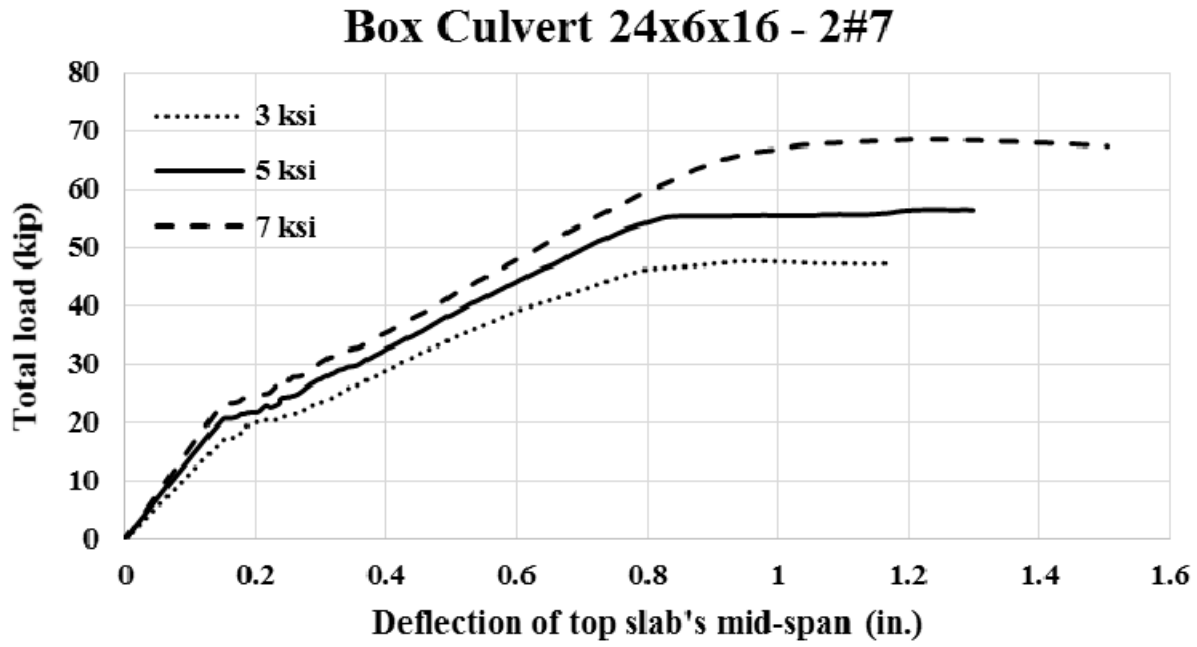
Box Culvert 24x6x16 - 2#7
3 ksi
5 ksi
7 ksi
Total load (kip)
0
10
20
30
40
50
60
70
80
0
0.2
0.4
0.6
0.8
1
1.2
1.4
1.6
Deflection of top slab's mid-span (in.)

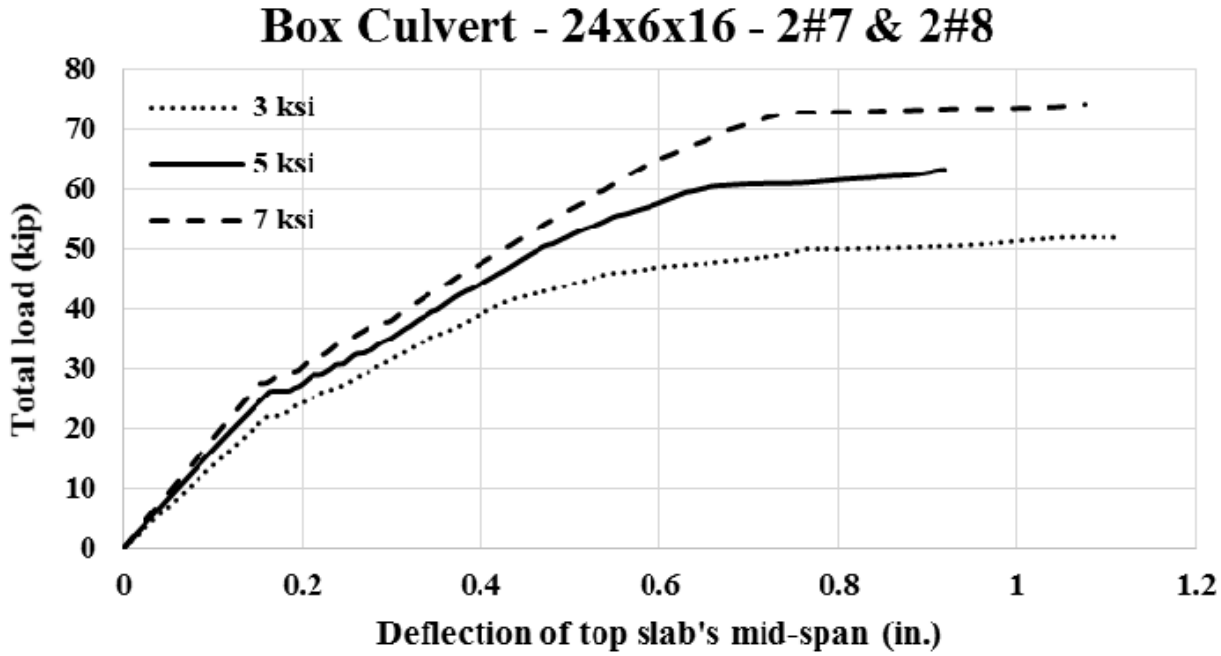
Box Culvert - 24x6x16 - 2#7 & 2#8
3 ksi
5 ksi
7 ksi
Total load (kip)
0
10
20
30
40
50
60
70
80
0
0.2
0.4
0.6
0.8
1
1.2
Deflection of top slab's mid-span (in.)

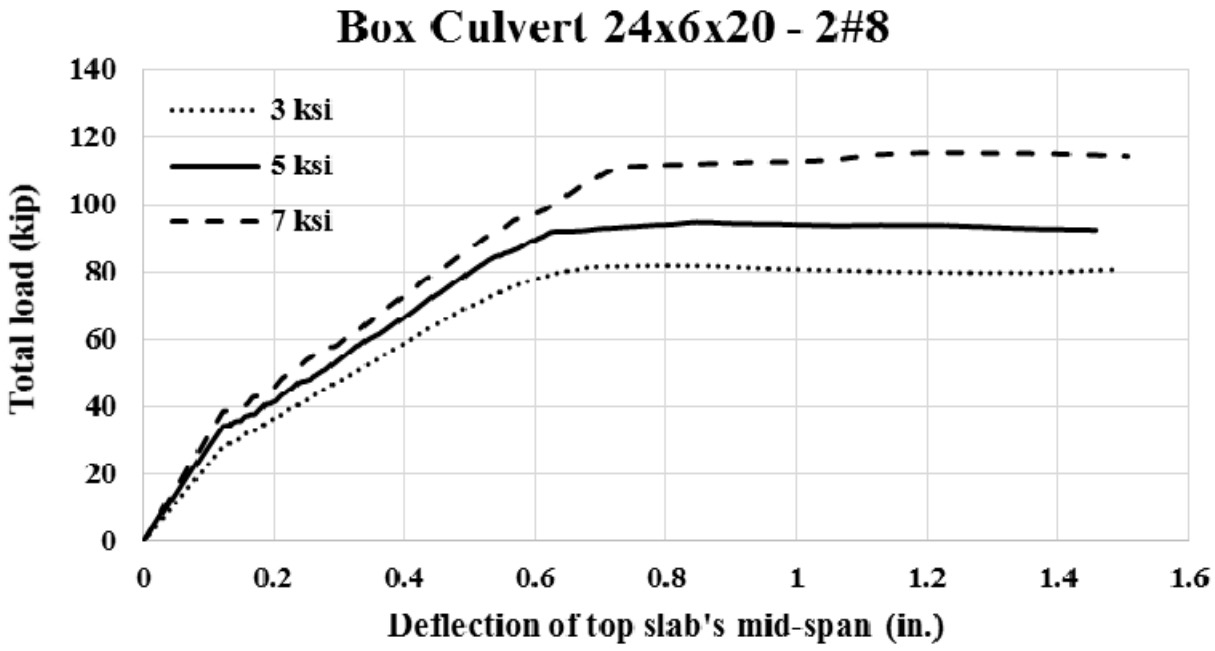
Box Culvert 24x6x20 - 2#8
3 ksi
5 ksi
7 ksi
Total load (kip)
Deflection of top slab's mid-span (in.)
0
20
40
60
80
100
120
140
0
0.2
0.4
0.6
0.8
1
1.2
1.4
1.6

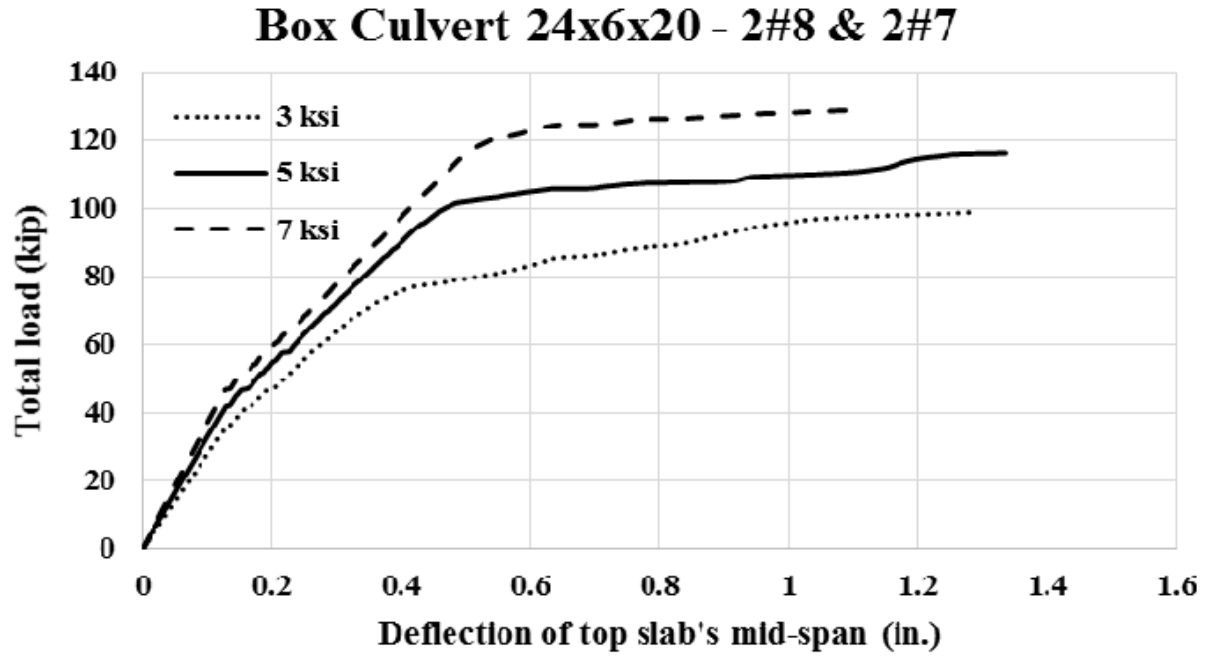
Box Culvert 24x6x20 - 2#8 & 2#7
3 ksi
5 ksi
7 ksi
Total load (kip)
Deflection of top slab's mid-span (in.)
0
20
40
60
80
100
120
140
0
0.2
0.4
0.6
0.8
1
1.2
1.4
1.6

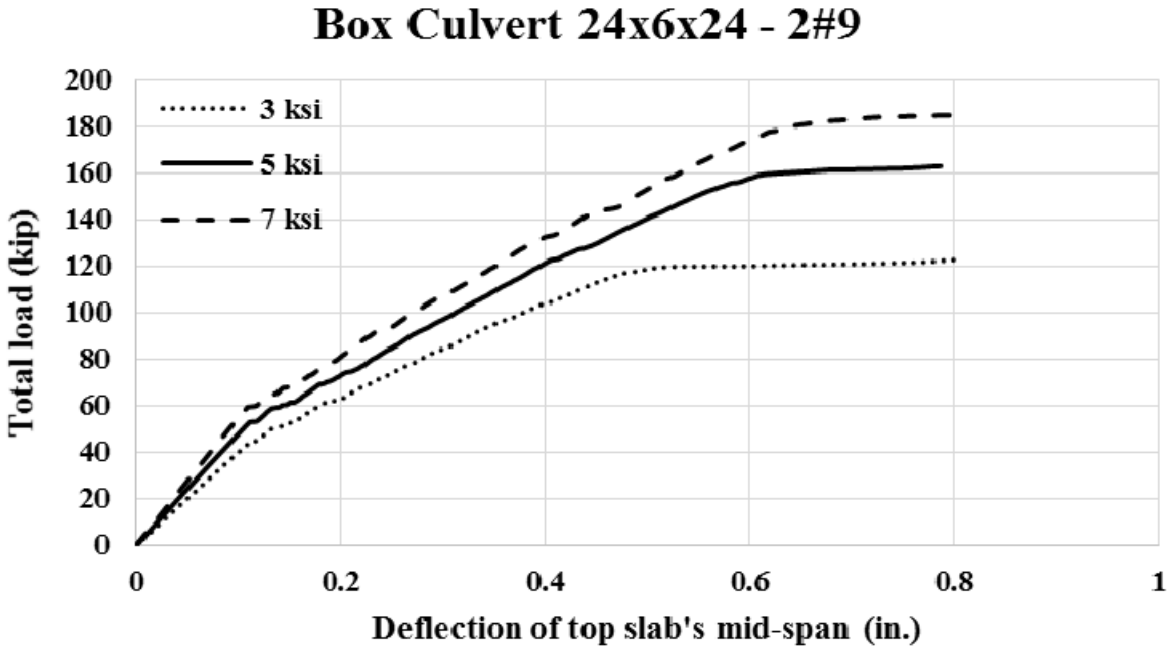
Box Culvert 24x6x24 - 2#9
3 ksi
5 ksi
7 ksi
Total load (kip)
200
180
160
140
120
100
80
60
40
20
0
0
0.2
0.4
0.6
0.8
1
Deflection of top slab's mid-span (in.)

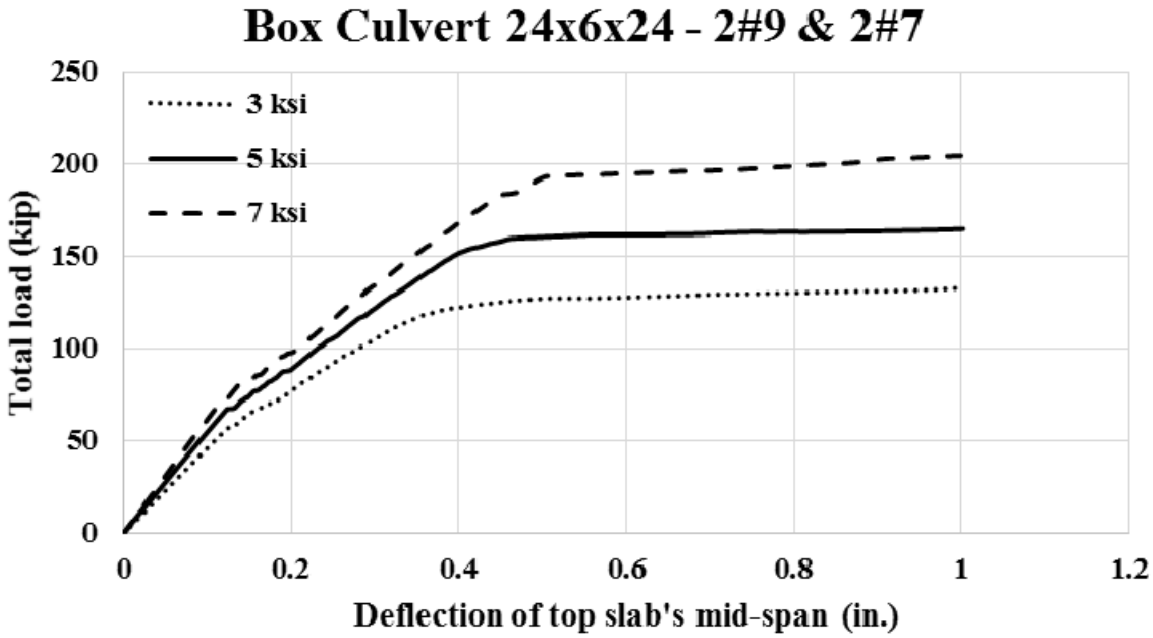
Box Culvert 24x6x24 - 2#9 & 2#7
3 ksi
5 ksi
7 ksi
Total load (kip)
250
200
150
100
50
0
0
0.2
0.4
0.6
0.8
1
1.2
Deflection of top slab's mid-span (in.)

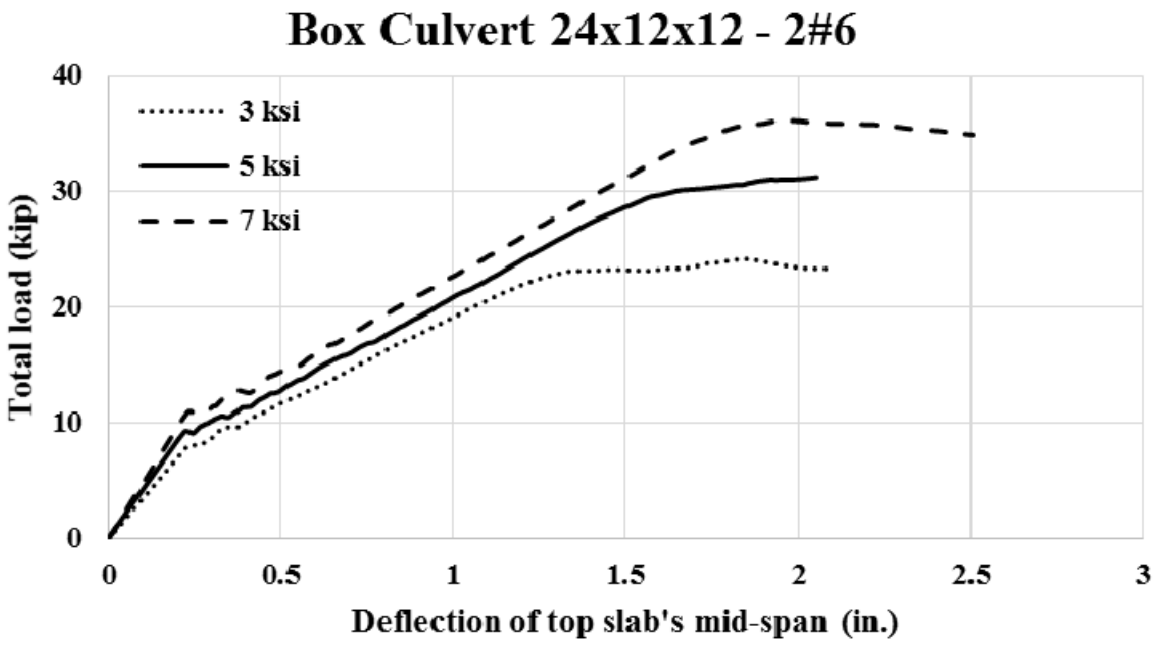
Box Culvert 24x12x12 - 2#6
3 ksi
5 ksi
7 ksi
Total load (kip)
Deflection of top slab's mid-span (in.)
0
10
20
30
40
0
0.5
1
1.5
2
2.5
3

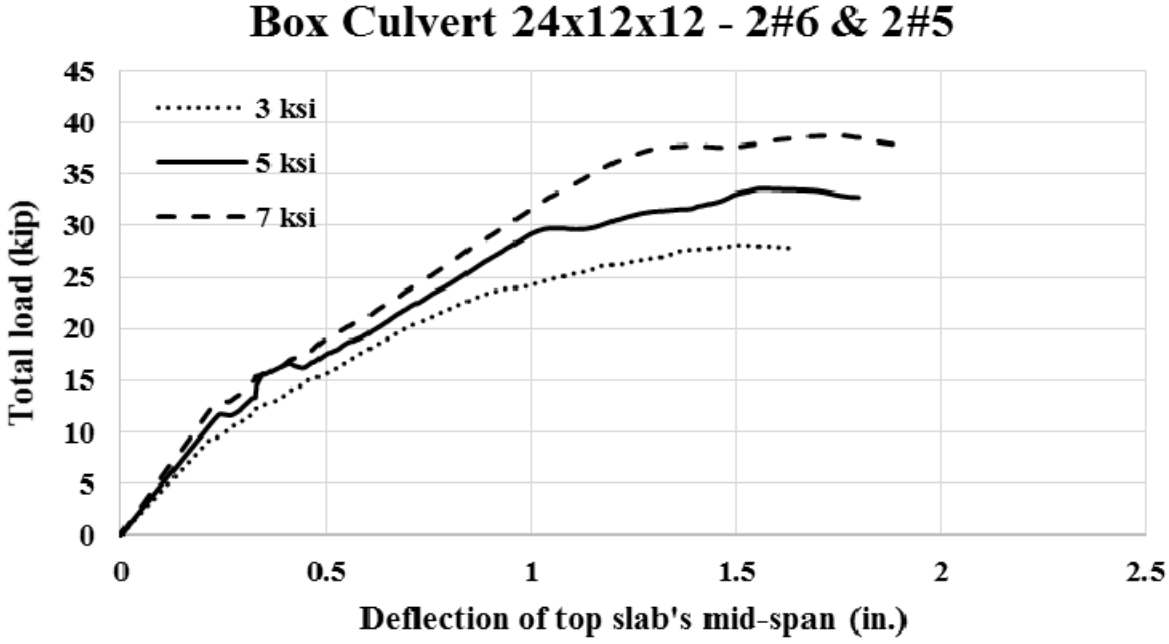
Box Culvert 24x12x12 - 2#6 & 2#5
3 ksi
5 ksi
7 ksi
Total load (kip)
Deflection of top slab's mid-span (in.)
0
5
10
15
20
25
30
35
40
45
0
0.5
1
1.5
2
2.5

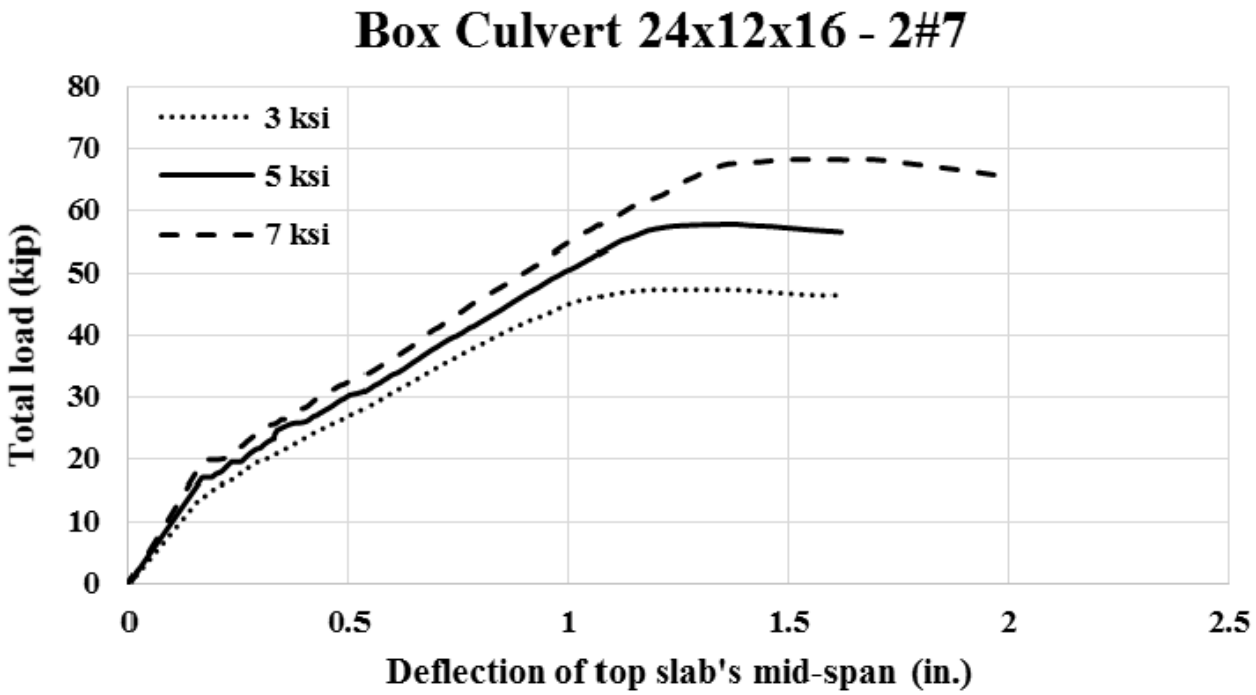
Box Culvert 24x12x16 - 2#7
3 ksi
5 ksi
7 ksi
Total load (kip)
0
10
20
30
40
50
60
70
80
0
0.5
1
1.5
2
2.5
Deflection of top slab's mid-span (in.)

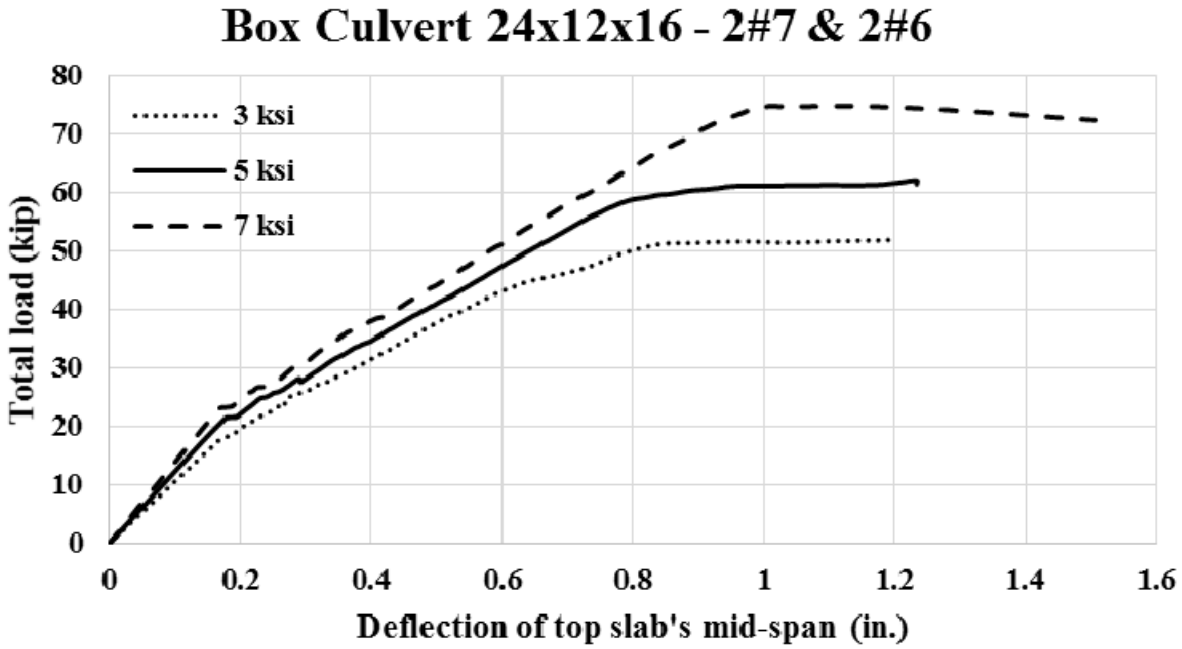
Box Culvert 24x12x16 - 2#7 & 2#6
3 ksi
5 ksi
7 ksi
Total load (kip)
0
10
20
30
40
50
60
70
80
0
0.2
0.4
0.6
0.8
1
1.2
1.4
1.6
Deflection of top slab's mid-span (in.)

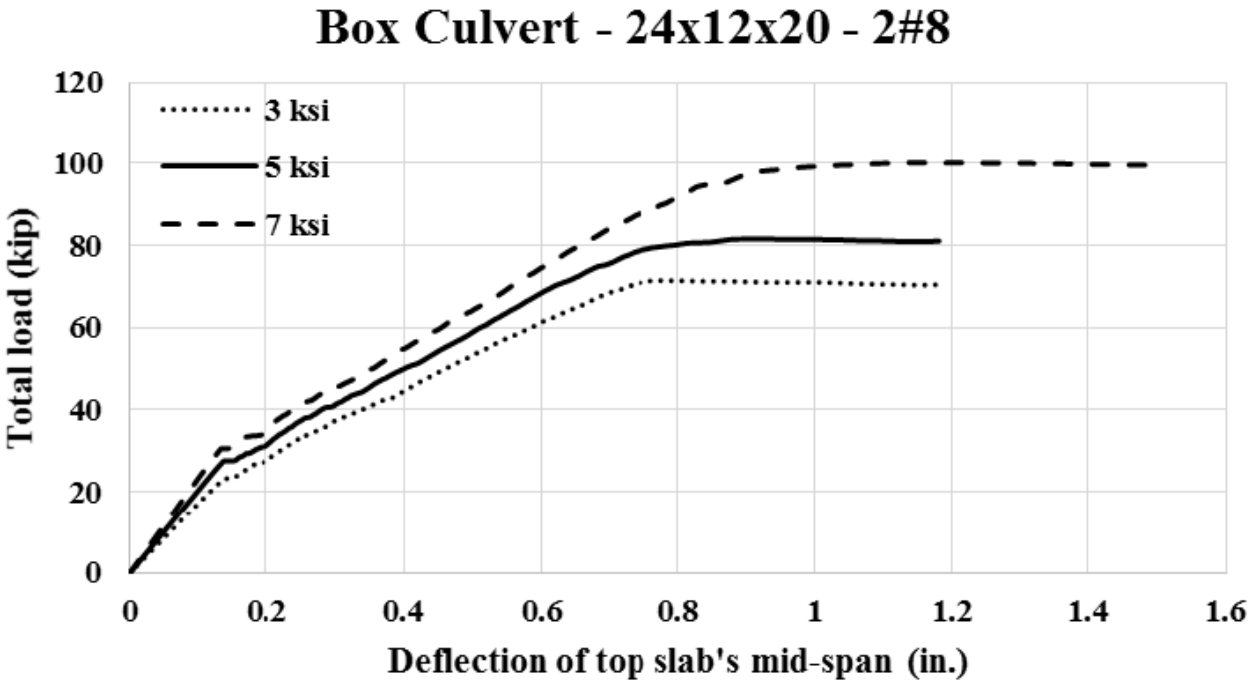
Box Culvert - 24x12x20 - 2#8
3 ksi
5 ksi
7 ksi
Total load (kip)
120
100
80
60
40
20
0
0
0.2
0.4
0.6
0.8
1
1.2
1.4
1.6
Deflection of top slab's mid-span (in.)

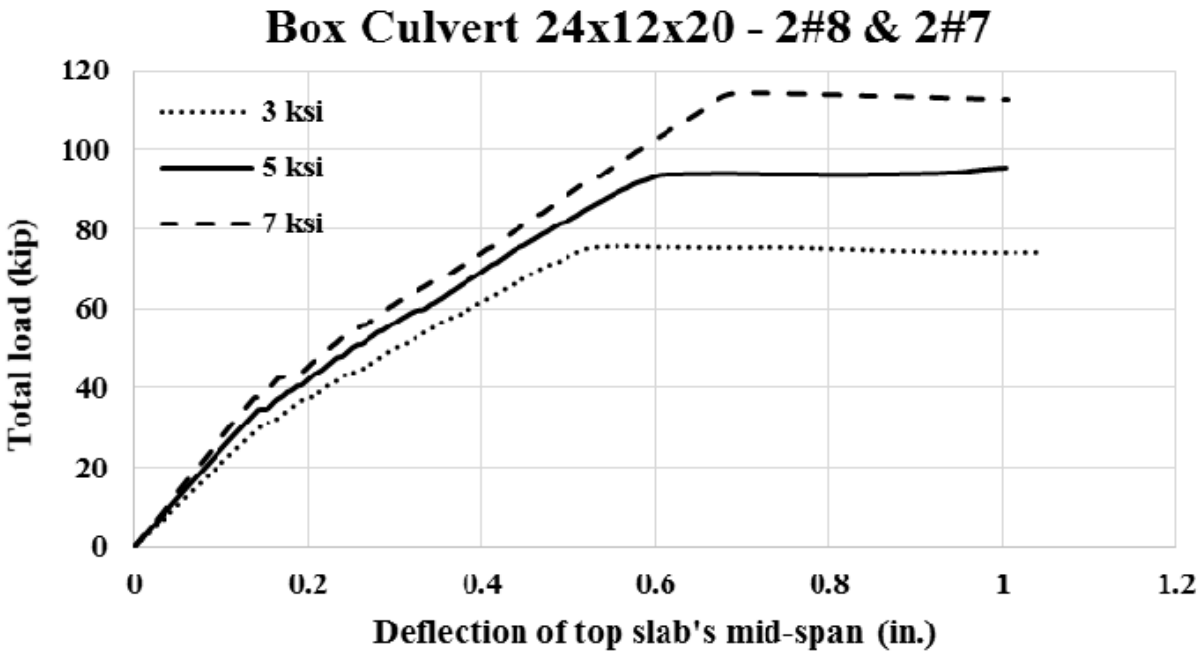
Box Culvert 24x12x20 - 2#8 & 2#7
3 ksi
5 ksi
7 ksi
Total load (kip)
120
100
80
60
40
20
0
0
0.2
0.4
0.6
0.8
1
1.2
Deflection of top slab's mid-span (in.)

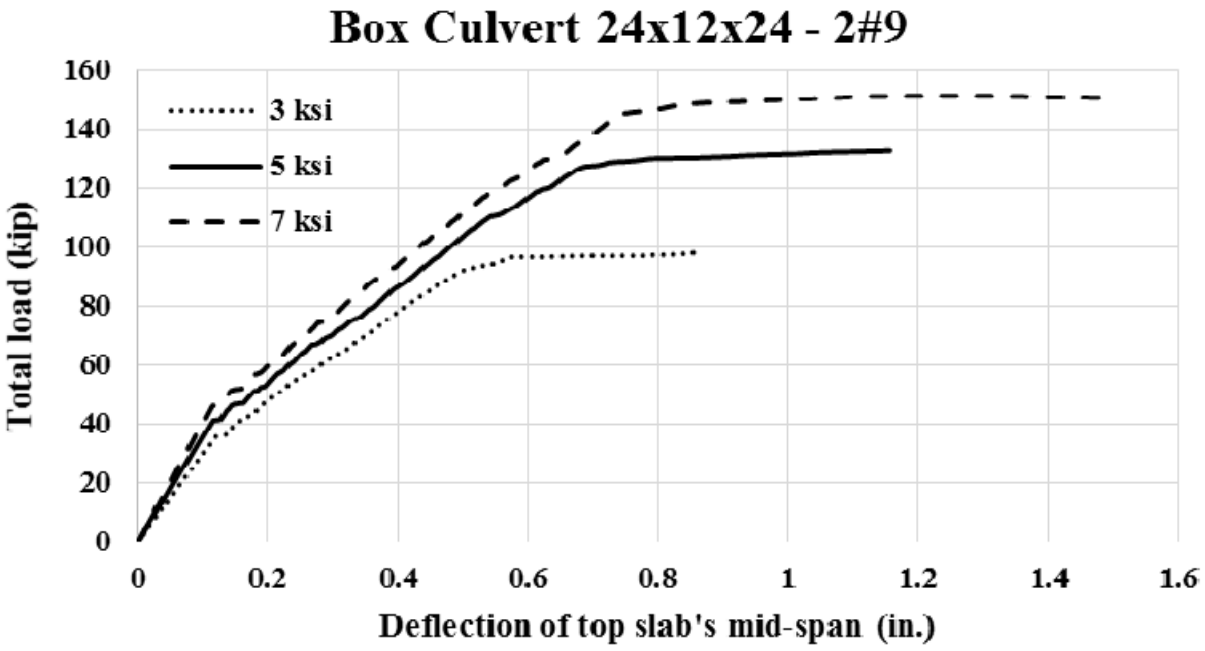
Box Culvert 24x12x24 - 2#9
3 ksi
5 ksi
7 ksi
Total load (kip)
Deflection of top slab's mid-span (in.)
0
20
40
60
80
100
120
140
160
0
0.2
0.4
0.6
0.8
1
1.2
1.4
1.6

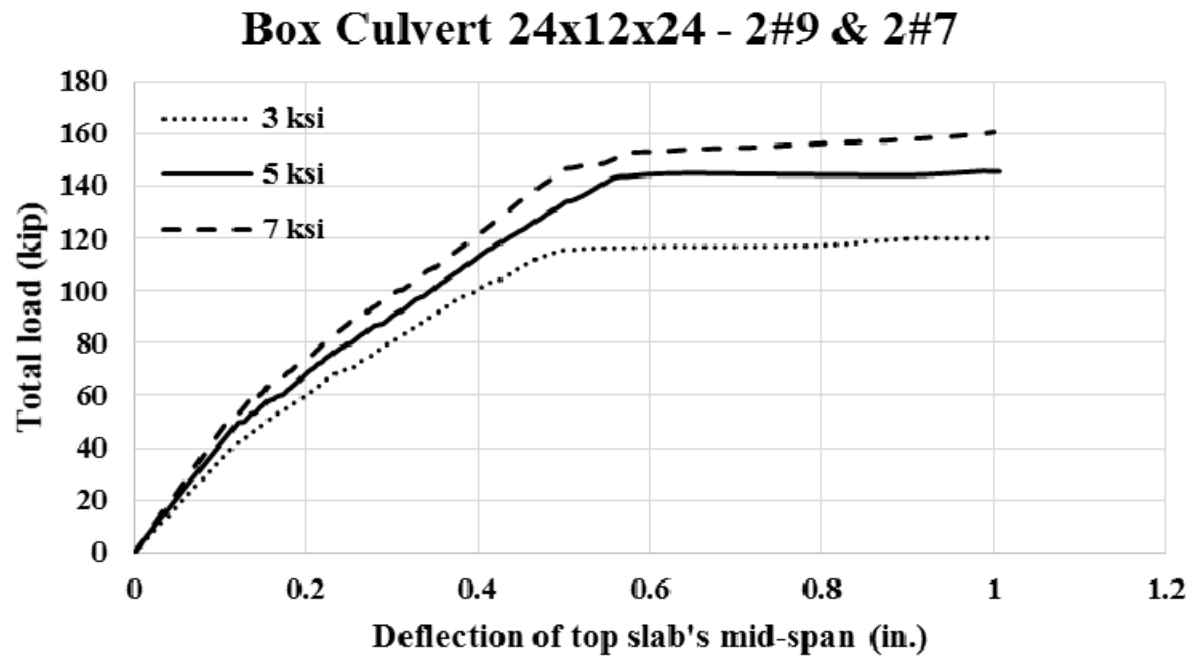
Box Culvert 24x12x24 - 2#9 & 2#7
3 ksi
5 ksi
7 ksi
Total load (kip)
Deflection of top slab's mid-span (in.)
0
20
40
60
80
100
120
140
160
180
0
0.2
0.4
0.6
0.8
1
1.2

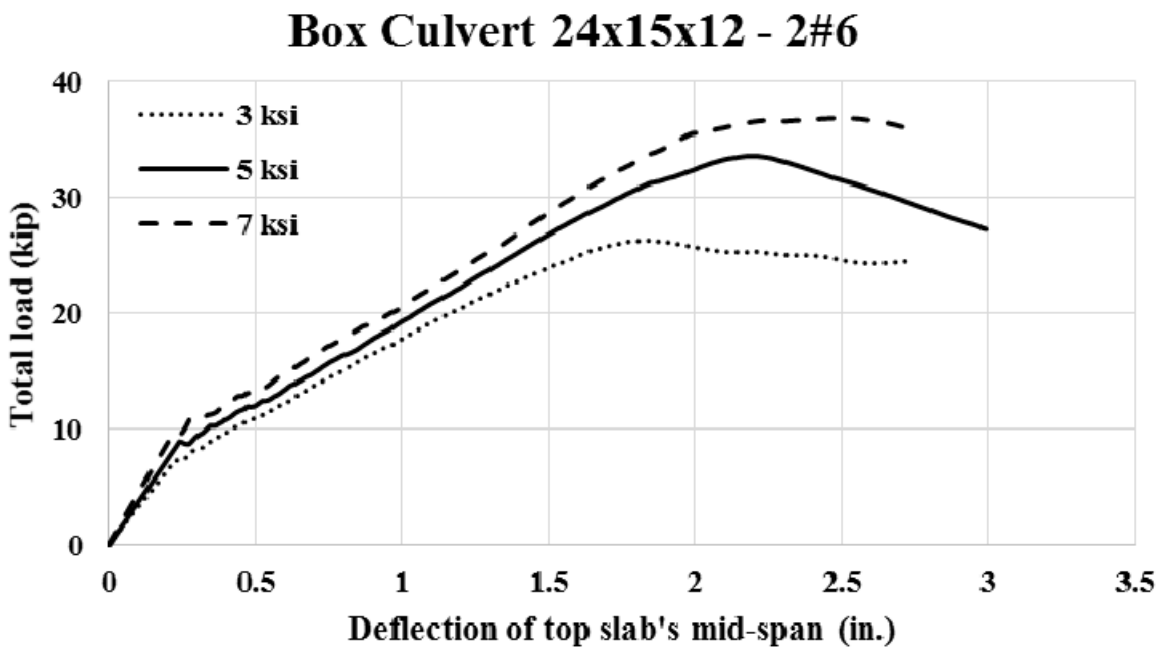
Box Culvert 24x15x12 - 2#6
3 ksi
5 ksi
7 ksi
Total load (kip)
Deflection of top slab's mid-span (in.)
0
10
20
30
40
0
0.5
1
1.5
2
2.5
3
3.5

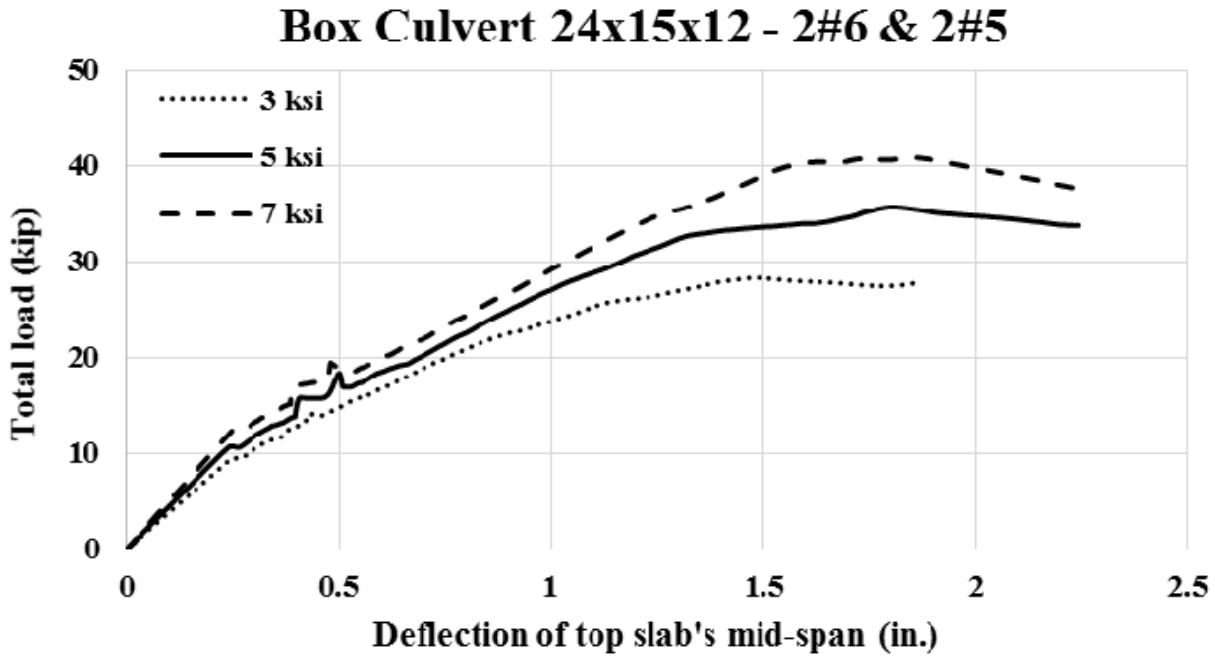
Box Culvert 24x15x12 - 2#6 & 2#5
3 ksi
5 ksi
7 ksi
Total load (kip)
Deflection of top slab's mid-span (in.)
0
10
20
30
40
50
0
0.5
1
1.5
2
2.5

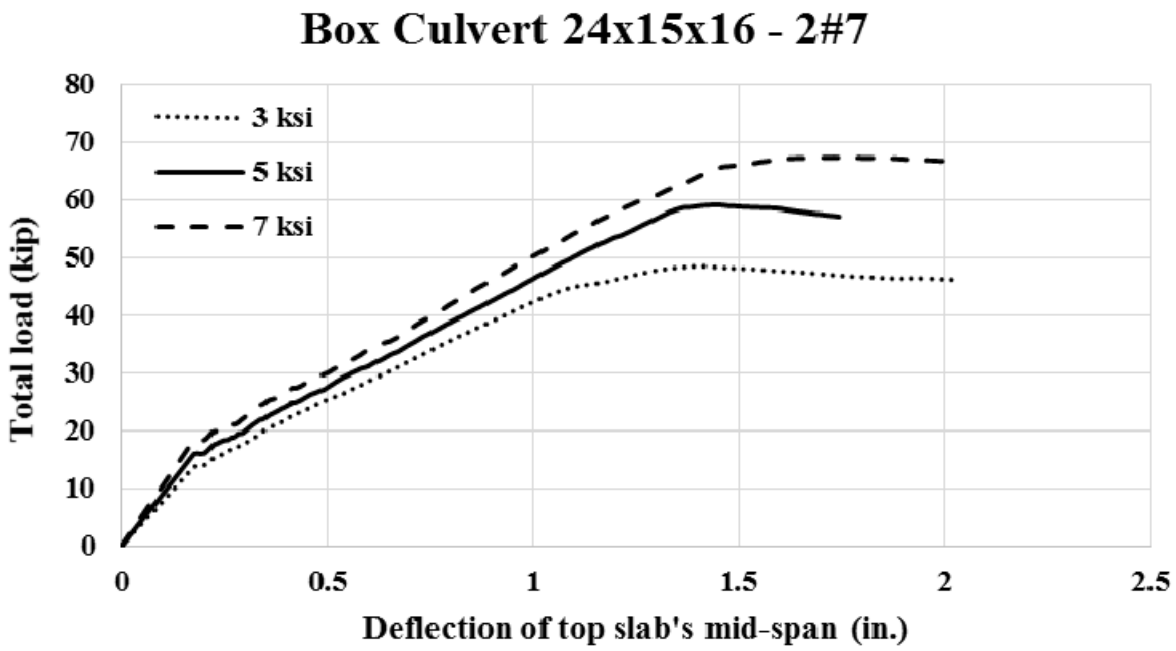
Box Culvert 24x15x16 - 2#7
3 ksi
5 ksi
7 ksi
Total load (kip)
0
10
20
30
40
50
60
70
80
0
0.5
1
1.5
2
2.5
Deflection of top slab's mid-span (in.)

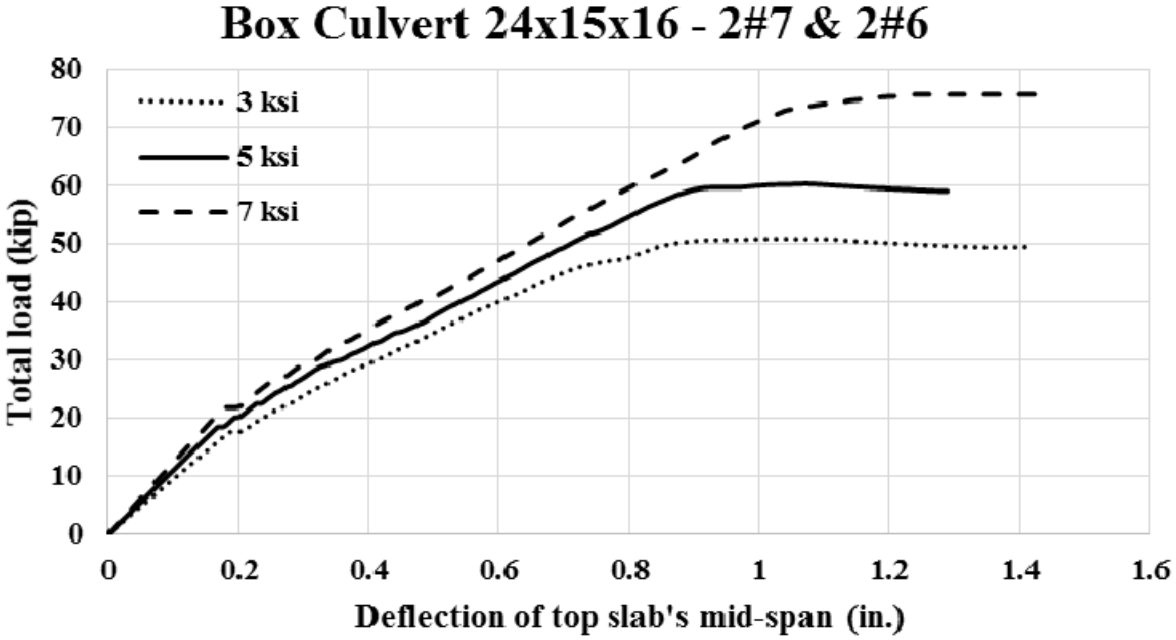
Box Culvert 24x15x16 - 2#7 & 2#6
3 ksi
5 ksi
7 ksi
Total load (kip)
0
10
20
30
40
50
60
70
80
0
0.2
0.4
0.6
0.8
1
1.2
1.4
1.6
Deflection of top slab's mid-span (in.)

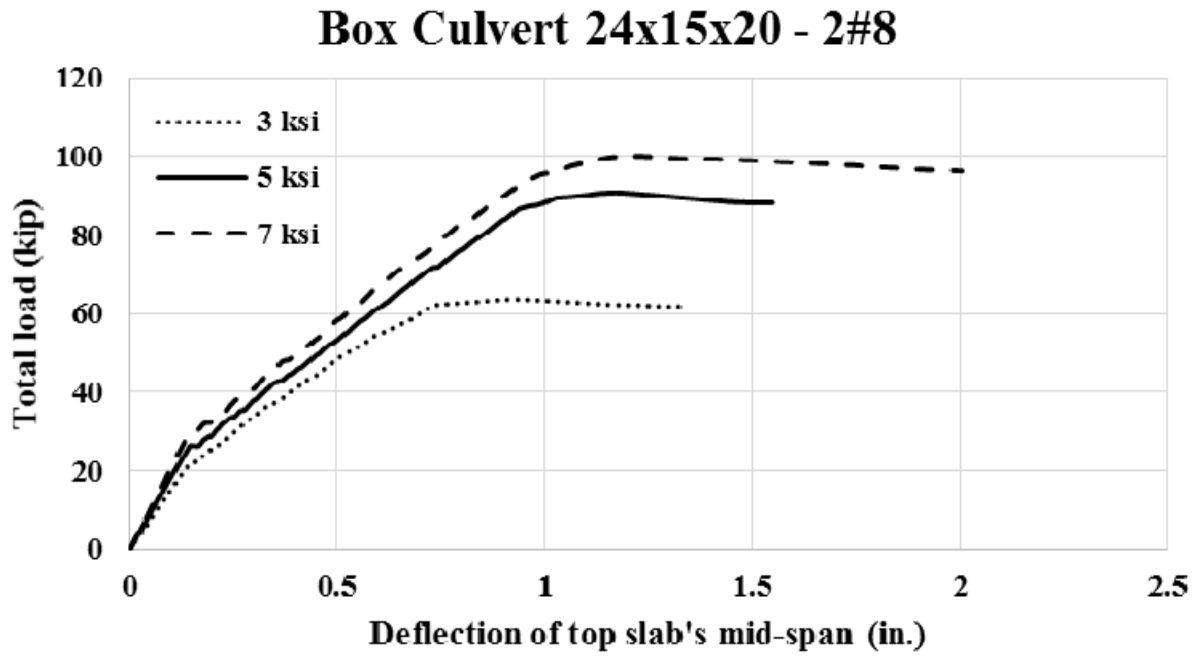
Box Culvert 24x15x20 - 2#8
3 ksi
5 ksi
7 ksi
Total load (kip)
120
100
80
60
40
20
0
0
0.5
1
1.5
2
2.5
Deflection of top slab's mid-span (in.)

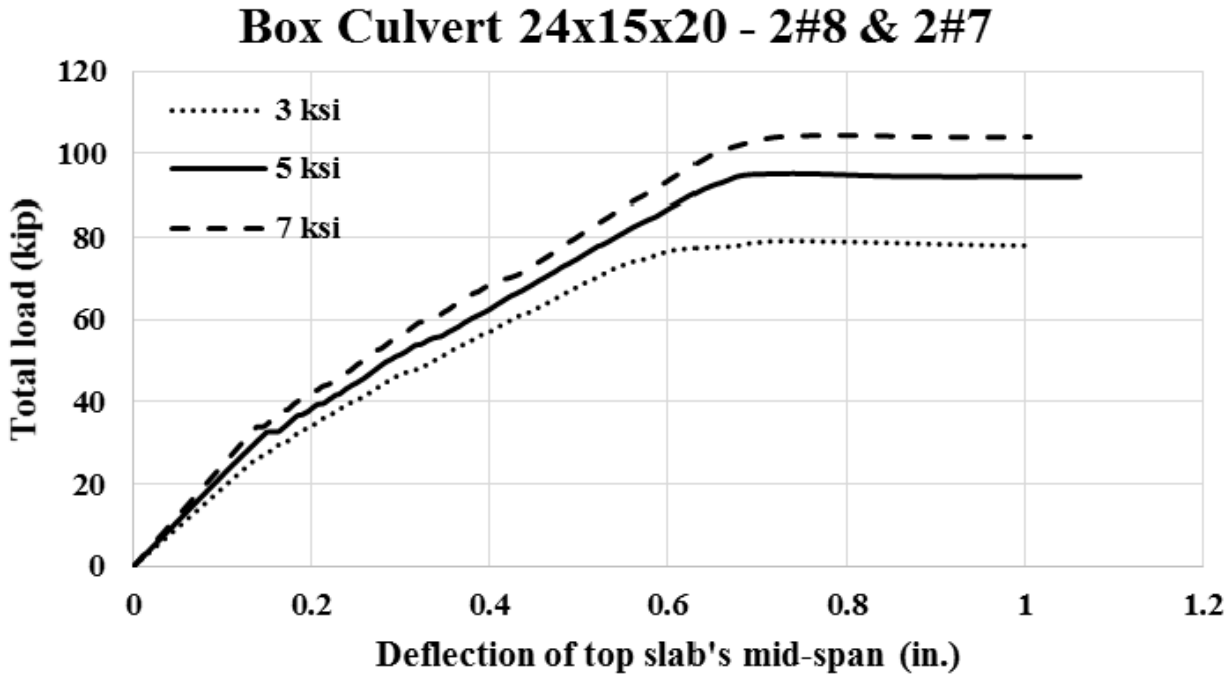
Box Culvert 24x15x20 - 2#8 & 2#7
3 ksi
5 ksi
7 ksi
Total load (kip)
120
100
80
60
40
20
0
0
0.2
0.4
0.6
0.8
1
1.2
Deflection of top slab's mid-span (in.)

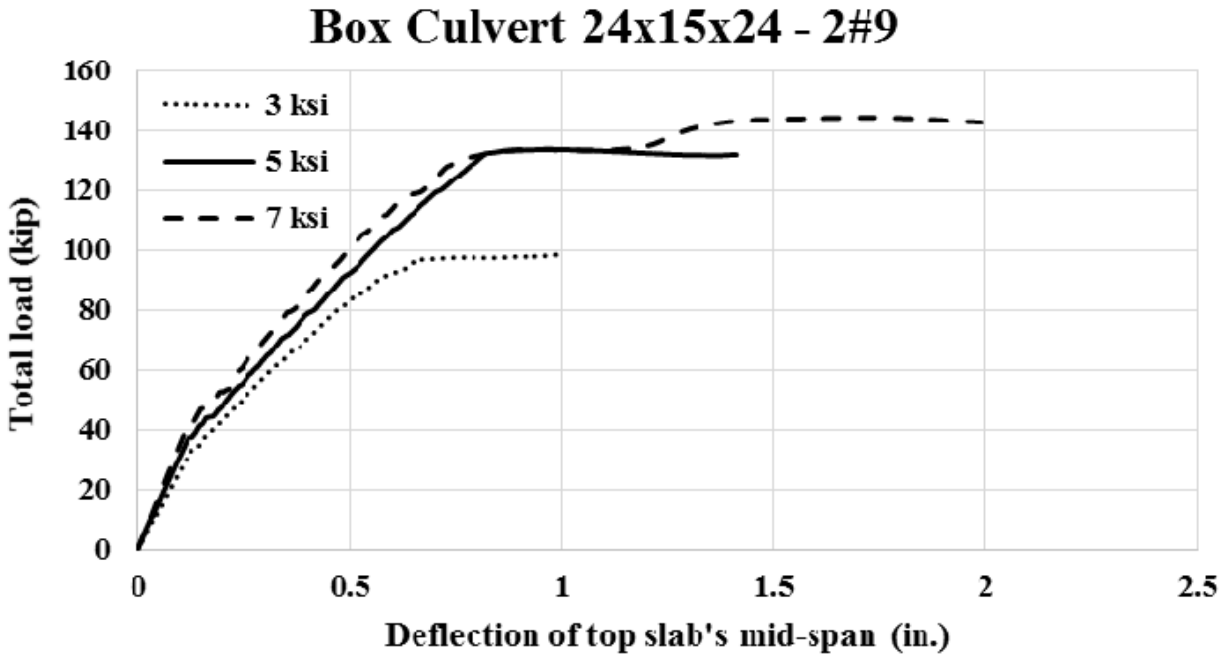
Box Culvert 24x15x24 - 2#9
3 ksi
5 ksi
7 ksi
Total load (kip)
0
20
40
60
80
100
120
140
160
0
0.5
1
1.5
2
2.5
Deflection of top slab's mid-span (in.)

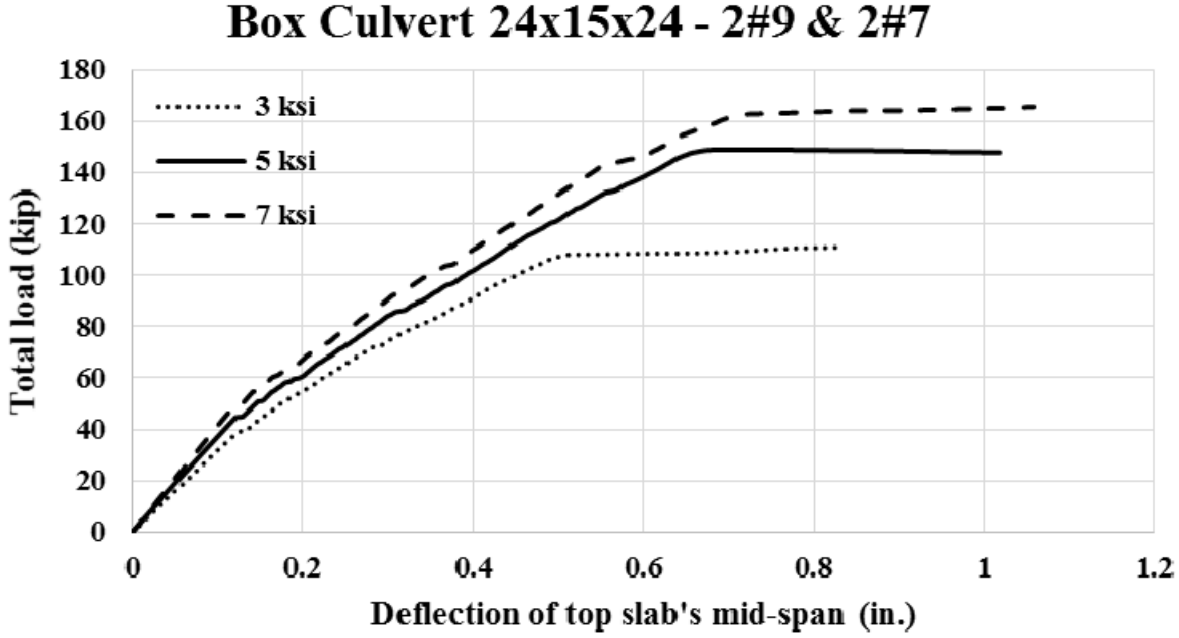
Box Culvert 24x15x24 - 2#9 & 2#7
3 ksi
5 ksi
7 ksi
Total load (kip)
0
20
40
60
80
100
120
140
160
180
0
0.2
0.4
0.6
0.8
1
1.2
Deflection of top slab's mid-span (in.)

APPENDIX 2. CRACKING PATTERN

Box Culvert 6 × 6 × 12

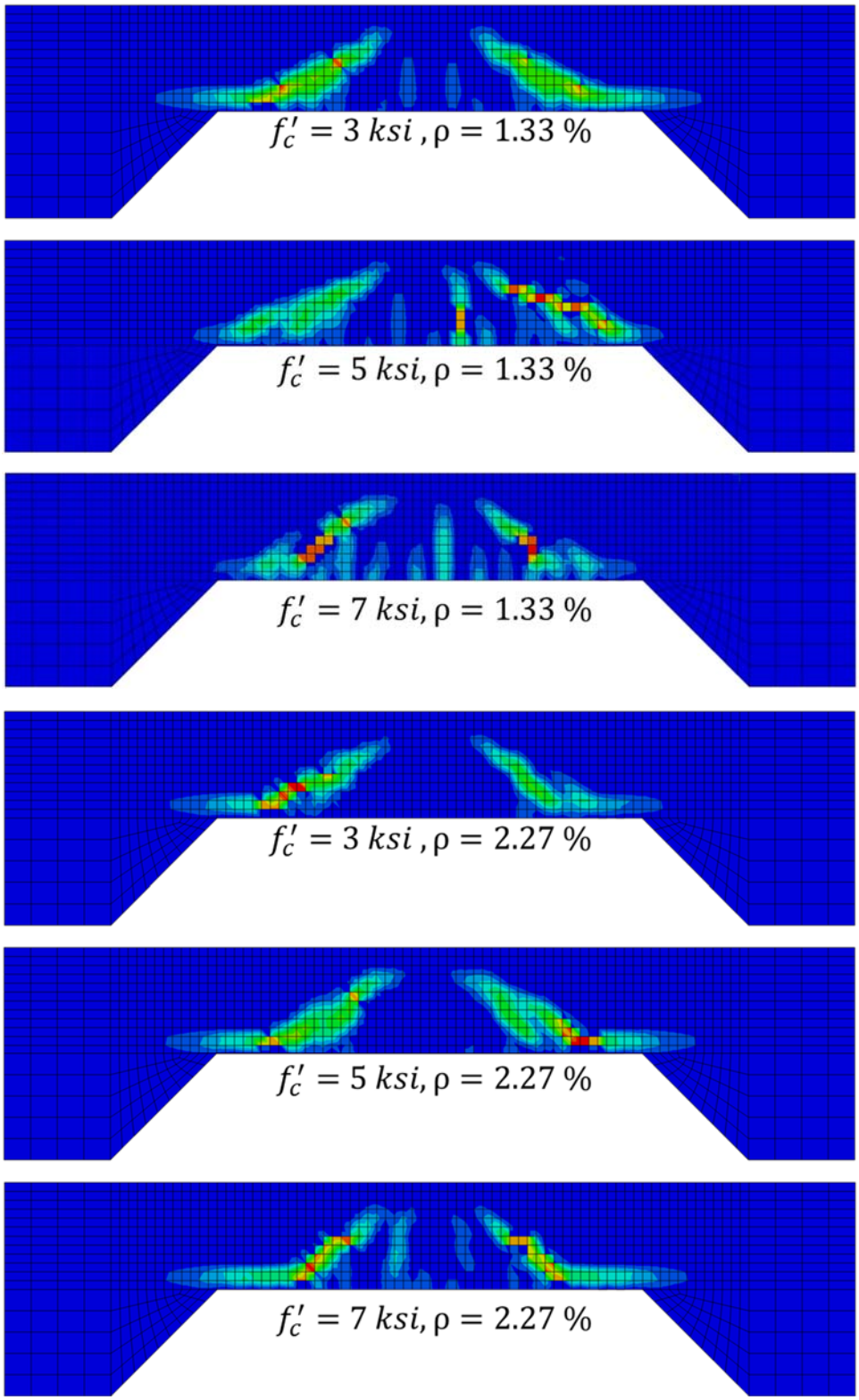

Box Culvert 6 × 6 × 16

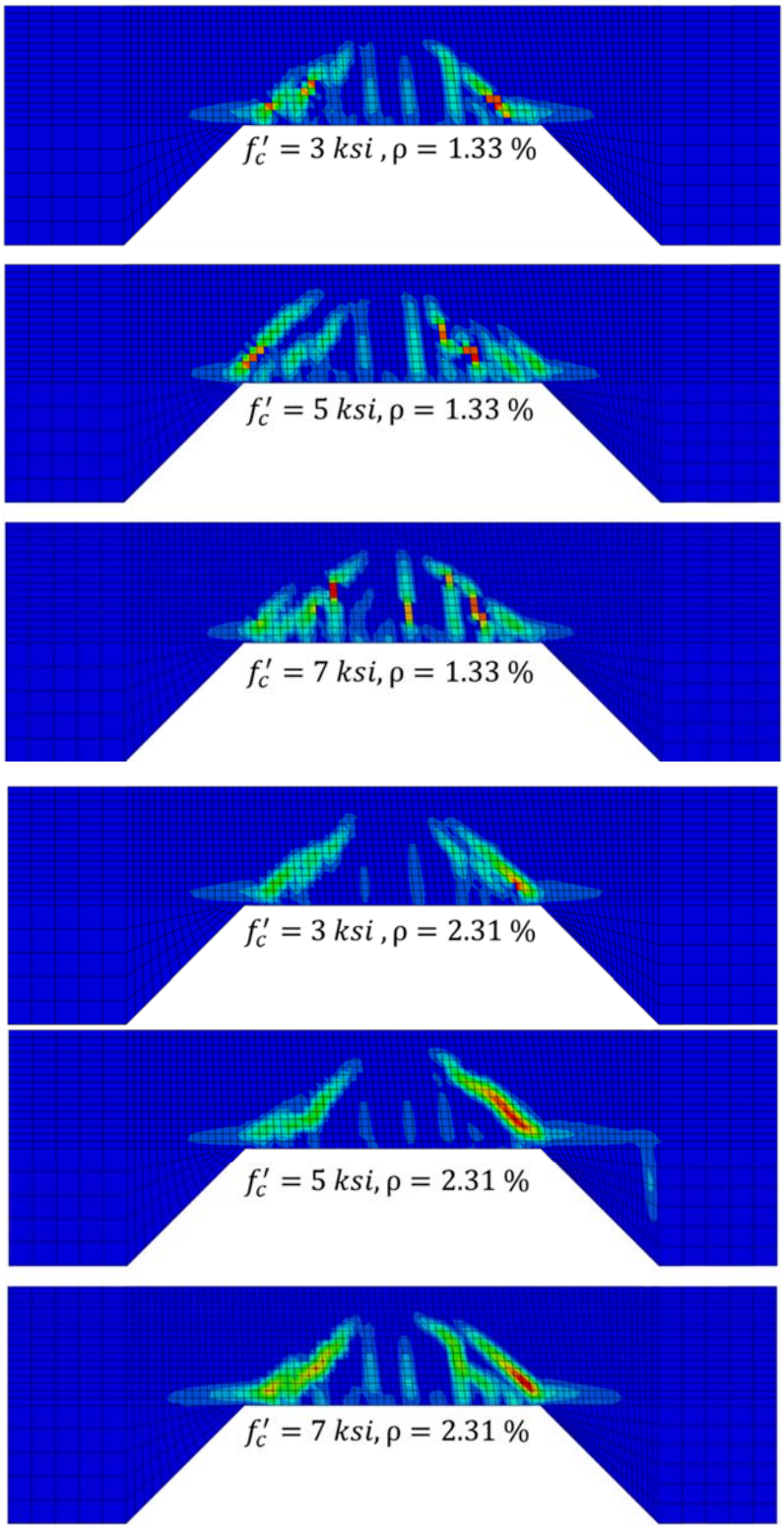

Box Culvert $6 \times 6 \times 20$

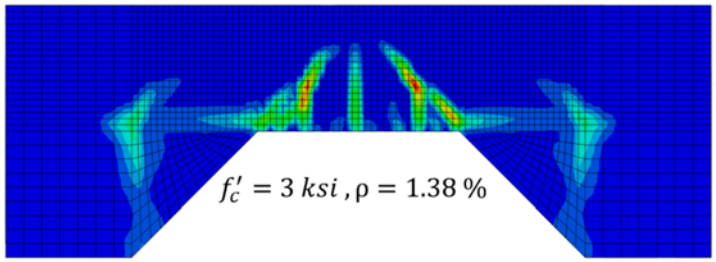

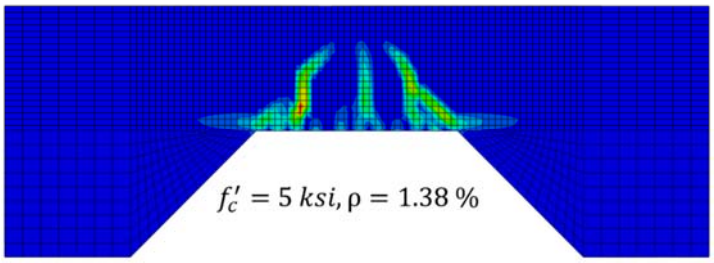

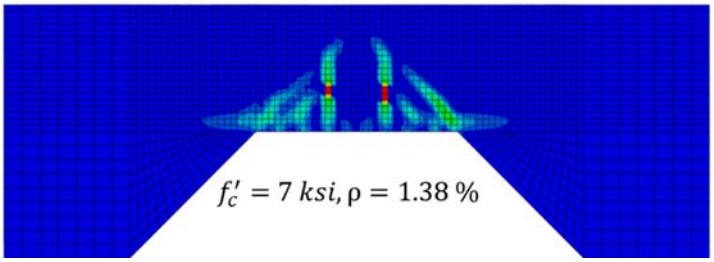

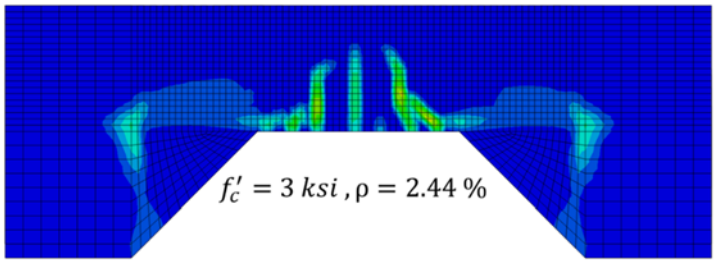

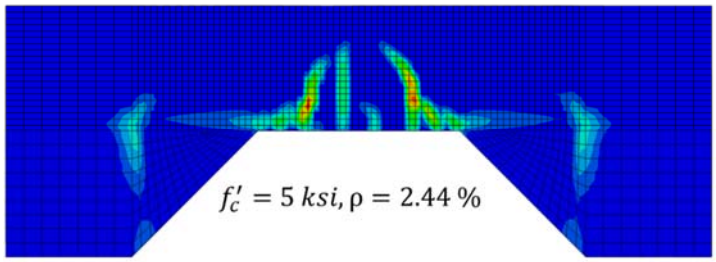

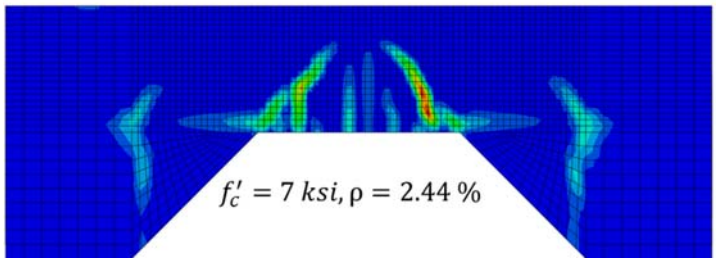

Box Culvert $6 \times 6 \times 24$

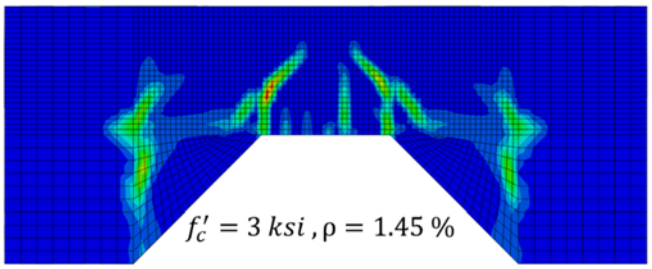

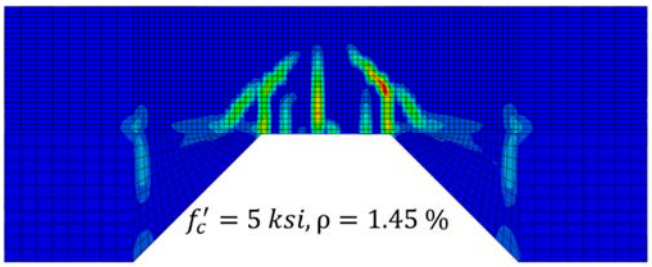

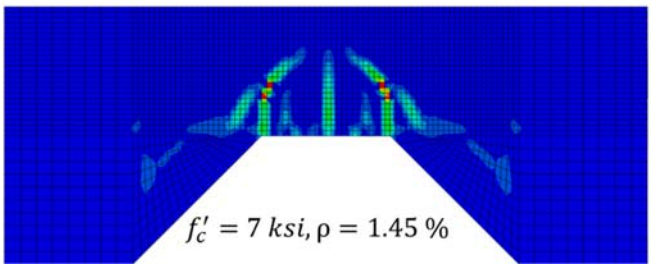

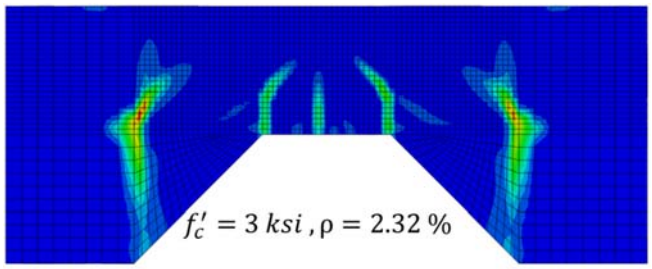

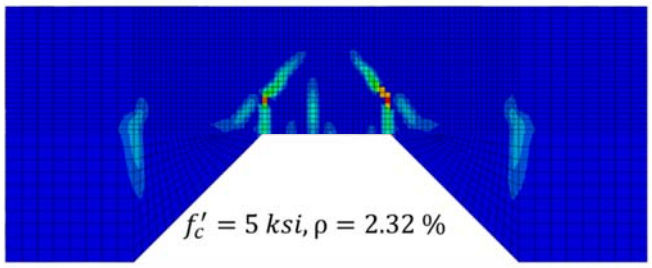

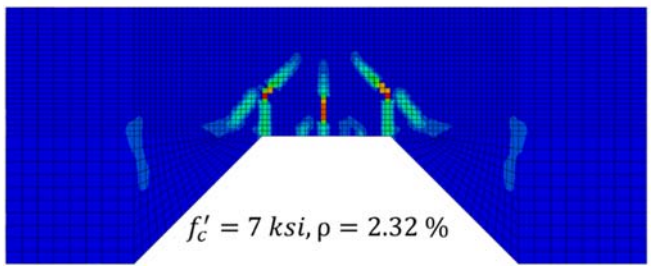

Box Culvert 6 × 12 × 12

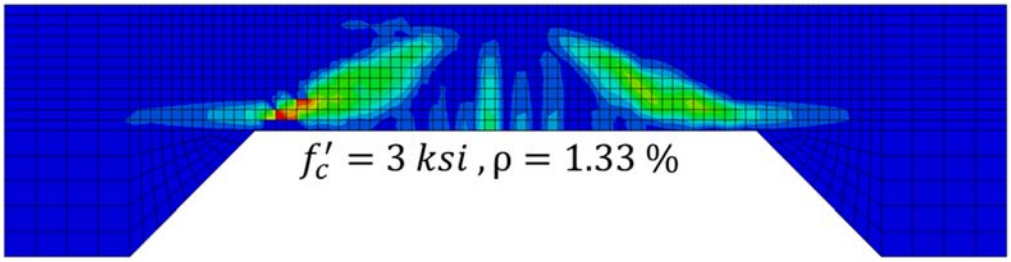

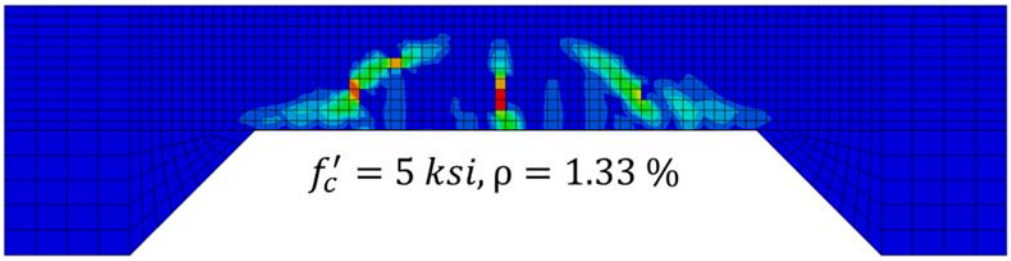

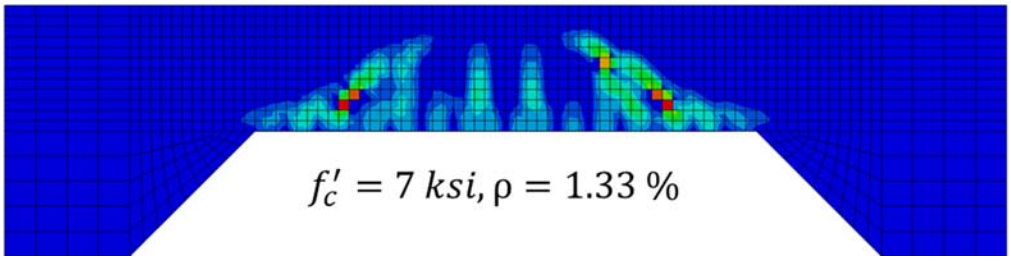

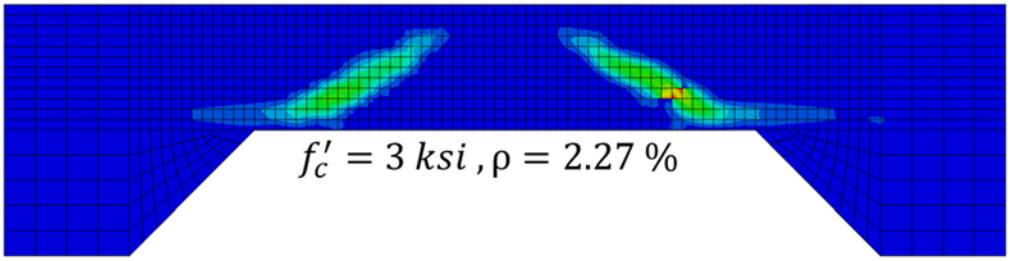

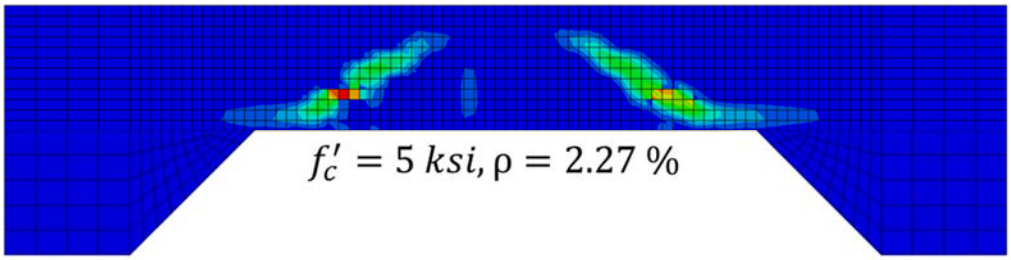

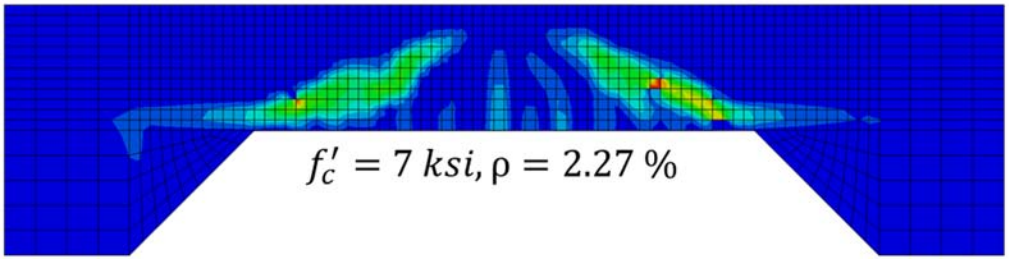

Box Culvert 6 × 12 × 16

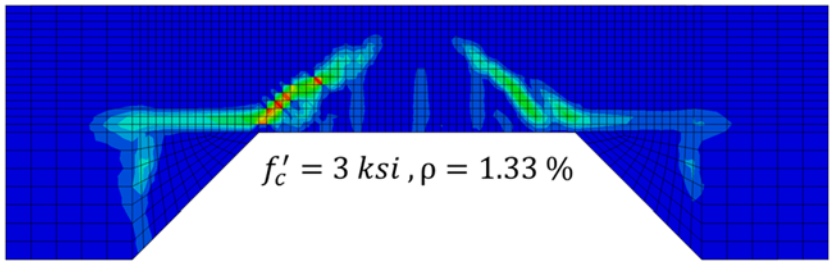

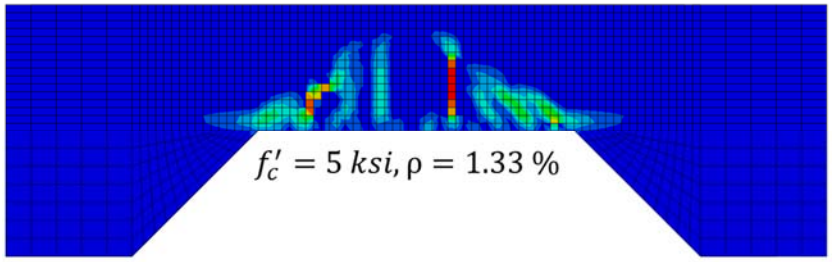

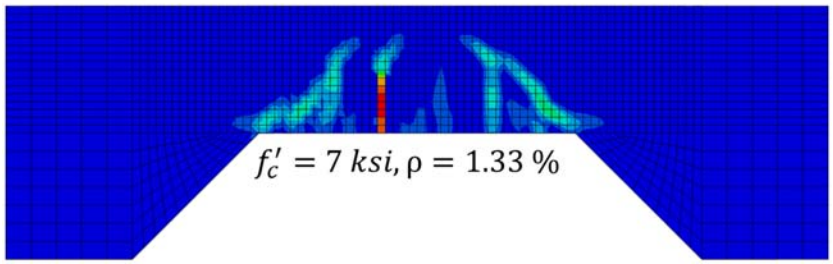

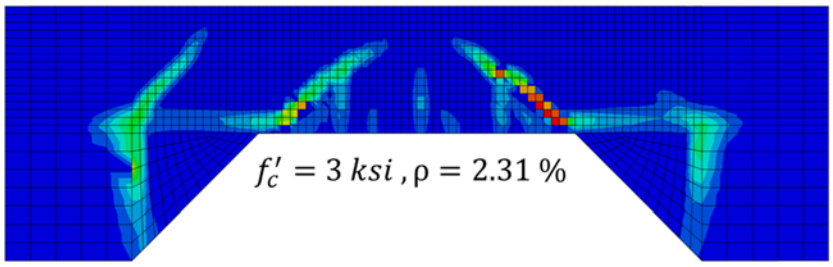

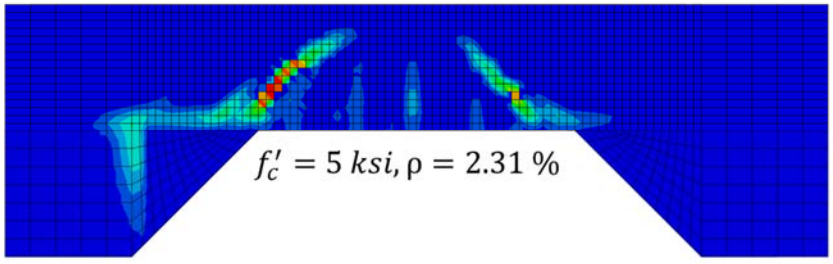

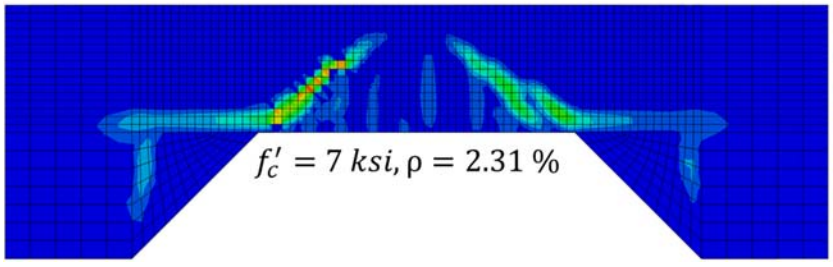

Box Culvert $6 \times 12 \times 20$

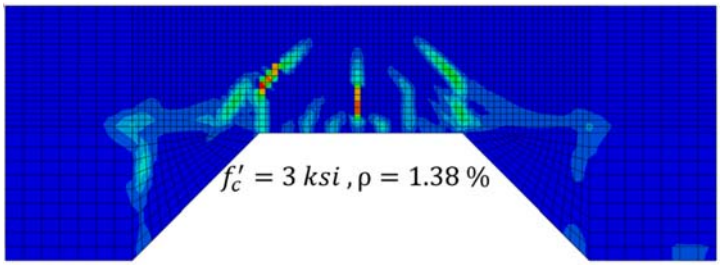

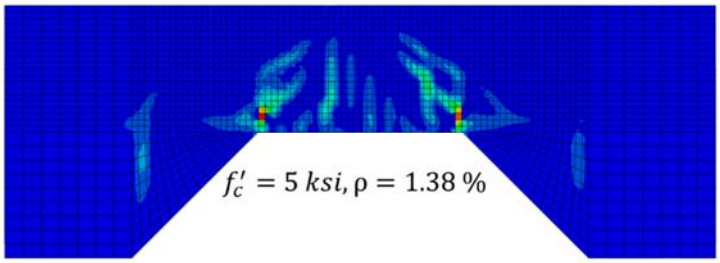

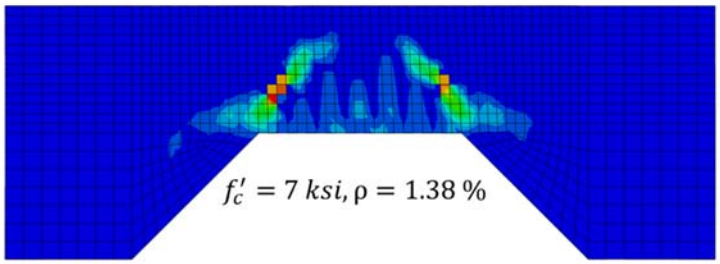

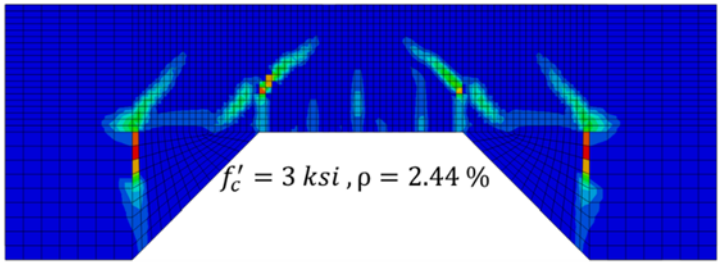

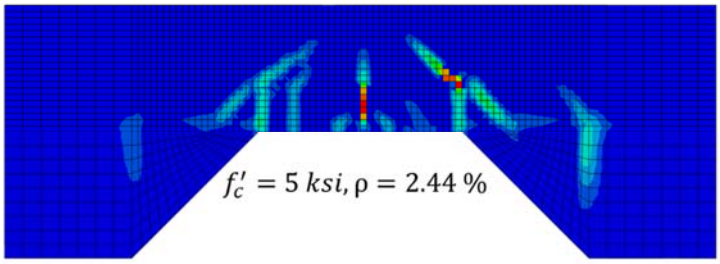

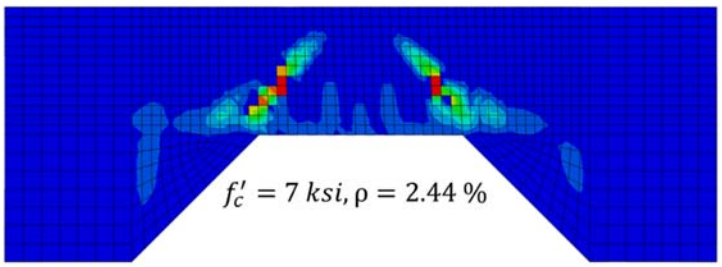

Box Culvert $6 \times 12 \times 24$

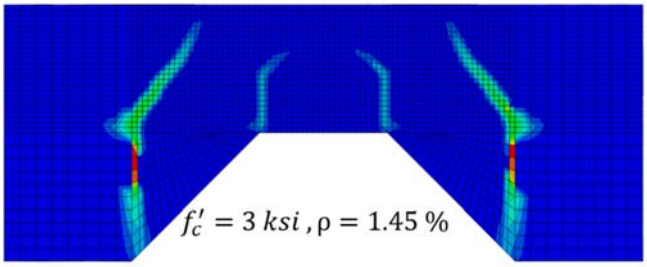

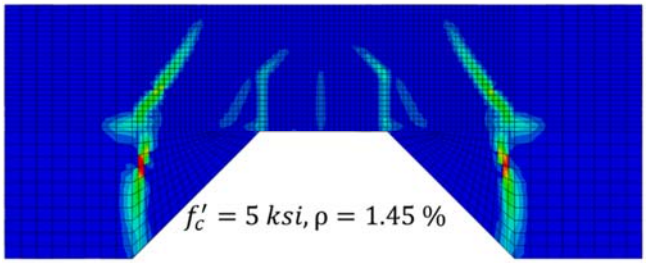

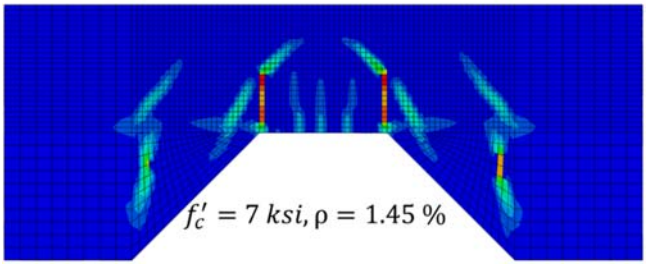

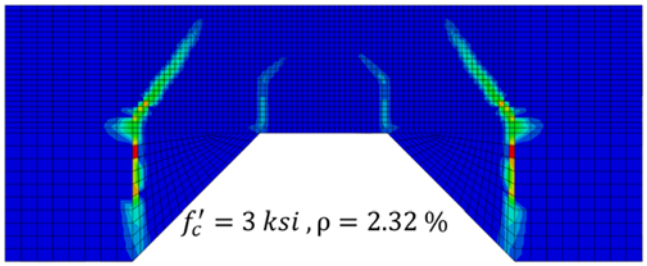

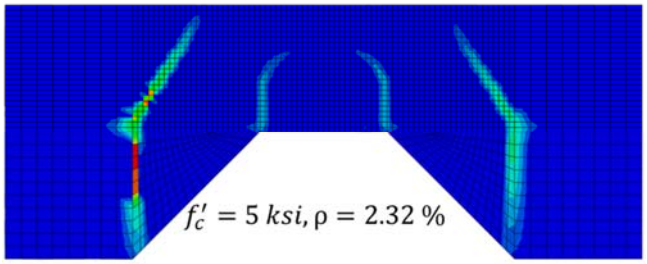

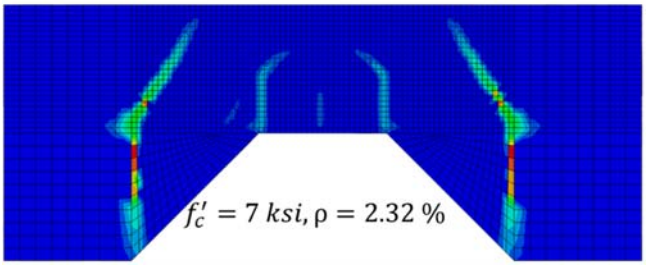

Box Culvert 6 × 15 × 12

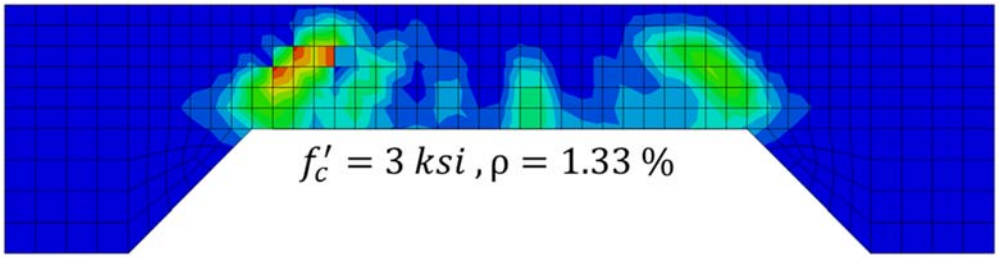

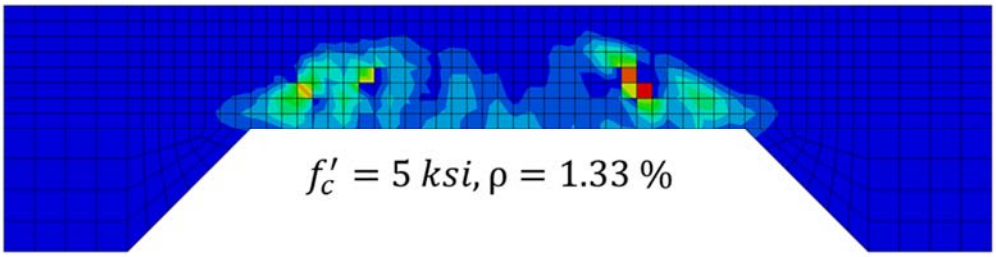

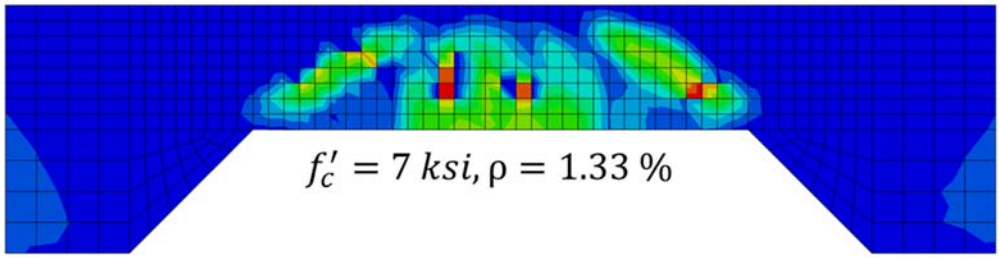

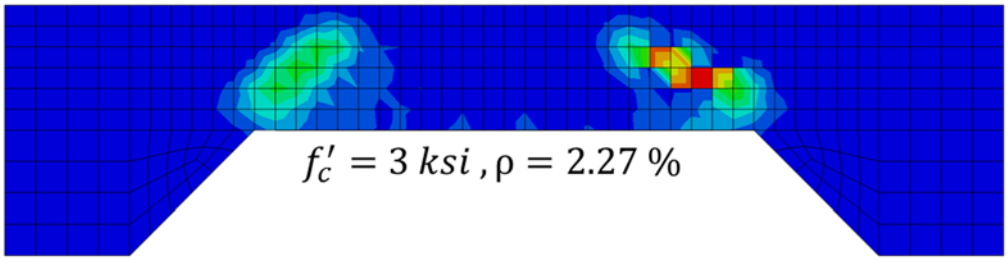

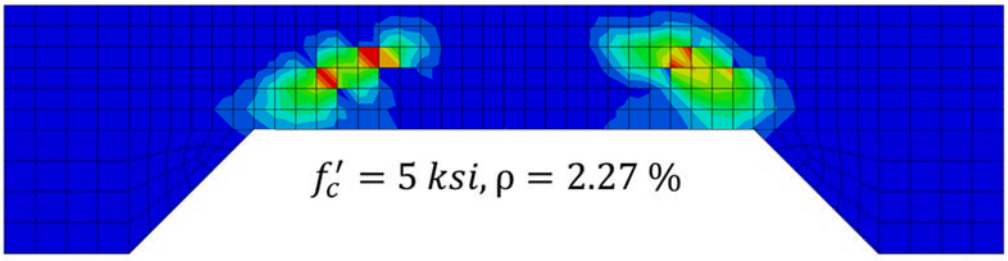

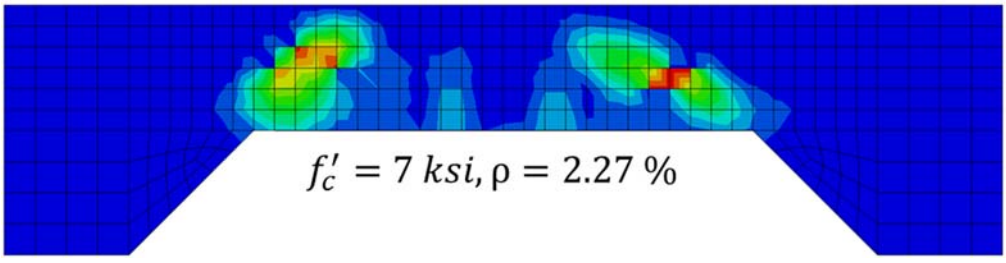

Box Culvert 6 × 15 × 16

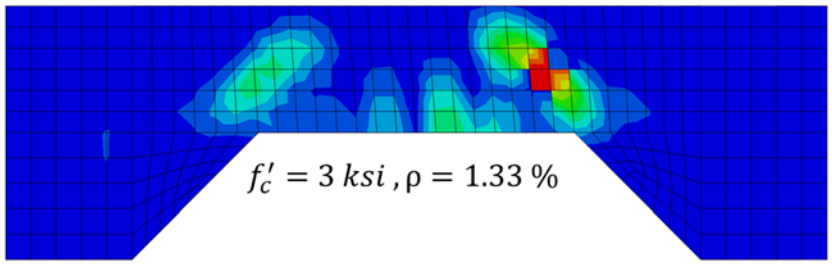

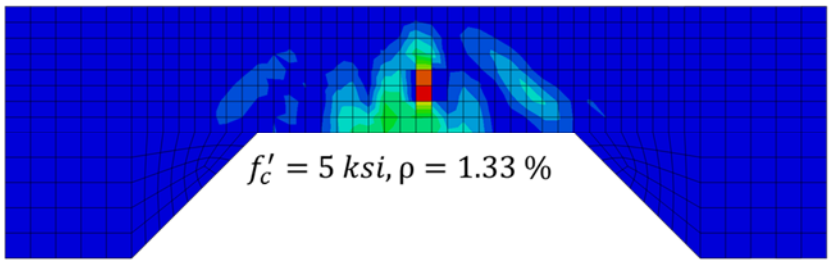

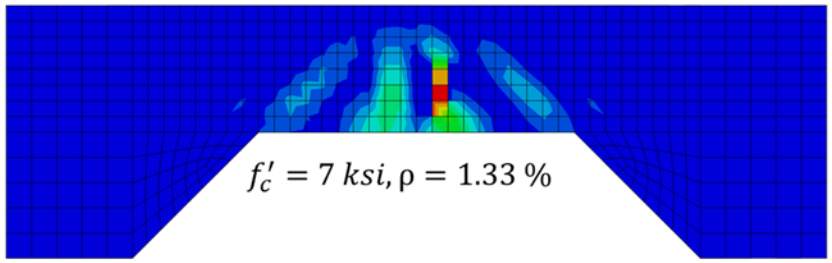

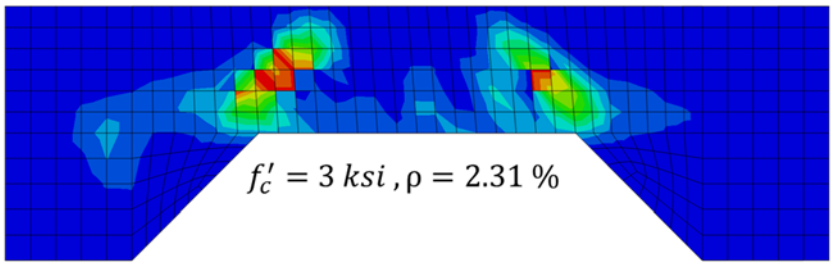

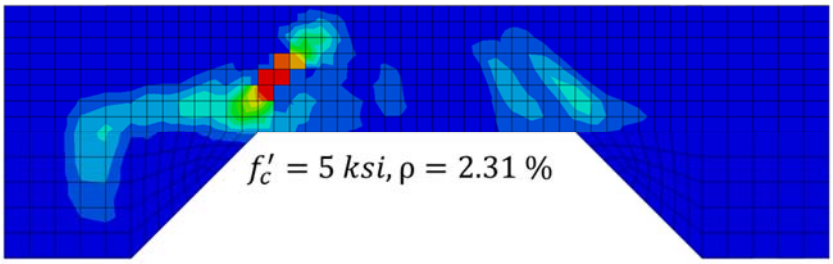

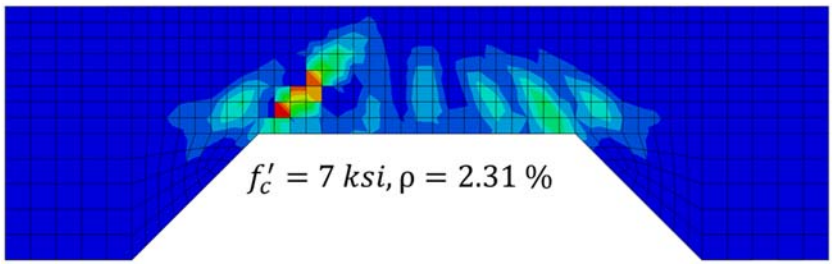

Box Culvert $6 \times 15 \times 20$

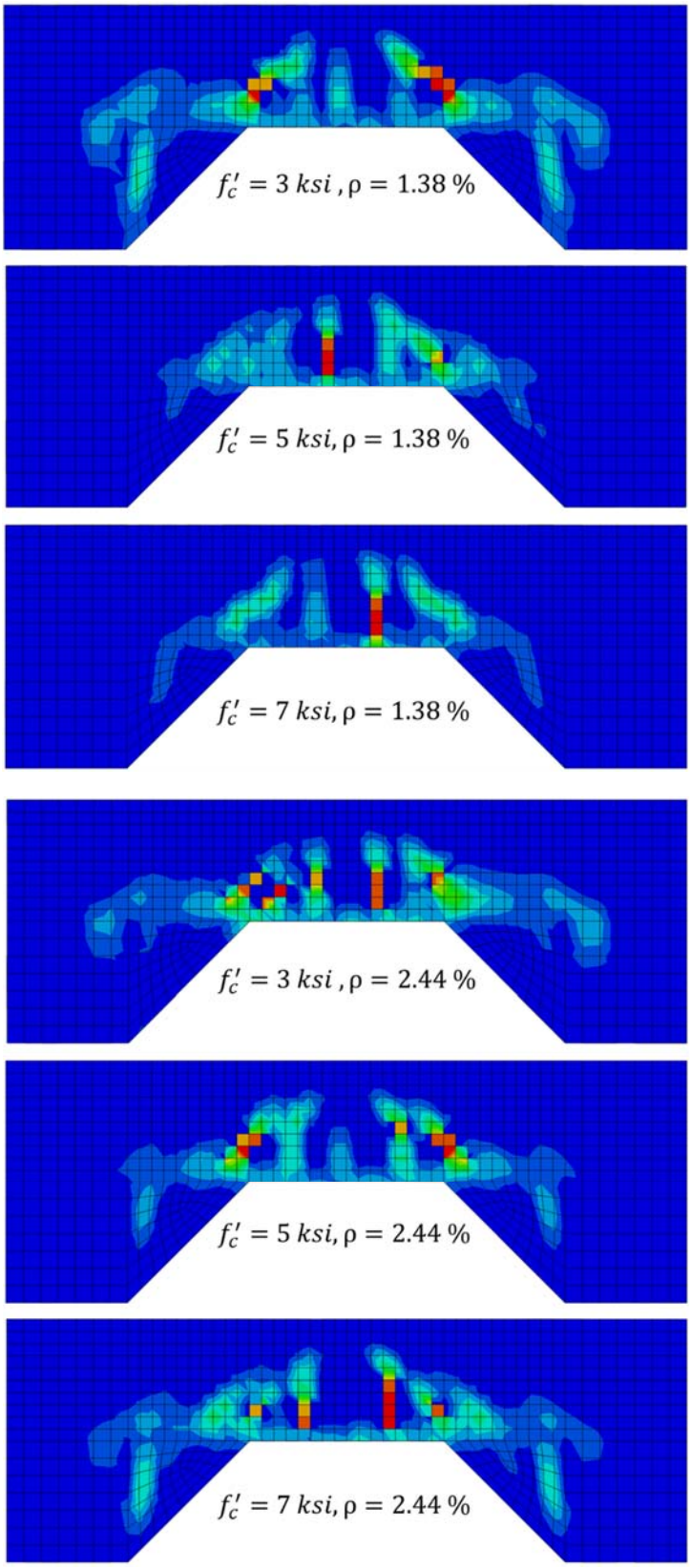

Box Culvert $6 \times 15 \times 24$

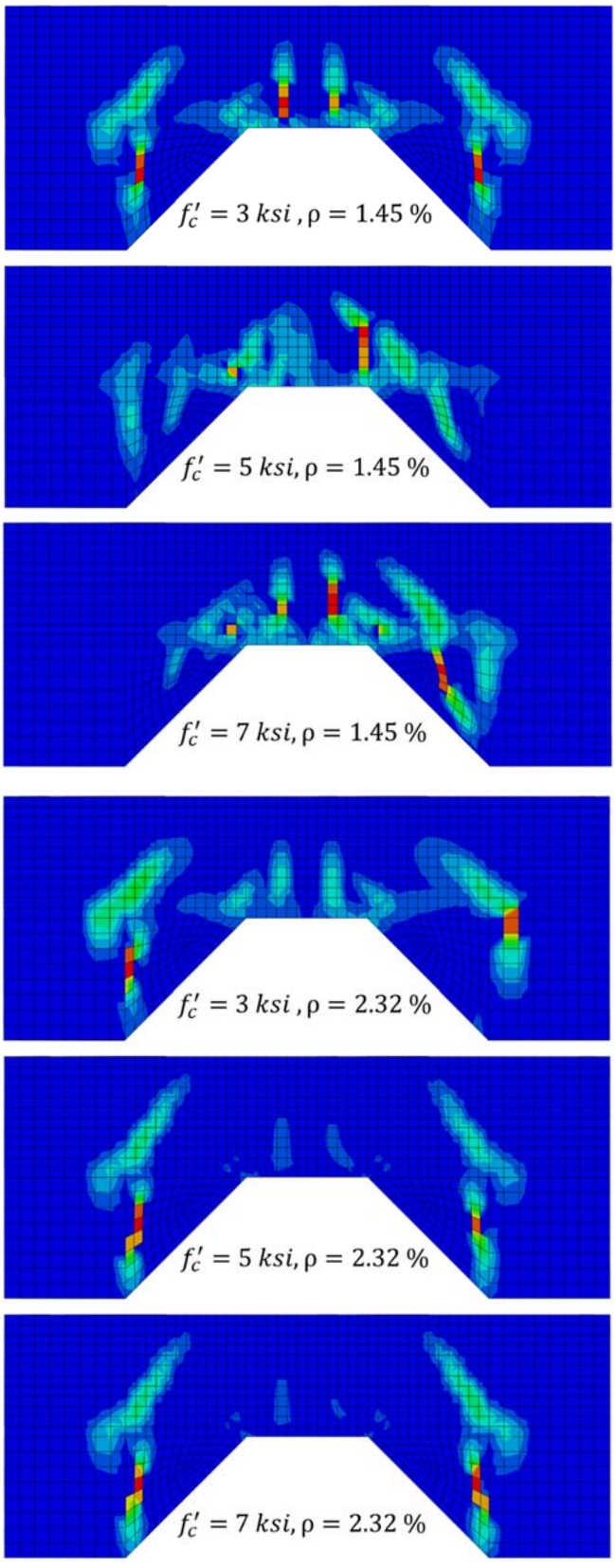

Box Culvert $12 \times 6 \times 12$

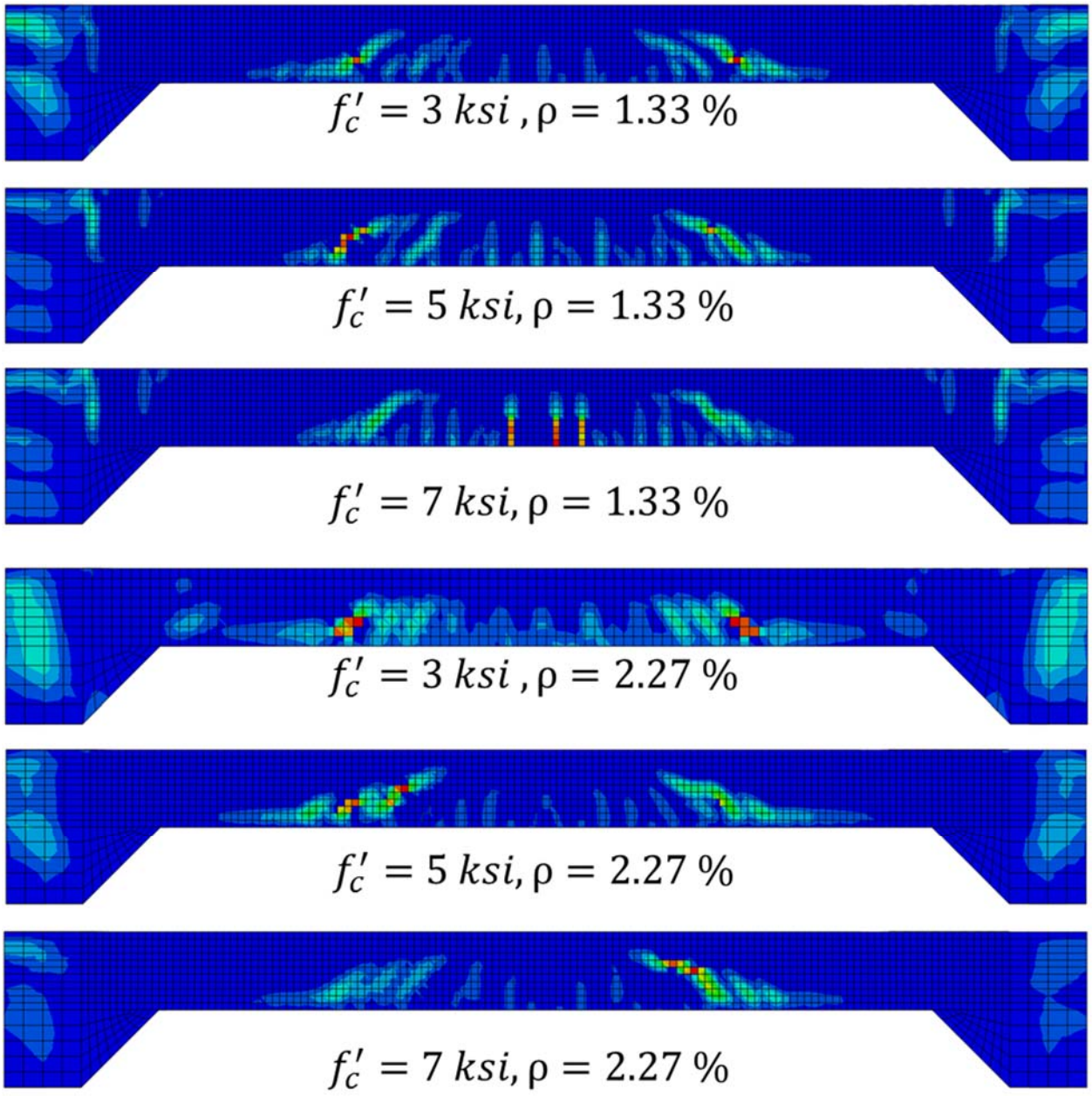

Box Culvert $12 \times 6 \times 16$

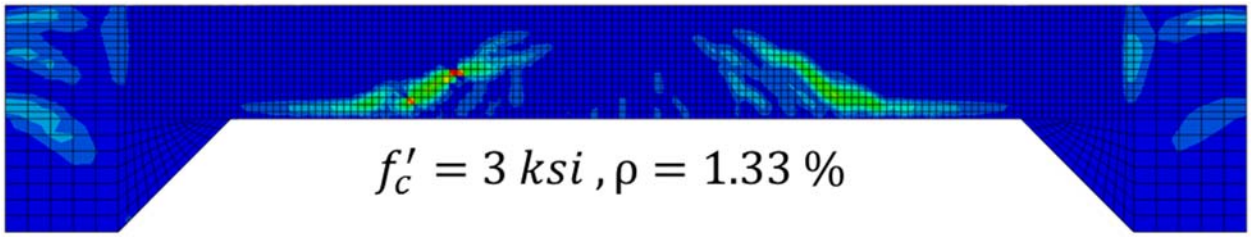

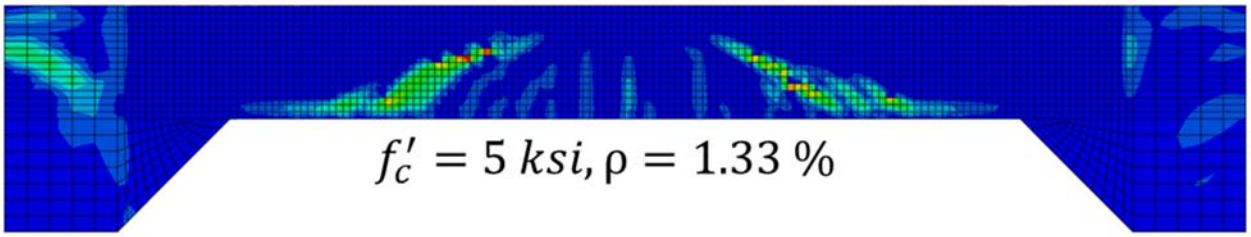

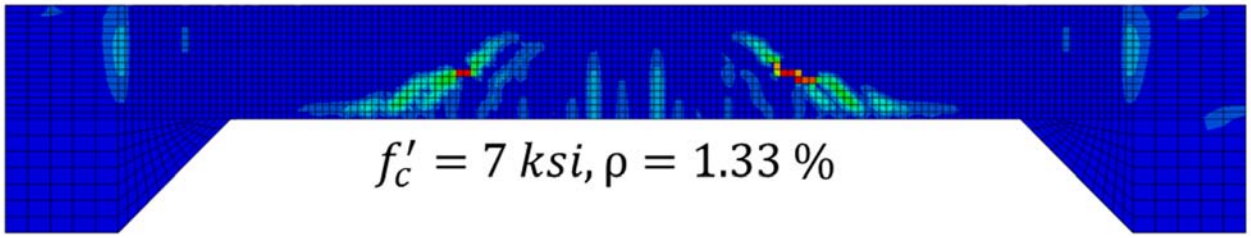

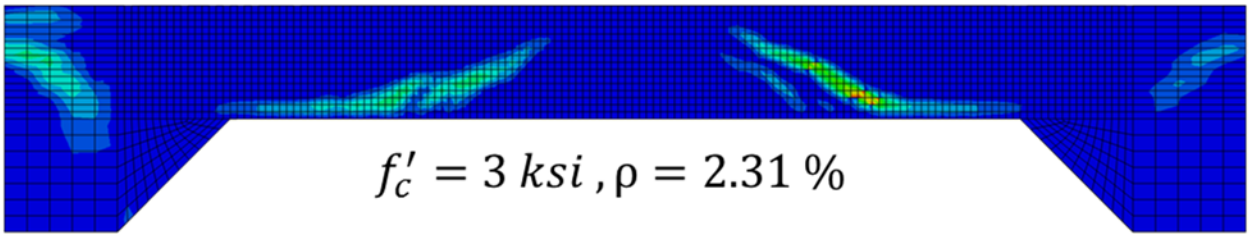

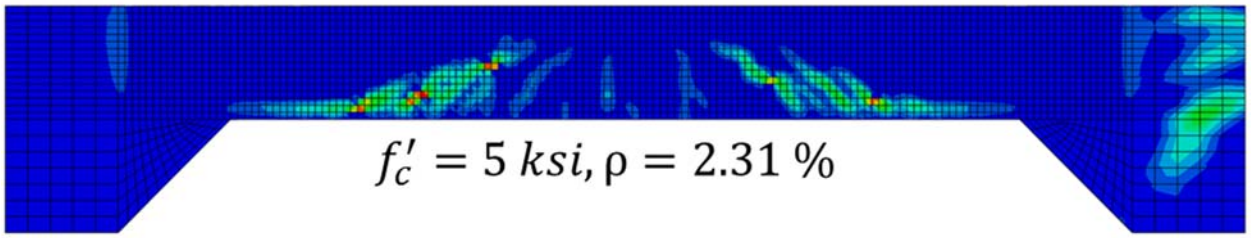

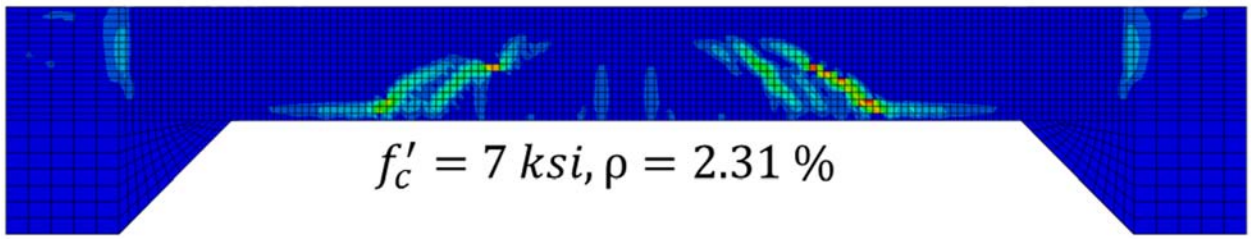

Box Culvert $12 \times 6 \times 20$

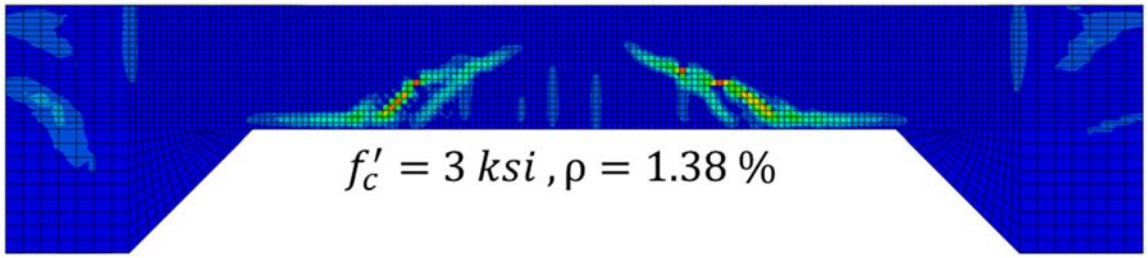

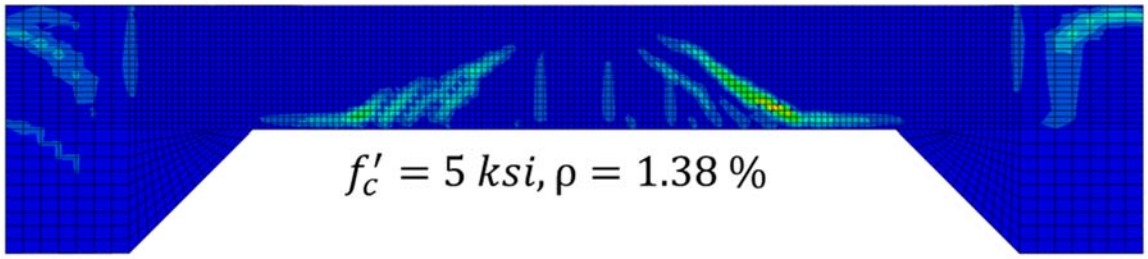

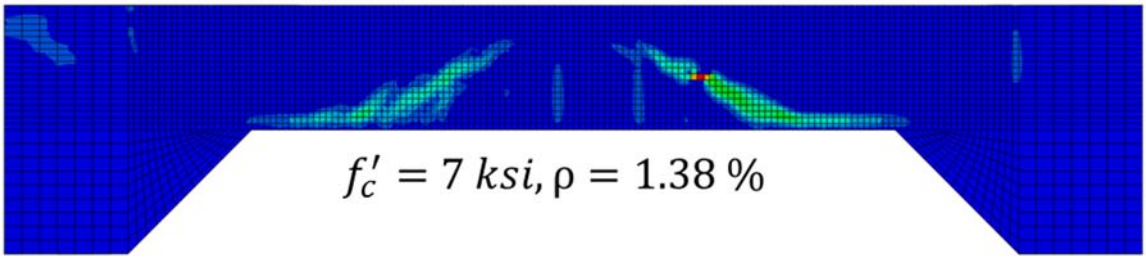

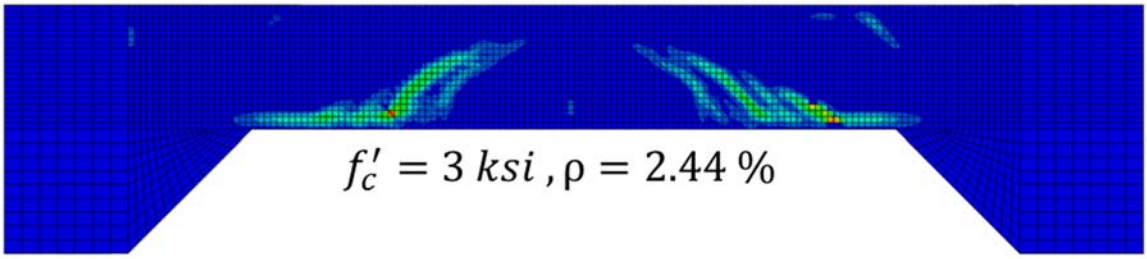

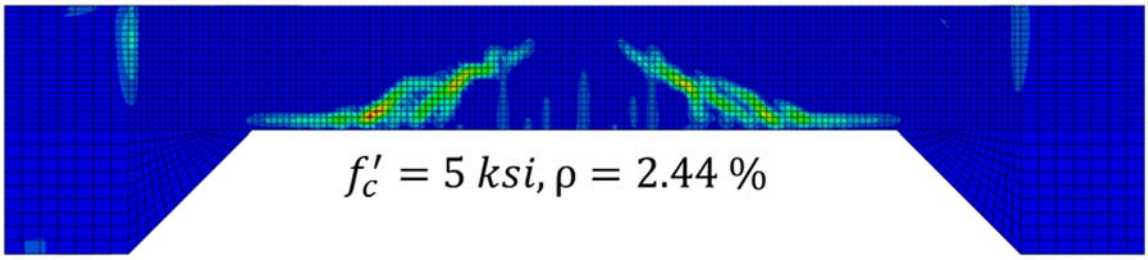

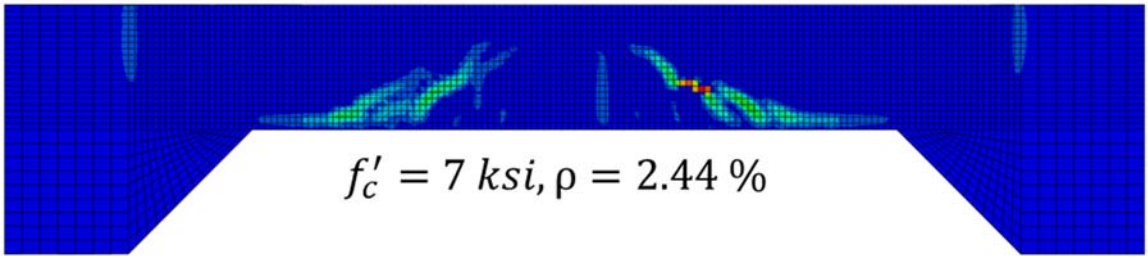

Box Culvert $12 \times 6 \times 24$

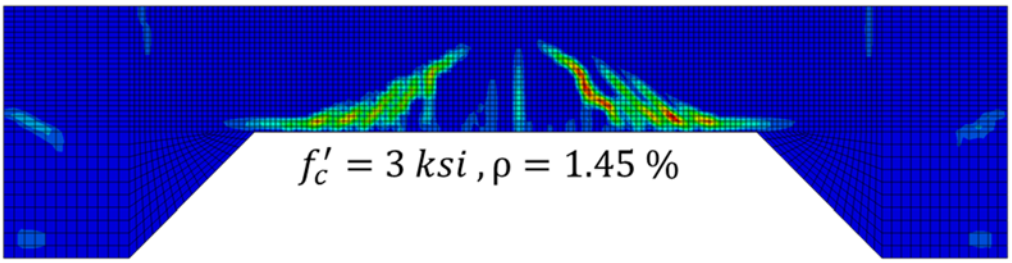

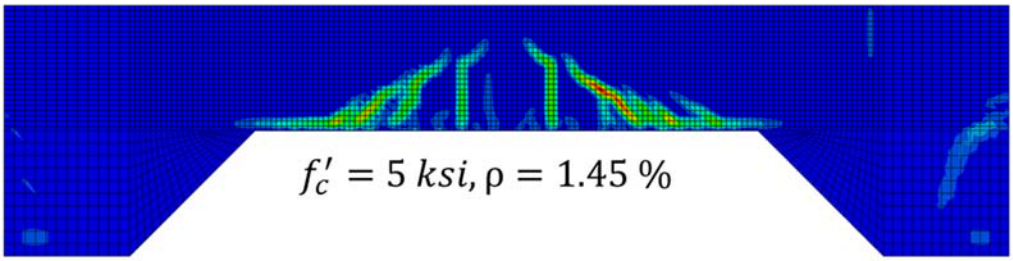

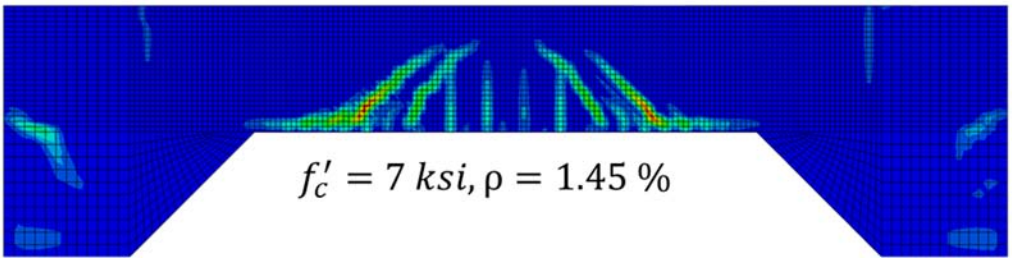

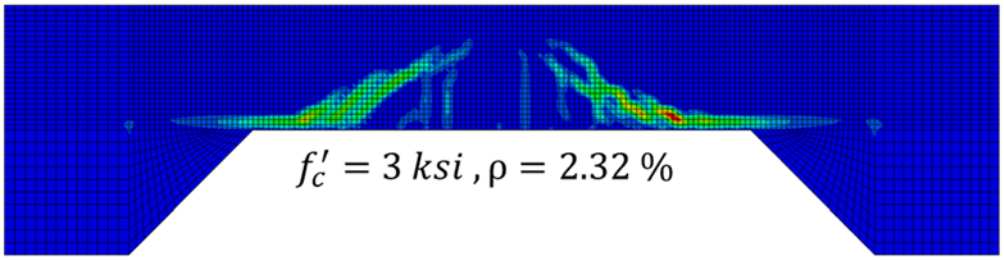

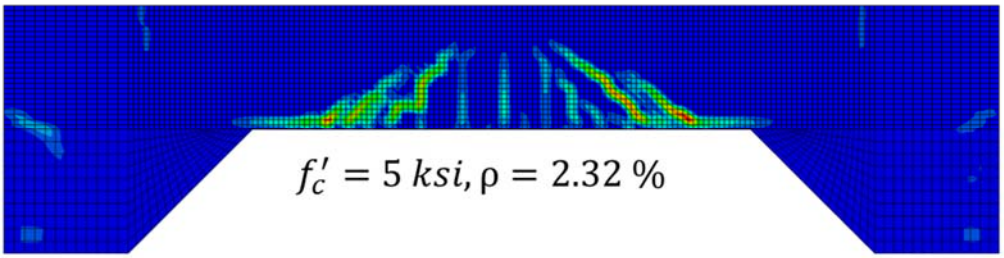

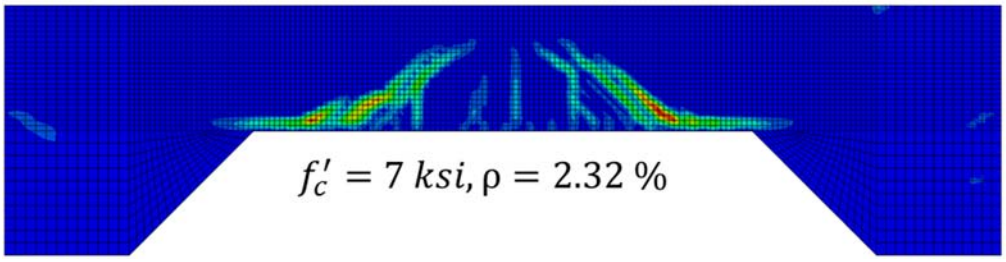

Box Culvert $12 \times 12 \times 12$

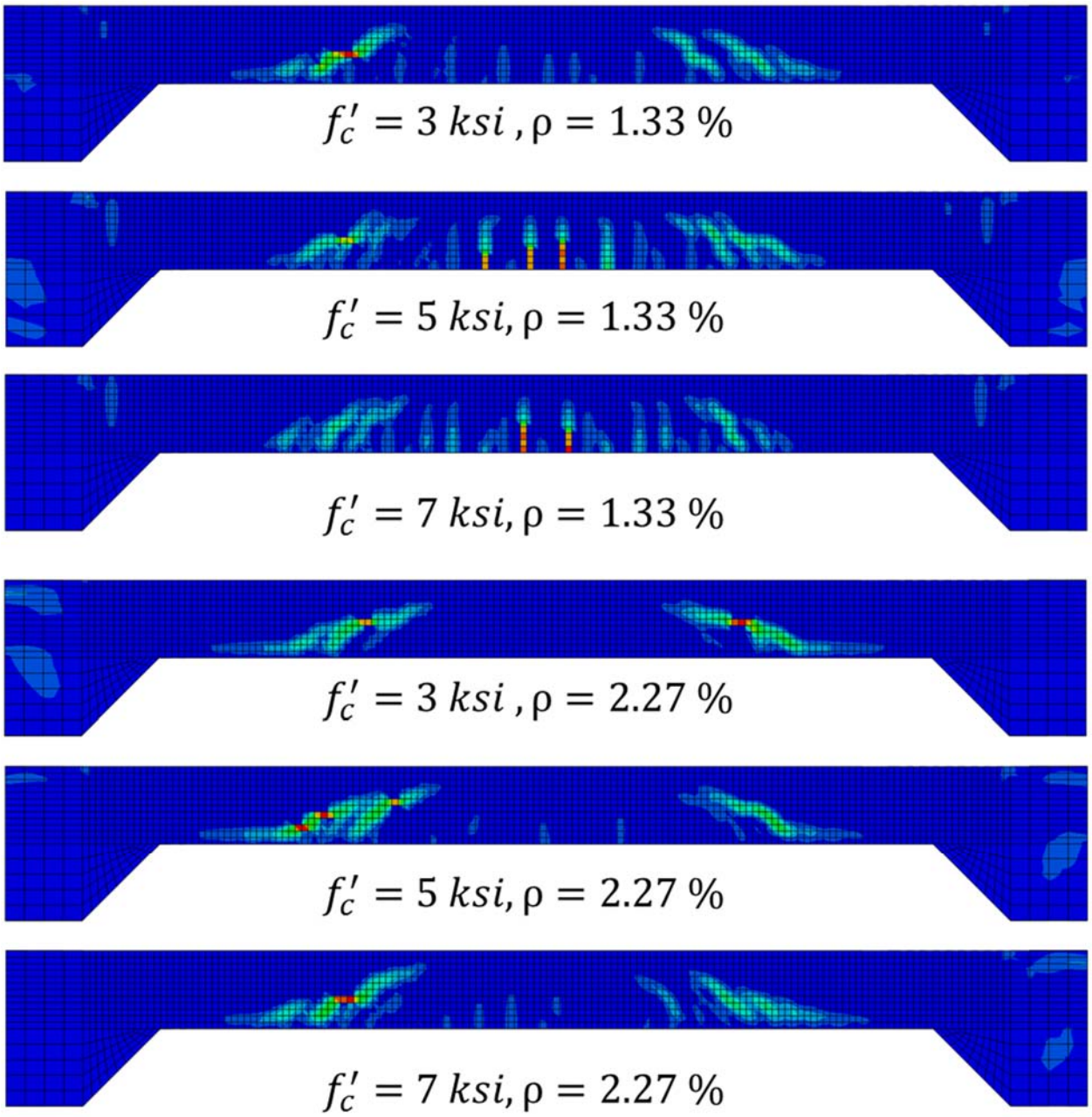

Box Culvert 12 × 12 × 16

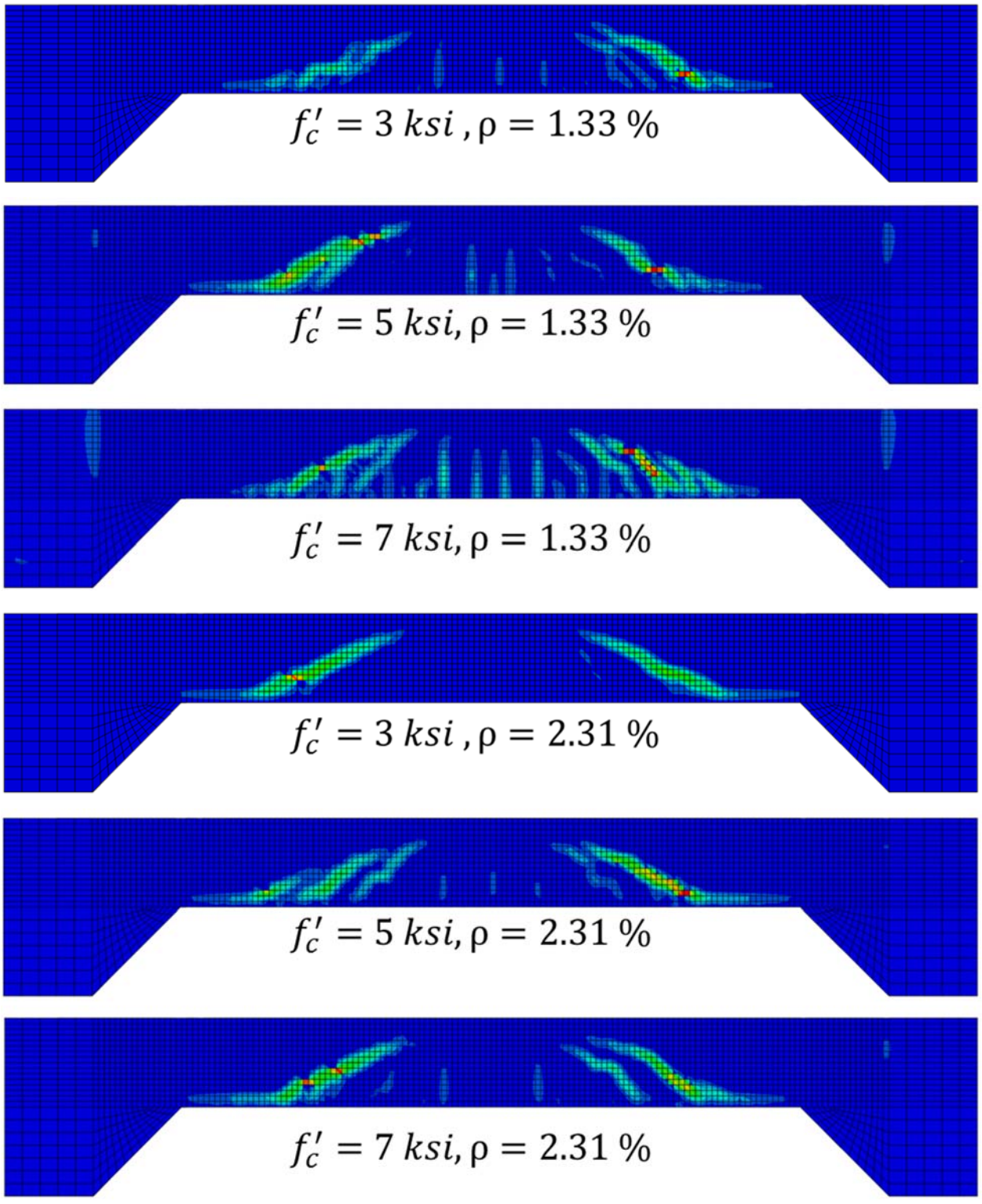

Box Culvert $12 \times 12 \times 20$

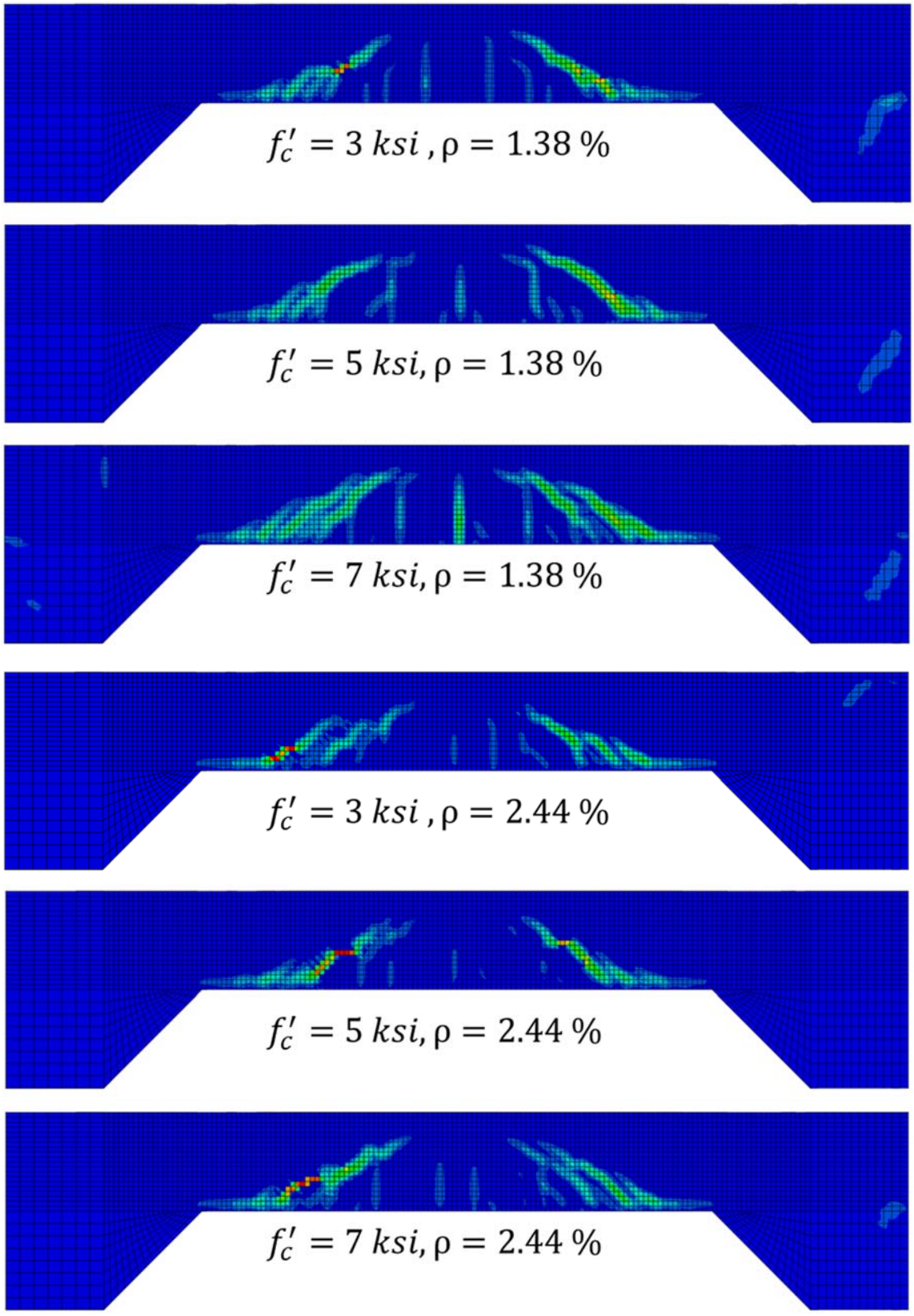

Box Culvert $12 \times 12 \times 24$

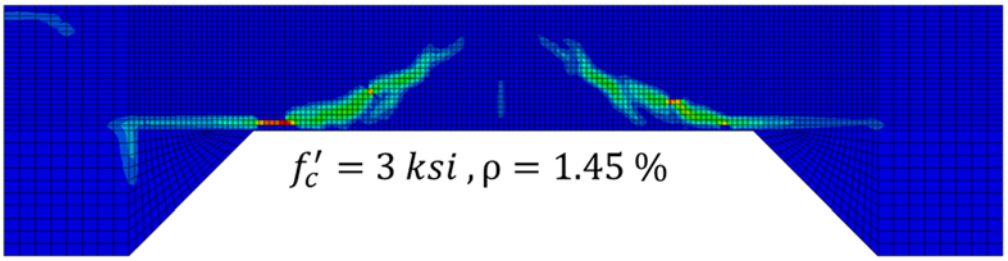

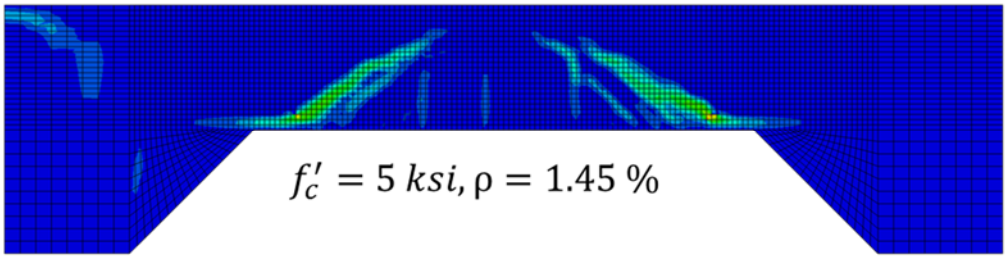

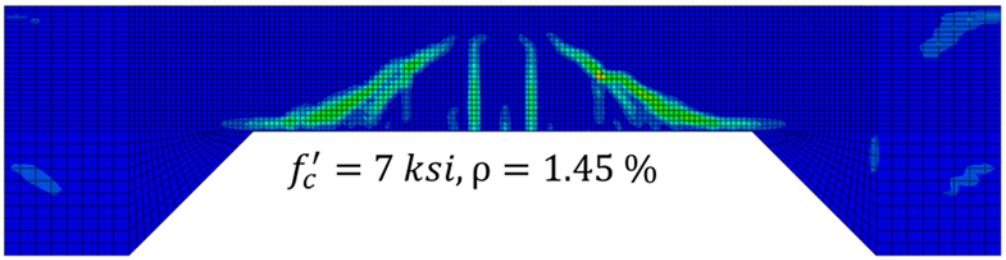

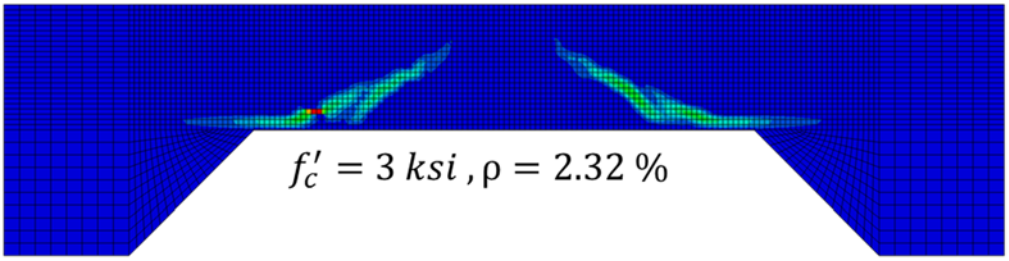

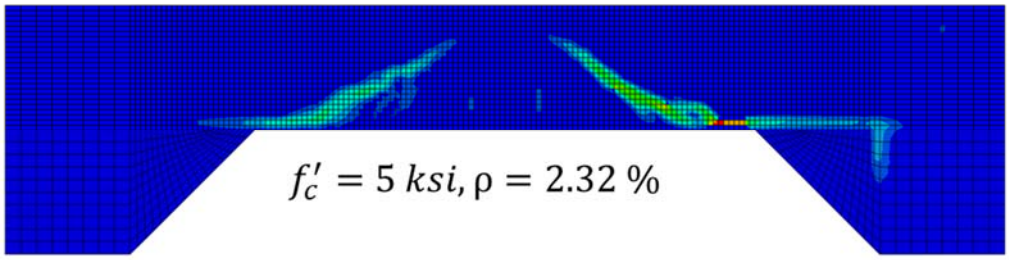

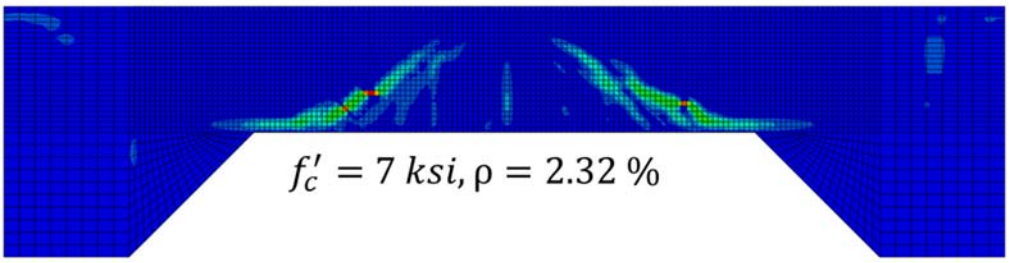

Box Culvert $12 \times 15 \times 12$

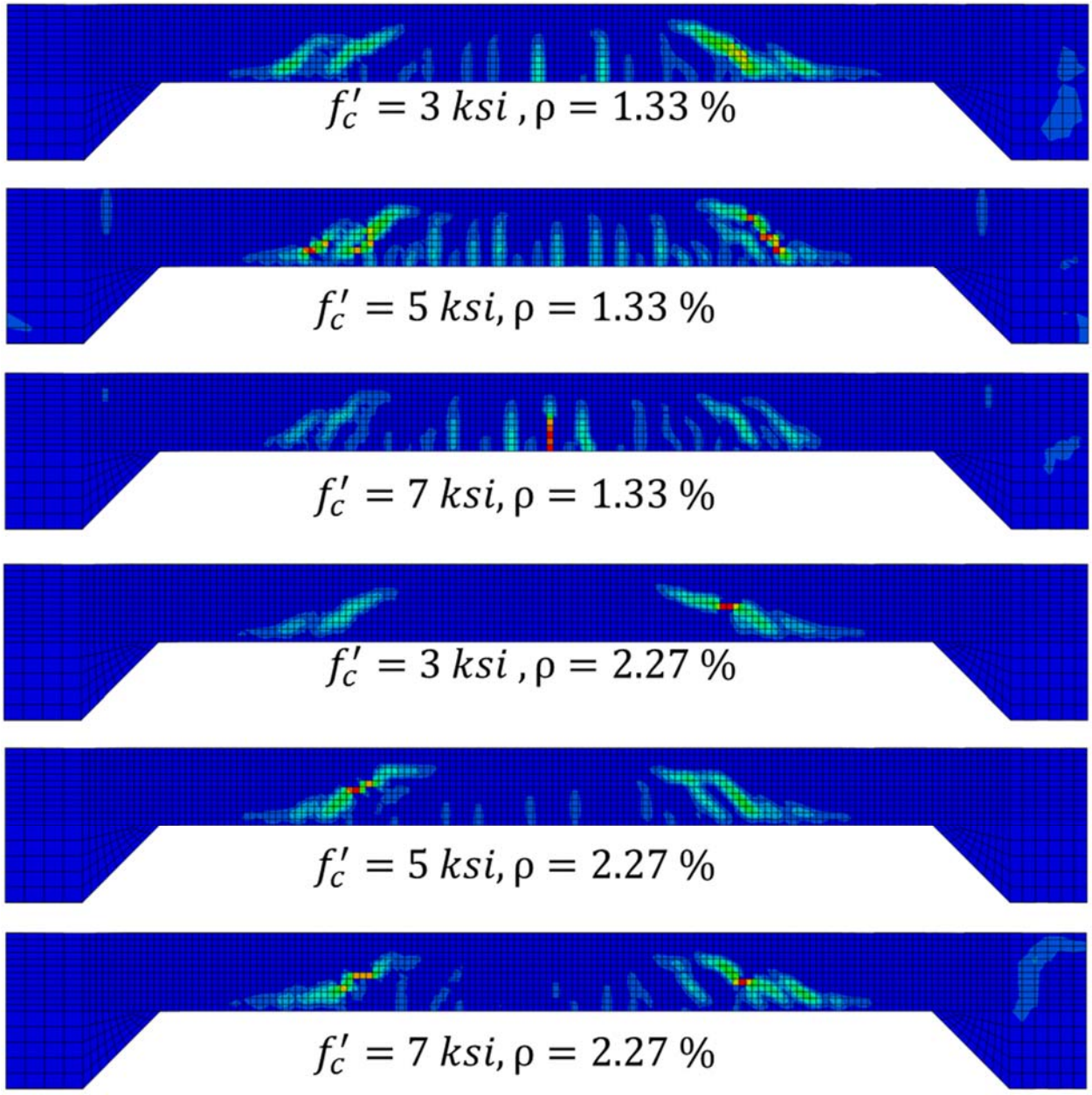

Box Culvert 12 × 15 × 16

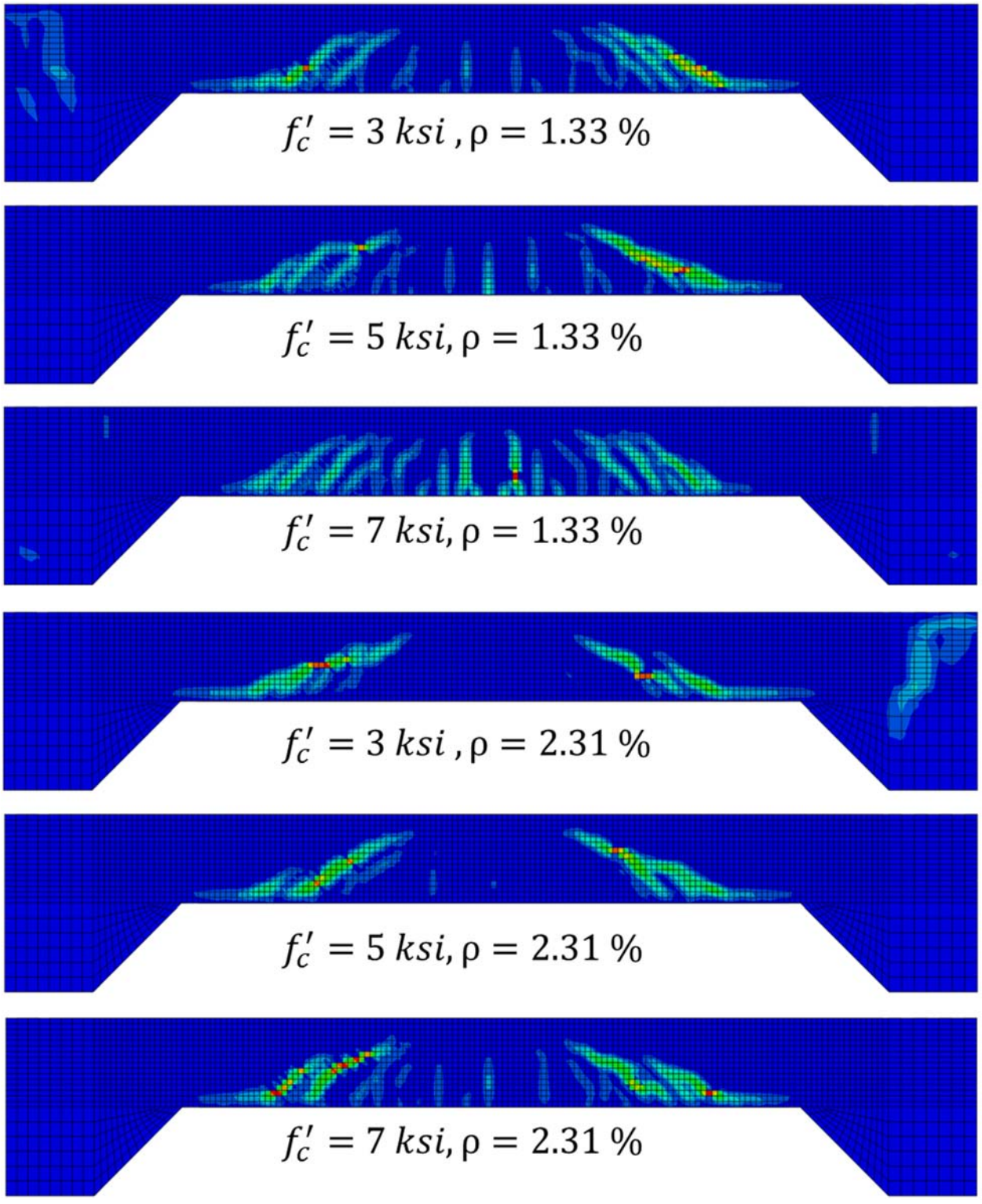

Box Culvert $12 \times 15 \times 20$

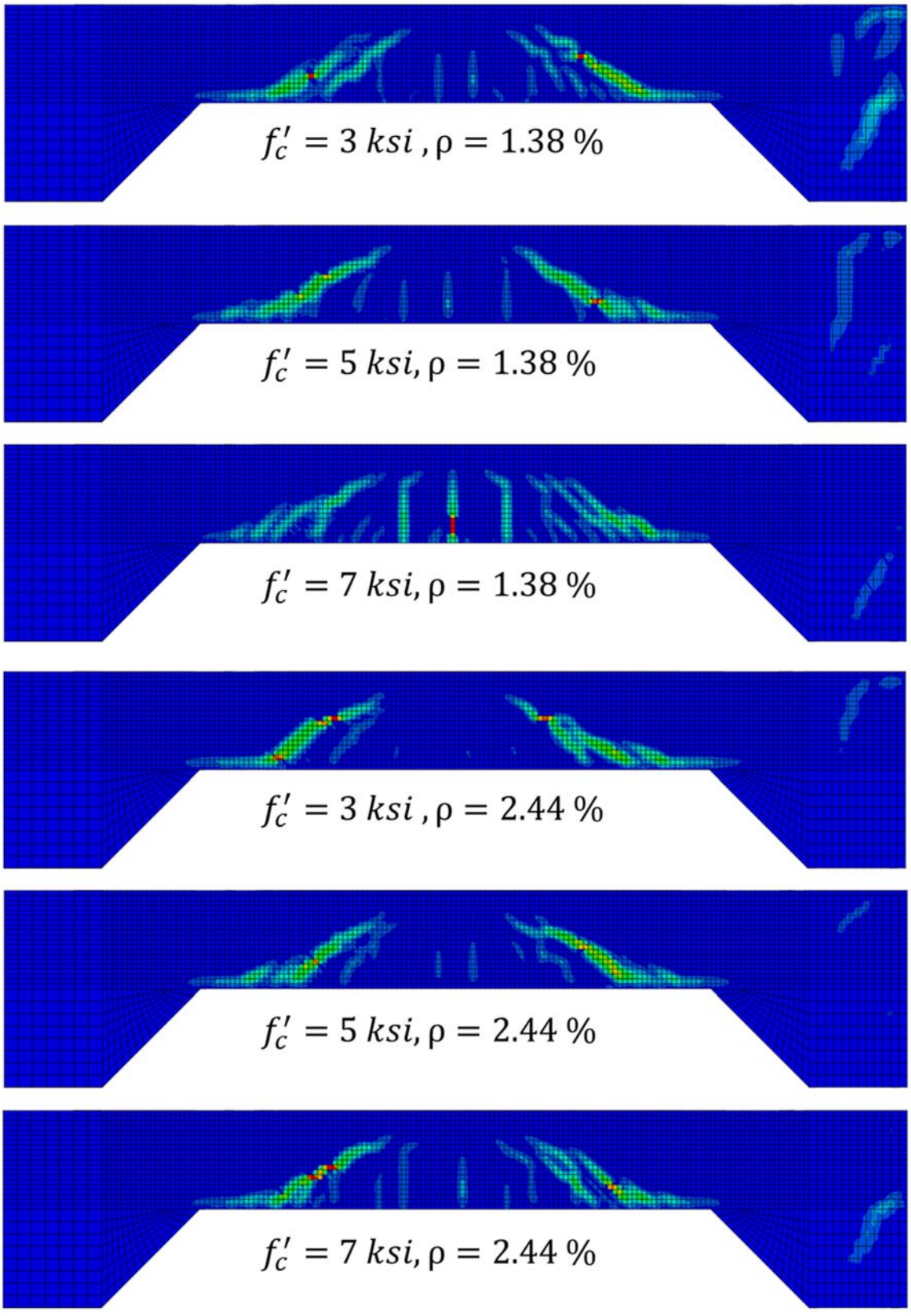

Box Culvert $12 \times 15 \times 24$

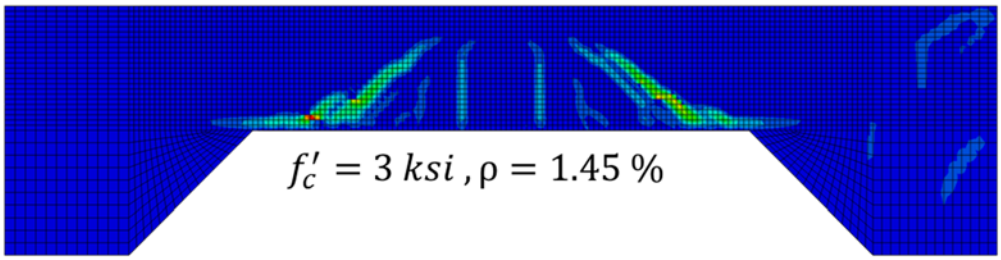

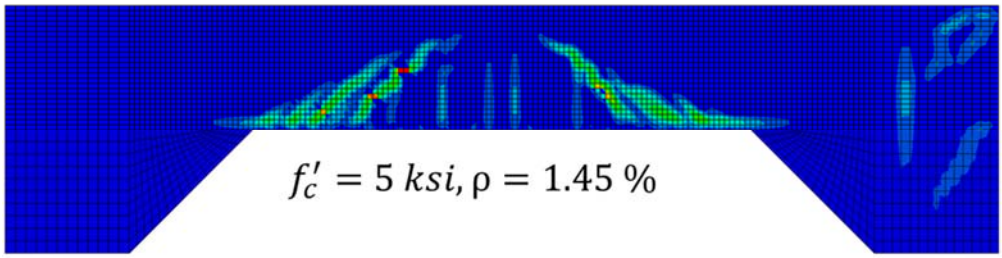

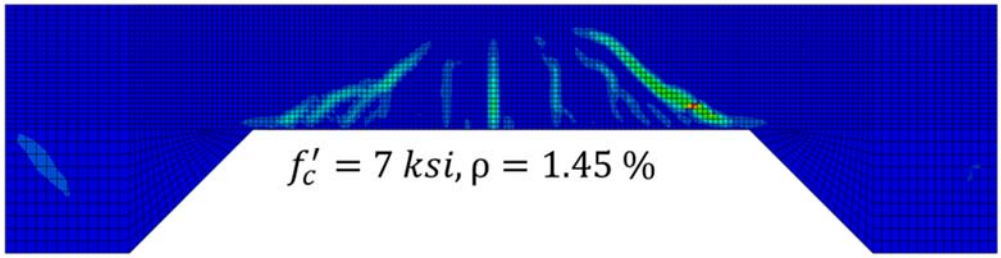

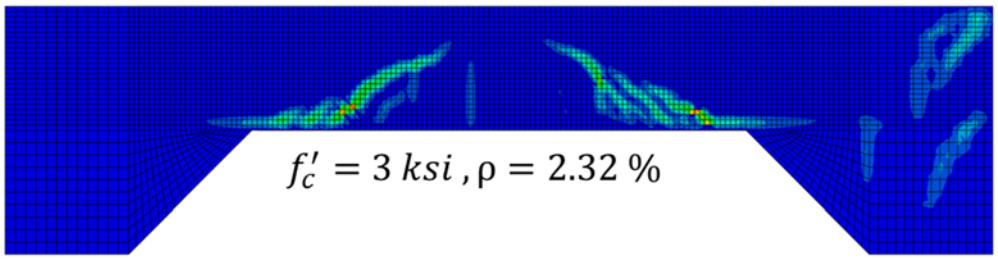

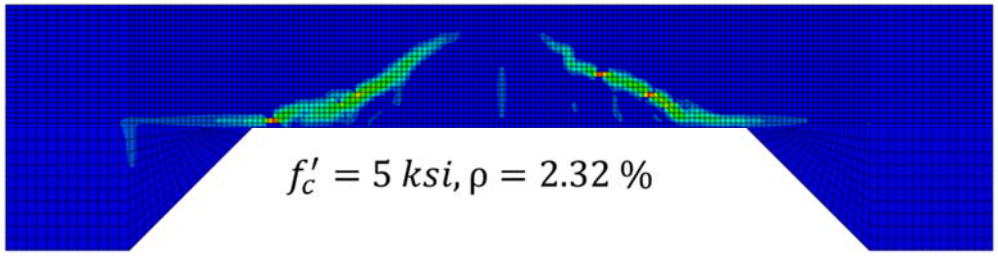

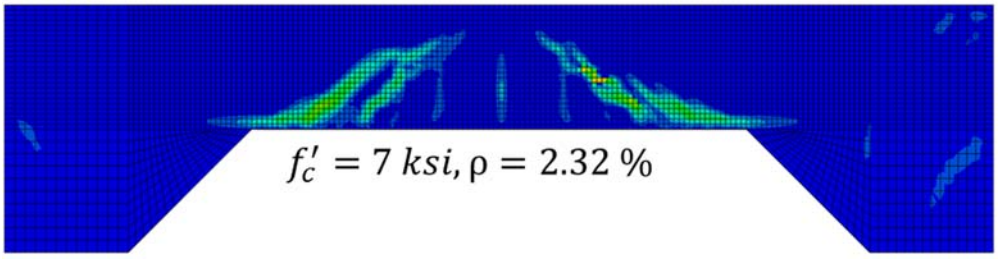

Box Culvert $18 \times 6 \times 12$

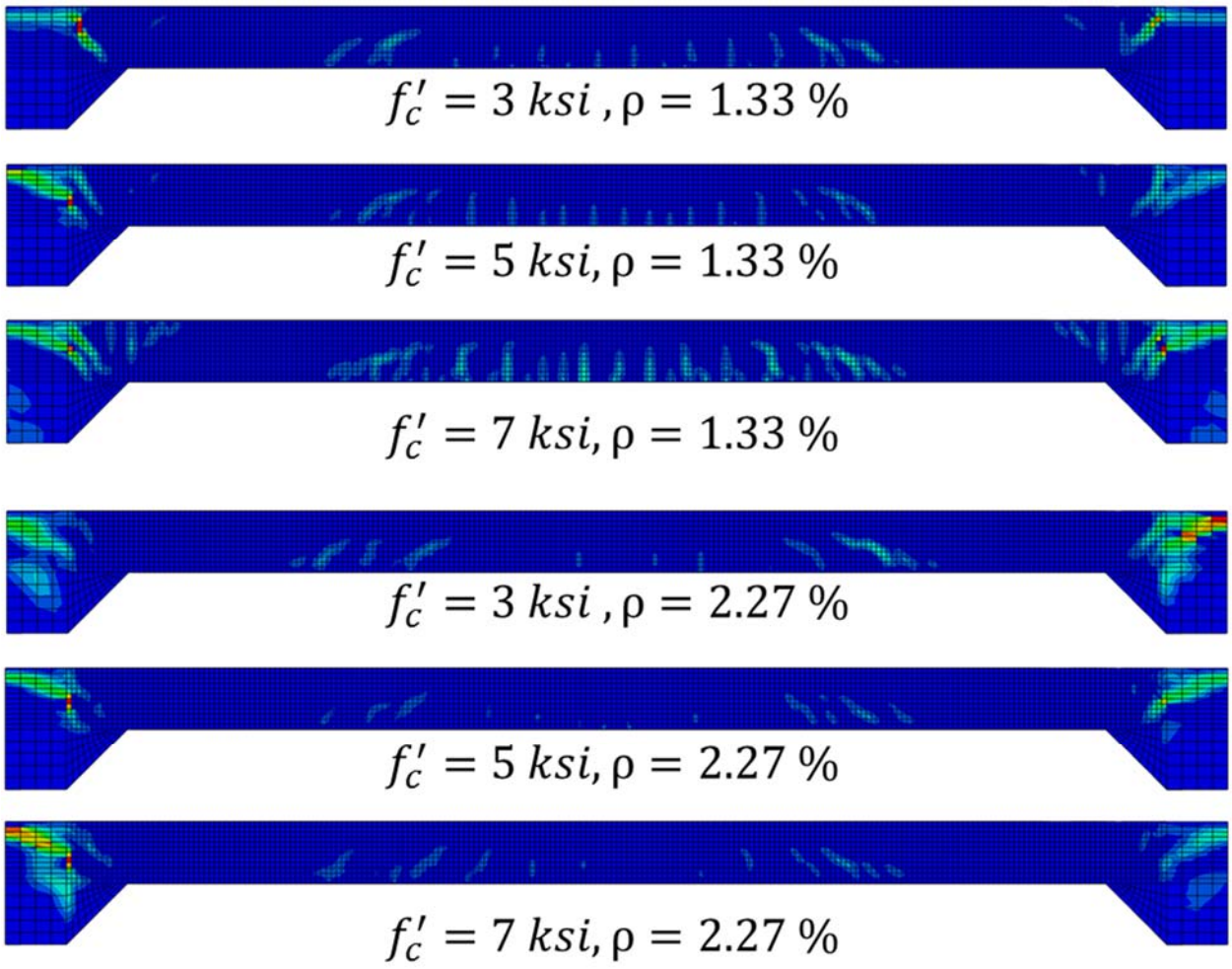

Box Culvert $18 \times 6 \times 16$

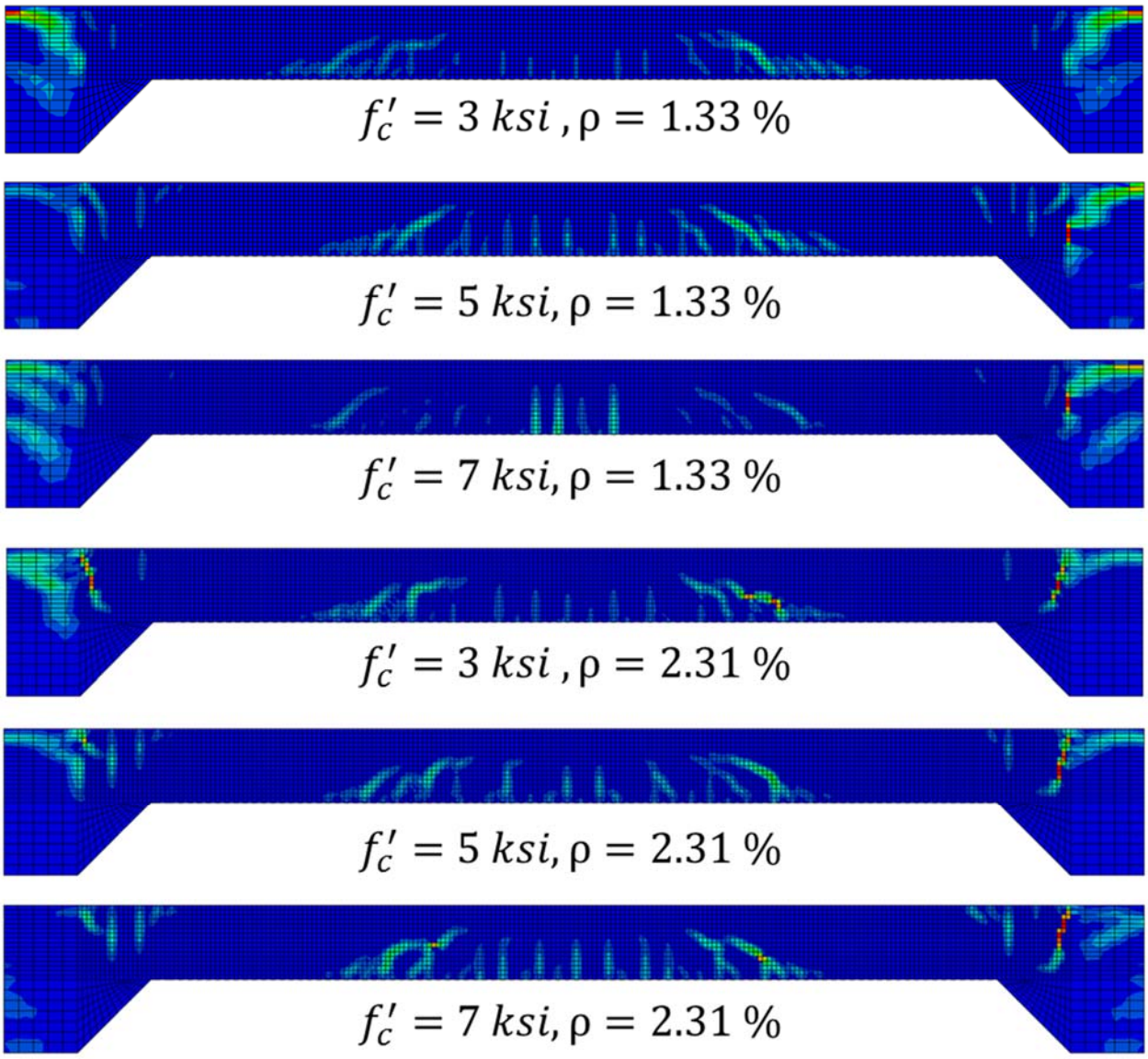

Box Culvert $18 \times 6 \times 20$

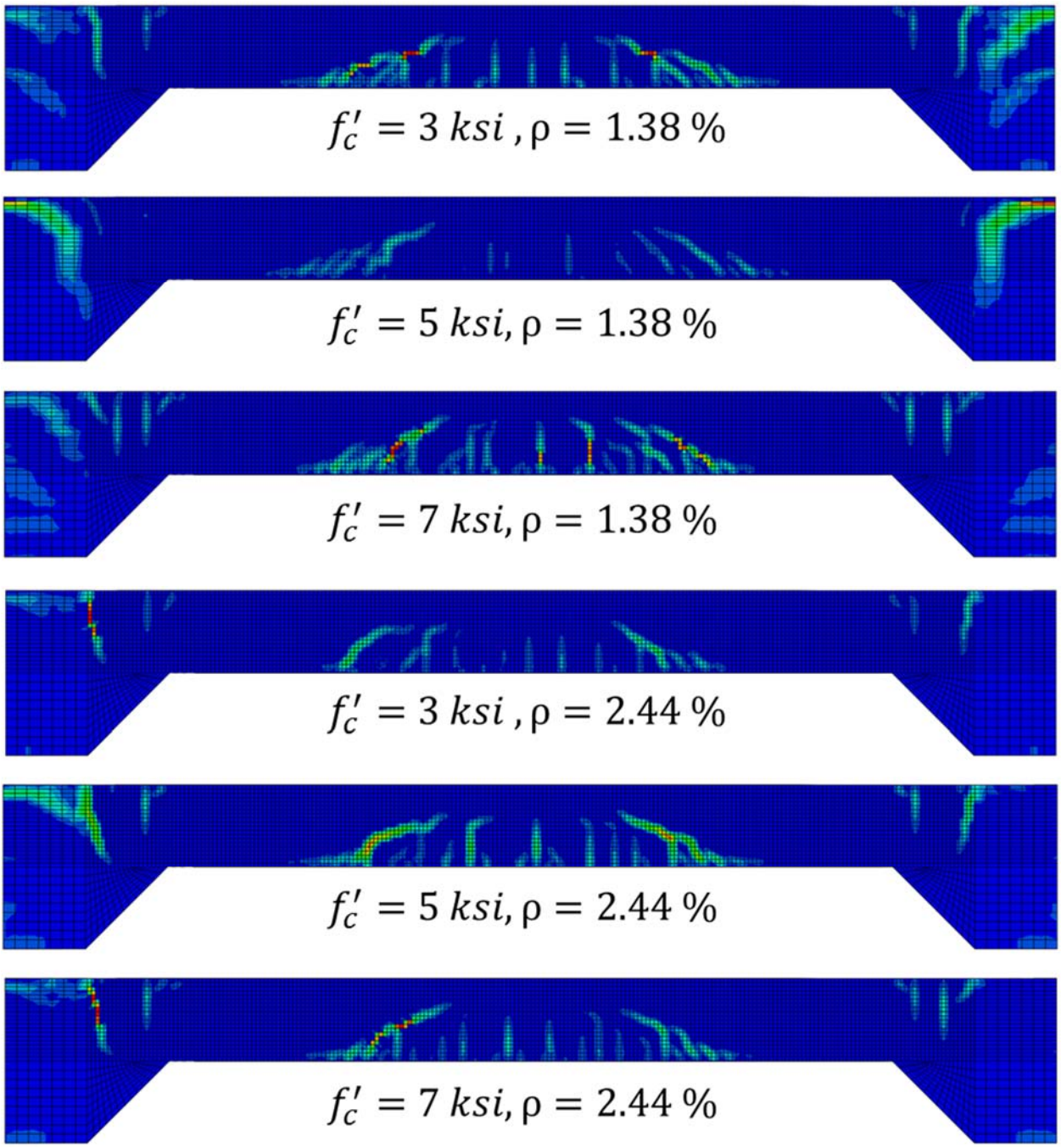

Box Culvert $18 \times 6 \times 24$

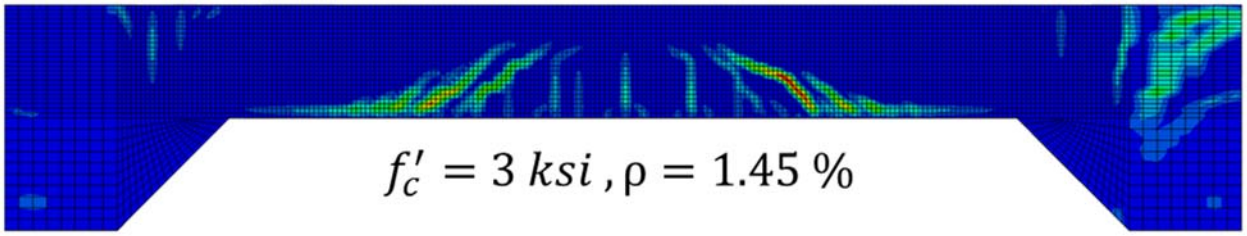

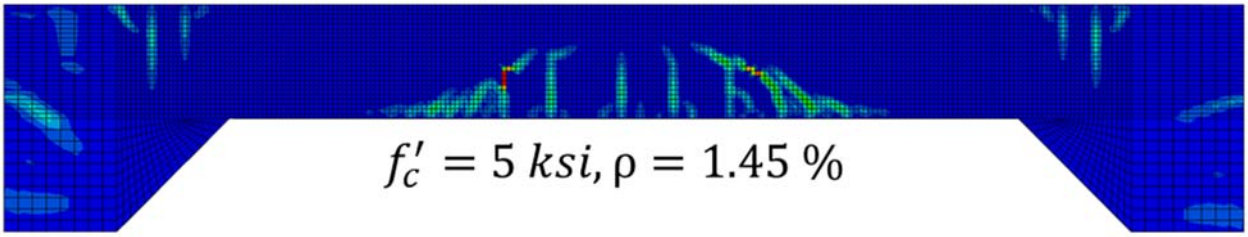

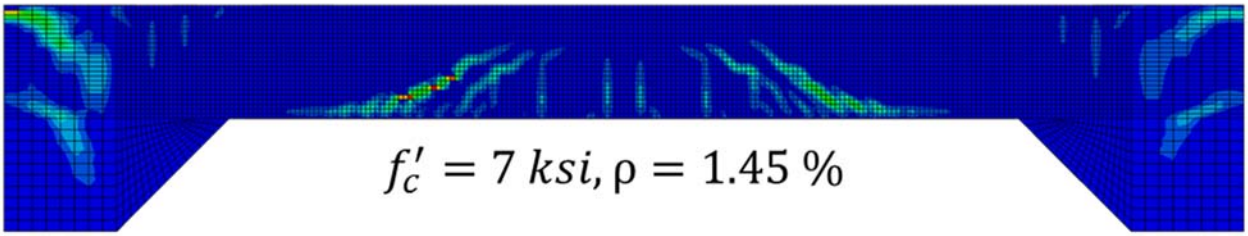

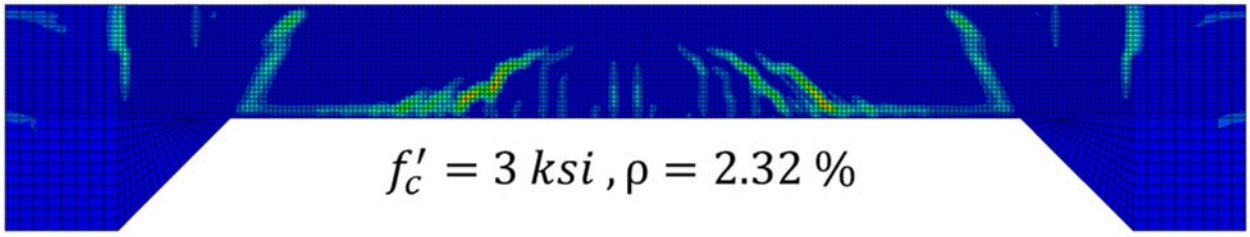

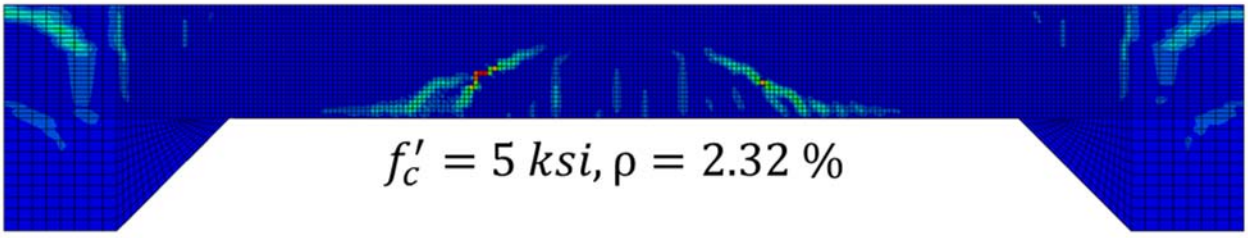

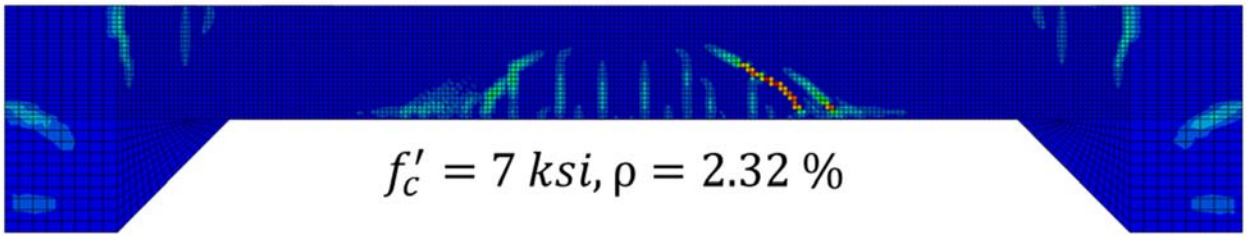

Box Culvert 18 × 12 × 12

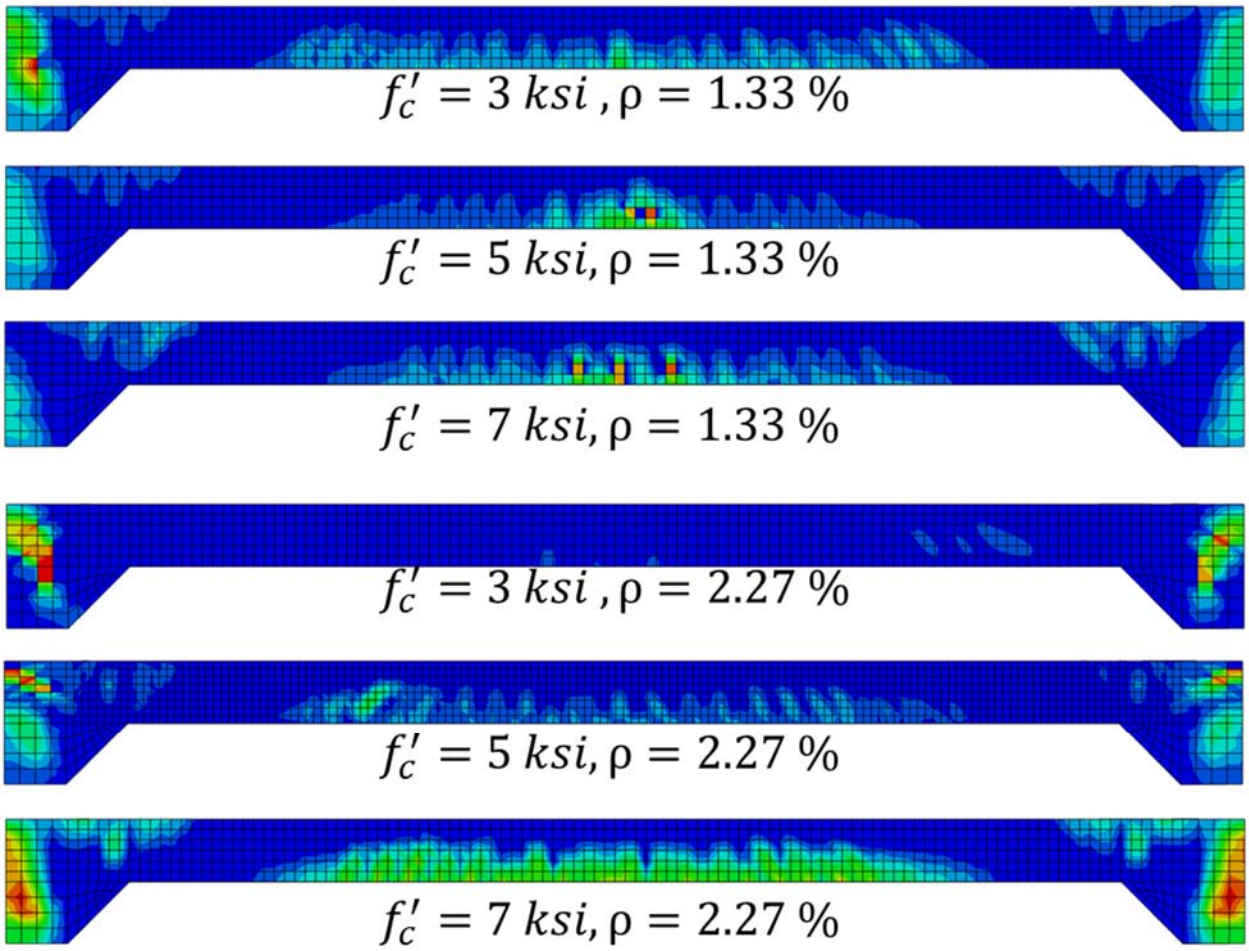

Box Culvert $18 \times 12 \times 16$

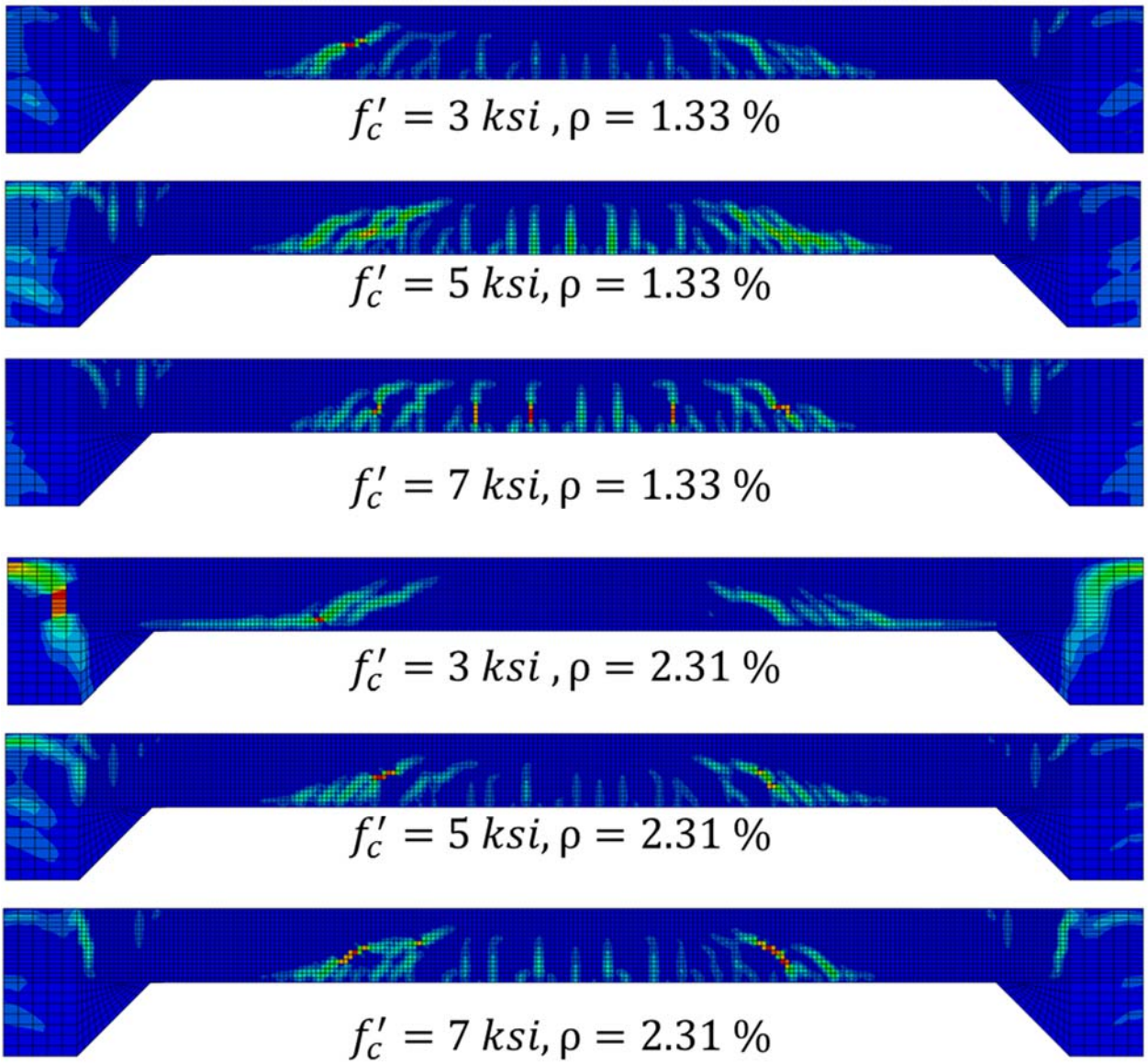

Box Culvert $18 \times 12 \times 20$

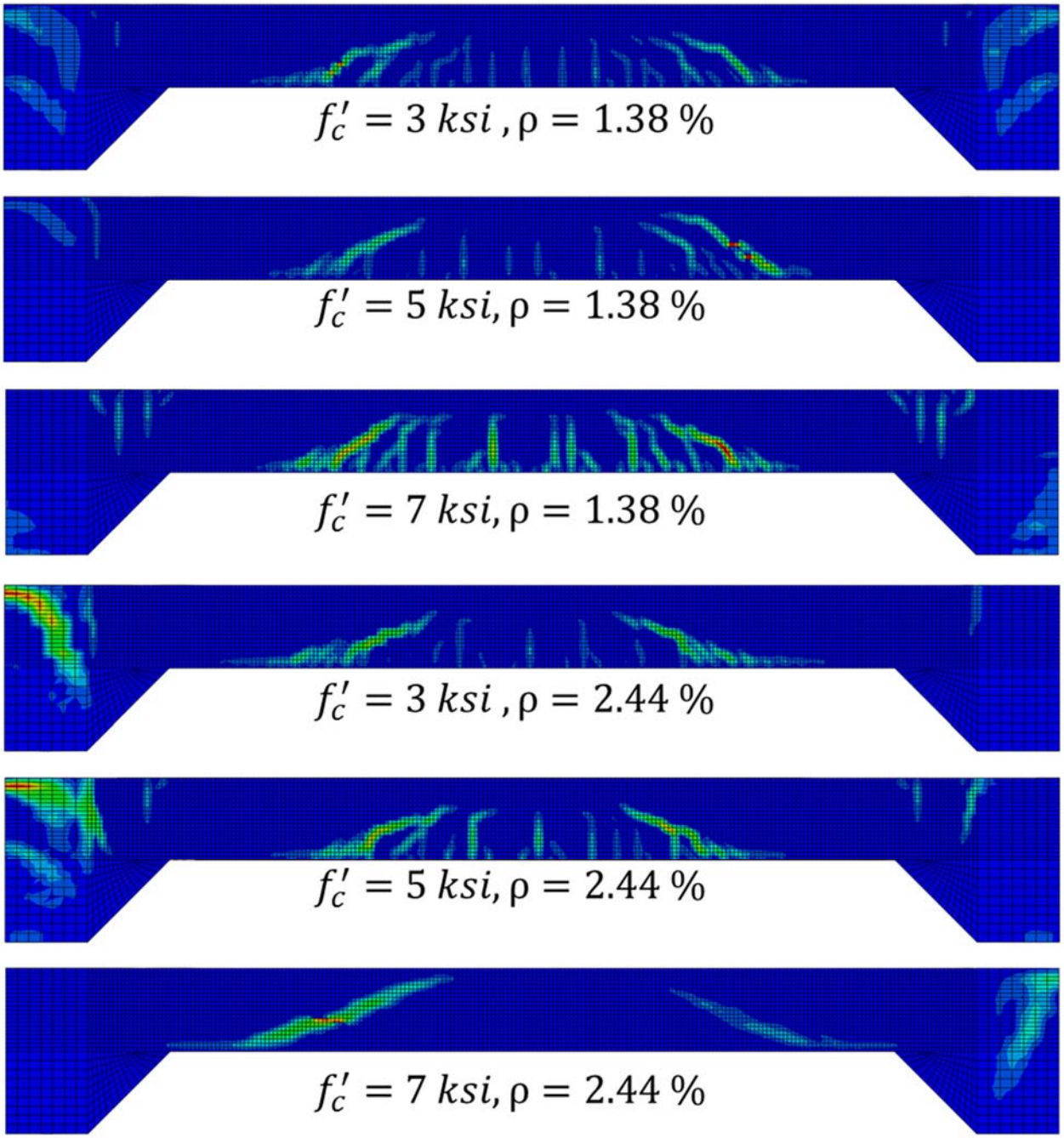

Box Culvert $18 \times 12 \times 24$

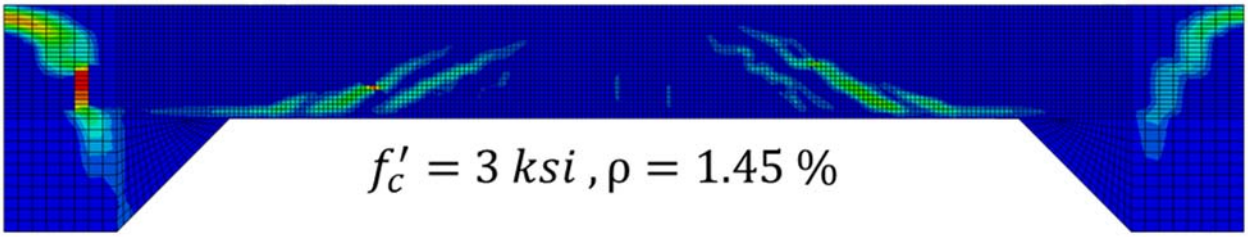

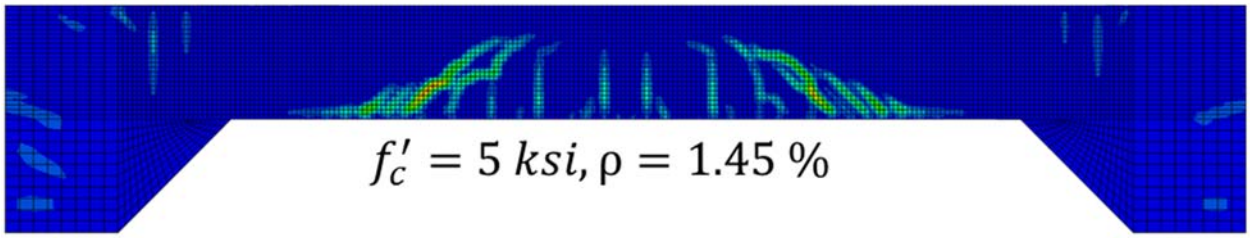

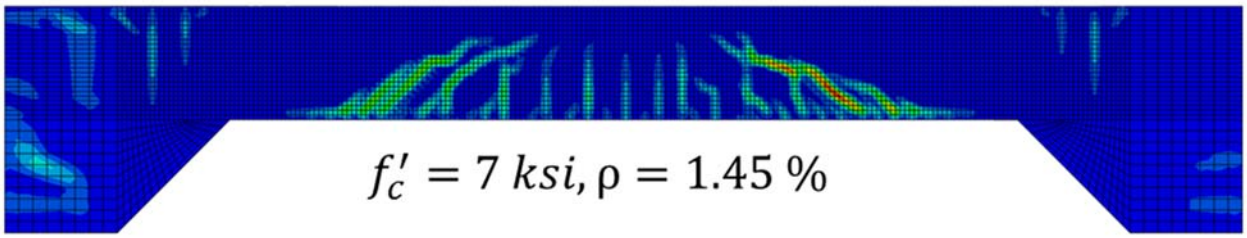

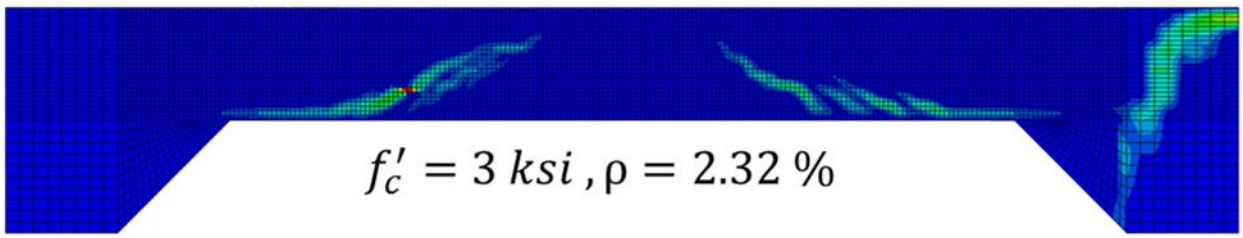

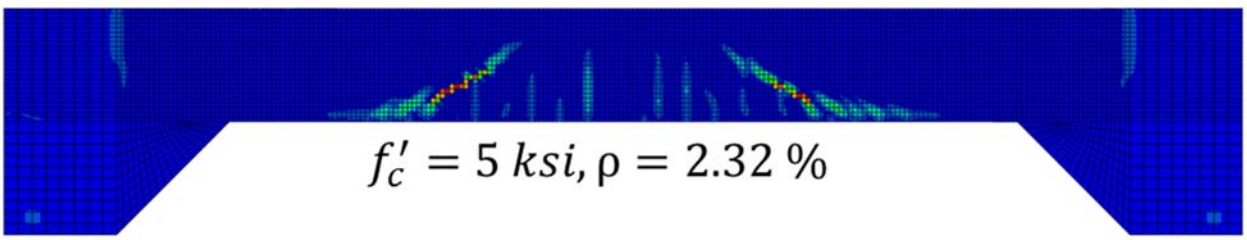

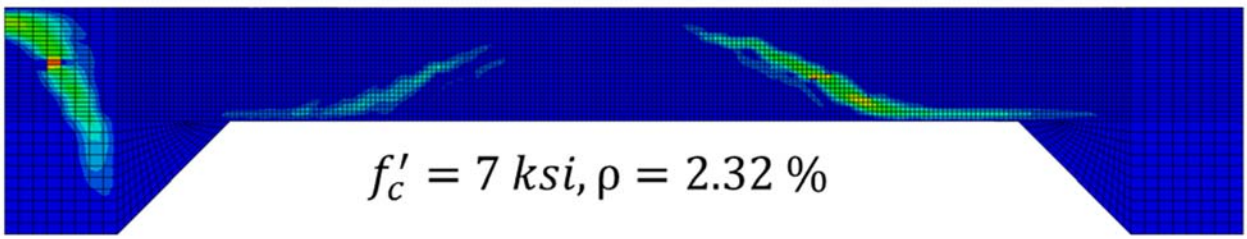

Box Culvert $18 \times 15 \times 12$

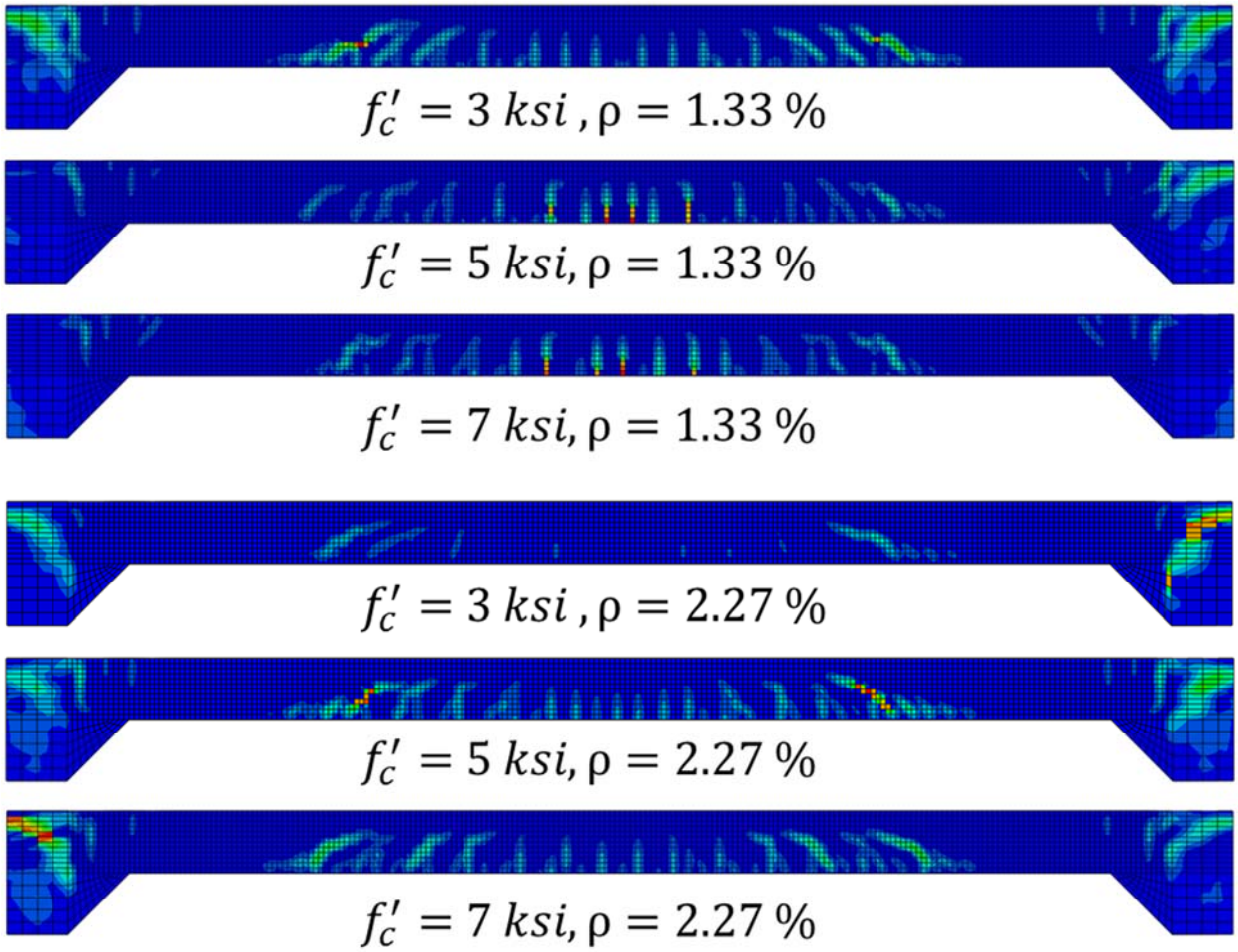

Box Culvert $18 \times 15 \times 16$

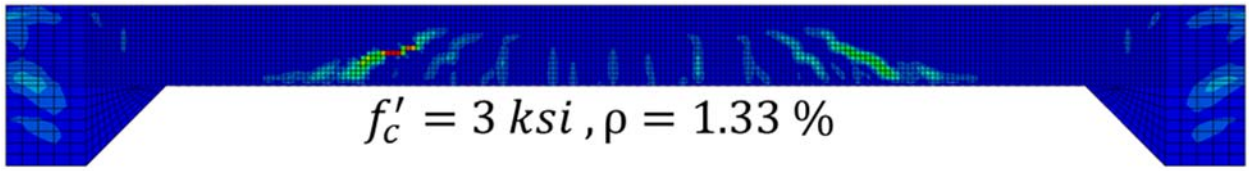

$f_c' = 3\ ksi\ , \rho = 1.33\ \%$

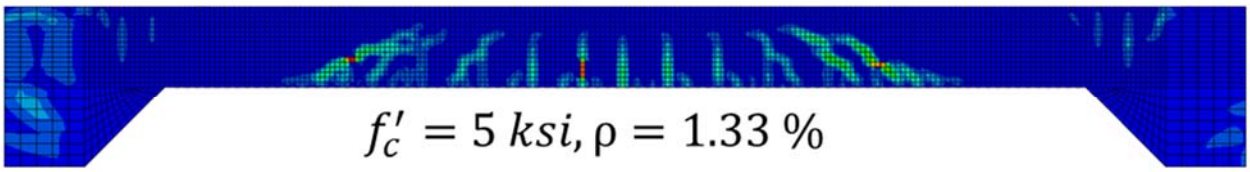

$f_c' = 5\ ksi, \rho = 1.33\ \%$

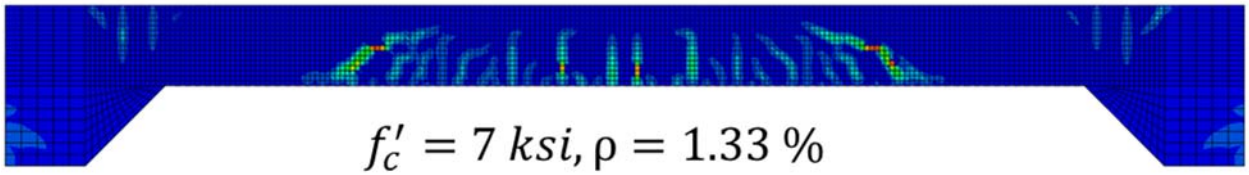

$f_c' = 7\ ksi, \rho = 1.33\ \%$

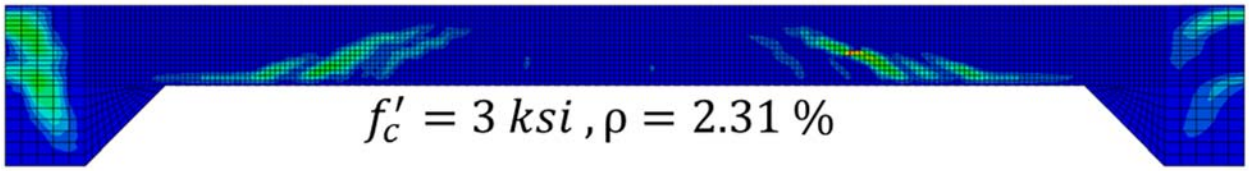

$f_c' = 3\ ksi\ , \rho = 2.31\ \%$

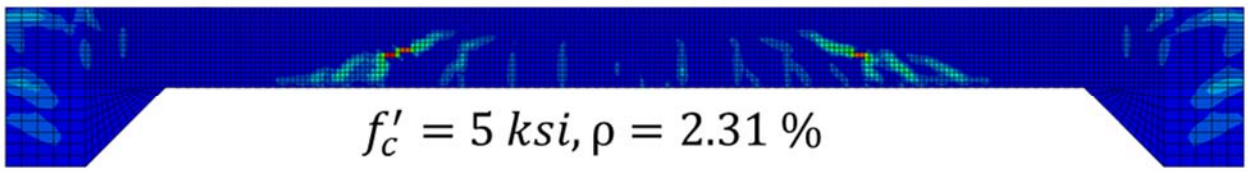

$f_c' = 5\ ksi, \rho = 2.31\ \%$

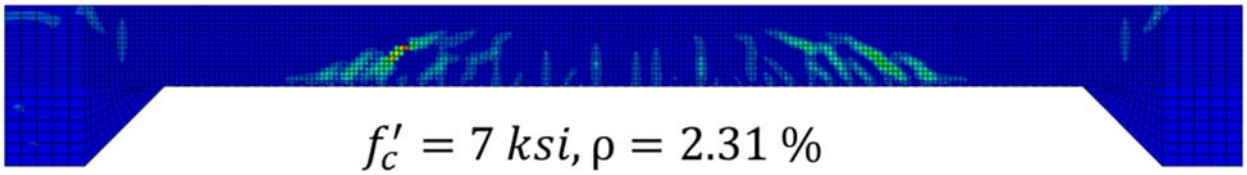

$f_c' = 7\ ksi, \rho = 2.31\ \%$

Box Culvert $18 \times 15 \times 20$

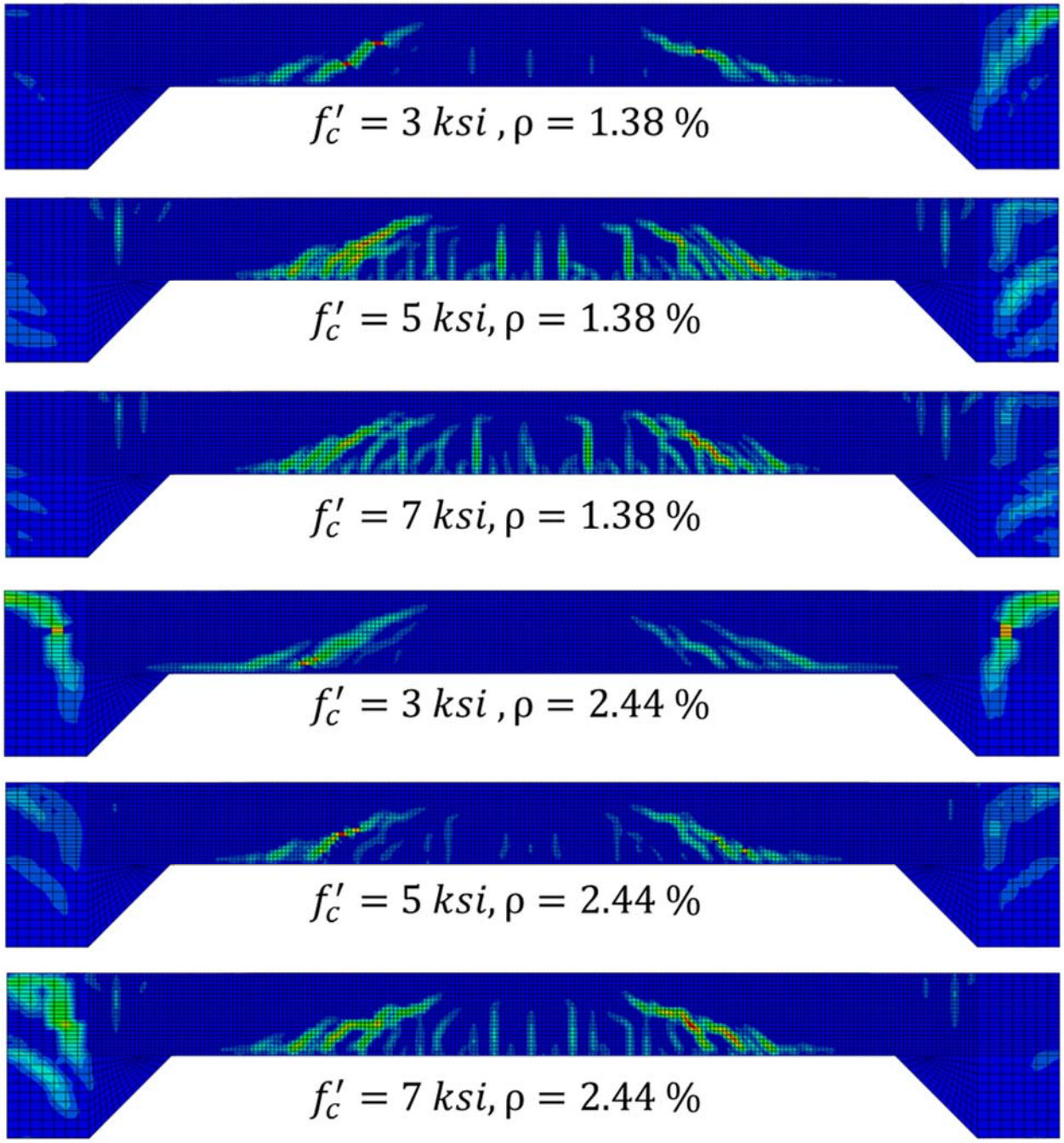

Box Culvert $18 \times 15 \times 24$

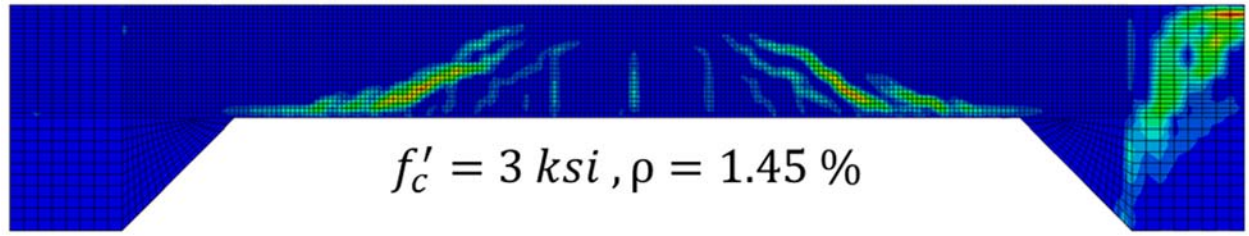

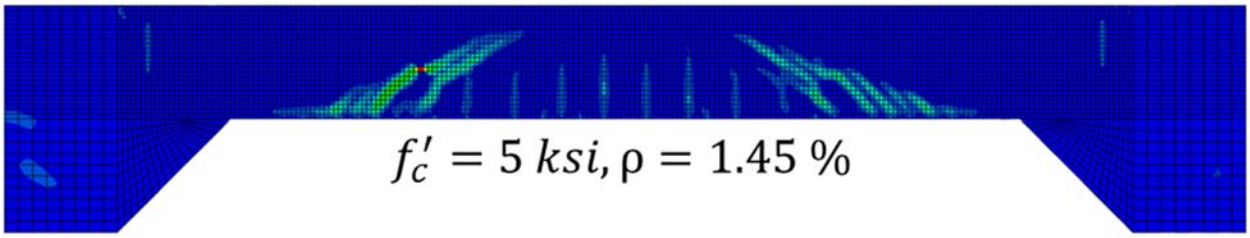

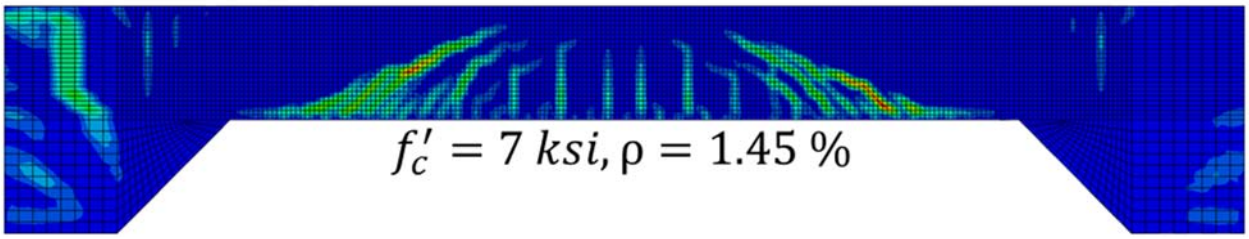

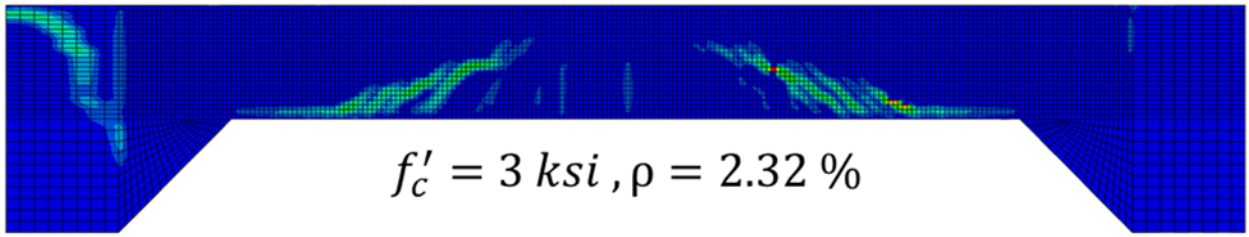

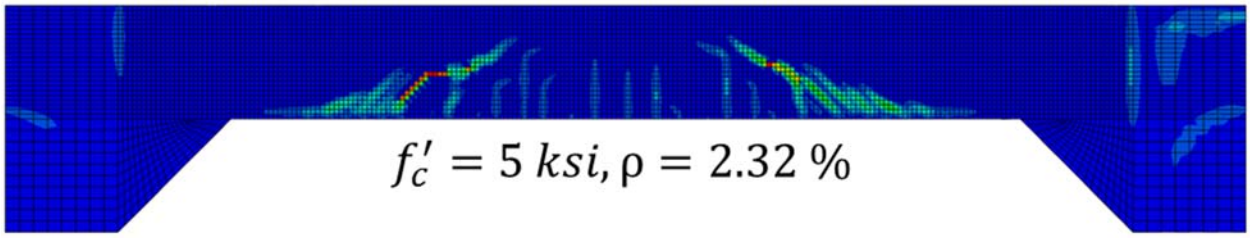

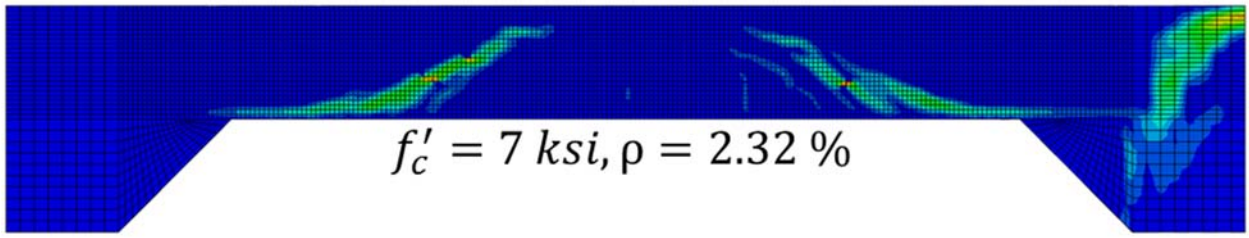

Box Culvert $24 \times 6 \times 12$

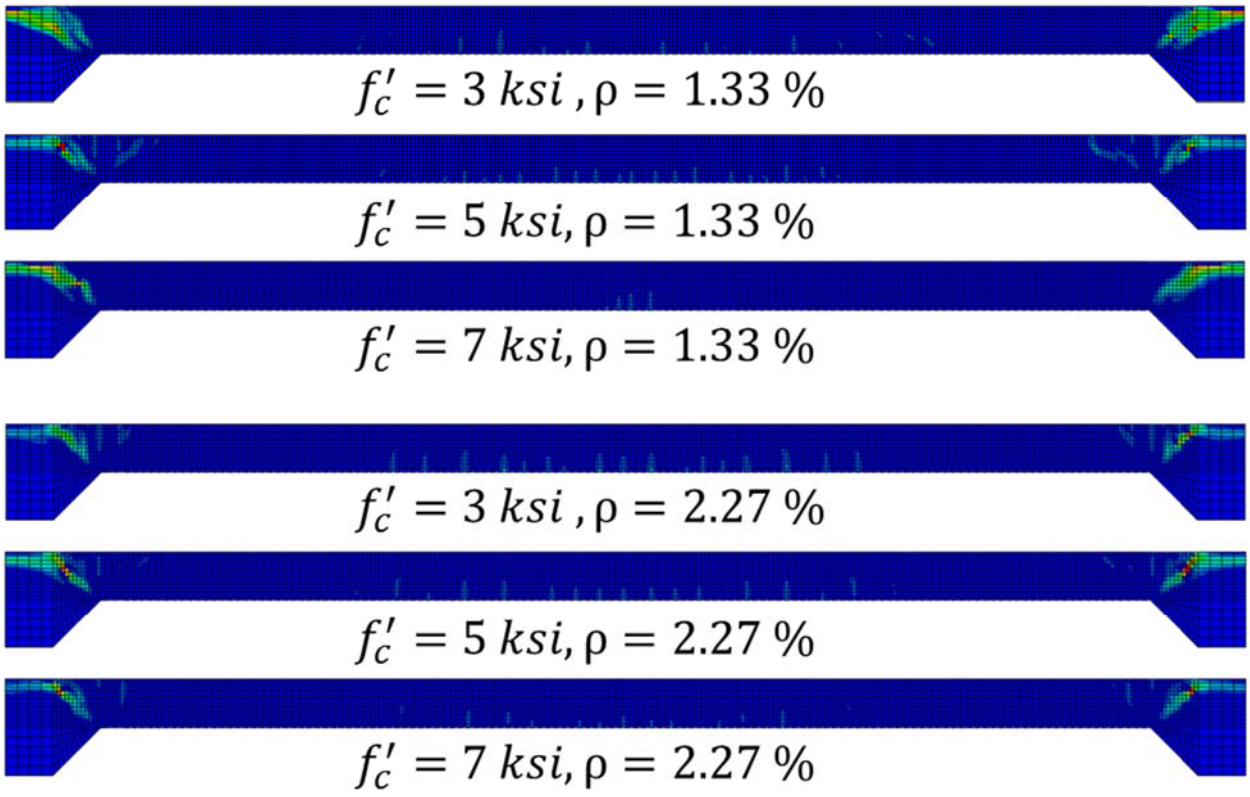

Box Culvert $24 \times 6 \times 16$

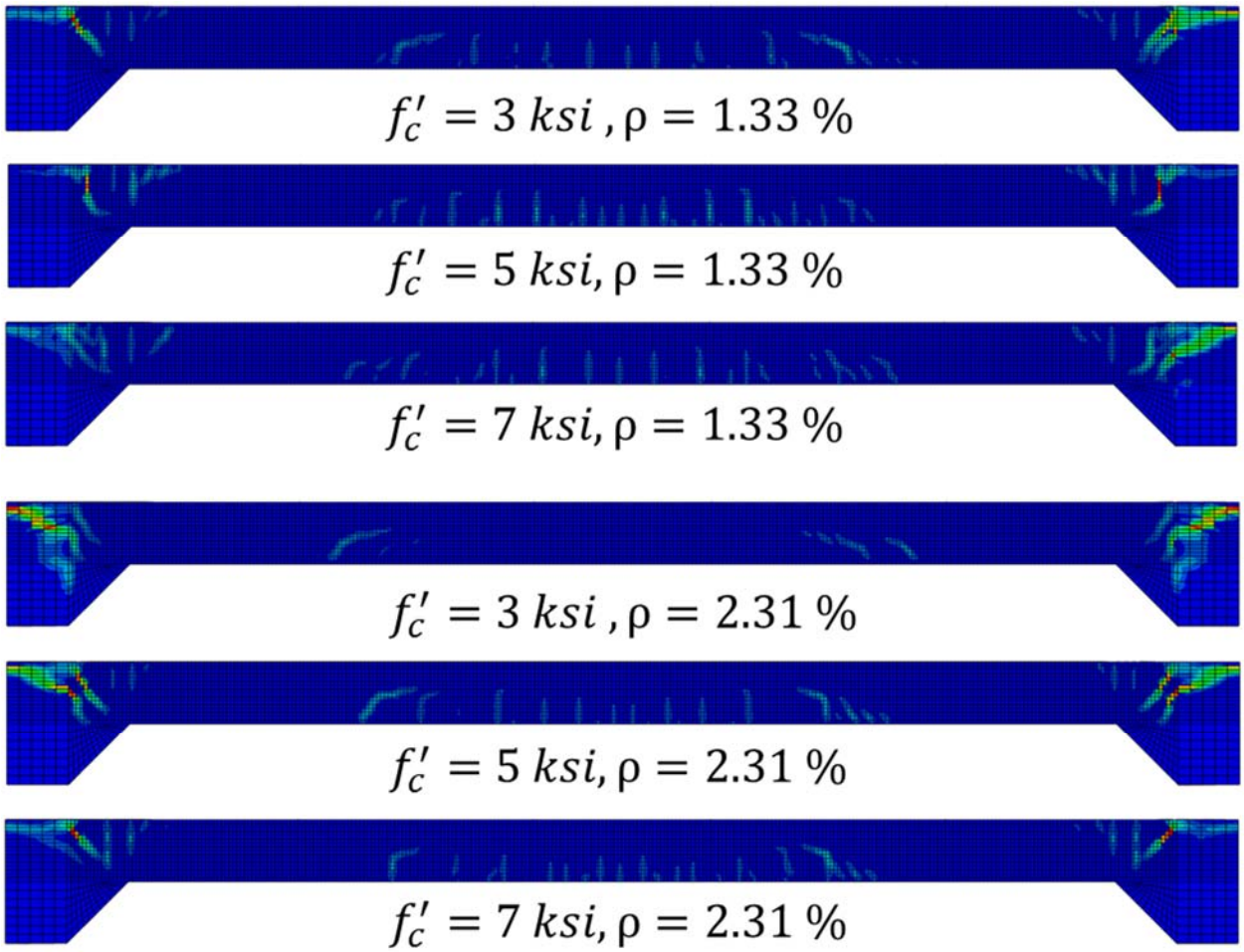

Box Culvert $24 \times 6 \times 20$

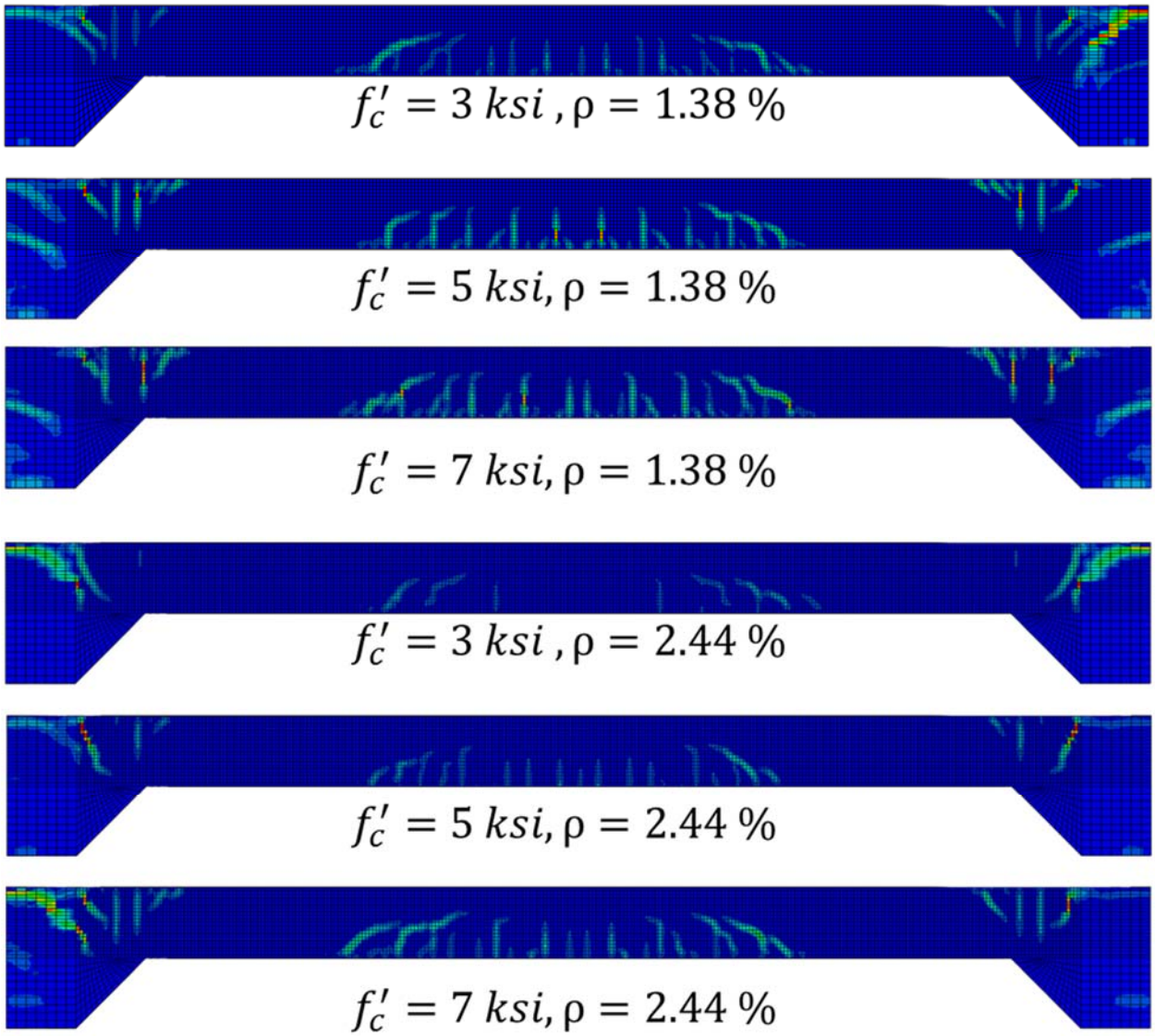

Box Culvert $24 \times 6 \times 24$

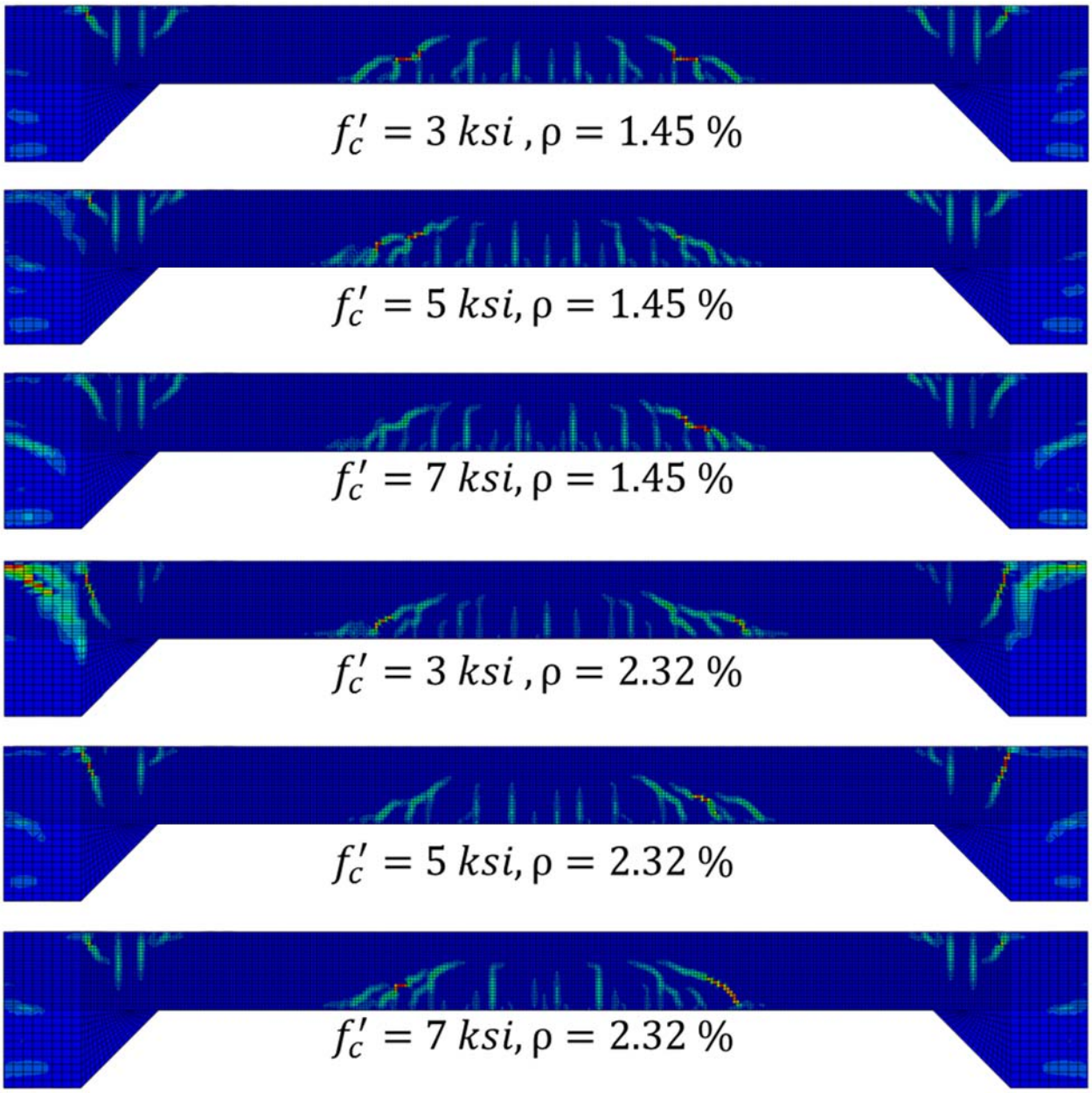

Box Culvert 24 × 12 × 12

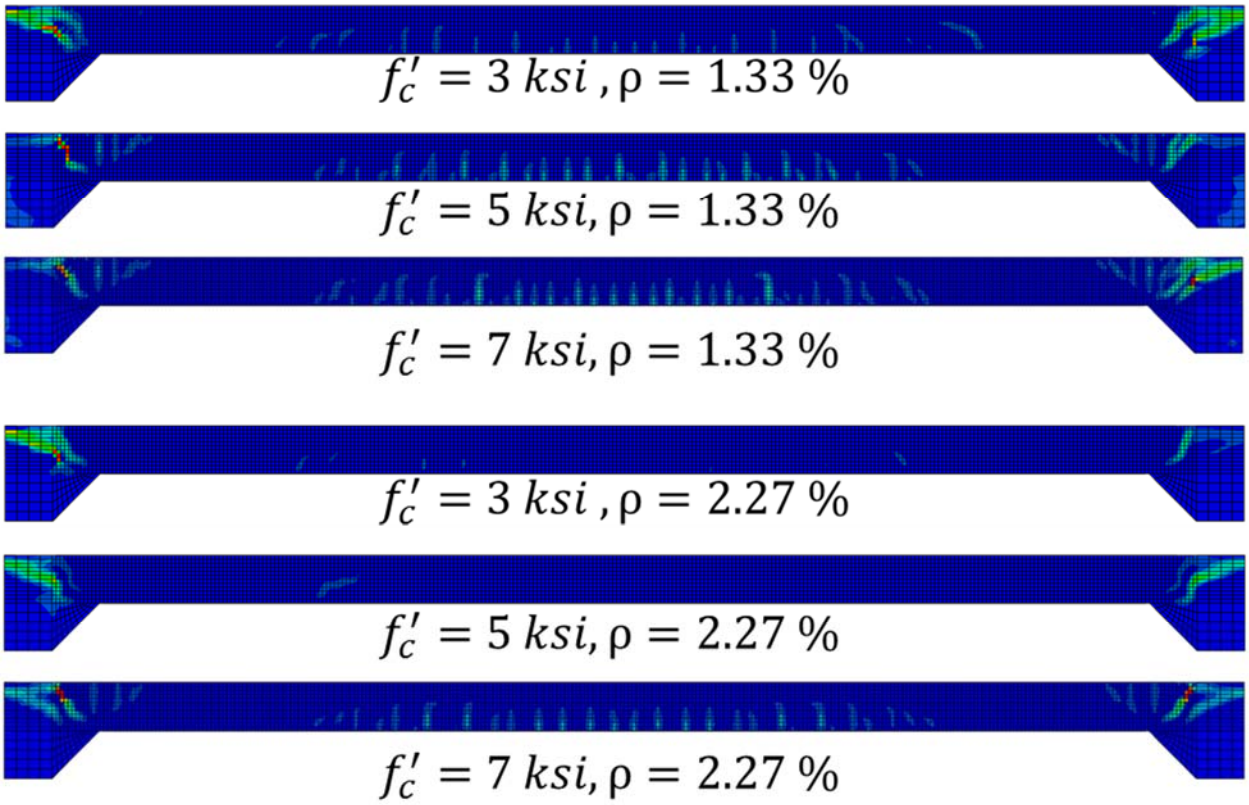

Box Culvert $24 \times 12 \times 16$

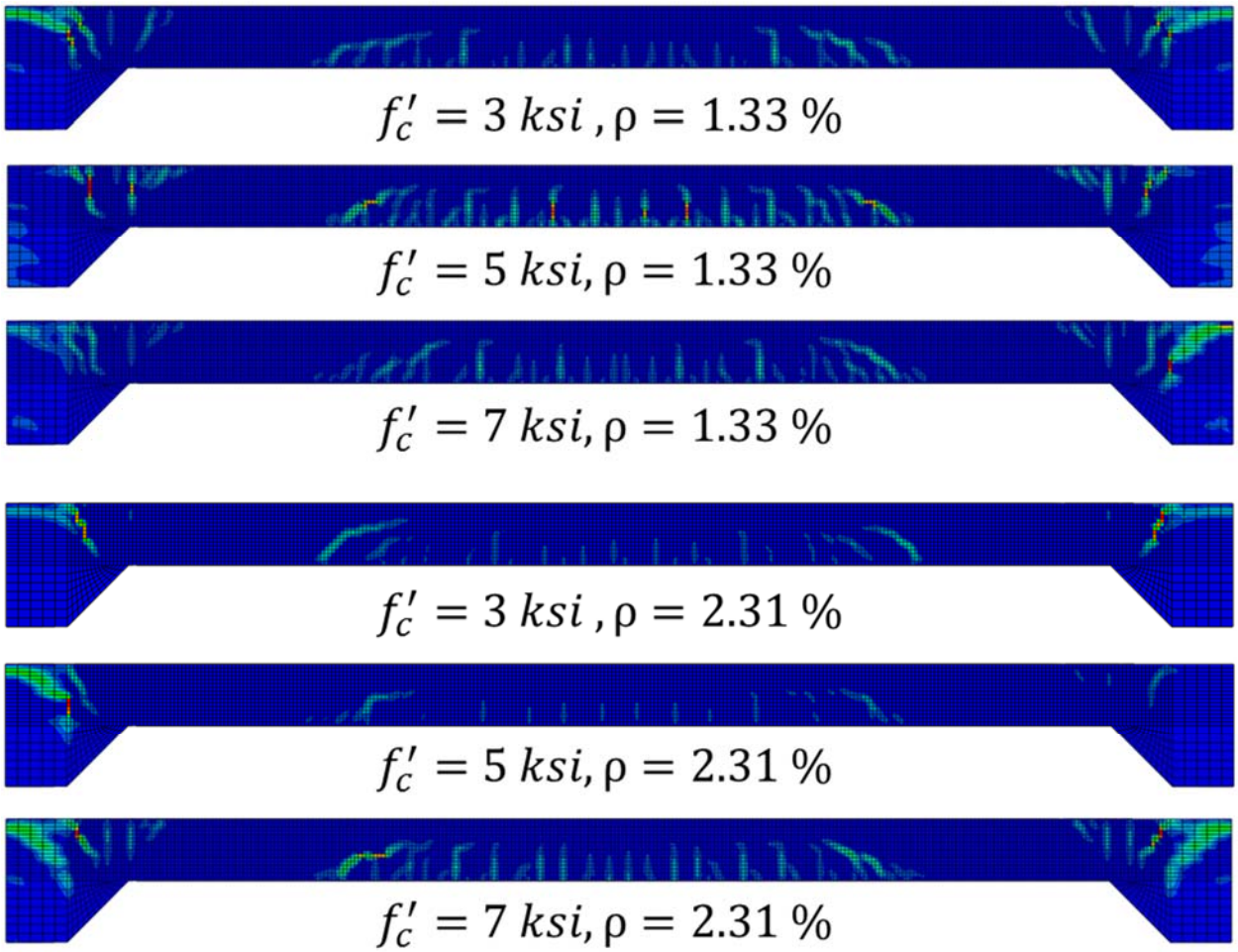

Box Culvert $24 \times 12 \times 20$

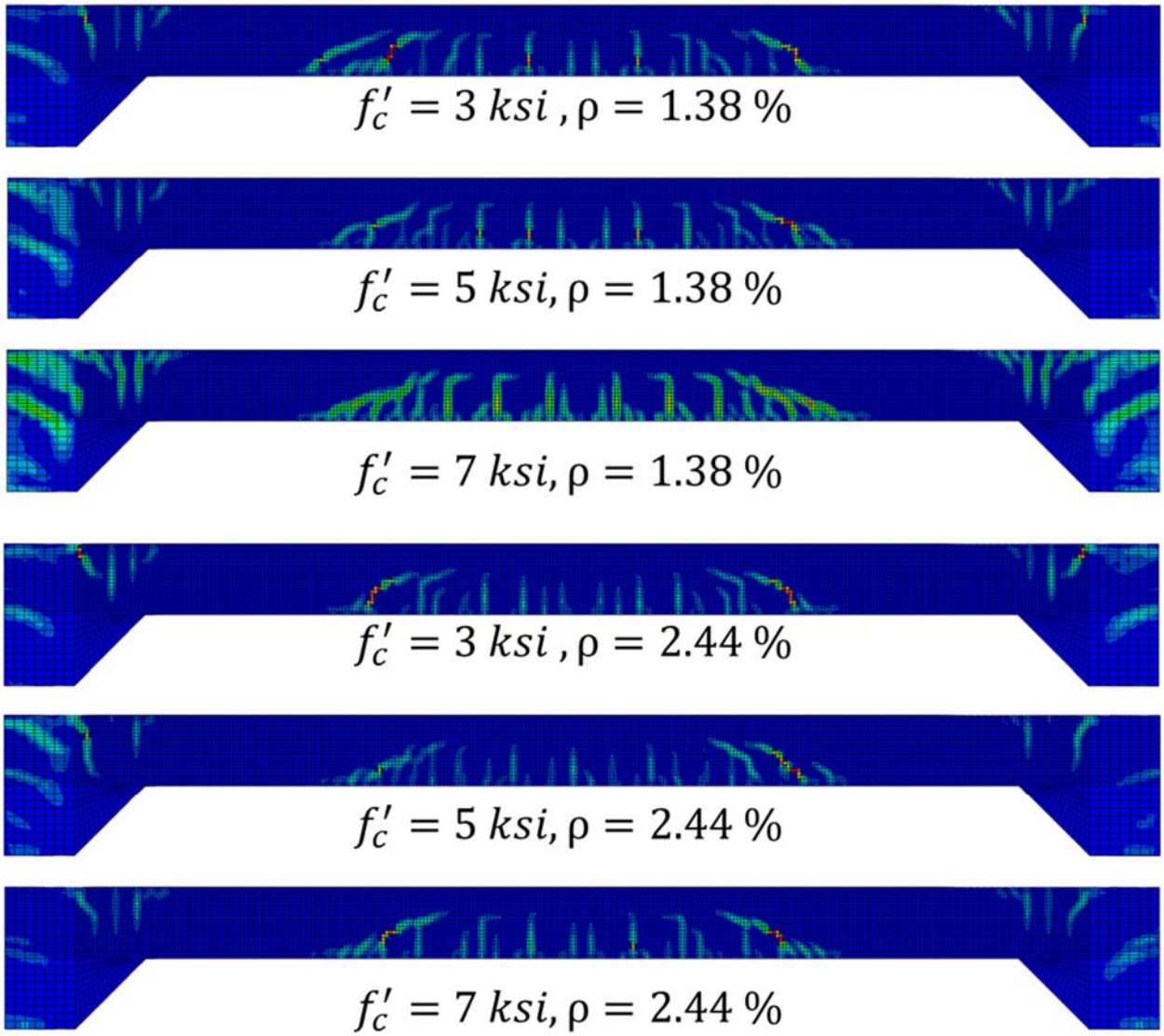

Box Culvert $24 \times 12 \times 24$

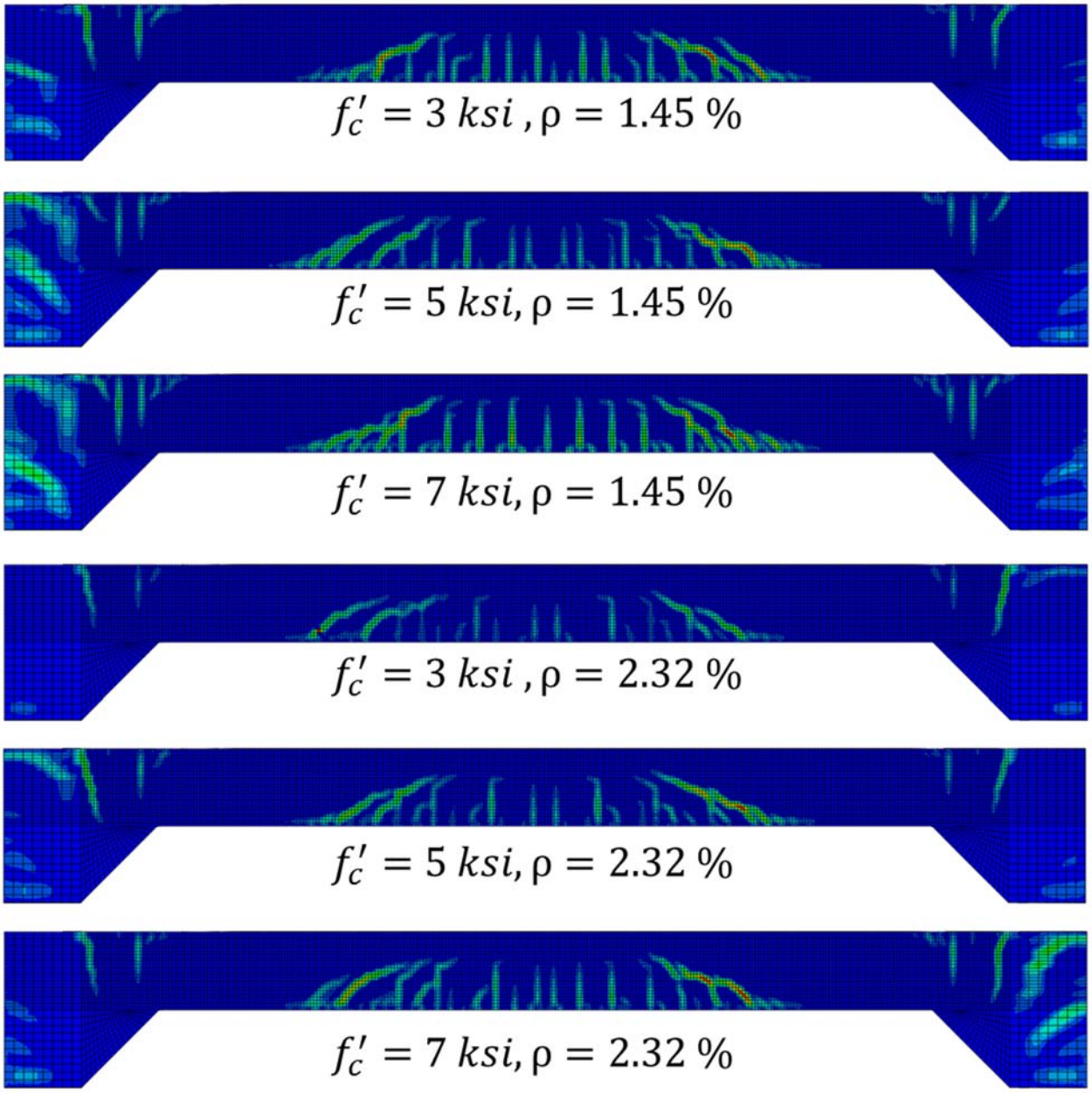

Box Culvert $24 \times 15 \times 12$

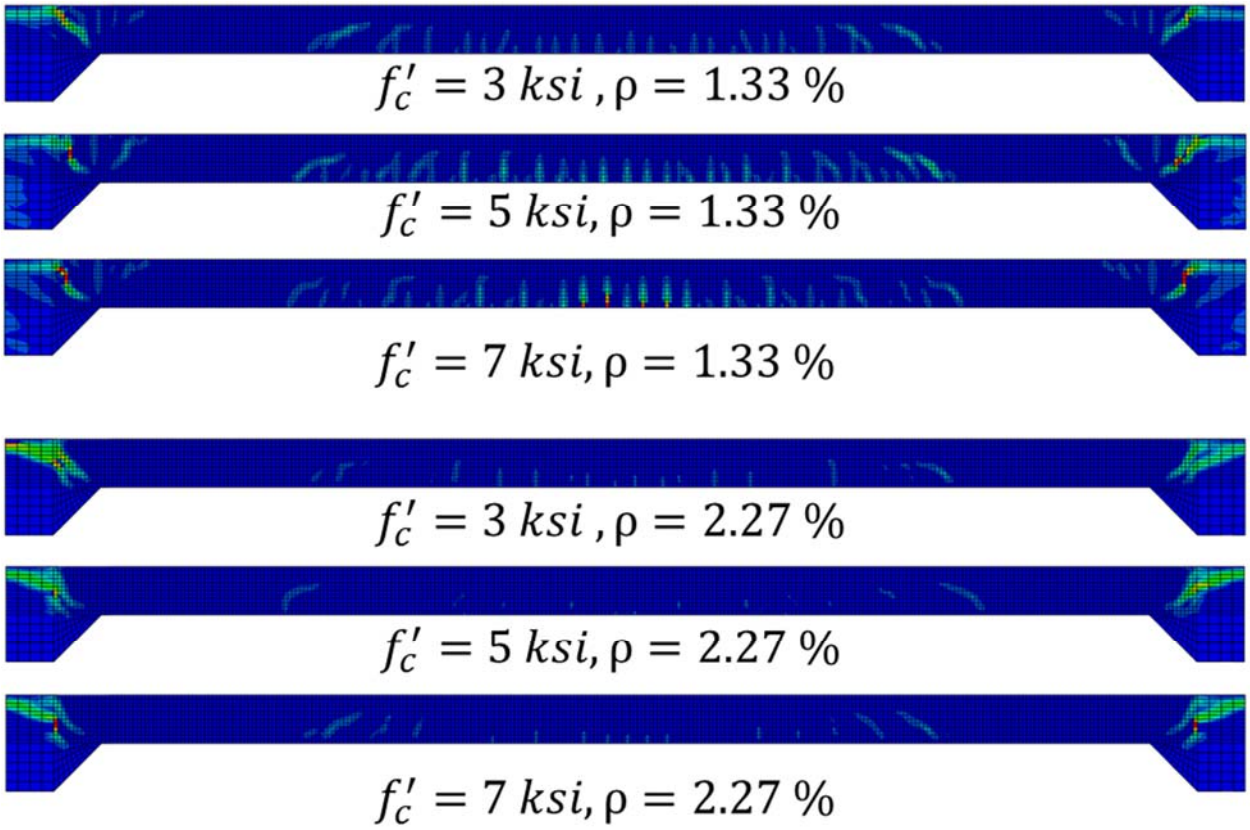

Box Culvert $24 \times 15 \times 16$

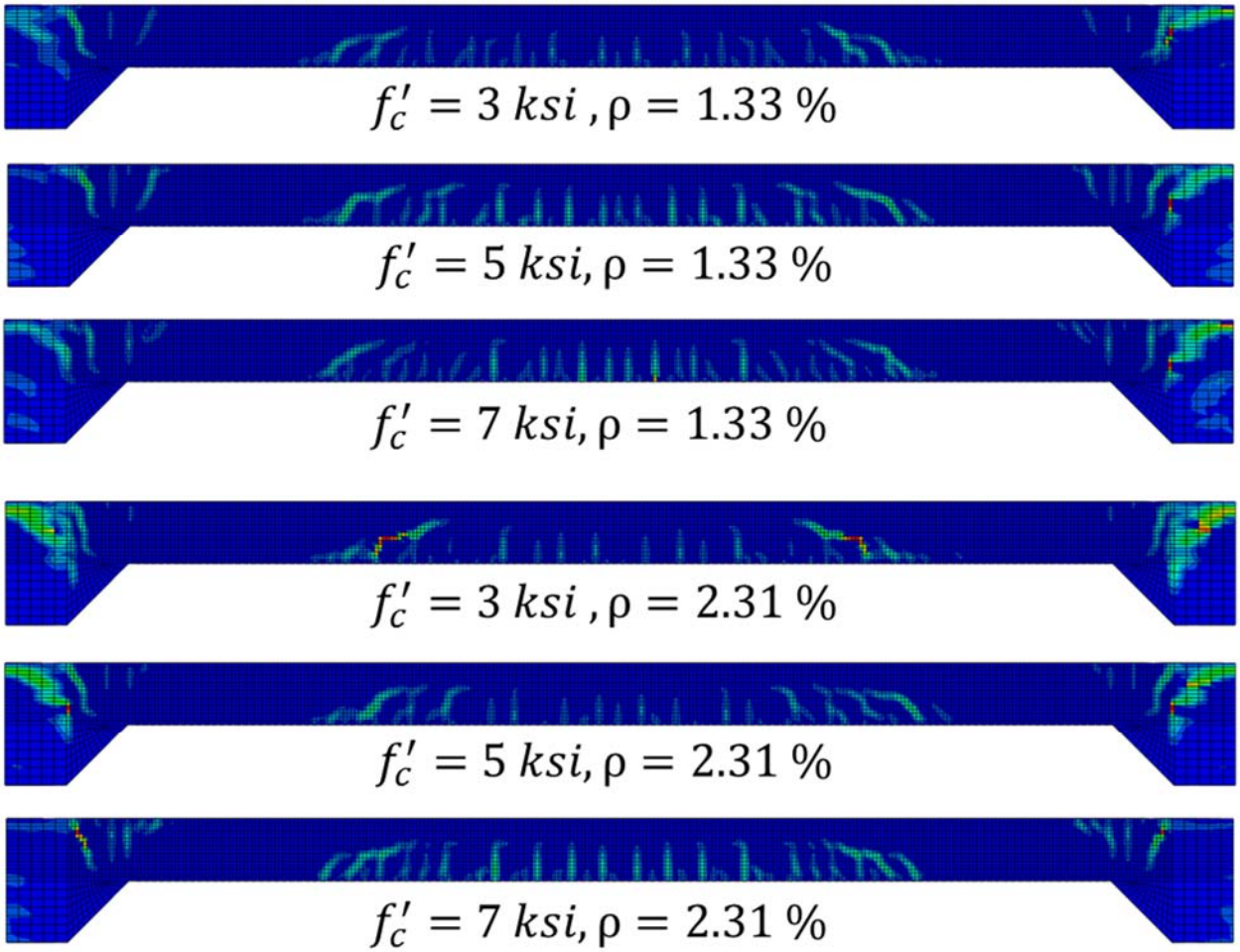

Box Culvert $24 \times 15 \times 20$

Box Culvert $24 \times 15 \times 24$

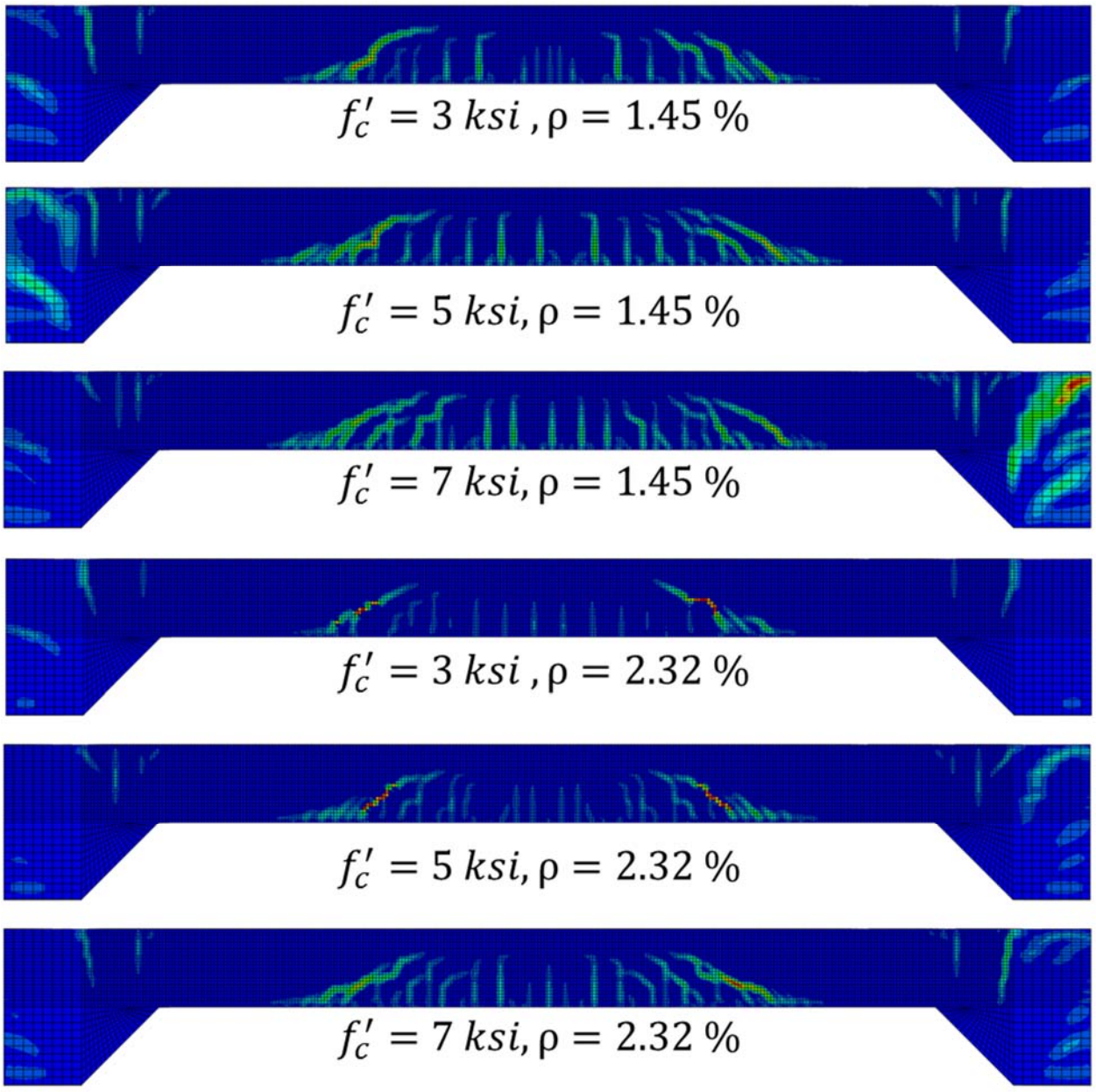

APPENDIX 3. RESULTS OF PARAMETRIC STUDY

Results of all case studies and comparison with AASHTO specification:

Size ($ft.\times ft.\times in.$)	ρ (%)	f'_c	Total failure load (lbs.)	Shear force in the section "d" from haunch at failure (lbs.)	Bending moment in the section "d" from haunch at failure (lbs.in.)	Strain in longitudinal rebar in the section "d" from haunch at failure from FEM ($\times 10^{-3}$)	Strain in longitudinal rebar in the section "d" from haunch at failure from AASHTO ($\times 10^{-3}$)	Ratio ($\frac{FEM}{AASHTO}$)	β from FEM	β from AASHTO	Ratio ($\frac{FEM}{AASHTO}$)
6 × 6 × 12	1.33	3	155038	25484.705	104398.5	2.082	1.371	1.52	7.05	2.37	2.98
6 × 6 × 12	2.27	3	149103	24587.62	99566.25	1.19	0.773	1.54	6.80	3.04	2.24
6 × 6 × 16	1.33	3	241777	15479.955	267066	1.802	0.956	1.88	3.14	2.74	1.15
6 × 6 × 16	2.31	3	245582	15758.624	215338.25	1.256	0.499	2.52	3.20	3.42	0.93
6 × 6 × 20	1.38	3	291875	13195.253	419720.5	1.311	0.770	1.70	2.11	2.80	0.75
6 × 6 × 20	2.44	3	284325	12947.9	370076	0.623	0.402	1.55	2.07	3.39	0.61
6 × 6 × 24	1.45	3	339462	43681.484	429145	0.762	1.075	0.71	5.78	2.31	2.50
6 × 6 × 24	2.32	3	336193	43538.977	375086	0.431	0.645	0.67	5.76	2.81	2.05
6 × 12 × 12	1.33	3	133582	21441.545	82782	3.029	1.135	2.67	5.93	2.59	2.29
6 × 12 × 12	2.27	3	128249	21273.246	80676.5	1.385	0.658	2.11	5.88	3.21	1.83
6 × 12 × 16	1.33	3	196603	11979.682	237398	1.886	0.799	2.36	2.43	2.94	0.83
6 × 12 × 16	2.31	3	193919	12486.332	213674	1.092	0.443	2.46	2.53	3.53	0.72
6 × 12 × 20	1.38	3	186795	21361.709	427453	1.24	0.957	1.30	3.42	2.57	1.33
6 × 12 × 20	2.44	3	228677	10209.345	304957.5	0.71	0.326	2.18	1.64	3.55	0.46
6 × 12 × 24	1.45	3	269082	34166.289	347329	0.915	0.849	1.08	4.52	2.55	1.77
6 × 12 × 24	2.32	3	276459	35182.957	322798	0.583	0.530	1.10	4.65	2.99	1.56
6 × 15 × 12	1.33	3	115808	18105.309	102719	2.085	1.075	1.94	5.01	2.66	1.88
6 × 15 × 12	2.27	3	120746	19317.178	112853.5	1.428	0.680	2.10	5.34	3.18	1.68
6 × 15 × 16	1.33	3	234812	18325.43	224114.5	3.285	0.956	3.44	3.72	2.74	1.36
6 × 15 × 16	2.31	3	223189	15974.904	208795	1.427	0.496	2.88	3.24	3.43	0.94
6 × 15 × 20	1.38	3	254371	9996.739	325105	1.718	0.592	2.90	1.60	3.06	0.52
6 × 15 × 20	2.44	3	283935	10572.873	246698.5	1	0.292	3.42	1.69	3.62	0.47
6 × 15 × 24	1.45	3	263969	36254.18	372258	1.1	0.904	1.22	4.80	2.49	1.93
6 × 15 × 24	2.32	3	282979	40201.684	306497	0.714	0.577	1.24	5.32	2.91	1.82
12 × 6 × 12	1.33	3	65240.4	20217.83	7075.75	0.689	0.817	0.84	5.59	2.98	1.88
12 × 6 × 12	2.27	3	78922.4	24424.199	6481.25	0.196	0.575	0.34	6.76	3.35	2.01
12 × 6 × 16	1.33	3	123445	30355.879	41158	1.282	0.951	1.35	6.16	2.75	2.24
12 × 6 × 16	2.31	3	132060	32004.551	82818	1.159	0.622	1.86	6.49	3.21	2.02

12 × 6 × 20	1.38	3	197831	36894.703	217269	1.184	1.055	1.12	5.91	2.47	2.40
12 × 6 × 20	2.44	3	215984	40408.457	173659	0.838	0.615	1.36	6.47	3.02	2.14
12 × 6 × 24	1.45	3	264342	42533.625	451441	1.079	1.072	1.01	5.63	2.32	2.43
12 × 6 × 24	2.32	3	268573	43662.887	441168	1.073	0.677	1.58	5.78	2.77	2.09
12 × 12 × 12	1.33	3	62244.8	19429.945	14734.5	0.951	0.814	1.17	5.37	2.98	1.80
12 × 12 × 12	2.27	3	69244	21376.734	3426	0.931	0.499	1.87	5.91	3.49	1.69
12 × 12 × 16	1.33	3	115704	28924.23	40027	1.396	0.908	1.54	5.87	2.80	2.10
12 × 12 × 16	2.31	3	121232	30271.502	63737	1.173	0.572	2.05	6.14	3.29	1.87
12 × 12 × 20	1.38	3	168903	34750.02	209660	1.823	0.999	1.82	5.57	2.52	2.20
12 × 12 × 20	2.44	3	186492	37977.75	189909	1.098	0.595	1.85	6.08	3.05	1.99
12 × 12 × 24	1.45	3	284871	40200.336	430370	1.581	1.016	1.56	5.32	2.37	2.24
12 × 12 × 24	2.32	3	292001	45662.934	385978	1.031	0.673	1.53	6.04	2.78	2.18
12 × 15 × 12	1.33	3	62462.7	19248.918	13185.5	0.944	0.801	1.18	5.32	3.00	1.78
12 × 15 × 12	2.27	3	70568	22350.773	5985.5	0.873	0.526	1.66	6.18	3.44	1.80
12 × 15 × 16	1.33	3	110282	26861.703	94795.5	1.641	0.953	1.72	5.45	2.74	1.99
12 × 15 × 16	2.31	3	124080	31494.758	53042.5	1.264	0.581	2.18	6.39	3.28	1.95
12 × 15 × 20	1.38	3	161259	33192.254	237520	1.9	0.997	1.91	5.32	2.53	2.10
12 × 15 × 20	2.44	3	186447	35389.809	164390	1.067	0.546	1.95	5.67	3.13	1.81
12 × 15 × 24	1.45	3	242820	37578.188	450455	1.594	0.986	1.62	4.97	2.40	2.07
12 × 15 × 24	2.32	3	251566	39201.328	399477.5	1.072	0.610	1.76	5.19	2.87	1.81
18 × 6 × 12	1.33	3	39623.9	14697.879	13570.75	0.663	0.624	1.06	4.07	3.27	1.24
18 × 6 × 12	2.27	3	45185.6	16840.104	44439	0.156	0.480	0.32	4.66	3.53	1.32
18 × 6 × 16	1.33	3	76099.1	23647.385	22596.5	0.474	0.723	0.66	4.80	3.05	1.57
18 × 6 × 16	2.31	3	80914.7	23147.416	44785	0.58	0.433	1.34	4.70	3.55	1.32
18 × 6 × 20	1.38	3	119900	35636.063	43607	0.398	0.828	0.48	5.71	2.72	2.09
18 × 6 × 20	2.44	3	117582	35549.781	63121.5	0.08	0.482	0.17	5.69	3.24	1.76
18 × 6 × 24	1.45	3	193059	56693.707	98092	1.358	1.051	1.29	7.50	2.34	3.21
18 × 6 × 24	2.32	3	183299	45623.813	127695	0.528	0.551	0.96	6.04	2.95	2.04
18 × 12 × 12	1.33	3	44773.5	16264.146	28913.75	0.343	0.740	0.46	4.50	3.09	1.46
18 × 12 × 12	2.27	3	49233	18003.908	72819	0.649	0.566	1.15	4.98	3.37	1.48
18 × 12 × 16	1.33	3	73936.4	22654.758	27660.5	0.349	0.704	0.50	4.60	3.08	1.49
18 × 12 × 16	2.31	3	83988.2	25921.473	43051	1.239	0.477	2.60	5.26	3.46	1.52
18 × 12 × 20	1.38	3	102485	31438.326	55903	0.862	0.750	1.15	5.03	2.83	1.78
18 × 12 × 20	2.44	3	127883	31938.814	121316	1.054	0.475	2.22	5.12	3.26	1.57
18 × 12 × 24	1.45	3	152108	40323.281	288996	1.62	0.912	1.78	5.33	2.48	2.15
18 × 12 × 24	2.32	3	177360	53291.891	84872	1.041	0.614	1.70	7.05	2.86	2.47
18 × 15 × 12	1.33	3	38885.8	14545.012	6157.25	0.262	0592	0.44	4.02	3.32	1.21
18 × 15 × 12	2.27	3	41490.9	15856.191	25090.75	0.145	0.417	0.35	4.39	3.66	1.20
18 × 15 × 16	1.33	3	75008.9	23316.859	24725	0.715	0.717	1.00	4.73	3.06	1.55
18 × 15 × 16	2.31	3	83807.8	25074.697	57772	1.295	0.480	2.70	5.09	3.46	1.47
18 × 15 × 20	1.38	3	104166	32851.348	4195	1.227	0.722	1.70	5.26	2.87	1.84

18 × 15 × 20	2.44	3	121387	37419.762	103341	1.169	0.532	2.20	5.99	3.16	1.90
18 × 15 × 24	1.45	3	158251	47539.535	100805	1.573	0.895	1.76	6.29	2.50	2.52
18 × 15 × 24	2.32	3	181317	38322.301	258540	1.195	0.534	2.24	5.07	2.98	1.70
24 × 6 × 12	1.33	3	22841	8611.746	18436.625	0.603	0.403	1.50	2.38	3.69	0.65
24 × 6 × 12	2.27	3	22078.7	8273.373	57458.75	0.372	0.310	1.20	2.29	3.89	0.59
24 × 6 × 16	1.33	3	47585	18143.512	73865.75	0.56	0.663	0.84	3.68	3.14	1.17
24 × 6 × 16	2.31	3	51302.4	19214.168	48213.5	0.131	0.372	0.35	3.90	3.68	1.06
24 × 6 × 20	1.38	3	81749	26067.439	86107.5	0.247	0.668	0.37	4.17	2.94	1.42
24 × 6 × 20	2.44	3	81191.2	25375.91	8190.25	0.036	0.320	0.11	4.06	3.56	1.14
24 × 6 × 24	1.45	3	118616	37120.277	75693.5	0.117	0.697	0.17	4.91	2.74	1.79
24 × 6 × 24	2.32	3	127351	39430.07	72419.5	0.02	0.459		5.22	3.11	1.68
24 × 12 × 12	1.33	3	24080.9	9083.032	6552.25	0.601	0.379	1.58	2.51	3.74	0.67
24 × 12 × 12	2.27	3	28071.7	10129.325	23091.375	0.238	0.281	0.85	2.80	3.96	0.71
24 × 12 × 16	1.33	3	47362.7	17710.066	6426.25	0.534	0.521	1.02	3.59	3.38	1.06
24 × 12 × 16	2.31	3	50592.9	18960.479	52182.625	0.144	0.372	0.39	3.85	3.68	1.05
24 × 12 × 20	1.38	3	71238.9	22219.896	52466	0.168	0.545	0.31	3.56	3.13	1.14
24 × 12 × 20	2.44	3	75793	23742.887	14118	0.047	0.304	0.15	3.80	3.60	1.06
24 × 12 × 24	1.45	3	95386.8	30202.311	394.25	0.03	0.521	0.06	4.00	3.00	1.33
24 × 12 × 24	2.32	3	115499	35815.16	8177	0.103	0.390	0.26	4.74	3.23	1.47
24 × 15 × 12	1.33	3	26313.3	9792.659	26303	0.71	0.477	1.49	2.71	3.53	0.77
24 × 15 × 12	2.27	3	28358	10521.033	1393	0.286	0.245	1.17	2.91	4.06	0.72
24 × 15 × 16	1.33	3	48327.3	17997.572	14698.5	0.4	0.545	0.73	3.65	3.34	1.09
24 × 15 × 16	2.31	3	50889.9	19126.52	3157.875	0.095	0.321	0.30	3.88	3.79	1.02
24 × 15 × 20	1.38	3	63883.1	19974.215	43094.625	0.053	0.485	0.11	3.20	3.24	0.99
24 × 15 × 20	2.44	3	79155.9	25115.863	25029.25	0.051	0.328	0.16	4.02	3.54	1.13
24 × 15 × 24	1.45	3	96836.9	30597.16	28618.75	0.094	0.549	0.17	4.05	2.96	1.37
24 × 15 × 24	2.32	3	108047	33604.152	35337.5	0.081	0.379	0.21	4.45	3.25	1.37
6 × 6 × 12	1.33	5	185731	30485.64	156476.5	2.027	1.752	1.16	6.53	2.07	3.15
6 × 6 × 12	2.27	5	207373	34364.28	164296	1.62	1.133	1.43	7.36	2.59	2.84
6 × 6 × 16	1.33	5	330095	19909.61	413258	2.097	1.364	1.54	3.13	2.33	1.35
6 × 6 × 16	2.31	5	359281	20770.39	322828.5	1.428	0.701	2.04	3.26	3.08	1.06
6 × 6 × 20	1.38	5	397929	18364.27	621650	1.355	1.115	1.22	2.28	2.41	0.95
6 × 6 × 20	2.44	5	400423	18354.08	544125	0.952	0.583	1.63	2.28	3.07	0.74
6 × 6 × 24	1.45	5	469642	58158.94	645364	1.038	1.487	0.70	5.96	1.97	3.02
6 × 6 × 24	2.32	5	463832	58268.15	539759	0.655	0.881	0.74	5.97	2.51	2.37
6 × 12 × 12	1.33	5	154103	25372.98	151872	2.003	1.535	1.30	5.44	2.23	2.44
6 × 12 × 12	2.27	5	167980	27692.58	146675	1.791	0.943	1.90	5.93	2.81	2.11
6 × 12 × 16	1.33	5	288774	18291.31	299803.5	1.844	1.100	1.68	2.87	2.58	1.12
6 × 12 × 16	2.31	5	233944	14531.46	324198	1.252	0.599	2.09	2.28	3.25	0.70
6 × 12 × 20	1.38	5	292070	13163.24	480523	1.562	0.839	1.86	1.63	2.71	0.60
6 × 12 × 20	2.44	5	296832	13549.33	436882	0.952	0.453	2.10	1.68	3.30	0.51

6 × 12 × 24	1.45	5	398995	50459.188	577382	1.33	1.303	1.02	5.17	2.11	2.45
6 × 12 × 24	2.32	5	354001	42847.59	487699	0.782	0.690	1.13	4.39	2.75	1.60
6 × 15 × 12	1.33	5	160634	25191.73	132270	2.42	1.458	1.66	5.40	2.29	2.35
6 × 15 × 12	2.27	5	159999	25808.66	103164	2.026	0.809	2.50	5.53	2.99	1.85
6 × 15 × 16	1.33	5	301830	17125.27	244556.5	1.817	0.961	1.89	2.69	2.73	0.98
6 × 15 × 16	2.31	5	289492	18913.52	205009	1.823	0.540	3.38	2.97	3.35	0.89
6 × 15 × 20	1.38	5	467265	18273.64	399240	2.015	0.857	2.35	2.27	2.69	0.84
6 × 15 × 20	2.44	5	334004	13009.55	422455	1.287	0.437	2.94	1.61	3.33	0.49
6 × 15 × 24	1.45	5	394186	52581.92	655719	1.601	1.398	1.15	5.39	2.04	2.64
6 × 15 × 24	2.32	5	351787	47175.83	450721	0.942	0.720	1.31	4.83	2.71	1.78
12 × 6 × 12	1.33	5	80897.7	25137.44	12897.25	0.324	1.031	0.31	5.39	2.71	1.99
12 × 6 × 12	2.27	5	107386	33438.301	6193.5	0.605	0.782	0.77	7.16	3.03	2.37
12 × 6 × 16	1.33	5	157718	39153.56	32887.5	1.412	1.188	1.19	6.15	2.49	2.47
12 × 6 × 16	2.31	5	167868	40073	111672	1.131	0.788	1.44	6.30	2.96	2.13
12 × 6 × 20	1.38	5	254399	47013.07	309363	1.503	1.381	1.09	5.83	2.17	2.69
12 × 6 × 20	2.44	5	264634	57532.43	245933	1.243	0.874	1.42	7.14	2.67	2.68
12 × 6 × 24	1.45	5	331053	49248.27	615029	1.048	1.310	0.80	5.05	2.11	2.40
12 × 6 × 24	2.32	5	350736	54725.31	570765	0.895	0.857	1.04	5.61	2.54	2.21
12 × 12 × 12	1.33	5	73006	22899.85	13314.25	0.651	0.945	0.69	4.91	2.81	1.75
12 × 12 × 12	2.27	5	86248.6	26805.12	6435	0.889	0.630	1.41	5.74	3.26	1.76
12 × 12 × 16	1.33	5	141874	34788.44	36007	1.577	1.069	1.48	5.47	2.61	2.09
12 × 12 × 16	2.31	5	155503	38472.6	28220	1.23	0.669	1.84	6.05	3.13	1.93
12 × 12 × 20	1.38	5	194169	36595.83	267078	1.52	1.105	1.37	4.54	2.41	1.88
12 × 12 × 20	2.44	5	232556	39570.18	398845	1.487	0.751	1.98	4.91	2.82	1.74
12 × 12 × 24	1.45	5	370246	59186.25	683820	2.039	1.533	1.33	6.07	1.94	3.12
12 × 12 × 24	2.32	5	398775	55727.53	574266	1.36	0.870	1.56	5.71	2.53	2.26
12 × 15 × 12	1.33	5	65793.1	20238.7	957.75	1.01	0.796	1.27	4.34	3.00	1.44
12 × 15 × 12	2.27	5	84807.6	25610.922	3261	0.833	0.596	1.40	5.49	3.32	1.65
12 × 15 × 16	1.33	5	129461	31608.48	30728.5	1.749	0.967	1.81	4.97	2.73	1.82
12 × 15 × 16	2.31	5	147336	36252.03	48710	1.284	0.655	1.96	5.70	3.15	1.81
12 × 15 × 20	1.38	5	199233	36803.32	304496	1.887	1.153	1.64	4.57	2.37	1.93
12 × 15 × 20	2.44	5	233808	41315.81	384587	1.503	0.764	1.97	5.13	2.81	1.83
12 × 15 × 24	1.45	5	308015	47972.71	710936	2.004	1.360	1.47	4.92	2.07	2.38
12 × 15 × 24	2.32	5	349066	55613.66	589655	1.332	0.876	1.52	5.70	2.52	2.26
18 × 6 × 12	1.33	5	46060.6	17476.27	31634.5	0.741	0.797	0.93	3.74	3.00	1.25
18 × 6 × 12	2.27	5	50864.4	19016.74	273	0.226	0.438	0.52	4.07	3.61	1.13
18 × 6 × 16	1.33	5	92102.4	28253.16	10681.75	0.266	0.832	0.32	4.44	2.90	1.53
18 × 6 × 16	2.31	5	102955	31670.51	9024.25	0.066	0.535	0.12	4.98	3.36	1.48
18 × 6 × 20	1.38	5	147871	45178.2	50444	0.762	1.044	0.73	5.60	2.48	2.26
18 × 6 × 20	2.44	5	155054	19118.63	440428.5	0.196	0.525	0.37	2.37	3.17	0.75
18 × 6 × 24	1.45	5	222015	59357.1	12624	0.541	1.033	0.52	6.08	2.35	2.58

18 × 6 × 24	2.32	5	233128	58699.96	152358.5	0.386	0.704	0.55	6.02	2.73	2.20
18 × 12 × 12	1.33	5	53480.4	19603.13	66438.5	1.212	1.005	1.21	4.20	2.74	1.53
18 × 12 × 12	2.27	5	58391.5	21707.96	13261.37	0.599	0.527	1.14	4.65	3.44	1.35
18 × 12 × 16	1.33	5	91918	28400.87	47744.75	0.778	0.908	0.86	4.46	2.80	1.59
18 × 12 × 16	2.31	5	97608.5	30679.78	19609.25	0.451	0.530	0.85	4.82	3.37	1.43
18 × 12 × 20	1.38	5	136396	41541.49	78999	0.485	0.997	0.49	5.15	2.53	2.04
18 × 12 × 20	2.44	5	144739	45315.2	9114	0.317	0.568	0.56	5.62	3.10	1.82
18 × 12 × 24	1.45	5	183277	47091.69	52657	0.259	0.851	0.30	4.83	2.55	1.89
18 × 12 × 24	2.32	5	200100	50109.28	62943.5	0.189	0.569	0.33	5.14	2.93	1.75
18 × 15 × 12	1.33	5	47681.8	17814.059	24760.5	0.696	0.786	0.89	3.82	3.02	1.26
18 × 15 × 12	2.27	5	53588.5	19960.04	10487.75	0.494	0.481	1.03	4.28	3.53	1.21
18 × 15 × 16	1.33	5	86145.2	27498.99	41991.75	0.751	0.871	0.86	4.32	2.85	1.52
18 × 15 × 16	2.31	5	99980.1	31239.7	27141.5	0.407	0.548	0.74	4.91	3.33	1.47
18 × 15 × 20	1.38	5	115397	36771.42	5846.5	0.38	0.809	0.47	4.56	2.75	1.66
18 × 15 × 20	2.44	5	142177	44095.47	18336	0.203	0.559	0.36	5.47	3.11	1.76
18 × 15 × 24	1.45	5	188499	48633.78	117770.5	0.289	0.927	0.31	4.98	2.46	2.02
18 × 15 × 24	2.32	5	195106	48127.59	72057	0.113	0.552	0.20	4.93	2.95	1.67
24 × 6 × 12	1.33	5	30368.9	11414.57	80573.5	1.128	0.734	1.54	2.45	3.10	0.79
24 × 6 × 12	2.27	5	29277.5	10981.23	55825.25	0.609	0.369	1.65	2.35	3.76	0.63
24 × 6 × 16	1.33	5	55046.4	20555.5	129142.5	1.008	0.838	1.20	3.23	2.89	1.12
24 × 6 × 16	2.31	5	61513.8	23054.48	54925	0.566	0.443	1.28	3.62	3.53	1.03
24 × 6 × 20	1.38	5	91900	29020.03	167385	0.901	0.826	1.09	3.60	2.73	1.32
24 × 6 × 20	2.44	5	101976	32140.32	141140	0.541	0.491	1.10	3.99	3.23	1.24
24 × 6 × 24	1.45	5	159801	50538.52	130801	0.824	0.969	0.85	5.18	2.42	2.14
24 × 6 × 24	2.32	5	156714	48698.42	106052	0.483	0.574	0.84	4.99	2.92	1.71
24 × 12 × 12	1.33	5	29682.8	11091.04	66944.5	1.054	0.673	1.57	2.38	3.19	0.75
24 × 12 × 12	2.27	5	33595.8	12766.04	17052	0.52	0.329	1.58	2.74	3.85	0.71
24 × 12 × 16	1.33	5	57653.9	21724.82	7210.5	0.67	0.638	1.05	3.41	3.18	1.07
24 × 12 × 16	2.31	5	61066.4	23281.81	24518.5	0.336	0.413	0.81	3.66	3.59	1.02
24 × 12 × 20	1.38	5	81564.1	25570.43	28357	0.121	0.591	0.20	3.17	3.06	1.04
24 × 12 × 20	2.44	5	94168.8	32818.78	32447.5	0.134	0.428	0.31	4.07	3.34	1.22
24 × 12 × 24	1.45	5	129984	41619.51	3318	0.222	0.720	0.31	4.27	2.71	1.57
24 × 12 × 24	2.32	5	144388	45812.93	14348	0.167	0.500	0.33	4.69	3.04	1.55
24 × 15 × 12	1.33	5	33607.3	12564.84	56141	0.858	0.692	1.24	2.69	3.16	0.85
24 × 15 × 12	2.27	5	35685.1	13376.51	2350.25	0.365	0.312	1.17	2.87	3.89	0.74
24 × 15 × 16	1.33	5	59050.1	21966.14	22417.5	0.509	0.674	0.76	3.45	3.12	1.10
24 × 15 × 16	2.31	5	60192.5	22538.52	15285	0.13	0.391	0.33	3.54	3.64	0.97
24 × 15 × 20	1.38	5	90805.7	28417.83	6145.5	0.098	0.627	0.16	3.53	3.00	1.17
24 × 15 × 20	2.44	5	95087.6	30058.27	19954.5	0.044	0.386	0.11	3.73	3.42	1.09
24 × 15 × 24	1.45	5	133692	42869.54	49696	0.49	0.776	0.63	4.39	2.64	1.66
24 × 15 × 24	2.32	5	149013	45922.95	55647	0.223	0.521	0.43	4.71	3.00	1.57

6 × 6 × 12	1.33	7	208317	34524.398	188941	1.966	2.026	0.97	6.25	1.91	3.28
6 × 6 × 12	2.27	7	275240	45359.504	228735.5	2.045	1.521	1.34	8.21	2.24	3.66
6 × 6 × 16	1.33	7	413035	25650.303	502995.5	3.054	1.701	1.80	3.41	2.07	1.65
6 × 6 × 16	2.31	7	436686	26790.869	514761.5	1.725	1.013	1.70	3.56	2.67	1.33
6 × 6 × 20	1.38	7	506187	23065.289	805524	1.703	1.429	1.19	2.42	2.13	1.13
6 × 6 × 20	2.44	7	502706	23760.168	743026	1.244	0.780	1.60	2.49	2.79	0.89
6 × 6 × 24	1.45	7	612217	78468.875	912314	1.34	2.037	0.66	6.80	1.65	4.11
6 × 6 × 24	2.32	7	606889	77757.188	765937	0.825	1.197	0.69	6.73	2.20	3.06
6 × 12 × 12	1.33	7	169801	28000.043	154500	2.093	1.648	1.27	5.07	2.15	2.36
6 × 12 × 12	2.27	7	224173	36540	204790	2.047	1.268	1.61	6.62	2.46	2.69
6 × 12 × 16	1.33	7	337504	19859.33	345882	17.65	1.233		2.64	2.44	1.08
6 × 12 × 16	2.31	7	350100	656.189	451176	1.908	0.510	3.74	2.8	2.89	0.97
6 × 12 × 20	1.38	7	567781	21606.75	508972	20.12	1.056		2.27	2.46	0.92
6 × 12 × 20	2.44	7	506597	24165.561	657100	1.622	0.729	2.23	2.53	2.86	0.89
6 × 12 × 24	1.45	7	473135	59902.914	735128	1.513	1.584	0.96	5.19	1.91	2.72
6 × 12 × 24	2.32	7	455363	57564.922	653268	0.951	0.926	1.03	4.99	2.46	2.02
6 × 15 × 12	1.33	7	175966	27603.754	141768	19.94	1.587		5.00	2.19	2.28
6 × 15 × 12	2.27	7	185889	29141.561	153621	2.067	0.991	2.09	5.28	2.75	1.92
6 × 15 × 16	1.33	7	315405	18644.844	320593	18.43	1.150		2.48	2.53	0.98
6 × 15 × 16	2.31	7	464296	26602.865	224936	18.48	0.690		3.53	3.10	1.14
6 × 15 × 20	1.38	7	537802	19018.459	522165	19.36	1.015		1.99	2.51	0.80
6 × 15 × 20	2.44	7	440411	16687.516	603887	1.612	0.601	2.68	1.75	3.04	0.57
6 × 15 × 24	1.45	7	487434	65445.313	730682	1.965	1.676	1.17	5.67	1.85	3.06
6 × 15 × 24	2.32	7	453927	62190.609	632280	1.181	0.966	1.22	5.39	2.42	2.22
12 × 6 × 12	1.33	7	90308.8	28106.307	24752.25	0.158	1.190	0.13	5.09	2.54	2.01
12 × 6 × 12	2.27	7	126717	39534.344	14053	0.487	0.938	0.52	7.16	2.82	2.54
12 × 6 × 16	1.33	7	189317	47221.332	1410	1.173	1.360	0.86	6.27	2.33	2.69
12 × 6 × 16	2.31	7	205279	50940.246	19281	0.885	0.866	1.02	6.77	2.85	2.37
12 × 6 × 20	1.38	7	333185	60813.156	366551	1.811	1.748	1.04	6.38	1.91	3.34
12 × 6 × 20	2.44	7	331091	65640.594	503373	1.65	1.143	1.44	6.88	2.38	2.89
12 × 6 × 24	1.45	7	413944	66634.695	804913	1.255	1.752	0.72	5.77	1.80	3.20
12 × 6 × 24	2.32	7	459152	75419.531	909682	1.5	1.239	1.21	6.53	2.16	3.02
12 × 12 × 12	1.33	7	84184	26281.521	39797.5	0.537	1.172	0.46	4.76	2.55	1.86
12 × 12 × 12	2.27	7	103980	32877.766	42428.5	1.077	0.844	1.28	5.95	2.94	2.03
12 × 12 × 16	1.33	7	154763	39587.512	4435	1.472	1.146	1.28	5.26	2.53	2.08
12 × 12 × 16	2.31	7	185949	47194.781	33547	1.423	0.819	1.74	6.27	2.91	2.15
12 × 12 × 20	1.38	7	250442	47761.699	293262	1.92	1.379	1.39	5.01	2.17	2.31
12 × 12 × 20	2.44	7	277874	57843.227	363323	1.753	0.955	1.84	6.06	2.57	2.36
12 × 12 × 24	1.45	7	410355	63433.547	832245	2.027	1.718	1.18	5.49	1.83	3.01
12 × 12 × 24	2.32	7	462813	81757.313	862765	1.697	1.285	1.32	7.08	2.13	3.33
12 × 15 × 12	1.33	7	75855	23482.752	32916.75	0.582	1.037	0.56	4.25	2.70	1.58

12 × 15 × 12	2.27	7	100705	30374.861	15293.5	0.959	0.730	1.31	5.50	3.10	1.77
12 × 15 × 16	1.33	7	150927	36760.355	48440.5	1.483	1.149	1.29	4.88	2.53	1.93
12 × 15 × 16	2.31	7	179009	42962.066	172714	1.731	0.903	1.92	5.71	2.80	2.03
12 × 15 × 20	1.38	7	240961	44739.719	341001	1.788	1.368	1.31	4.69	2.18	2.15
12 × 15 × 20	2.44	7	264411	54609.117	385659	1.767	0.929	1.90	5.73	2.60	2.20
12 × 15 × 24	1.45	7	378024	49121.953	841051	2.119	1.477	1.43	4.25	1.98	2.15
12 × 15 × 24	2.32	7	401533	61976.383	828190	1.673	1.056	1.58	5.37	2.33	2.30
18 × 6 × 12	1.33	7	54467.3	20377.818	53297	0.961	0.988	0.97	3.69	2.76	1.34
18 × 6 × 12	2.27	7	61571.9	22536.027	86986	0.4	0.700	0.57	4.08	3.15	1.30
18 × 6 × 16	1.33	7	111760	33113.102	38602.5	0.465	1.025	0.45	4.40	2.66	1.65
18 × 6 × 16	2.31	7	113112	36397.633	11848.5	0.145	0.617	0.24	4.83	3.22	1.50
18 × 6 × 20	1.38	7	178878	54415.441	7505	0.146	1.196	0.12	5.71	2.33	2.45
18 × 6 × 20	2.44	7	195702	57335.762	92753	0.173	0.772	0.22	6.01	2.80	2.15
18 × 6 × 24	1.45	7	297943	72380.836	70262	1.283	1.301	0.99	6.27	2.11	2.97
18 × 6 × 24	2.32	7	285393	70703.695	149476	0.384	0.832	0.46	6.12	2.57	2.38
18 × 12 × 12	1.33	7	55611.6	20200.285	59468.5	0.968	1.003	0.96	3.66	2.74	1.34
18 × 12 × 12	2.27	7	76885.1	27789.223	54745.5	0.385	0.753	0.51	5.03	3.07	1.64
18 × 12 × 16	1.33	7	104915	31984.393	38620.5	0.332	0.993	0.33	4.25	2.70	1.58
18 × 12 × 16	2.31	7	120205	38525.738	69839	0.633	0.716	0.88	5.12	3.06	1.67
18 × 12 × 20	1.38	7	150137	41676.484	34987	0.83	0.950	0.87	4.37	2.58	1.69
18 × 12 × 20	2.44	7	188641	57630.984	68130	1.559	0.759	2.05	6.04	2.81	2.15
18 × 12 × 24	1.45	7	227756	49387.488	344387	1.526	1.110	1.38	4.28	2.28	1.88
18 × 12 × 24	2.32	7	264131	63626.73	452026	1.701	0.897	1.90	5.51	2.50	2.21
18 × 15 × 12	1.33	7	50083.7	18657.662	41947.25	0.708	0.881	0.80	3.38	2.89	1.17
18 × 15 × 12	2.27	7	65778.4	24568.047	31576	0.307	0.631	0.49	4.45	3.26	1.37
18 × 15 × 16	1.33	7	103085	31257.133	60823	0.265	1.015	0.26	4.15	2.67	1.55
18 × 15 × 16	2.31	7	118904	35958.488	55396	0.79	0.657	1.20	4.78	3.15	1.52
18 × 15 × 20	1.38	7	138758	37503.18	179	1.094	0.819	1.34	3.93	2.74	1.44
18 × 15 × 20	2.44	7	181031	47835.047	252790	1.615	0.758	2.13	5.02	2.81	1.78
18 × 15 × 24	1.45	7	216370	52259.051	255539	1.543	1.093	1.41	4.53	2.30	1.97
18 × 15 × 24	2.32	7	250487	75070.945	50442	1.634	0.833	1.96	6.50	2.57	2.53
24 × 6 × 12	1.33	7	34915.8	13120.546	103281	1.254	0.882	1.42	2.38	2.89	0.82
24 × 6 × 12	2.27	7	37809.4	14155.661	102120.25	0.681	0.539	1.26	2.56	3.42	0.75
24 × 6 × 16	1.33	7	68478	26075.301	102773	0.949	0.946	1.00	3.46	2.75	1.26
24 × 6 × 16	2.31	7	72601.1	27159.637	135602.5	0.463	0.600	0.77	3.61	3.24	1.11
24 × 6 × 20	1.38	7	110507	34527.887	211696	0.497	0.997	0.50	3.62	2.53	1.43
24 × 6 × 20	2.44	7	123075	37791.586	85372	0.244	0.524	0.47	3.96	3.17	1.25
24 × 6 × 24	1.45	7	180140	56181.758	155367	0.215	1.085	0.20	4.87	2.30	2.11
24 × 6 × 24	2.32	7	192271	60067.906	166014	0.1	0.725	0.14	5.20	2.71	1.92
24 × 12 × 12	1.33	7	36032.1	13643.737	96252.5	1.037	0.878	1.18	2.47	2.89	0.85
24 × 12 × 12	2.27	7	37587.1	14064.658	63830.75	0.63	0.457	1.38	2.55	3.58	0.71

24 × 12 × 16	1.33	7	68016.3	25688.188	26329.25	0.885	0.789	1.12	3.41	2.96	1.15
24 × 12 × 16	2.31	7	74642.3	27957.061	20102.25	0.414	0.486	0.85	3.71	3.45	1.08
24 × 12 × 20	1.38	7	99171.5	31311.391	86646	0.182	0.783	0.23	3.28	2.78	1.18
24 × 12 × 20	2.44	7	114049	35731.77	92930.25	0.147	0.504	0.29	3.75	3.20	1.17
24 × 12 × 24	1.45	7	146872	46137.066	26735.25	0.041	0.816		4.00	2.59	1.54
24 × 12 × 24	2.32	7	153130	47610.871	55592.25	0.075	0.539	0.14	4.12	2.97	1.39
24 × 15 × 12	1.33	7	36899.4	13820.547	86649.25	1.046	0.850	1.23	2.50	2.93	0.85
24 × 15 × 12	2.27	7	40778.1	15294.247	26405	0.521	0.407	1.28	2.77	3.68	0.75
24 × 15 × 16	1.33	7	67231.6	25412.24	35159.5	0.761	0.798	0.95	3.37	2.94	1.15
24 × 15 × 16	2.31	7	73171.7	27541.551	74954.75	0.379	0.539	0.70	3.66	3.35	1.09
24 × 15 × 20	1.38	7	99995.6	31330.994	9955.25	0.123	0.695	0.18	3.28	2.90	1.13
24 × 15 × 20	2.44	7	104444	32713.412	4645.5	0.033	0.409		3.43	3.38	1.01
24 × 15 × 24	1.45	7	144540	48458.84	5698.5	0.712	0.840	0.85	4.20	2.56	1.64
24 × 15 × 24	2.32	7	162857	50399.695	62181	0.176	0.572	0.31	4.37	2.92	1.49
							Mean	**1.19**	**Mean**		**1.68**

Cases used to assess ACI318-14 code and comparison results

Case study	Box culvert Size ($ft.\times ft.\times in.$)	ρ^* (%)	f'_c, ksi	Total shear load at failure (lbs.)	Shear force in CS ** at failure (lbs.)	Bending moment in CS ** at failure (lbs.in)	ACI318-14's Prediction (lbs.) (Section 22.5.5)	Ratio ($\frac{FEM}{ACI}$)
1	6 × 6 × 12	1.33	3	155038	29600.6	71158	10613.94	2.79
2	6 × 6 × 12	2.27	3	149103	28525.1	62932.75	9062.94	3.15
3	6 × 6 × 16	1.33	3	241777	44528	193914	14563.56	3.06
4	6 × 6 × 16	2.31	3	245582	45457.5	184472	12358.56	3.68
5	12 × 6 × 12	1.33	3	65240.4	12063	119043.25	9314.58	1.30
6	12 × 6 × 12	2.27	3	78922.4	14692.3	101510	9062.94	1.62
7	12 × 6 × 16	1.33	3	123445	17152.3	223557	12810.03	1.34
8	12 × 6 × 16	2.31	3	132060	24811	189095.5	12471.06	1.99
9	12 × 6 × 20	1.38	3	197831	34232	336450	18817.67	1.82
10	12 × 6 × 20	2.44	3	215984	37626	280589.5	15654.17	2.40
11	12 × 12 × 12	1.33	3	62244.8	11646.7	93711	9868.58	1.18
12	12 × 12 × 12	2.27	3	69244	12649.7	110191.75	9062.94	1.40
13	12 × 12 × 16	1.33	3	115704	21773.4	142889	14563.56	1.50
14	12 × 12 × 16	2.31	3	121232	26315	136642	12471.06	2.11
15	12 × 12 × 20	1.38	3	168903	34647	295510.5	18817.67	1.84
16	12 × 12 × 20	2.44	3	186492	38060	189060.5	15796.67	2.41
17	18 × 6 × 20	1.38	3	119900	15718.8	347095.5	15247.81	1.03
18	18 × 6 × 20	2.44	3	117582	15804.6	287132.5	15996.17	0.99
19	18 × 6 × 24	1.45	3	193059	32471.4	469557	22317.89	1.45
20	18 × 6 × 24	2.32	3	183299	22718	418559	19122.29	1.19
21	18 × 12 × 20	1.38	3	102485	18922	304420	16508.53	1.15
22	18 × 12 × 20	2.44	3	127883	26555.8	253352.5	15996.17	1.66
23	18 × 12 × 24	1.45	3	152108	31551.2	368745	22365.29	1.41
24	18 × 12 × 24	2.32	3	177360	42568.5	293800	19122.29	2.23
25	18 × 15 × 20	1.38	3	104166	18354.3	345237.5	15836.48	1.16
26	18 × 15 × 20	2.44	3	121387	29147.4	272076	15996.17	1.82
27	18 × 15 × 24	1.45	3	158251	36868.2	381240	22365.29	1.65
28	18 × 15 × 24	2.32	3	181317	38320.3	378765	19122.29	2.00
29	24 × 12 × 20	1.38	3	71238.9	13307.6	222966	16323.73	0.82
30	24 × 12 × 20	2.44	3	75793	14131.1	197669.5	15996.17	0.88
31	24 × 12 × 24	1.45	3	95386.8	16212.6	336283	19908.34	0.81
32	24 × 12 × 24	2.32	3	115499	21404.1	252634.5	19122.29	1.12
33	24 × 15 × 20	1.38	3	63883.1	11988	222697.75	15886.29	0.75
34	24 × 15 × 20	2.44	3	79155.9	15226.8	230386.25	15996.17	0.95
35	24 × 15 × 24	1.45	3	96836.9	18458.5	304657	21332.39	0.87
36	24 × 15 × 24	2.32	3	108047	20099.6	259493.25	18949.79	1.06
37	6 × 6 × 12	1.33	5	185731	35147.3	94281	12612.62	2.79
38	6 × 6 × 12	2.27	5	207373	38384.4	130193	11061.62	3.47
39	6 × 6 × 16	1.33	5	330095	40954.7	382366	16899.37	2.42
40	6 × 6 × 16	2.31	5	359281	69310.2	178498	15084.03	4.59
41	12 × 6 × 12	1.33	5	80897.7	15028.5	146161	11349.17	1.32
42	12 × 6 × 12	2.27	5	107386	19993.3	179387.5	11061.62	1.81

43	12 × 6 × 16	1.33	5	157718	23463.9	314499	15440.46	1.52
44	12 × 6 × 16	2.31	5	167868	33244.3	239396	15196.53	2.19
45	12 × 6 × 20	1.38	5	254399	47196.7	306524	22269.93	2.12
46	12 × 6 × 20	2.44	5	264634	50504.9	388830	19106.43	2.64
47	12 × 12 × 12	1.33	5	73006	13530.8	116382	11673.63	1.16
48	12 × 12 × 12	2.27	5	86248.6	21496.2	99100.5	11061.62	1.94
49	12 × 12 × 16	1.33	5	141874	26041.5	220227	17289.03	1.51
50	12 × 12 × 16	2.31	5	155503	34530.8	155270	15196.53	2.27
51	12 × 12 × 20	1.38	5	194169	36498	339493	22269.93	1.64
52	12 × 12 × 20	2.44	5	232556	43367.1	442171	19248.93	2.25
53	18 × 6 × 20	1.38	5	147871	19378.8	486635	18291.73	1.06
54	18 × 6 × 20	2.44	5	155054	25871.6	378495	19448.43	1.33
55	18 × 6 × 24	1.45	5	222015	31557.8	677801.5	23897.32	1.32
56	18 × 6 × 24	2.32	5	233128	29549.6	682049	23301.34	1.27
57	18 × 12 × 20	1.38	5	136396	24990.7	296909.5	21605.66	1.16
58	18 × 12 × 20	2.44	5	144739	27328.6	308657	19448.43	1.41
59	18 × 12 × 24	1.45	5	183277	33076.2	426096	26544.34	1.25
60	18 × 12 × 24	2.32	5	200100	37200.2	460831	23301.34	1.60
61	18 × 15 × 20	1.38	5	115397	22650.8	362211.5	19988.97	1.13
62	18 × 15 × 20	2.44	5	142177	26582.3	346760	19448.43	1.37
63	18 × 15 × 24	1.45	5	188499	33783	434378	26544.34	1.27
64	18 × 15 × 24	2.32	5	195106	36653.3	480879	23301.34	1.57
65	24 × 12 × 20	1.38	5	81564.1	15443.7	315899	18969.21	0.81
66	24 × 12 × 20	2.44	5	94168.8	20998.6	307498.5	19448.43	1.08
67	24 × 12 × 24	1.45	5	129984	24845	481243	24480.38	1.01
68	24 × 12 × 24	2.32	5	144388	27764.9	415712	23301.34	1.19
69	24 × 15 × 20	1.38	5	90805.7	17095.3	379484	18682.30	0.92
70	24 × 15 × 20	2.44	5	95087.6	18191.8	246059	19448.43	0.94
71	24 × 15 × 24	1.45	5	133692	23883	525819	23766.33	1.00
72	24 × 15 × 24	2.32	5	149013	25356.8	537139	23128.84	1.10
73	6 × 6 × 12	1.33	7	208317	34524.4	188941	14237.22	2.42
74	6 × 6 × 12	2.27	7	275240	45359.5	228735.5	12686.22	3.58
75	6 × 6 × 16	1.33	7	413035	51861.7	461838	19347.49	2.68
76	6 × 6 × 16	2.31	7	436686	67650.4	480399.5	17299.39	3.91
77	12 × 6 × 12	1.33	7	90308.8	14273.6	191683	12289.26	1.16
78	12 × 6 × 12	2.27	7	126717	15745.2	265567.5	12686.22	1.24
79	12 × 6 × 16	1.33	7	189317	27277	363468	17675.54	1.54
80	12 × 6 × 16	2.31	7	205279	38553.6	306913	17411.89	2.21
81	12 × 6 × 20	1.38	7	333185	43065.4	678235	22866.95	1.88
82	12 × 6 × 20	2.44	7	331091	76832.2	439742	21912.56	3.51
83	12 × 12 × 12	1.33	7	84184	15555.5	144693	13086.88	1.19
84	12 × 12 × 12	2.27	7	103980	19830.1	165320.5	12686.22	1.56
85	12 × 12 × 16	1.33	7	154763	29795.7	233298.5	19504.39	1.53
86	12 × 12 × 16	2.31	7	185949	35494.3	265120	17411.89	2.04
87	12 × 12 × 20	1.38	7	250442	47761.7	396271	25076.06	1.90
88	12 × 12 × 20	2.44	7	277874	57843.3	467213	22055.06	2.62
89	18 × 6 × 20	1.38	7	178878	27906.4	484366.5	22427.40	1.24
90	18 × 6 × 20	2.44	7	195702	28137.6	504990.5	22254.56	1.26
91	18 × 6 × 24	1.45	7	297943	53751.7	790074	29765.02	1.81
92	18 × 6 × 24	2.32	7	285393	39581.8	740990	26698.23	1.48
93	18 × 12 × 20	1.38	7	150137	30742.8	451293	23212.59	1.32
94	18 × 12 × 20	2.44	7	188641	45386.8	348194	22254.56	2.04

95	$18 \times 12 \times 24$	1.45	7	227756	49327.1	645143	29941.23	1.65
96	$18 \times 12 \times 24$	2.32	7	264131	50479.2	722136	26698.23	1.89
97	$18 \times 15 \times 20$	1.38	7	138758	27922.2	407358	23244.20	1.20
98	$18 \times 15 \times 20$	2.44	7	181031	30380.1	615809.5	22254.56	1.37
99	$18 \times 15 \times 24$	1.45	7	216370	38665.5	664239	28634.76	1.35
100	$18 \times 15 \times 24$	2.32	7	250487	43727.6	649126	26698.23	1.64
101	$24 \times 12 \times 20$	1.38	7	99171.5	18887.4	330299.25	22395.15	0.84
102	$24 \times 12 \times 20$	2.44	7	114049	21476.9	363960.5	22254.56	0.97
103	$24 \times 12 \times 24$	1.45	7	146872	24902.4	598170.5	26727.18	0.93
104	$24 \times 12 \times 24$	2.32	7	153130	28514	448648	26698.23	1.07
105	$24 \times 15 \times 20$	1.38	7	99995.6	19105.4	298149.5	22910.56	0.83
106	$24 \times 15 \times 20$	2.44	7	104444	19681.9	356685.5	22254.56	0.88
107	$24 \times 15 \times 24$	1.45	7	144540	23706.8	635988	26226.06	0.90
108	$24 \times 15 \times 24$	2.32	7	162857	30092.9	539868	21937.23	1.37
							Average	**1.66**

APPENDIX 4. GALLERY OF BEAM TEST PICTURES

P1. Pin support

P2. Roller Support

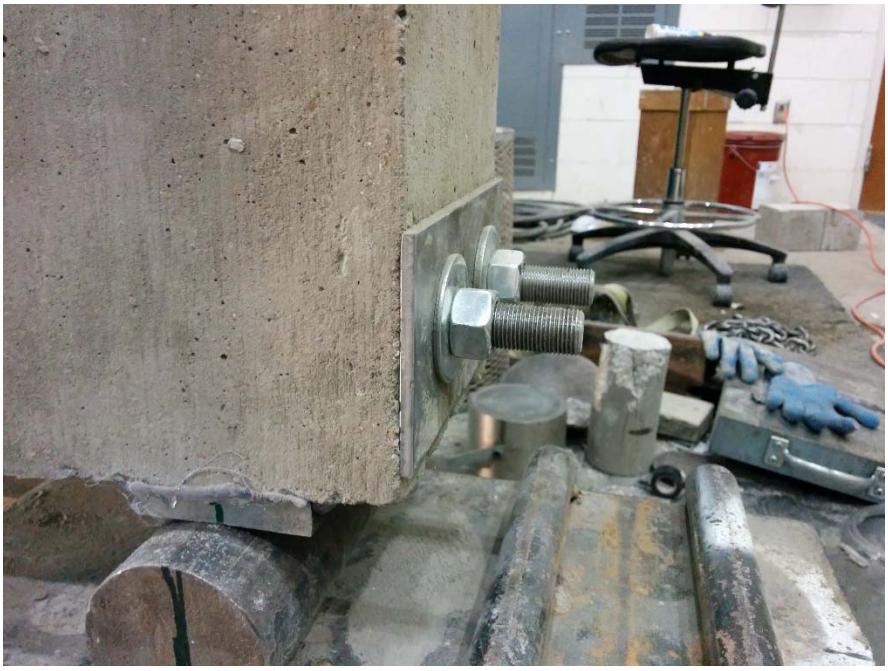

P3. Anchorage of longitudinal rebar

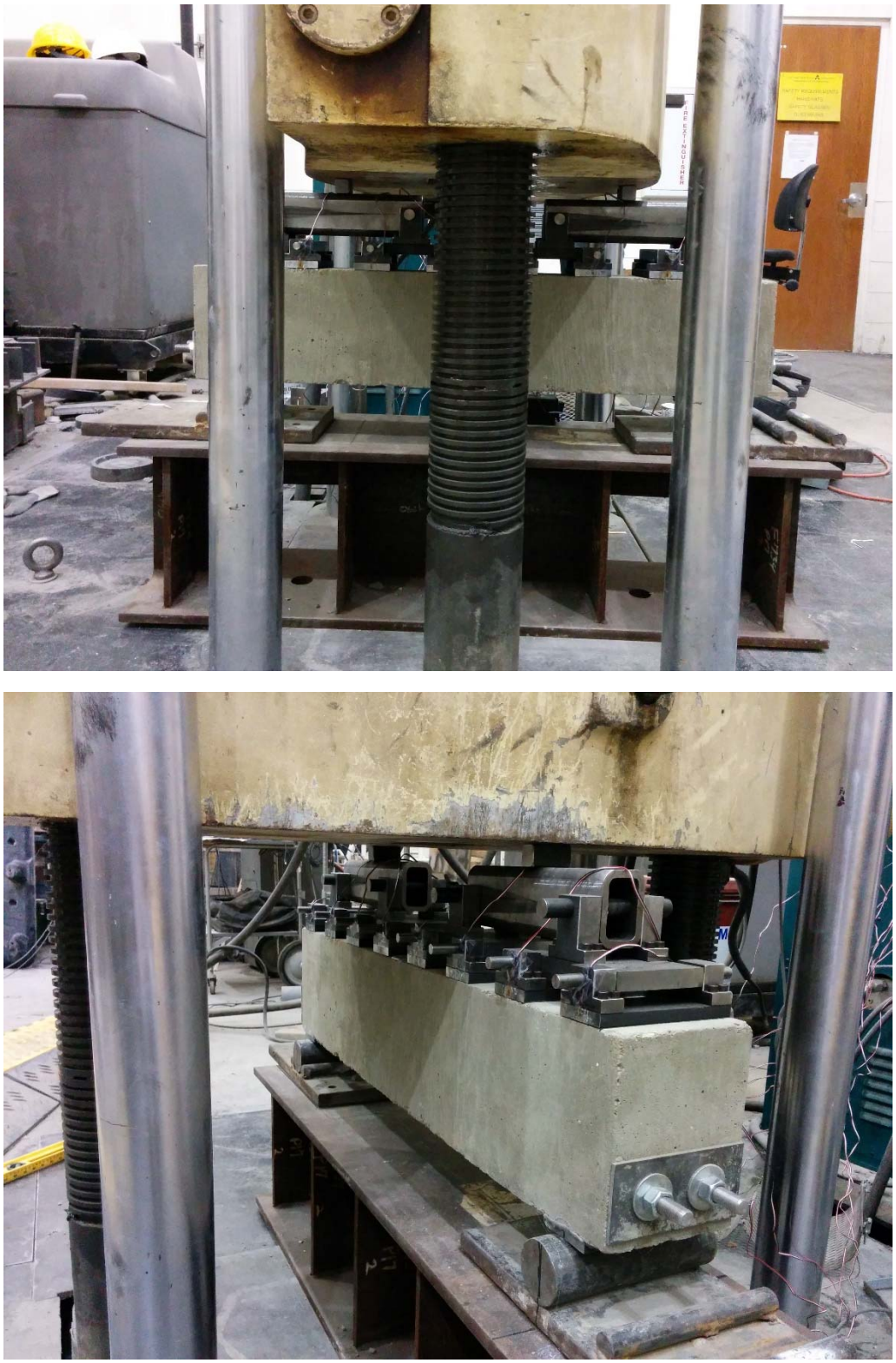

P4. Test setup

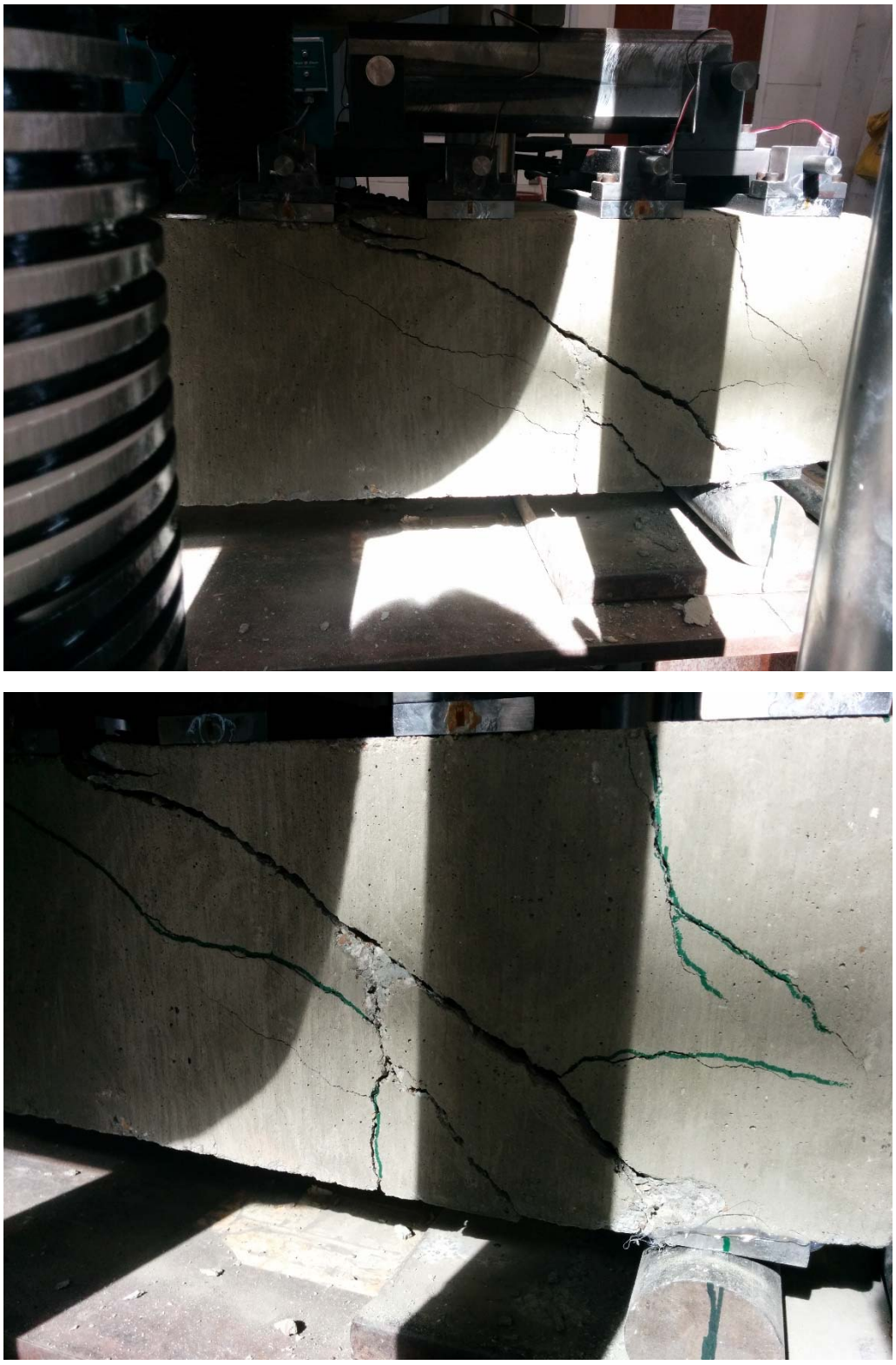

P5. Shear Cracking (continued)

P5. Shear Cracking (continued)

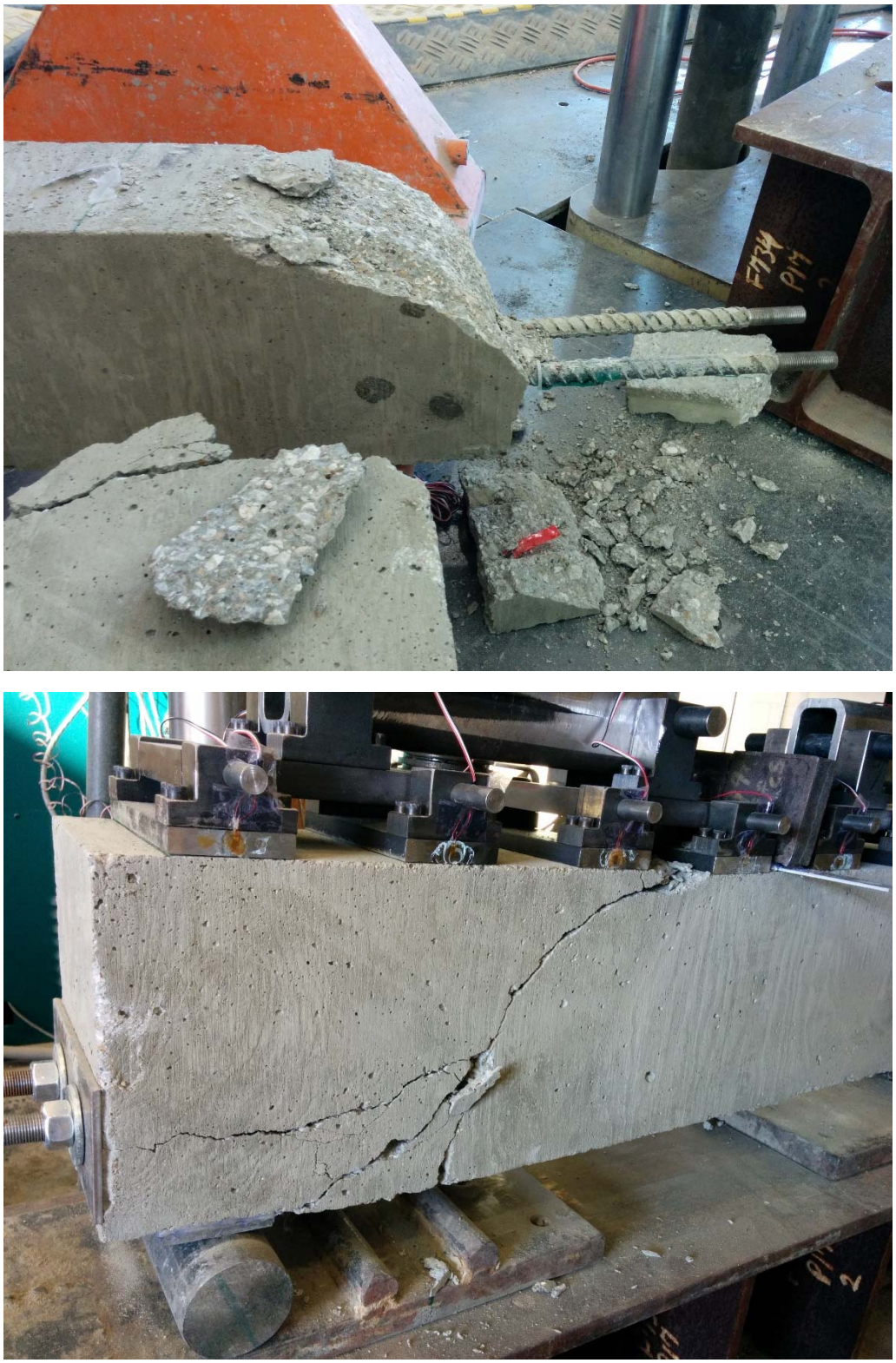

P5. Shear Cracking (continued)

P5. Shear Cracking

APPENDIX 5. GALLERY OF BOX CULVERT TESTS

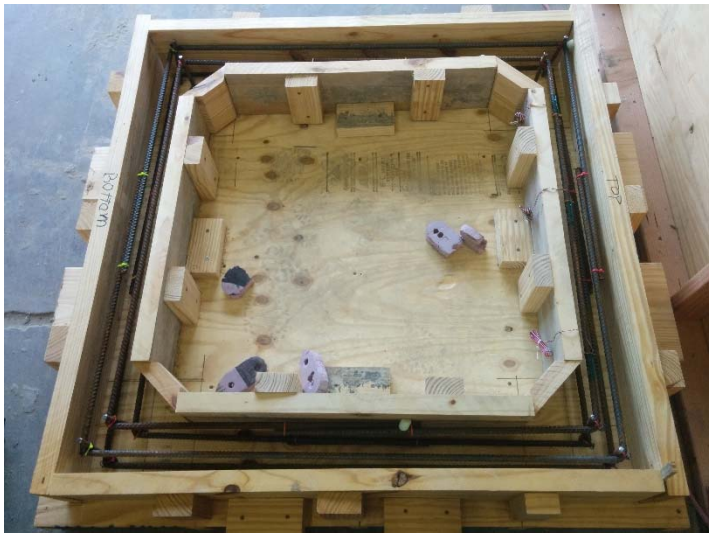

P1. Construction of molds

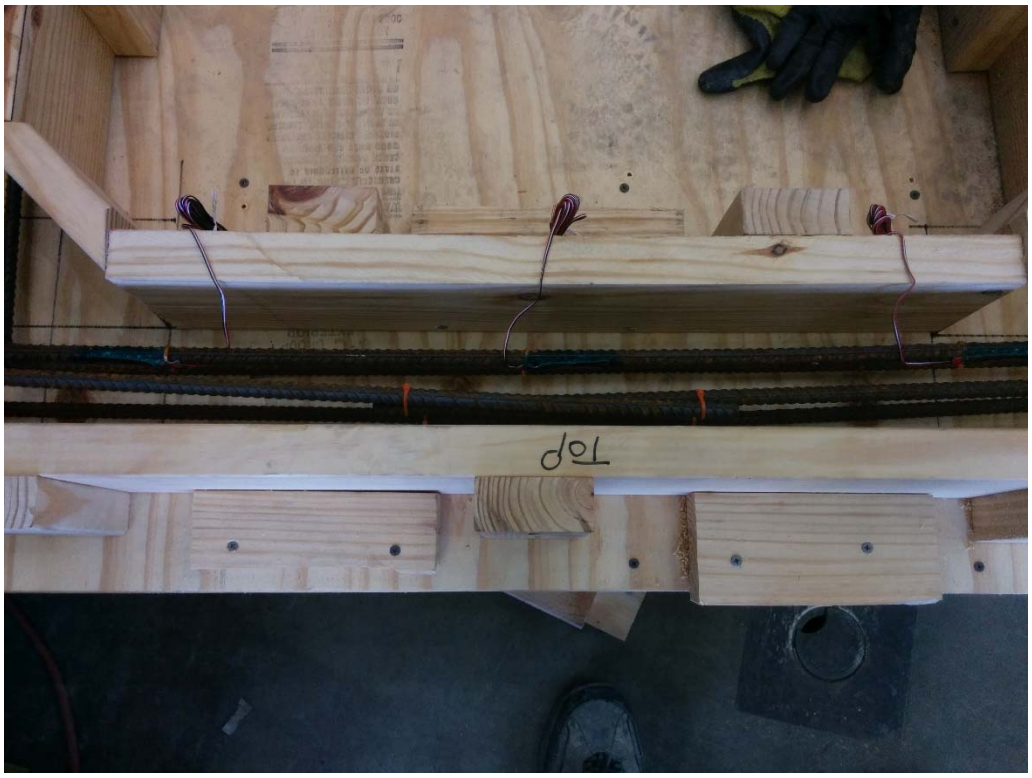

P2. Installation of strain gauge before casting

P3. Casting concrete- $f'_c = 6.5$ ksi (continued)

P3. Casting concrete- $f_c' = 6.5$ ksi

P4. Curing for 28 days. Needed water was provided periodically.

P5. Test setup for first series of test- $f'_c = 6.5$ ksi (continued)

P5. Test setup for first series of test- $f'_c = 6.5$ ksi

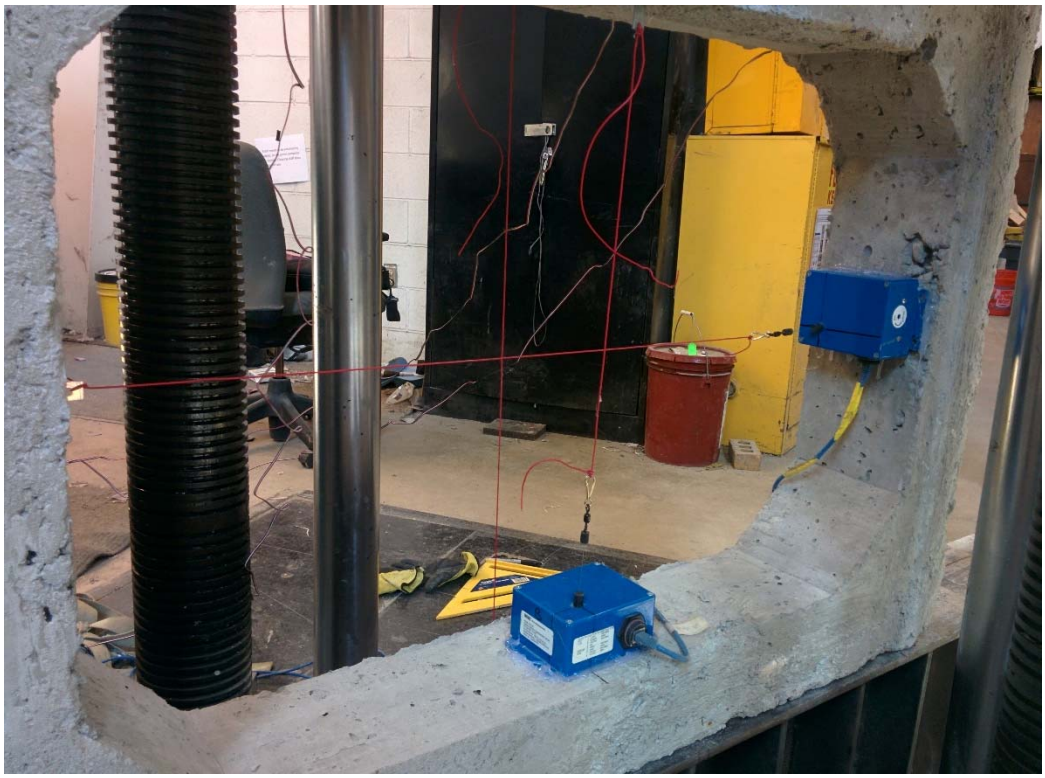

P6. Instrumentations- $f'_c = 6.5$ ksi

P7. Data Acquisition system- $f_c' = 6.5$ ksi

P8. Shear cracking- $f_c' = 6.5$ ksi (continued)

P8. Shear cracking- $f_c' = 6.5$ ksi (continued)

P8. Shear cracking- $f_c' = 6.5$ ksi (continued)

P8. Shear cracking- $f_c' = 6.5$ ksi

P9. Building box culverts for the second series of testing- $f'_c = 4.8$ ksi

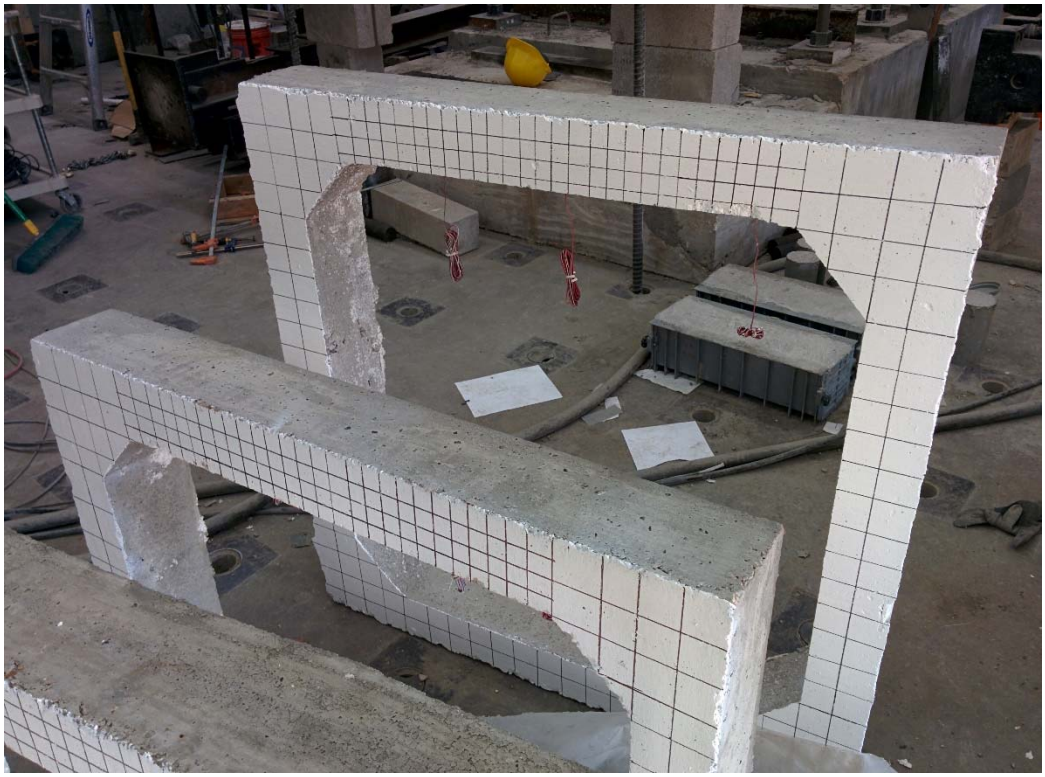

P10. Making grid on one surface of box culverts- $f'_c = 4.8$ ksi (continued)

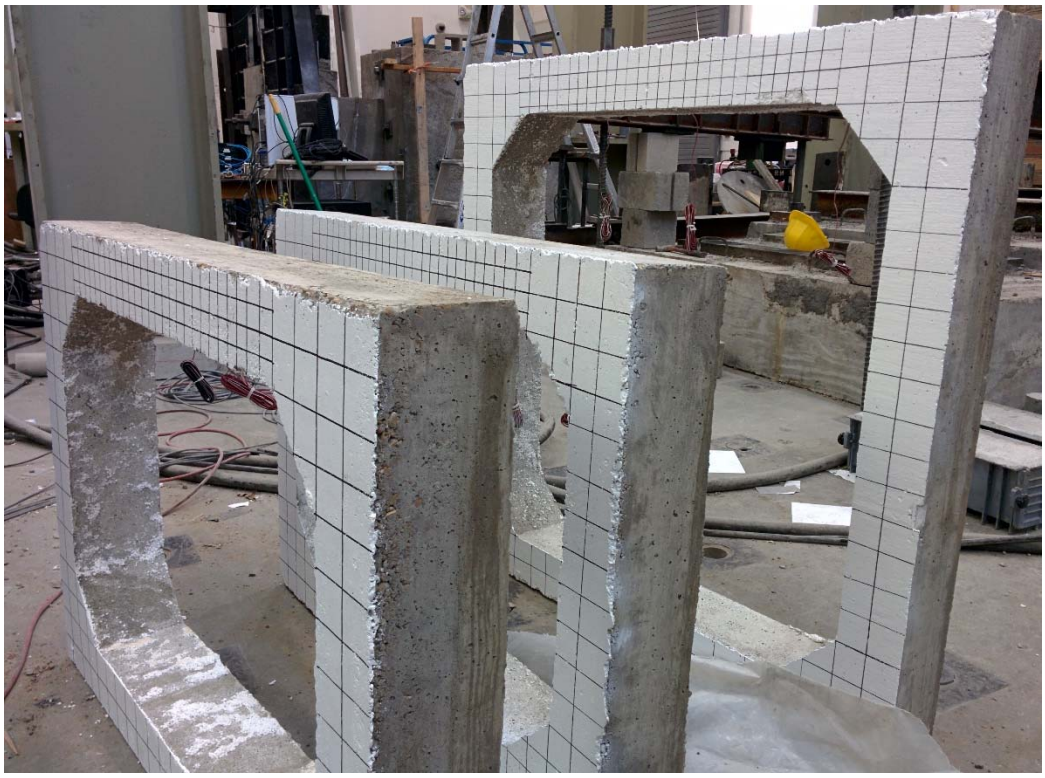

P10. Making grid on one surface of box culverts- $f_c' = 4.8$ ksi

P11. Applying the framework on the top of the box culverts- $f_c' = 4.8$ ksi

P12. Flexural cracks on the side walls- $f'_c = 4.8$ ksi

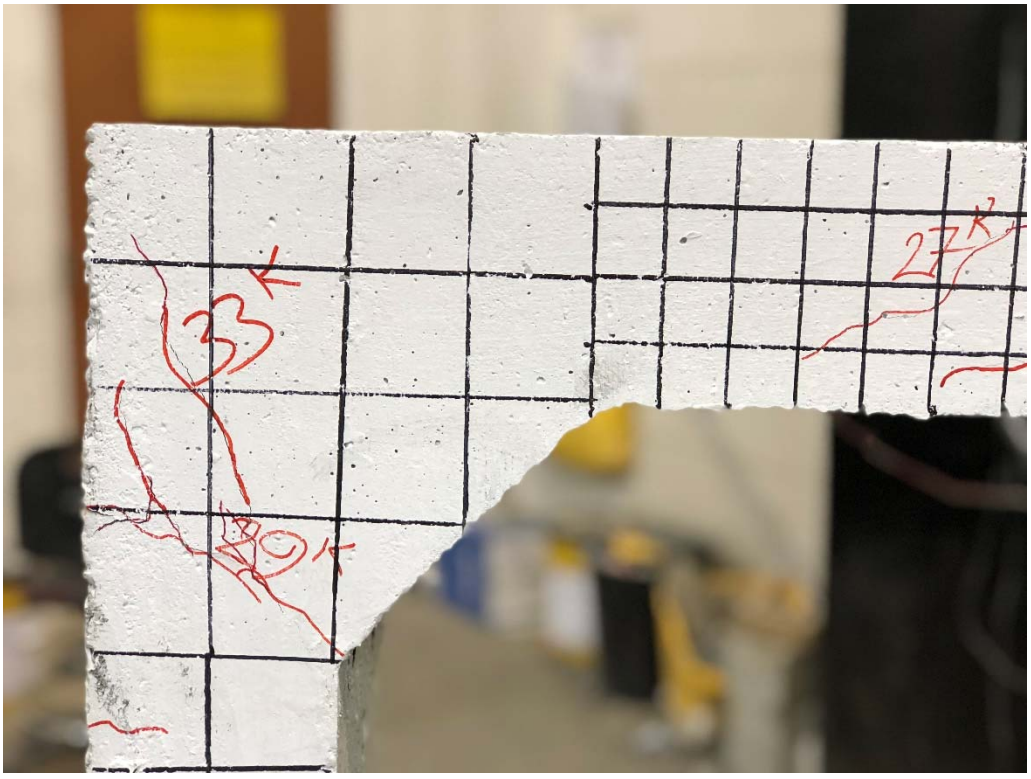

P13. Flexural cracks in connection of slab and wall- $f'_c = 4.8$ ksi

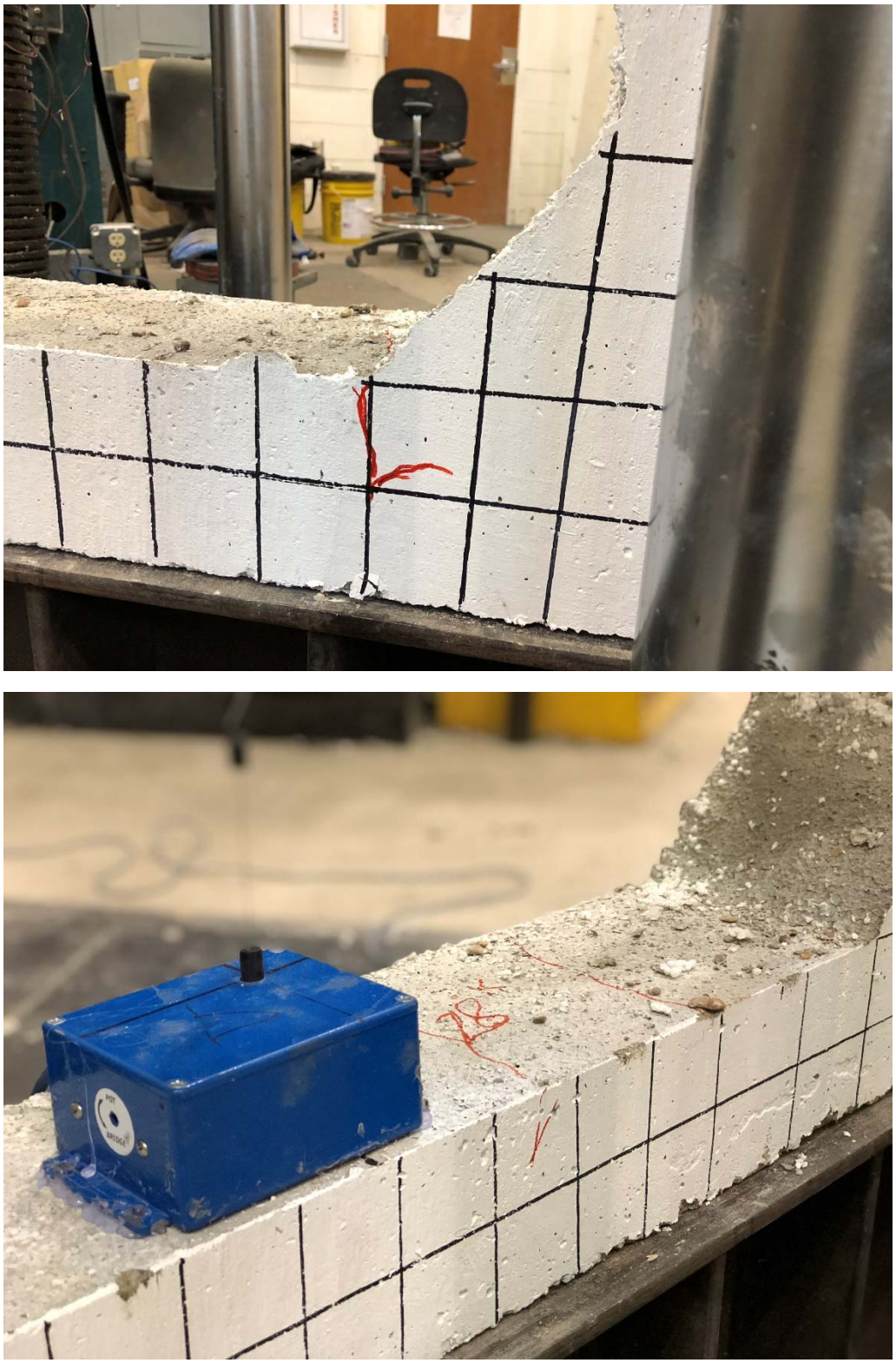

P14. Minor cracks in the bottom slab- $f_c' = 4.8$ ksi

P15. Shear cracking- $f_c' = 4.8$ ksi (continued)

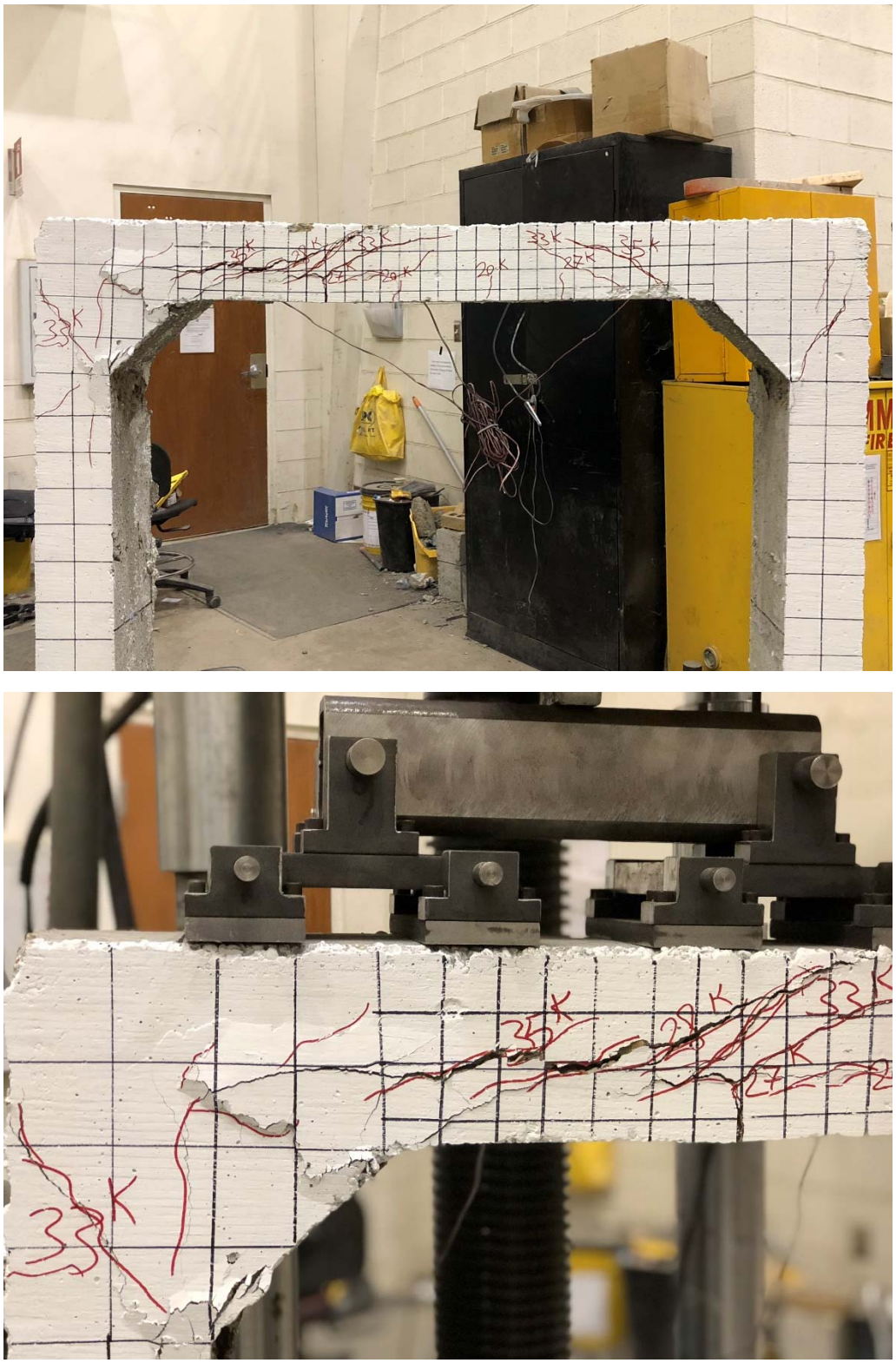

P15. Shear cracking- $f_c' = 4.8$ ksi (continued)

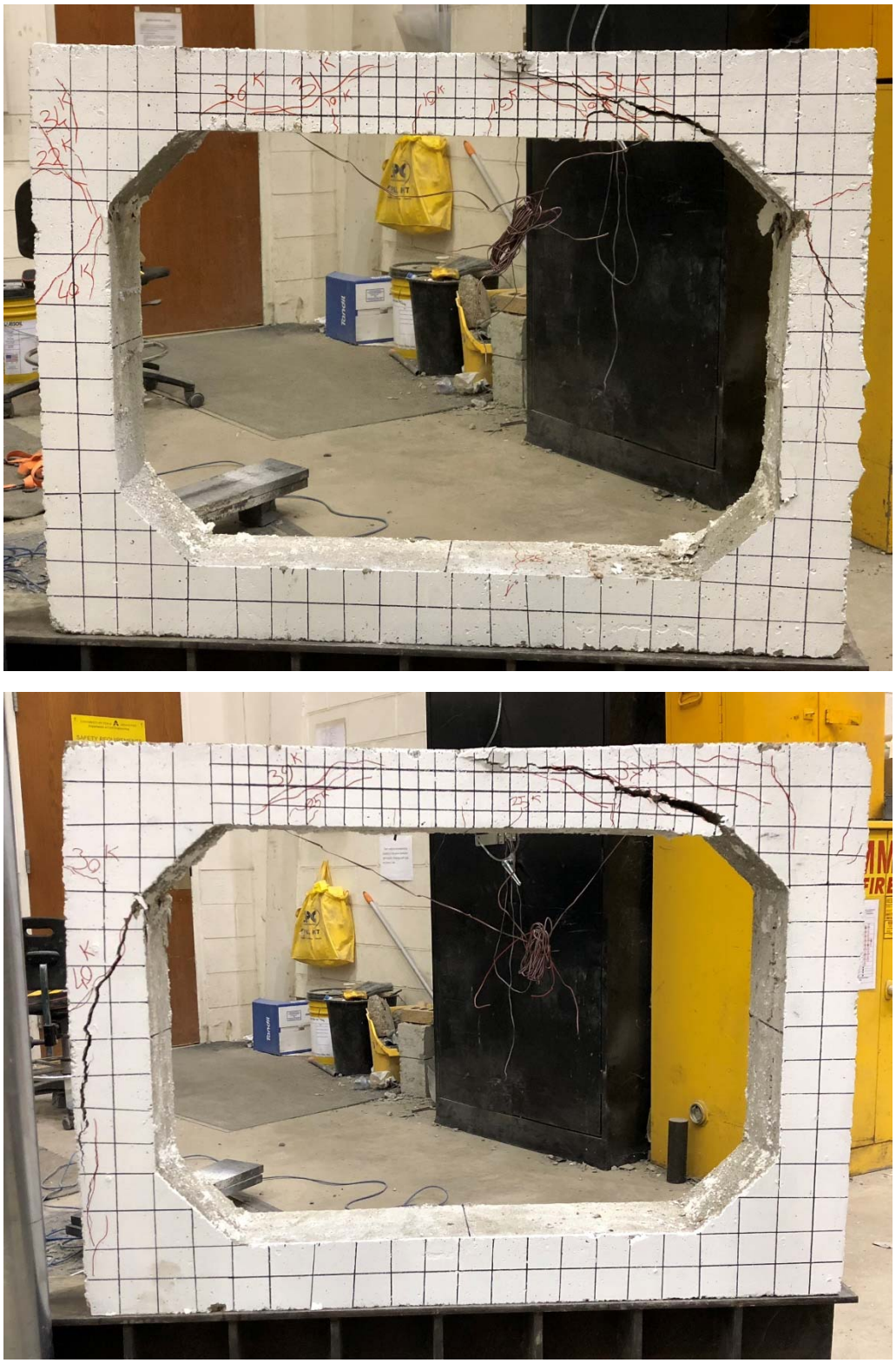

P15. Shear cracking- $f'_c = 4.8$ ksi (continued)

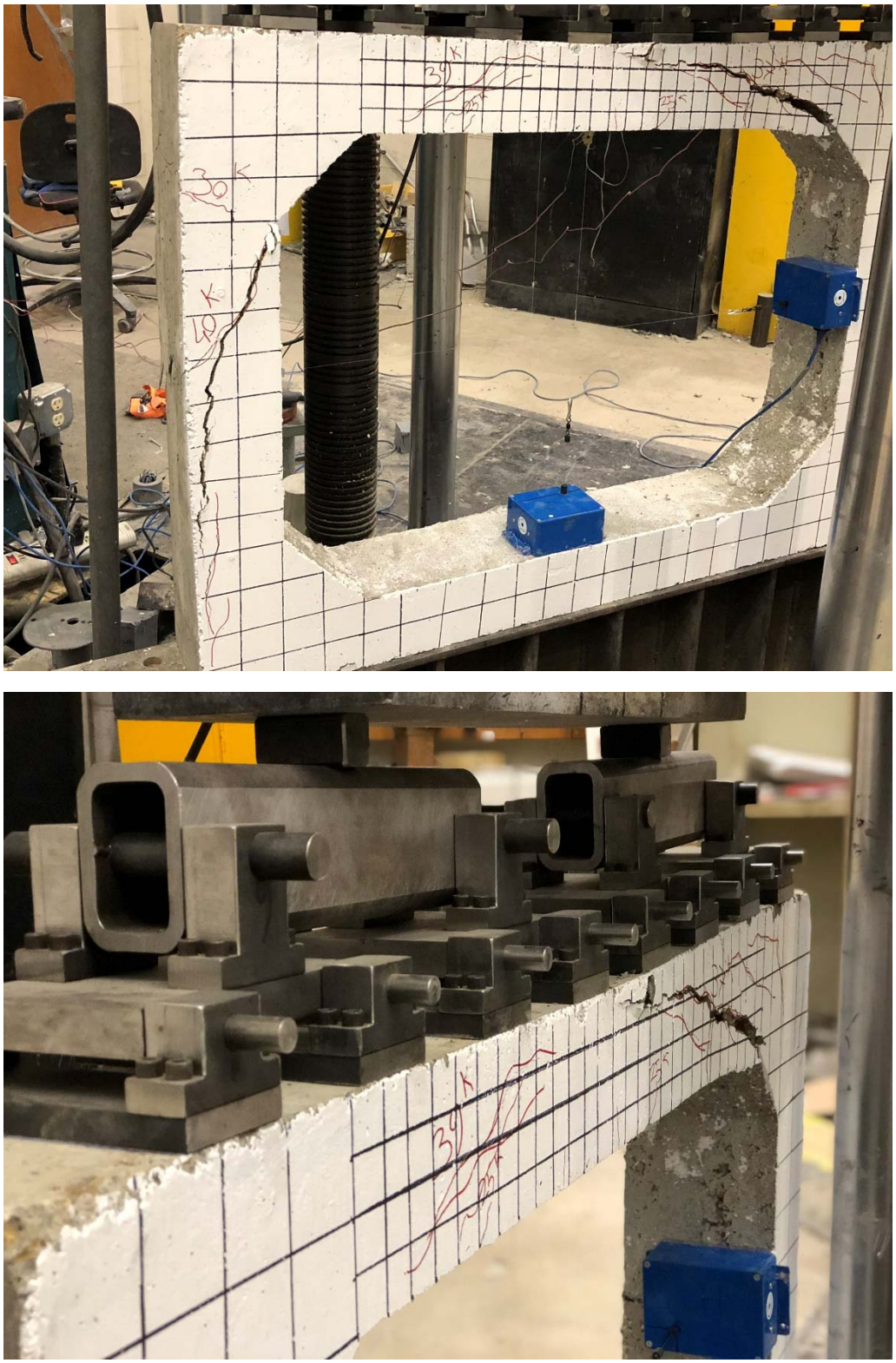

P15. Shear cracking- $f_c' = 4.8$ ksi (continued)

P15. Shear cracking- $f'_c = 4.8$ ksi

References

[1] Box Culverts applications and uses | BPDA | BPDA, 2018, https://www.precastdrainage.co.uk/page/box-culverts-applications

[2] Shawprecastsolutions.ca, 2018, http://shawprecastsolutions.ca/spans-crossings/box-culverts/advantages/

[3] AASHTO (American Association of State Highway and Transportation Officials). 2017. "AASHTO LRFD Bridge Design Specification." 8th Edition.

[4] ASTM (American Society for Testing and Materials) Specification C1577. 2017. "Precast Reinforced Concrete Monolithic Box Sections for Culverts, Storm Drains, and Sewers Designed According to AASHTO LRFD." ASTM International, West Conshohocken, PA.

[5] Hassan, T. K.; Seliem, H. M.; Dwairi, H.; Rizkalla, S. H.; and Zia, P. 2008. “Shear behavior of large concrete beams reinforced with high-strength steel.” ACI Structural Journal, Vol.105, No.2, 173-179.

[6] Zarrinpour, M.R. and Chao, S.H. 2017. “Shear strength enhancement mechanisms of steel fiber-reinforced concrete slender beams.” ACI Structural Journal, Vol. 114, No. 3, 729-742.

[7] Bazant, Z.P. and Kim, J.K. 1983. “Size effect in shear failure of longitudinally reinforced beams.” ACI Structural Journal, Vol. 81, 456-468.

[8] Vecchio, F. J. and Shim, W. 2004. “Experimental and analytical reexamination of classic concrete beam tests.” Journal of Structural Engineering, Vol. 130, No.3, 460-469.

[9] Bentz, E. C.; Vecchio, F. J.; and Collins, M. P. 2006. “Simplified modified compression field theory for calculating shear strength of reinforced concrete elements.” ACI Structural Journal, Vol. 103, No. 4, 614-624.

[10] Collins, M. P.; Mitchell, D.; Adebar, P.; and Vecchio, F. J. 1996. “A general shear design method.” ACI Structural Journal. Vol. 93, No. 1, 36-45.

[11] Vecchio, F. J. and Collins, M. P. 1986. “The modified compression-field theory for reinforced concrete element subjected to shear.” ACI Journal. 219-231.

[12] Abolmaali, A. and Garg, A.K. 2008. “Effect of wheel live load on shear behavior of precast reinforced concrete box culverts.” Journal of Bridge Engineering. Vol. 13, No.1, 93-99.

[13] Mostafazadeh, M. 2017. “Shear behavior of synthetic fiber-reinforced concrete box culverts.” Department of Civil Engineering, University of Texas at Arlington

[14] Yee, R.A. 2003. “Shear behavior of concrete box culverts.” Department of Civil Engineering, University of Toronto.

[15] CHBDC. 2000. “Canadian Highway Bridge Design Code” Canadian Standards Association. Toronto.

[16] Sherwood, E. G.; Lubell, A. S.; Bentz, E. C.; and Collins, M. P. 2006. “One-way shear strength of thick slabs and wide beams.” ACI Structural Journal. Vol. 103, No.6. 794-802.

[17] Orton, S.L.; Loehr, J.E.; Boeckmann, A.; and Havens, G. 2015. “Live-load effect in reinforced concrete box culverts under soil fill.” Journal of Bridge Engineering, Vol. 20, No. 11.

[18] AASHTO (American Association of State Highway and Transportation Officials). 2012. "AASHTO LRFD Bridge Design Specification." 6th Edition.

[19] Kim, K. and Yoo, C.H. 2005. “Design loading on deeply buried box culverts.” Journal of Geotechnical and Geoenvironmental Engineering, Vol. 131, No. 1.

[20] Ghahremannejad, M. and Abolmaali, A. 2018. “Prediction of shear strength of reinforced concrete beams using displacement control finite element analysis.” Engineering Structures Journal, Vol. 169, 226-237

[21] Pang, P.L.R. and Millar, M.A. 1978. “Experimental behavior of a fixed ended beam under simulated uniformly distributed load.” International Journal of Mechanical Science, Vol.20, pp 675-683.

[22] Brown, M. D. and Bayrak, O. 2007. “Investigation of deep beams with various load configurations.” ACI Structural Journal. Vol. 104, No.5. 518-611.

[23] Zararis, P. D. and Zararis, I. P. 2008. “Shear strength of reinforced concrete beams under uniformly distributed loads.” ACI Structural Journal, Vol. 105, No. 6, 711-719.

[24] Iguro, M.; Shioya, T.; Nojiri, Y.; and Akiyama, H. 1985. “Experimental studies on shear strength of large reinforced concrete beams under uniformly distributed load.” Concrete Library of JSCE, No.5.

[25] Klaus, T.P.R. 2007. “Shear behavior of reinforced concrete box culverts.” Department of Civil Engineering, University of Toronto.

[26] ACI Committee 318. 2014. “Building Code Requirements for Structural Concrete (ACI 318-14) and Commentary (ACI 318R-14).” American Concrete Institute, Farmington Hills, MI, 520.

[27] Vecchio, F. J. and Collins, M. P. 1986. “The modified compression-field theory for reinforced concrete element subjected to shear.” ACI Journal. 219-231.

[28] Ghahremannejad, M. and Park, Y. “Impact on the number of floors of a reinforced concrete building subjected to sudden column removal.” Journal of Engineering Structures 2016. Vol. 111, pp. 11-23.

[29] May, I. M.; Naji, J. H.; and Ganaba, T. H. 1998. “Displacement control for the non-linear analysis of reinforced concrete structures.” Journal of Engineering Computations, Vol. 5, Issue: 4, pp 266-273.

[30] Zheng, H.; Liu, D. F.; Lee, C. F.; and Tham, L. G. 2005. “Displacement-controlled method and its applications to material non-linearity.” International Journal for Numerical and Analytical Methods in Geomechanics, Vol. 29, pp 209-226.

[31] ASTM. 2016. “Standard Specification for Deformed and Plain Carbon-Steel Bars for Concrete Reinforcement.” A615- 615M.

[32] ABAQUS 6.14 Documentation. 2016. ABAQUS Manual, version 6.14, Pawtucket, R.I.

[33] Jankowiak, T. and Lodygowski, T. 2005. “Identification of parameters of concrete damage plasticity constitutive model.” Foundations of Civil and Environmental Engineering, No.6, 53-69.

[34] Vecchio, F. J. and Shim, W. 2004. “Experimental and analytical reexamination of classic concrete beam tests.” Journal of Structural Engineering, Vol. 130, No.3, 460-469.

[35] Hosseinzadeh, N.; Kazem, H.; Ghahremannejad, M.; Ahmadi, E.; and Kazem, N. “Comparison of API650-2008 provision with FEM analyses for seismic assessment of existing steel oil storage tanks.” Journal of Loss Prevention in the Process Industries 2013. Vol. 26, Issue 4, pp. 666-675.

[36] Kazem, H.; Rizkalla, S.; and Kobayashi, A. 2018. “Shear strengthening of steel plates using small-diameter CFRP strands.” Journal of Composite Structures, Vol. 184, pp. 78-91.

[37] Shafieifar, M., Farzad, M. and Azizinamini, A. “Experimental and numerical study on mechanical properties of ultra-high performance concrete (UHPC).” Journal of Construction and Building Materials 2017. Vol. 156, pp. 402-411.

[38] Shafieifar, M.; Farzad, M.; and Azizinamini, A. “A comparison of existing analytical methods to predict the flexural capacity of ultra-high performance concrete (UHPC) beams.” 2018. Journal of Construction and Building Materials, Vol. 172, pp. 10-18.

[39] Mahdavi, M.; Davoodi, M.R.; and Mostafavian, A. “Determination of joint stiffness of a three-story steel frame by finite element model updating.” 15th World Conference on Earthquake Engineering 2012.

[40] Amleh, L. and Ghosh, A. 2006. “Modeling the effect of corrosion on bond strength at the steel-concrete interface with finite-element analysis.” Canadian Journal of Civil Engineering, Vol. 33, pp. 673-682.

[41] Belakhdar, K. 2008. “Nonlinear finite element analysis of reinforced concrete slab strengthened with shear bolts.” Jordan Journal of Civil Engineering, Vol. 2, No. 1, pp. 32-44

[42] An, X.; Maekawa, K.; and Okamura, H. 1997. “Numerical simulation of size effect in shear strength of RC beams.” Journal of Materials Conc. Struct., Pavements, JSCE, No. 564, Vol. 35, pp 297-316.

[43] Bates, D. M. and Watts, D. G. “Nonlinear regression analysis and its applications.” John Wiley & Sons Inc., Second Edition.

[44] XLSTAT 2017: Data Analysis and Statistical Solution for Microsoft Excel. Addinsoft, Paris, France.

[45] Ghahremannejad, Masoud; Mahdavi, Maziar; Emami, Arash; Sina Abhaee, Saleh; and Abolmaali, Ali. “Experimental investigation and identification of single and multiple cracks in synthetic fiber concrete beams.” Case Study in Construction Material Journal, Vol. 9, 2018, e00182.

Biographical Information

Masoud Ghahremannejad was born on March 21, 1987 in the northwest part of Iran. His only sibling is a one-year older brother who is an electrical engineer. His father was a consultant or a telecommunication company in Iran. Due to his father's job, they moved to Tehran, the capital of Iran, when Masoud was five years old. He finished his elementary, mid-school, and high-school in Tehran. Then, in 2005, he moved to Tabriz, Iran for four years to pursue his undergraduate degree in civil engineering at the University of Tabriz. He was admitted to Amirkabir University of Technology (Tehran Polytechnic), where he received his Master of Science degree in structural engineering in 2011. After working in industry for four years, including two years in the construction field and two years as a consultant, Masoud decided to continue his education while pursuing a PhD program abroad. He was admitted to the University of Texas at Arlington in 2014 and began the PhD program in spring 2015. Since then, he has been active in student and engineering organizations on campus. Masoud was involved in various research projects in the areas of advanced concrete materials and evaluation of infrastructures performance. The outcomes of his research were several journal papers that were published in prestigious international scientific journals. He graduated in summer 2018 with a PhD degree in civil engineering.